



Rubén Rellán Álvarez

Long distance iron transport and metabolomics of plant iron deficiency

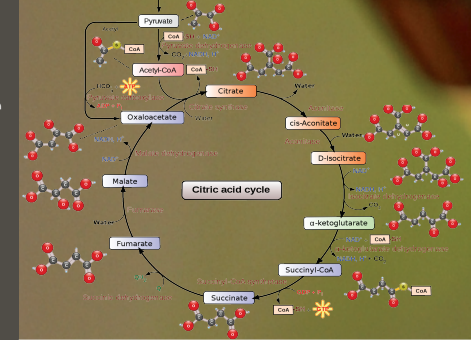
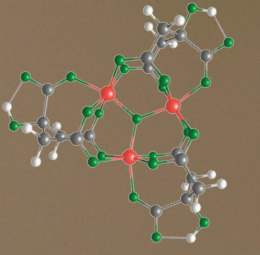
2010


TESIS DOCTORAL

Rubén Rellán Álvarez
Zaragoza, 2010

Transporte de hierro a larga distancia y metabolómica de la deficiencia de hierro en plantas

Long distance iron transport and metabolomics of plant iron deficiency



 **Plant Stress Physiology**



 **CSIC**

Estación Experimental de Aula Dei
Consejo Superior de Investigaciones Científicas (CSIC)



Departamento de Biología
Universidad Autónoma de Madrid

TESIS DOCTORAL

UNIVERSIDAD AUTÓNOMA DE MADRID
FACULTAD DE CIENCIAS DEPARTAMENTO DE BIOLOGÍA

Consejo Superior de Investigaciones Científicas (CSIC)

Estación Experimental Aula Dei

Departamento de Nutrición Vegetal

Plant Stress Physiology Group

Zaragoza



CSIC



Plant Stress Physiology

TESIS DOCTORAL:

Transporte de hierro a larga distancia y metabolómica de la deficiencia de hierro en plantas

Long distance iron transport and metabolism changes in iron deficient plants

Memoria presentada por Rubén Rellán Álvarez, Licenciado en Ciencias Ambientales, para optar al grado de Doctor en Ciencias.

D. Rubén Rellán Álvarez,
Zaragoza, Noviembre de 2010

AUTORIZACIÓN DE LOS DIRECTORES PARA LA PRESENTACIÓN DE TESIS DOCTORAL

ANA MARÍA ÁLVAREZ FERNÁNDEZ, Científica Titular del Consejo Superior de Investigaciones Científicas (CSIC), y JAVIER ABADÍA BAYONA, Profesor de Investigación del mismo organismo.

AUTORIZAN

La presentación de la siguiente memoria de Tesis Doctoral, titulada “TRANSPORTE DE HIERRO A LARGA DISTANCIA Y METABOLÓMICA DE LA DEFICIENCIA DE HIERRO EN PLANTAS” presentada por D. RUBÉN RELLÁN ÁLVAREZ para optar al grado de Doctor por la Universidad Autónoma de Madrid.

Y para que conste a los efectos oportunos expide la presente autorización

En Zaragoza, Noviembre de 2010

Fdo. Ana María Álvarez-Fernández

Fdo. Javier Abadía Bayona

**AUTORIZACIÓN DEL TUTOR ACADÉMICO PARA LA PRESENTACIÓN DE
TESIS DOCTORAL**

Luis Eduardo Hernández Rodríguez, Profesor Titular de la Universidad Autónoma de Madrid.

AUTORIZA

La presentación de la siguiente memoria de Tesis Doctoral, titulada “TRANSPORTE DE HIERRO A LARGA DISTANCIA Y METABOLÓMICA DE LA DEFICIENCIA DE HIERRO EN PLANTAS” presentada por D. RUBÉN RELLÁN ÁLVAREZ para optar al grado de Doctor por la Universidad Autónoma de Madrid.

Y para que conste a los efectos oportunos expide la presente autorización

En Madrid, Noviembre de 2010

Fdo. Luis Eduardo Hernández Rodríguez

UNIVERSIDAD AUTÓNOMA DE MADRID
FACULTAD DE CIENCIAS DEPARTAMENTO DE
BIOLOGÍA

**Transporte de hierro a larga distancia y metabólica de
la deficiencia de hierro en plantas**

**Long distance iron transport and metabolism changes in
iron deficient plants**

Memoria presentada por Rubén Rellán Álvarez para optar
al grado de Doctor en Ciencias Biológicas por la
Universidad Autónoma de Madrid.

Los directores:

Dr. Javier Abadía

Dpto. Nutrición Vegetal

EEAD, CSIC

Dra. Ana Álvarez

Dpto. Nutrición Vegetal

EEAD, CSIC

El Doctorando:

Rubén Rellán Álvarez

**UNIVERSIDAD AUTÓNOMA DE MADRID
FACULTAD DE CIENCIAS DEPARTAMENTO DE
BIOLOGÍA**

**Transporte de hierro a larga distancia y metabólica de
la deficiencia de hierro en plantas**

**Long distance iron transport and metabolism changes in
iron deficient plants**

TESIS DOCTORAL

Rubén Rellán Álvarez

Zaragoza, 2010

Agradecimientos

El trabajo que ha llevado a la realización de este tesis doctoral no hubiese sido posible sin la colaboración de un gran equipo de personas, que de una u otra manera han colaborado conmigo durante todos estos años, ellos y ellas bien saben todo lo que han hecho, pero desde aquí quiero aprovechar para expresarles mi mas sincero agradecimiento.

En primer lugar, gracias a Ana y a Javier, mis dos directores de tesis. Gracias por confiar en mi desde que llegue a Aula Dei. Gracias, porque habéis sido un ejemplo de profesionalidad y porque con vuestras enseñanzas he crecido como investigador y porque sois un espejo en el que ver el científico que me gustaría ser el día de mañana.

Gracias al profesor Oliver Fiehn, que no solamente me abrió las puertas de su laboratorio y me enseñó todo lo que se de metabólomica sino que también me abrió las puertas de su casa y su familia y me hizo sentir en Davis realmente a gusto. Siempre que he vuelto ha sido como regresar a casa. Gracias también a todos los miembros de su laboratorio por su ayuda y enseñanzas, especialmente a Martin, Nabil y Tobias.

Gracias a mi paisano, el profesor José Ignacio García Alonso, porque siempre es un orgullo volver a la tierra donde uno nació para trabajar en uno de los mejores laboratorios del mundo de ICP-MS y comprobar que se está haciendo un trabajo de primerísimo nivel. Gracias también a Justo y Jose, por todas las noches en vela que pasamos enfrente del ICP, al final mereció la pena.

Gracias también al profesor Antonio Segura por acogerme en su laboratorio de Granada, si bien los resultados no acompañaron, en esas 3 semanas me sentí realmente a gusto y aprendí con el genio de la electroforesis capilar, David.

Gracias a mi tutor de Tesis, Luis Eduardo, mi primer guía en esto de la ciencia, sin ti no habría llegado a donde he llegado.

Gracias a todo mi grupo de investigación en Aula Dei, con todos nuestros defectos y cosas por mejorar podemos sentirnos my orgullosos del trabajo que desarrollamos, a la vista están los resultados. Gracias a Monona por mantener la cordura y hacer que todo marche como deba y sin que se note. Gracias a Aurora, sabes que tengo un cariño especial, tu y tu prima Maribel sois dos personas muy adelantadas a vuestro tiempo, que un “guaje” como yo se sienta tan a gusto con vosotras así lo demuestra. Gracias a Ana Flor y Fermín, siempre habéis sido un ejemplo para mi, y ha sido un orgullo continuar de alguna manera el trabajo que empezasteis vosotros. Gracias también al resto de mis compañeros de laboratorio que me han acompañado durante todo este tiempo, Sofía, María, Irene, Iñaki, Piluca, Nacho, Hamdi, Jorge, Ruth, Victoria, Victor, Ade, Saúl y Giuseppe, la vida en el laboratorio salvo contadas excepciones ha sido muy fácil con vosotros. Sabéis que podéis contar conmigo para lo que queráis.

Gracias al resto de compañeros de Aula Dei, especialmente aquellos que se dedican a sumar e intentar que esta maquina funcione mejor, quiero reconocer especialmente el trabajo de personas como David Camón, Yolanda Pechero o Lola Márquez, que dan sentido a la palabra *servidor* público, ojala se extendiese el ejemplo.

Gracias también a todos los amigos que he hecho en todo este tiempo entre los ciudadanos de Aula Dei, especialmente a mis amigos Jorge, Nacho y Manu y el resto de la tropa de Peñaflo, Vicente, Alfonso, Ana y Raúl.

Gracias por ultimo a mis padres, que siempre han puesto los medios y me han dado la libertad para que llegue a ser todo lo que me proponga. Si alguien me ha enseñado en primer lugar el valor del trabajo bien hecho y el esfuerzo habéis sido vosotros, estoy seguro que mis hermanos piensan igual. Me siento orgulloso de vosotros y quizás debería demostrároslo más a menudo.

Gracias también a ti Erika, la historia de esta tesis es casi paralela a nuestra historia, hemos estado lejos ahora estamos cerca, hemos pasado por momentos tristes y por momentos muy felices y hemos construido algo hermoso entre los dos que lleva camino de convertirse en algo mucho bonito.

Gracias por hacerme feliz Erika.

A mis padres, hermanos y abuelos

A Erik@

Funding

This Thesis was supported by the Spanish MICINN (projects AGL2004- 00194 and AGL2007-61948, co-financed with FEDER), the European Commission (Thematic Priority 5- Food Quality and Safety, 6th Framework RTD Programme, Contract no. FP6- FOOD-CT-2006-016279) and the Aragón Government (group A03). Rubén Rellán Álvarez was supported by a FPI fellowship from the Spanish Ministry of Science and Innovation (MICINN).

Index

1. Summary/Resumen	1
2. Introduction: Long distance iron transport and metabolism changes in iron deficient plants. An integrated mass spectrometry approach.	9
3. Objectives/Objetivos	23
4. Formation of metal-nicotianamine complexes as affected by pH, ligand exchange with citrate and metal exchange. A study by electrospray ionization time-of-flight mass spectrometry	27
5. Identification of a tri-iron(III), tri-citrate complex in the xylem sap of iron-deficient tomato resupplied with iron: new insights into plant iron long-distance transport	45
6. Low molecular weight organic acid determination in plant tissue extracts by liquid chromatography – electrospray time of flight mass spectrometry	71
7. Changes in the proteomic and metabolic profiles of <i>Beta vulgaris</i> root tips in response to iron deficiency and resupply	85
8. Metabolite profile changes of xylem sap and leaves of Strategy I plants in response to iron deficiency and iron resupply	105
9. Conclusions/Conclusiones	127
10. Anex I (Other articles of the Master's Thesis)	131
11. Anex II (Other collaboration articles)	155
12. Anex III (<i>Curriculum vitae</i>)	161

SUMMARY/RESUMEN

Summary

Background

Iron is an essential element for plants, since it participates in important processes such as chlorophyll synthesis and photosynthetic electron transport. Iron deficiency is one of the major agriculture limiting factors, in spite of being the fourth most abundant element in terrestrial crust. Iron deficiency is induced by a low Fe soil bioavailability, especially in calcareous soils. Moreover, Fe deficiency can be also associated to metabolic and physiological processes that lead to low Fe availability inside the plant. On the other hand, Fe can be toxic, since it participates in the production of reactive species of oxygen. Thus, plants must carefully regulate Fe acquisition, transport and partitioning within different organ and cell compartments, in order to prevent excess accumulation while obtaining an adequate intake.

The elucidation of the molecular identity of metal complexes in plant compartments is still one of the biggest challenges in plant metal transport. In the case of xylem sap, Fe is assumed to be transported as complexed forms. Iron xylem loading, transport and unloading studies have mainly used indirect approaches: i) mutants that show an impaired synthesis of putative Fe ligands and transporter proteins of ligands or complexes, ii) *in silico* chemical speciation of Fe in plant fluids. These studies proposed different molecules as Fe carriers in the xylem: organic acids (*e.g.*, citric acid), a non-proteinogenic aminoacid like nicotianamine (NA) and phytosiderophores (*e.g.* mugineic acid). However, there was still no direct determination of Fe-complexes with these ligands in plant fluids. Such determinations require the use of analytical techniques that are: i) sensitive, since Fe concentrations in plant fluids are usually very low and ii) selective, since plant fluids are complex matrixes. Moreover, the analytical methodologies should maintain the original sample conditions (*e.g.*, pH), since the Fe speciation can be affected. The combined use of highly selective and sensitive molecular (*e.g.*, ESI-MS) and metal-specific (*e.g.*, ICP-MS) mass spectrometry techniques can be used for the determination of metal complexes, especially in plant fluids where direct analysis can be carried out.

The most characteristic Fe-deficiency symptom in plants is a decrease in chlorophyll levels in young leaves, associated to a reduction in photosynthetic CO₂ fixation. Iron-deficient plants develop different physiological and biochemical changes to maximize Fe mobilization and uptake from the soil. Iron deficiency also causes increases in the root activity of phosphoenolpyruvate carboxylase (PEPC) and several enzymes of the glycolytic pathway and the TCA cycle. This leads to an anaplerotic root fixation of C, which is then exported as organic acids *via* xylem to leaves. This may allow maintaining basic processes in Fe-deficient leaves, which have otherwise reduced photosynthetic rates. Most of the metabolic changes induced by Fe deficiency have been characterized using traditional physiological and biochemical studies, which cover a reduced group of metabolites and/or enzymes. The complete set of metabolites (*ca.* 250.000 in plants) is the end product of the gen-transcript-protein-metabolite chain, and is called “metabolome” by analogy with the terms genome and proteome. Metabolomics aims to analyze simultaneously and un-biasedly as much metabolites as possible, and together with genomics, transcriptomics and proteomics has broaden our knowledge of how plants acclimate to different environmental conditions, including abiotic stresses. Although the study of Fe deficiency in plants has been tackled by proteomics and genomics approaches, no metabolomics studies had been carried out so far.

Objectives

The general objectives of this Thesis are: i) to develop and apply new analytical methodologies for the determination of the Fe forms involved in long-distance Fe transport in plants, and ii) to study the metabolite profile of plants grown under Fe-deficiency conditions.

In order to achieve these general objectives the specific objectives are:

1. To study the formation of metal complexes with nicotianamine as affected by pH, ligand and metal exchange by means of electrospray time-of-flight mass spectrometry (ESI-TOFMS).
2. To develop a method for the determination of naturally occurring Fe complexes in xylem sap, using high performance liquid chromatography coupled to ESI-TOFMS and inductively coupled plasma mass spectrometry (HPLC-ESI-TOFMS and HPLC-ICP-MS, respectively).
3. To develop an HPLC-ESI-TOFMS method for the determination of organic acids in plant tissues.
4. To characterize the changes induced in the metabolite profile of plant roots in response to Fe deficiency and resupply, using gas chromatography coupled to mass spectrometry (GC-MS).
5. To characterize the changes induced in the metabolite profile of xylem sap and leaves of plants in response to Fe deficiency and resupply, using GC-MS.

Concluding remarks

Formation of metal-nicotianamine complexes as affected by pH, ligand exchange with citrate and metal exchange using ESI-TOFMS

We showed that Fe-NA complexes can be determined using ESI-TOFMS. We found that relatively small changes in pH and changes in the concentrations of citrate and metals could have significant effects in NA speciation in conditions similar to those present in plant fluids such as xylem and phloem sap. In the xylem sap, NA is not likely to complex Fe, due to exchange reactions with citrate and other metals, whereas it could chelate other metals such as Cu and Ni. In the phloem sap, NA could still be a good candidate to chelate Fe, specially in the Fe(II) form. Our work and other recent studies have shown the feasibility of using ESI-MS to study metal-complexes within plant fluids, but some drawbacks inherent to the technique need to be addressed, including: i) the need to maintain as much as possible the pH of the plant compartment under study through the whole extraction, separation and analysis process, ii) the possible changes in metal speciation due to the complex metal-ligand chemistry, iii) the difficulty to assess the true pH value in solutions which have a considerable amount of organic solvent, and iv) the possibility that metal redox reactions may occur in the ESI process. Our work also showed that *in silico* predictions may fail to accurately speciate NA in non-equilibrium solutions such as plant fluids.

Identification of a tri-iron, tri-citrate complex in tomato xylem sap using an integrated mass spectrometry approach

We reported the first direct and unequivocal identification of a natural Fe complex in plant xylem sap. A tri-Fe(III), tri-citrate complex (Fe_3Cit_3) was found in the xylem sap of Fe-deficient *Solanum lycopersicum* Mill. plants resupplied with Fe, by using an integrated mass spectrometry approach based on exact molecular mass, isotopic signature and Fe determination and chromatographic mobility. This complex was modeled as having an oxo-bridged tri-Fe core. A second complex, a di-Fe(III), di-citrate complex was also detected in Fe-citrate standards along with Fe_3Cit_3 , with the Fe-to-citrate ratio driving the balance between the two complexes. These results provide evidence for Fe-citrate complex xylem transport in plants. The consequences for the role of the Fe-to-citrate ratio in long-distance Fe xylem transport were also discussed.

Development of an HPLC-ESI-TOFMS method to determine organic acids in plant tissue extracts

Carboxylates are possible candidates for playing a role in Fe homeostasis in plants. An HPLC-ESI-TOFMS method was developed to determine organic acids (oxalic, cis-aconitic, 2-oxoglutaric, citric, malic, quinic, ascorbic, shikimic, succinic and fumaric acids) in different plant tissues (xylem sap, leaves and fruit juice) with high selectivity, sensitivity and reproducibility. Quantification was accomplished using ^{13}C isotope-labeled malic and succinic acids as internal standards. Limits of detection were between 0.13 and 255 pmol. The intraday repeatability values were approximately 0.1 and 1.6 % for retention time and peak area, respectively whereas the interday repeatability values were

about 0.1 and 4.4%, respectively for retention time and peak area. Good recoveries (90-110%) were obtained for most of the organic acids with the exception of oxalic, 2-oxoglutaric and ascorbic acids in some plant tissues. Due to the importance of carboxylates in cellular metabolism, oxidative stress response and possibly metal speciation, this method may permit to obtain useful information about the plant responses to specific environmental stresses such as Fe deficiency and others.

Changes in the metabolite and protein profiles of sugar beet root tips as affected by Fe deficiency and resupply using GC-MS

The protein and metabolite profiles of root tips from *Beta vulgaris* plants were found to be affected by Fe deficiency and resupply. Two novel and major findings were the increases in DMRL synthase protein concentration and gene expression, and some RFO sugars (*e.g.*, raffinose and galactinol). These findings give new perspectives to the knowledge of plant responses to Fe deficiency. Changes found in glycolysis and TCA cycle metabolites and proteins confirmed previous studies.

Changes in the metabolite profiles of xylem sap and leaves of different plant species in response to Fe deficiency and resupply using GC-MS

The main changes in the metabolite profile of xylem sap from *Solanum lycopersicum* and *Lupinus albus* in response to Fe deficiency were an increase in TCA cycle metabolites and a decrease in aminoacids and carbohydrates. The xylem sap metabolite profile of Fe-deficient *Solanum lycopersicum* plants becomes similar to that of Fe-sufficient controls one day after Fe resupply. In *Solanum lycopersicum* and *Beta vulgaris* Fe deficient leaves, the main changes in the metabolite profile were the increases in TCA cycle metabolites, aminoacids and carbohydrates. A high correlation between selected pairs of aminoacids and TCA cycle metabolites suggest that leaves of Fe-deficient *Beta vulgaris* plants use aminoacids as a anaplerotic C source.

Resumen

Antecedentes

El hierro es un elemento esencial para las plantas ya que participa en importantes procesos metabólicos como la síntesis de clorofila y el transporte electrónico en la fotosíntesis. La deficiencia de hierro es uno de los principales factores limitantes en la agricultura, a pesar de que este elemento es el cuarto más abundante en la corteza terrestre. La deficiencia de Fe es inducida por una baja biodisponibilidad del Fe en el suelo, especialmente en los suelos calizos. Además, la deficiencia de Fe también puede ser debida a procesos metabólicos y fisiológicos que conducen a una baja disponibilidad de este elemento dentro de la planta. El Fe también puede ser tóxico, ya que participa en la producción de especies reactivas de oxígeno. Por lo tanto, las plantas deben regular cuidadosamente la adquisición de Fe, el transporte y su distribución entre los diferentes órganos y compartimentos celulares con el fin de evitar un exceso de dicho elemento y conseguir absorber una cantidad suficiente.

La especiación química de los metales en los diferentes órganos y compartimentos celulares de la planta sigue siendo uno de los mayores retos en el transporte de metales en plantas. En el caso de la savia de xilema, se asume que el Fe es transportado en forma de complejo. Los estudios realizados sobre la carga, transporte y descarga de Fe en xilema han utilizado principalmente métodos indirectos como: i) el estudio de mutantes que muestran una alteración en la síntesis de posibles ligandos de Fe y/o de proteínas transportadoras de ligandos o complejos metálicos, ii) la especiación química *in silico* del Fe en fluidos vegetales. Estos estudios han propuestos diferentes moléculas como ligandos de Fe en fluidos vegetales: ácidos orgánicos (ej., citrato), el aminoácido no proteínogénico nicotianamina (NA) y fitosideróforos (ej., ácido mugineico). Sin embargo, aún no existe una determinación directa de complejos de estos compuestos con Fe en fluidos vegetales. Tales determinaciones requieren de técnicas analíticas que sean: i) sensibles, ya que las concentraciones de Fe en fluidos vegetales suelen ser bajas, ii) selectivas, puesto que los fluidos vegetales son matrices complejas. Además, las metodologías de análisis deben preservar las condiciones originales (por ejemplo, el pH) de la muestra ya que los complejos de Fe son muy sensibles a cambios de algunas de estas condiciones. La utilización combinada de técnicas de espectrometría de masas, altamente selectivas y sensibles con especificidad molecular (ej., ESI-MS) y atómica (por ejemplo, ICP-MS) podría resultar muy eficaz en la especiación de metales especialmente en la fluidos vegetales.

El síntoma más característico de la deficiencia Fe es la disminución de los niveles de clorofila en las hojas jóvenes que está asociada a una reducción en la fijación de CO₂ mediante la fotosíntesis. En las plantas deficientes en Fe, se producen diferentes cambios fisiológicos y bioquímicos con el fin de maximizar la movilización y absorción de Fe a nivel radicular y su transporte dentro de la planta. La deficiencia de Fe también provoca un aumento en la actividad de la fosfoenolpiruvato carboxilasa (PEPC) y en varias enzimas de la glicólisis y del ciclo de Krebs. Esto lleva a una fijación anaplerótica de C en raíz, que luego se exporta en forma de ácidos orgánicos a través del xilema a las hojas. Una vez en las hojas, esta fuente de C permitiría el mantenimiento de procesos metabólicos básicos en hojas deficientes que tienen bajas tasas fotosintéticas. La mayor parte de los cambios metabólicos inducidos por la deficiencia de Fe en plantas, se han caracterizado mediante estudios fisiológicos y bioquímicos que cubren un reducido grupo de metabolitos y/o enzimas. El conjunto completo de metabolitos (alrededor de 250.000 en plantas) es el producto final de la cadena gen-transcrito-proteína-metabolito y se denomina metaboloma por analogía con los términos genoma y proteoma. La metabolómica pretende analizar de forma no sesgada y simultáneamente tantos metabolitos como sea posible y, junto con la genómica, la transcriptómica y la proteómica, está ampliando nuestro conocimiento de cómo las plantas se aclimatan a diferentes condiciones ambientales, como los estreses abióticos. Aunque el estudio de la deficiencia de Fe en las plantas ha sido abordado desde el punto de vista de la proteómica y la genómica, todavía no se han llevado a cabo estudios metabolómicos.

Objetivos

Los objetivos generales de esta tesis doctoral son: a) desarrollar y aplicar nuevas metodologías analíticas que permitan la especiación química del Fe en los fluidos vegetales involucrados en el transporte a larga distancia de este elemento en plantas y b) estudiar el perfil de metabolitos de plantas cultivadas en condiciones de deficiencia de Fe.

Para alcanzar estos objetivos generales se plantean los siguientes objetivos específicos:

1. Estudiar el efecto del pH y las reacciones de intercambio del metal o el ligando sobre la formación de complejos metálicos con nicotianamina mediante espectrometría de masas (MS) con analizador de tiempo de vuelo (TOF) y fuente de electrospray (ESI).
2. Desarrollar un método que permita la determinación de complejos naturales de Fe en plantas involucrados en el transporte de este elemento *vía* xilema mediante cromatografía líquida de alta resolución (HPLC) acoplada a ESI-TOFMS y espectrometría de masas con fuente de plasma de acoplamiento inductivo (ICP-MS).
3. Desarrollar un método que permita la determinación de ácidos orgánicos en tejidos vegetales mediante HPLC-ES-TOFMS.
4. Caracterizar los cambios en el perfil de metabolitos que se producen en condiciones de deficiencia y reaporte de Fe en las raíces de las plantas mediante cromatografía de gases acoplada a espectrometría de masas (GC-MS).
5. Caracterizar los cambios en el perfil de metabolitos que se producen en condiciones de deficiencia y reaporte de Fe en la savia de xilema y las hojas de las plantas mediante GC-MS.

Principales resultados y discusión

Formación de complejos metálicos con nicotianamina y efecto sobre los mismos del pH, y de las reacciones de intercambio del metal o el ligando mediante ESI-TOFMS.

Se ha conseguido determinar los complejos de Fe-NA mediante ESI-TOFMS. Cambios relativamente pequeños en el pH y en las concentraciones de citrato y metales podrían tener efectos significativos en la especiación de NA en fluidos vegetales como la savia de xilema y floema. En la savia de xilema, la NA no es probable que forme complejos con Fe debido a reacciones de intercambio con citrato y con metales, mientras que si podría quelar otros metales como el Cu y Ni. Sin embargo, en la savia de floema, la NA, es un buen candidato para quelar Fe, especialmente Fe(II). Este estudio así como el de otros investigadores ha demostrado la viabilidad de la técnica de ESI-MS para el estudio de complejos metálicos en fluidos vegetales, pero es necesario considerar algunos de los inconvenientes inherentes a la técnica, en concreto: i) la necesidad de mantener, en la medida de lo posible, el pH del fluido vegetal en estudio durante todo el proceso de extracción, separación, y análisis, ii) los posibles cambios en la especiación de los complejos metálicos en estudio, iii) la dificultad para evaluar el verdadero valor de pH en soluciones con una considerable cantidad de disolvente orgánico, y iv) la posibilidad de que ocurran reacciones redox en el proceso de ionización. Además, las predicciones *in silico* pueden ser inexactas para especiar la NA en soluciones que no están en equilibrio, como los fluidos vegetales.

Identificación de un complejo formado por tres moléculas de citrato y tres átomos de Fe en xilema de tomate utilizando espectrometría de masas elemental y molecular

Se ha logrado por primera vez la identificación directa e inequívoca de un complejo natural de Fe en savia de xilema. El complejo formado por tres moléculas de citrato y tres átomos de Fe (Fe_3Cit_3) se encontró en la savia del xilema de plantas de *Solanum lycopersicum* deficientes en Fe después de haber realizado un reaporte de Fe, utilizando un enfoque integrado de espectrometría de masas basado en la determinación de la masa molecular exacta, la firma isotópica y el Fe junto con la movilidad cromatográfica. Cálculos *in silico* predicen que el complejo tiene un núcleo formado por tres átomos de Fe unidos por un O. Un segundo complejo, formado por dos átomos de Fe y dos moléculas de citrato (Fe_2Cit_2) también se detectó en soluciones estándar junto con con el Fe_3Cit_3 . La formación de

uno u otro compuesto dependió de la relación Fe:citrato. Estos resultados evidencian el papel del citrato en el transporte xilemático de Fe. La importancia de la relación Fe:citrato en el transporte de Fe a larga distancia es discutida.

Desarrollo de un método de HPLC-ESI-TOFMS para determinar ácidos orgánicos en extractos vegetales

Los carboxilatos son moléculas que pueden tener un papel importantes en la homeostasis de Fe en las plantas. Un método de HPLC-ESI-TOFMS con alta selectividad, sensibilidad y reproducibilidad fue desarrollado para determinar ácidos orgánicos (oxálico, cis-aconítico, 2-oxoglutárico, cítrico, málico, ácido quínico, ascórbico, shikímico, succínico y fumárico) en diferentes tejidos vegetales (savia de xilema, hojas y jugo de frutas). La cuantificación se realiza mediante la utilización como patrones internos de ácidos málico y succínico marcados isotópicamente con ^{13}C . Los límites de detección fueron entre 0.13 y 255 pmol. Los valores de repetibilidad fueron aproximadamente 0.1 y 1.6% para el tiempo de retención y área del pico, respectivamente, mientras que los valores de reproducibilidad estuvieron entre 0.1 y 4.4%, respectivamente, para el tiempo de retención y el área del pico. Los porcentajes de recuperación fueron aceptables (90-110%) para la mayoría de los ácidos orgánicos, con la excepción del ácido oxálico, 2-oxoglutárico y ascórbico en alguno de los tejidos. Debido a la importancia de los ácidos orgánicos en el metabolismo celular y en la respuesta al estrés oxidativo y posiblemente en la especiación de metales este método puede ser aplicado para obtener información sobre la respuesta de la planta a estreses ambientales específicos como la deficiencia de Fe entre otros.

*Estudio de los cambios en los perfiles de metabolitos y proteínas de raíz *Beta vulgaris* afectadas por deficiencia y reaporte de Fe.*

Los perfiles de proteínas y metabolitos de puntas de raíz de plantas de *Beta vulgaris* fueron afectados por la deficiencia y reaporte de Fe. Los cambios más relevantes fueron el incremento de i) la DMRL sintetasa tanto a nivel de proteínas como de expresión génica y ii) algunos azúcares de la familia de la rafinosa (ej., rafinosa y galactinol). Estos hallazgo no habían sido descrito hasta ahora en plantas deficientes en Fe y por consiguiente abren nuevas vías de estudio de este desorden nutricional. Cambios en la glucólisis y el ciclo de Krebs fueron también encontrados confirmando estudios previos.

Estudio de los cambios en los perfiles de metabolitos de la savia de xilema y de las hojas de diferentes especies de plantas en respuesta a la deficiencia y reaporte de Fe.

Los principales cambios en los perfiles de metabolitos de la savia del xilema de *Solanum lycopersicum* y *Lupinus albus* en respuesta a la deficiencia de Fe fueron un aumento en los metabolitos del ciclo de Krebs y una disminución general de aminoácidos y carbohidratos. El perfil de los metabolitos de la savia de xilema de las plantas de *Solanum lycopersicum* con deficiencia de Fe se acerca al de las plantas control en tan solo 24h después de un reaporte de Fe. En hojas deficiente en Fe de *Solanum lycopersicum* y *Beta vulgaris* los principales cambios en el perfil metabólico fueron los aumentos en los metabolitos del ciclo de Krebs, aminoácidos y carbohidratos. Correlaciones elevadas entre aminoácidos y ácidos orgánicos del ciclo de Krebs sugieren que en las hojas de plantas de *Beta vulgaris* deficientes en Fe se producen reacciones anapleróticas que utilizan aminoácidos como fuente de C.

INTRODUCTION

Long Distance Iron Transport and Metabolism Changes in Iron Deficient Plants.

An Integrated Mass Spectrometry Approach.

Long Distance Iron Transport and Metabolism Changes in Iron Deficient Plants. An Integrated Mass Spectrometry Approach.

Plant iron deficiency

Iron is an essential micronutrient for plants because it is a component of different proteins involved in processes such as chlorophyll synthesis and the maintenance of chloroplast structure (Terry and Abadía, 1986), respiration, nitrogen fixation (Clárk, 1983) and in DNA and hormone syntheses (Briat and Lobreaux, 1997). In plants, 80% of Fe is located in the chloroplasts and approximately 63% of Fe in leaves is associated with proteins that can be classified in: proteins with a hemo group, proteins with Fe-S clusters and phytoferritin.

Iron is the fourth most abundant element on earth crust. However, in calcareous and alkaline soils Fe is mainly found as oxides and hydroxides with a very low solubility. In this kind of soils bioavailable Fe concentration is around 0.1 nM, while the necessary levels for plants, are much higher (0.1 μ M, Marschner, 1995). Once inside the plants, Fe can reach sufficient concentrations for normal plant development and, however, some plants still can show Fe deficiency symptoms because Fe is in inactive forms not easily assimilated. This phenomenon is known as Fe chlorosis paradox (Morales et al., 1998). Different factors such as high phosphate concentrations and high apoplastic pH could cause Fe precipitation in the form of phosphates or ferric hydroxides (Mengel et al., 1994) making it not readily bio-available.

Iron deficient plants show different symptoms; among them the most common is the yellowing of the younger leaves, known as Fe chlorosis, due to a defective production of chlorophyll and a general malfunctioning of the different photosynthetic components (Abadía, 1992). If chlorosis is severe it can lead to leaf necrosis. Iron deficiency has been described in a great number of plant species with agronomical interest such as fruit trees and, if not treated properly, Fe deficiency can lead to reduced number and size in fruits with the consequent economical loss (Álvarez-Fernández et al., 2003).

Almost 30% of cultivated plants are grown in calcareous soils (Rombolà and Tagliavini, 2006) where Fe deficiency can represent a major problem for plant productivity. In this type of soils, one of the major costs for farmers is the use of Fe fertilizers to alleviate low Fe soil

availability. Fe fertilizers cost is around 200-400 € ha⁻¹ and year in fruit trees (Rombolà and Tagliavini, 2006).

Plants with Fe deficiency also pose a problem in the countries where human nutrition is mainly based on plants that do not have enough Fe concentration to fulfil Fe human requirements. In fact almost one third of human population is Fe deficient (www.harvestplus.org/content/iron).

Plant iron uptake strategies

Two different strategies of Fe uptake have been described in plants (see root part of Fig. 1). The so-called reduction strategy (or Strategy I), mainly used by non graminaceous plants, relies on the coordinated action of a membrane bound Fe reductase (FRO2), that reduces Fe(III) to Fe(II) (Robinson et al., 1999), an Fe(II) uptake transporter (IRT, Eide et al., 1996) and an H⁺-ATPase that lowers the pH of the rhizosphere (Santi and Schmidt, 2009). The expression of these genes is regulated by bHLH type proteins (Yuan et al., 2005; Bauer et al., 2007). Other possible components of this strategy have been suggested recently. This is the case of PDR9, an ABC type transporter that may efflux to the rhizosphere phenols, organic acids or flavins (Yang et al., 2010). The reduction strategy also includes root morphological changes such as root tip swelling, development of transfer cells and a higher number of lateral roots, all of them leading to an increase in the root surface in contact with the medium (Landsberg, 1982, 1986). The so-called chelation strategy (or Strategy II), which is mainly found in graminaceous plants, is based on the excretion of phytosiderophores (PS; low molecular weight compounds with a high affinity for Fe and other metals) to the rhizosphere. Phytosiderophores are synthesized from methionine and the components of this biosynthetic pathway are strongly upregulated under Fe deficiency, resulting in an increased PS release (Kobayashi et al., 2006). The first putative PS root plasma membrane transporter, TOM1 (Transporter Of MA), has just been recently described in rice (TOM1) and barley (HvTOM1); *TOM1* is up-regulated by Fe deficiency and plants over-expressing TOM1 excrete more PSs without increasing the rate of

synthesis (Nozoye et al., *In press*). Phytosideropores chelate Fe(III) and the Fe(III)-PS chelates are then subsequently transported into the root cells through specific transporters of the YSL family such as ZmYS1 or HVYS1 (Curie et al., 2001; Murata et al., 2006). The expression of these genes is regulated by a bHLH protein (Ogo et al., 2007) also under the control of another transcription factor (IDEF1) (Kobayashi et al., 2007). Even though plants have been traditionally divided in Strategy I or Strategy II plants, recent research points to the use of typical mechanisms of Strategy I plants by graminaceous plants and vice versa. For example, YSL transporters have been described to be up regulated in *Arabidopsis* Fe-deficient roots (Dinneny et al., 2008) and Fe(II) transporters (IRT) homologs have also been found in typical Strategy II plants such as rice (Ishimaru et al., 2006) and barley (Pedas et al., 2008). See the root part of Fig. 1 for a representation of all the transporters described here.

Long distance iron transport

Xylem loading

Iron xylem loading is still not very well characterized and a lot of questions remain unanswered, the major one being the chemical form(s) and mechanism(s) in which Fe is loaded. As it is commonly accepted, Fe in the cytosol is chelated with the non-proteinogenic aminoacid nicotianamine (NA) (von Wirén et al., 1999). Iron-NA complexes could be loaded into the xylem by an Fe-PS transporter from the YSL family. AtYSL2, which is expressed in the lateral membranes of xylem parenchyma cells, suggests a role in lateral movement within the veins; however there are contradictory results about its ability to transport Fe-NA (DiDonato et al., 2004; Schaaf et al., 2004). The rice ortholog, OsYSL2 also localizes to the lateral plasma membrane and transports Fe-NA (Koike et al., 2004). Other Fe transporter, IREG1 / FPN1 (Iron Regulated1 / Ferroportin1), has also been proposed to play a role in Fe xylem loading (Morrissey et al., 2009). The loss of FPN1 results in chlorosis and FPN1-GUS plants show staining in the plasma membrane in the vasculature of the root suggesting that FPN1 loads Fe into the vasculature; however, yeast complementation studies failed and no information on the Fe chemical form transported, and most precisely if Fe is transported as a complex or un-complexed,

is available (Morrissey et al., 2009). There are other components that may have a role in xylem Fe loading. FRD3, a transporter from the multidrug and toxin efflux family (MATE), localizes to the plasma membrane of the pericycle and the vascular cylinder. FRD3 mediates citrate efflux into the root vasculature and has been described in *Arabidopsis* (Durrett et al., 2007) and rice (Yokosho et al., 2009). *Frd3* plants show reduced citrate levels in the xylem and shoot, accumulate Fe in the root, are chlorotic, and exhibit constitutive expression of the Fe uptake components; therefore suggesting that FRD3 is necessary for efficient Fe translocation to the shoot, likely, as an Fe citrate complex (Yi and Guerinot, 1996; Rogers and Guerinot, 2002; Durrett et al., 2007; Yokosho et al., 2009). However, the exact role of this citrate transporters in Fe deficiency is not yet clear, since the chlorosis showed by these mutants might be explained by a pleiotropic effect due to an impaired C (citrate and probably other organic acids) transport to leaves (See the 'Metabolism changes induced by Fe deficiency' section for a more detailed description of this effect). The NA synthase NAS4 gene is induced in the *Arabidopsis frd3* mutant and the double mutant *nas4x-2/frd3* showed impaired growth and no Fe was measured in shoots (Schuler et al., 2010) suggesting that increased NA-Fe may alleviate the reduced citrate concentration in *FRD3* mutants. Unfortunately, the form in which Fe is loaded into the xylem sap as well as the exact role that FRD3 plays in the process are still big open questions. Whatever the transport system might be, it seems clear that the Fe complex originally present in the root cells is different of the one found in the xylem sap. It is also important to note that xylem pH is around 5.5 while the pH of root cells cytosol is around 7.2; since the formation of Fe-NA complexes is highly dependent on pH (von Wirén et al., 1999), specially at this critic pH range, ligand exchange reactions are expected to occur after Fe loading into the xylem sap.

Xylem transport

Once Fe is loaded into the xylem stream it is transported as a complex form, because free ionic forms can be toxic and are also prone to undergo precipitation at the neutral or slightly acidic pH values typical of xylem sap. Nicotianamine has been proposed to play a major role in symplastic and phloem Fe chelation while the possible

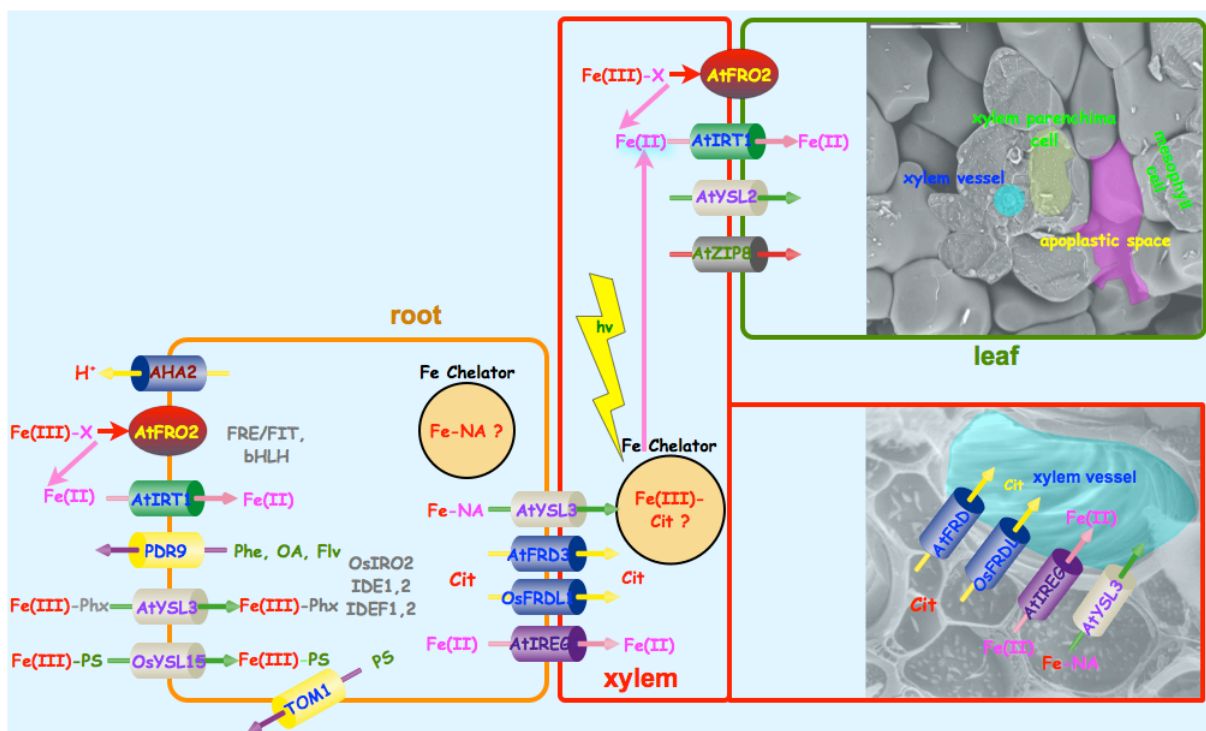


Figure 1. Acquisition and long distance Fe transport in plants. Represented are the main Fe uptake strategies in roots, Fe loading and unloading mechanism and the expected Fe complexes in the different plant compartments (*Pictures taken by Saül Vazquez*).

involvement of NA in long-distance metal transport in the xylem is still being explored (Klatte et al., 2009), see (Curie et al., 2009) for a review. Nicotianamine has been observed in the xylem at μM concentrations (Takahashi et al., 2003) however, it does not seem to be essential for Fe xylem transport since the NA-deficient tomato mutant chloronerva, can accumulate Fe in old leaves (Pich et al., 1994). Citrate has been considered the most likely candidate for Fe xylem transport since the early works of Tiffin and Brown (Tiffin and Brown, 1962; Tiffin, 1966, 1966). The identity and occurrence of Fe-Cit complexes in the xylem sap had only been hypothesized by means of *in silico* calculations using total concentrations of possible Fe complexing agents (including carboxylates) and Fe, and the known stability and protonation constants of Fe-containing complexes, always assuming that chemical equilibrium was achieved. For example, $[\text{FeCitOH}]^{-1}$ was proposed to be the most abundant Fe complex in the apoplast and xylem sap of control sugar beet plants while in chlorotic samples the main Fe species was $[\text{FeCit}_2]^{-3}$ in both plant fluids (López-Millán et al., 2000). However, when using apoplast samples of Fe sufficient and Fe deficient field cultivated pear trees the most abundant Fe

species found in both +Fe and -Fe samples was $[\text{FeCitOH}]^{-1}$. Using this approach, several Fe-Cit species were predicted to be the most abundant Fe complexes in the xylem sap whereas other potential plant metal chelators such as NA were ruled out as possible xylem Fe carriers (von Wirén et al., 1999).

The elucidation of the molecular identity of metal complexes in plant compartments is still considered one of the biggest challenges in plant biology and further investigation is needed to speciate Fe (and other metals) in plant fluids such as xylem sap (Hider et al., 2004). The recent development of methodologies based on integrated mass spectrometry techniques can help to solve this problem (Meija et al., 2006). Metal complex characterization by integrated mass spectrometry is based in the coupling of different separation techniques such as high performance liquid chromatography (HPLC) to complementary atomic (such as ICP-MS) and molecular detection (such as ESI-MS) techniques. Multi-element specificity and accurate quantification are the key features of ICP-MS, whereas molecular weight determination and structural information are those contributed by ESI-MS(-MS). After the metal-complex species have been detected and

identified using chromatography and MS techniques, it is common practice to simulate the chelation conditions using metal-ligand standard solutions. This approach allows careful exploration and characterization of the complexation phenomena by controlling different factors such as pH and also for signal optimization of detection systems. One of the main problems of this kind of approach is that samples need to be extracted before separation and analysis. This usually implies the combination of the different cell compartments into one single solution and since metal complex formation is pH dependent, artefacts can occur during the extraction process. Plant fluids such as xylem sap do not have this problem, since no tissue extraction is needed and in fact, a great part of the metal complex identifications studies are done with plant fluids such as xylem or phloem. Other non destructive techniques based on X-ray spectroscopy such as extended X-ray absorption fine structure (EXAFS) and X-ray absorption near edge structure (XANES) (Sarret et al., 2002; Küpper et al., 2004), and synchrotron X-ray fluorescence (SXRF) (Punshon et al., 2009) have also been used for metal complex speciation. However, X-ray techniques suffer from limited sensitivity (usually in the ppm range) and metal complex identification relies on comparison with metal-complex standards. The sensitivity limitations of X-TXRF have been recently improved by means of multilayer monochromators and bending magnet beamlines offering detection limits in the femtogram range for transition metals (Szoboszlai et al., 2009). See in the same publication a review of the application of this technique in different plant extracts and exudates.

Xylem unloading

Iron is unloaded from the vasculature into developed tissues through yet unknown mechanisms. These processes could take place via parenchyma cells and/or by passive diffusion to the apoplastic space driven by transpiration. The symplastic path could imply the participation of YSL transporters for Fe-NA or a reduction based mechanism for Fe-Cit complexes. Several YSL, FROs and ZIP proteins have been localized in the vascular cylinder and might play a role in Fe unloading (Guerinot, 2000; Mukherjee et al., 2006; Dinneny et al., 2008; Curie et al., 2009). Iron deficiency is also associated with lower leaf Fe reductase activities (Gonzalez-Vallejo et al.,

1998). Recent studies also show that the whole xylem system is not fully developed in chlorotic leaves and is clearly different from that of the Fe sufficient plants (Fernández et al., 2008; Eichert et al., 2010). These morphological differences between Fe sufficient and Fe deficient plants may imply different unloading rates or mechanisms of Fe unloading that could explain Fe immobilization in leaves of plants affected by Fe deficiency.

Phloem transport

Iron phloem transport is supposed to occur at least through two main mechanisms. The first one would be as a complex with NA. The neutral to basic pH values of the phloem sap are suitable to Fe-NA formation (von Wirén et al., 1999). Also YSL transporters, that are able to transport Fe-NA complexes have been described in *Arabidopsis* and rice phloem vascular tissues, see (Curie et al., 2009) for a review. In fact, some of these transporters could be facilitating xylem-phloem Fe exchange. The second mechanism would involve an Fe transporting protein (ITP) that has been described in the phloem sap of *Ricinus communis* (Krüger et al., 2002).

Metabolism changes induced by Fe deficiency

Any change in growth conditions (including Fe deficiency) requires an adjustment of metabolic pathways, aimed at achieving a new state of homeostasis in a process that is usually referred as acclimation. From the standpoint of metabolites this implies at least four different types of compounds: i) compounds involved in the acclimation process such as antioxidants, ii) by-products of stress that appear in cells because of the disruption of normal homeostasis, iii) signal transduction molecules involved in mediating the acclimation response and iv) molecules that enhance the acquisition and transport processes such as flavonoids. Under Fe deficiency, different reducing and chelating compounds (such as phenolics and flavins *e.g.*, riboflavin; Rbfl) can be accumulated in the root and/or released to the rhizosphere and may have a role in Fe acquisition (Susín et al., 1993; Jin et al., 2007; Cesco et al., 2010). For instance, Rbfl and derivatives could act as a redox bridge for electron transport to ferric reductases (López-Millán et al., 2000; Marsili et al., 2008). This is supported by the fact that root ferric chelate reductase (FRO2) belongs to a superfamily of flavocytochrome oxidoreductases (Robinson et

al., 1999) and by a recent study confirming that the FRO2 protein contains FAD sequence motifs on the inside of the membrane (Schagerl \ddot{o} f et al., 2006). Moreover, Fe deficiency perception and Rbfl excretion has been described to occur through basic helix-loop-helix (bHLH) transcription factors in *Arabidopsis thaliana* (Vorwieger et al., 2007) and Rbfl synthesis was also found to be down regulated by Fe in flavinogenic yeast strains and some bacteria (Worst et al., 1998; Stenchuk et al., 2001). Other Fe-deficiency mediated metabolic changes occurring at the root level include an increase in the activity of phosphoenolpyruvate carboxylase (PEPC) and several enzymes of the glycolytic pathway and the tricarboxylic acid (TCA) cycle (Abadía et al., 2002; López-Millán et al., 2009). Phosphoenolpyruvate carboxylase increases the rate of glycolysis by consuming phosphoenolpyruvate, which has a negative allosteric control on phosphofructokinase-1 and aldolase (Plaxton and Podesta, 2006). The increase in PEPC activity also induces an anaplerotic production of TCA carboxylates, mainly malate and citrate, in roots (Abadía et al., 2002). These carboxylates could then be exported to the xylem and might play an important role in the transport of Fe and C (López-Millán et al., 2000) to the shoots. In fact, increases of organic acids have been found in xylem sap, leaves, fruits, etc. of Fe-deficient strategy I plants (Abadía et al., 2002). The increase of organic acids would also help to increase the biosynthetic pathways (in particular the synthesis of amino acids) and along with the accumulation of dicarboxylic acid carrier (DTC) would increase the communication between the cytosolic and the mitochondrial pool of organic acids that maintain a high turnover of reducing equivalents (Vigani and Zocchi, 2009). The induction of C metabolism in roots of Fe-deficient plants would provide a source of reducing power, protons and ATP for the Fe(III) reductase and H⁺-ATPase enzymes (López-Millán et al., 2000). The higher energy requirements in Fe deficient root cells are tackled by increasing mitochondrial oxidative processes. For instance, roots from Fe-deficient plants showed enhanced respiratory activities and higher O₂ consumption rates (López-Millán et al., 2000; Vigani et al., 2009). However, the root mitochondrial respiratory chain is strongly affected under Fe-deficient conditions (Vigani et al., 2009; Vigani and Zocchi, 2009), since some

of its components are Fe-containing enzymes. All these processes can lead to an increase in reactive oxygen species (ROS), and in fact ROS detoxification strategies were enhanced in Fe-deficient sugar beet roots (Zaharieva et al., 2004). Furthermore, an increase in anaerobic metabolism has also been described in Fe-deficient roots (López-Millán et al., 2000), probably as a strategy to oxidize all the reducing power generated by glycolysis and TCA cycle that can not be easily oxidized in the respiratory chain.

In leaves, the most characteristic Fe-deficiency symptom is the greenish-yellow colour that is due to the fact that Fe deficiency decreases the amount of light-harvesting pigments, chlorophylls and carotenoids to different extents, causing a relative enrichment in carotenoids and also changes in the violaxanthin cycle (Larbi et al., 2004; Timperio et al., 2007). Leaves of Fe-deficient plants show a marked decrease in photosynthetic rates and in photosynthetic efficiency and electron transport rates (Terry, 1980). Iron deficiency is known to cause a reduction in the number of granal and stromal lamellae per chloroplast, and in the amounts of many thylakoid membrane components, including proteins, electron carriers and lipids (Abadía, 1992). The biochemical processes taking place in leaves under Fe deficiency is still not well study and the -omic studies more abundant in the roots are still scarce in leaves; most of them are proteomic studies and focused on specific leaf compartments such as thylakoids (Andaluz et al., 2006; Timperio et al., 2007; Laganowsky et al., 2009). Thylakoid proteomic changes of sugar beet and spinach Fe-deficient plants showed a decrease in the proteins involved in electron transfer, a reduction of large complexes and supercomplexes, and aggregation of proteins in small complexes (Andaluz et al., 2006; Timperio et al., 2007). Iron deficiency also lead to an increase in proteins participating in leaf C fixation-linked reactions (Andaluz et al., 2006) and in different antioxidant enzymes. At the metabolite level, most of the works done so far has been related with changes in leaf pigments, see above, or with organic acids (López-Millán et al., 2001; López-Millán et al., 2009). However, no metabolomics studies in Fe-deficient plant leaves have been done so far, even though is clear that Fe-deficiency changes the C

metabolism and a lot of compounds are expected to be altered in these conditions.

Iron resupply to Fe deficient plants, leads to increases in chlorophyll concentrations and photosynthetic rates within few days or weeks depending on the plant species (Larbi et al., 2003; Larbi et al., 2004; Timperio et al., 2007) and decreases the concentration of organic acids in the whole plant (López-Millán et al., 2001; López-Millán et al., 2001). Iron resupply short-term effects (1-2 days) have been less studied but there seems to be a lag phase between an increase in Fe concentration (López-Millán et al., 2001) and Chl synthesis, although other leaf pigments change more rapidly (Larbi et al., 2004). Therefore, it is interesting to study in more detail the metabolism changes that may occur after Fe-resupply at very short times (hours to 1-3 days) specially in the tissues that may respond more quickly to Fe-resupply such as root tips and xylem sap. In the case of xylem sap the lack of information is even more accentuated since the information available is limited to organic acid changes (see Abadía et al. (2002) for a review) and recent small RNAs studies about long distance nutrient regulating signals (Buhtz et al., 2010).

The most common approach used to study Fe deficiency effects on the metabolism is to analyze only a small number of genes, proteins and/or metabolites. A more comprehensive knowledge of the processes taking place in Fe-deficient roots has been recently provided by the application of modern techniques allowing for the simultaneous and un-targeted analysis of multiple genes (Thimm et al., 2001; Buhtz et al., 2010; Yang et al., 2010), or proteins (Herbik et al., 1996; Andaluz et al., 2006; Timperio et al., 2007; Brumbarova et al., 2008; Li et al., 2008; Laganowsky et al., 2009; Donnini et al., 2010; Lan et al., 2010; Li and Schmidt, 2010; Rodríguez-Celma et al., 2011, *Submitted*). However, the changes in the metabolic profile induced by Fe deficiency have not been studied so far from a metabolomics approach.

Metabolites are the end products of cellular regulatory processes, and their levels can be regarded as the ultimate response of biological systems to genetic or environmental changes. In parallel to the terms 'transcriptome' and 'proteome', the set of metabolites synthesized by a biological system constitute its 'metabolome' (Fiehn, 2002). Metabolomics aims at the

comprehensive and quantitative analysis of wide arrays of metabolites in biological samples. These wide array of metabolites have very diverse physico-chemical properties and occur at different abundance levels. Consequently, comprehensive metabolomics investigations are primarily a challenge for analytical chemistry and specifically MS has been widely used in this field (Dettmer et al., 2007; Scalbert et al., 2009). The most common approaches used in plant metabolomics research include metabolic fingerprinting, metabolite profiling and targeted analysis. Metabolic fingerprinting is used to identify metabolic signatures or patterns associated with a particular stress response without identification or precise quantification of all the different metabolites in the sample. Pattern recognition analysis is then performed on the data to identify features specific to a fingerprint. Fingerprinting can be performed with a variety of analytical techniques, including nuclear magnetic resonance NMR (Krishnan et al., 2005), MS (Goodacre et al., 2003), Fourier transform ion cyclotron resonance (FT-ICR) MS or Fourier transform infrared (FT-IR) spectroscopy (Johnson et al., 2003). Metabolite profiling pursues a simultaneous measurement of all (as much as possible) or a set of metabolites in a sample. Multiple analytical techniques can be used for metabolite profiling (Sumner et al., 2003). These techniques include NMR, GC-MS HPLC-MS, capillary electrophoresis-mass spectrometry (CE-MS) and FT-IR (Allwood and Goodacre, 2010). Metabolite untargeted profiling is particularly useful to obtain a global view of the metabolism of cells or identify new metabolites/pathways. However untargeted profiling is semiquantitative, i.e. it provides relative concentration data based on the use of internal standards or just simple response ratios based on the comparison of a given treatment metabolite signal with the corresponding value in the controls. These data have to be further validated using targeted quantitative assays. Targeted profiling is used when it is necessary to determine the precise concentration of a limited number of known metabolites and provides a very low limit of detection. Targeted analysis has been widely used to follow the dynamics of a limited number of metabolites (organic acids, aminoacids, hormones etc.) known to be involved in a particular plant stress such as plant Fe deficiency.

References

- Abadía J** (1992) Leaf responses to iron nutrition - A review. *J. Plant Nutr.* **15**: 1699-1713
- Abadía J, López-Millán AF, Rombolà AD, Abadía A** (2002) Organic acids and Fe deficiency: a review. *Plant Soil* **241**: 75-86
- Allwood JW, Goodacre R** (2010) An introduction to liquid chromatography-mass spectrometry instrumentation applied in plant metabolomic analyses. *Phytochem. Anal.* **21**: 33-47
- Álvarez-Fernández A, Paniagua P, Abadía J, Abadía A** (2003) Effects of Fe deficiency chlorosis on yield and fruit quality in peach (*Prunus persica* L. Batsch). *J. Agr. Food Chem.* **51**: 5738-5744
- Andaluz S, López-Millán A, Rivas J, Aro E, Abadía J, Abadía A** (2006) Proteomic profiles of thylakoid membranes and changes in response to iron deficiency. *Photosynth. Res.* **89**: 141-155
- Bauer P, Ling H-Q, Guerinot ML** (2007) FIT, the FER-like iron deficiency induced transcription factor in *Arabidopsis*. *Plant Physiol. Biochem.* **45**: 260-261
- Briat J, Lobreaux S** (1997) Iron transport and storage in plants. *Trends Plant Sci.* **2**: 187-193
- Brumbarova T, Matros A, Mock HP, Bauer P** (2008) A proteomic study showing differential regulation of stress, redox regulation and peroxidase proteins by iron supply and the transcription factor FER. *Plant J.* **54**: 321-334
- Buhtz A, Pieritz J, Springer F, Kehr J** (2010) Phloem small RNAs, nutrient stress responses, and systemic mobility. *BMC Plant Biol.* **10**: 64
- Cesco S, Neumann G, Tomasi N, Pinton R, Weisskopf L** (2010) Release of plant-borne flavonoids into the rhizosphere and their role in plant nutrition. *Plant Soil* **329**: 1-25
- Clárk R** (1983) Plant genotype differences in the uptake, translocation, accumulation, and use of mineral elements required for plant growth. *Plant Soil* **72**: 175-196
- Curie C, Cassin G, Couch D, Divol F, Higuchi K, Le Jean M, Misson J, Schikora A, Czernic P, Mari S** (2009) Metal movement within the plant: contribution of nicotianamine and yellow stripe 1-like transporters. *Ann. Bot.* **103**: 1-11
- Curie C, Panaviene Z, Loulergue C, Dellaporta S, Briat J, Walker E** (2001) Maize yellow stripe1 encodes a membrane protein directly involved in Fe(III) uptake. *Nature* **409**: 346-349
- Dettmer K, Aronov PA, Hammock BD** (2007) Mass spectrometry-based metabolomics. *Mass Spectrom. Rev.* **26**: 51-78
- DiDonato R, Roberts L, Sanderson T, Easley R, Walker E** (2004) *Arabidopsis* Yellow Stripe-Like2 (YSL2): a metal-regulated gene encoding a plasma membrane transporter of nicotianamine-metal complexes. *Plant J.* **39**: 403-414
- Dinneny JR, Long TA, Wang JY, Jung JW, Mace D, Pointer S, Barron C, Brady SM, Schiefelbein J, Benfey PN** (2008) Cell identity mediates the response of *Arabidopsis* roots to abiotic stress. *Science* **320**: 942-945
- Donnini S, Bhakti P, Negri AS, Vigani G, Espen L, Zocchi G** (2010) Proteomic characterization of iron deficiency response in *Cucumis sativus* L. roots. *BMC Plant Biol.* **10**: 268
- Durrett TP, Gassmann W, Rogers EE** (2007) The FRD3-Mediated efflux of citrate into the root vasculature is necessary for efficient iron translocation. *Plant Physiol.* **144**: 197-205
- Eichert T, Peguero-Piña JJ, Gil-Pelegrín E, Heredia A, Fernández V** (2010) Effects of iron chlorosis and iron resupply on leaf xylem architecture, water relations, gas exchange and stomatal performance of field-grown peach (*Prunus persica*). *Physiol. Plant.* **138**: 48-59
- Eide D, Brodenius M, Fett J, Guerinot M** (1996) A novel iron-regulated metal transporter from plants identified by functional expression in yeast. *Proc. Natl. Acad. Sci. USA* **93**: 5624-5628
- Fernández V, Del Río V, Pumariño L, Igartua E, Abadía J, Abadía A** (2008) Foliar fertilization of peach (*Prunus persica* (L.) Batsch) with different iron formulations: Effects on re-greening, iron concentration and mineral composition in treated and untreated leaf surfaces. *Scient. Hort.* **117**: 241-248

- Fiehn O** (2002) Metabolomics - the link between genotypes and phenotypes. *Plant Mol. Biol.* **48**: 155-171
- Gonzalez-Vallejo E, Susín S, Abadía A, Abadía J** (1998) Changes in sugar beet leaf plasma membrane Fe(III)-chelate reductase activities mediated by Fe-deficiency, assay buffer composition, anaerobiosis and the presence of flavins. *Protoplasma* **205**: 163-168
- Goodacre R, York EV, Heald JK, Scott IM** (2003) Chemometric discrimination of unfractionated plant extracts analyzed by electrospray mass spectrometry. *Phytochem.* **62**: 859-863
- Guerinot ML** (2000) The ZIP family of metal transporters. *BBA-Biomemb.* **1465**: 190-198
- Herbik A, Giritch A, Horstmann C, Becker R, Balzer H, Baumlein H, Stephan U** (1996) Iron and copper nutrition-dependent changes in protein expression in a tomato wild type and the nicotianamine-free mutant chloronerva. *Plant Physiol.* **111**: 533-540
- Hider R, Yoshimura E, Khodr H, von Wirén N** (2004) Competition or complementation: the iron-chelating abilities of nicotianamine and phytosiderophores. *New Phytol.* **164**: 204-208
- Ishimaru Y, Suzuki M, Tsukamoto T, Suzuki K, Nakazono M, Kobayashi T, Wada Y, Watanabe S, Matsushashi S, Takahashi M, Nakanishi H, Mori S, Nishizawa N** (2006) Rice plants take up iron as an Fe³⁺-phytosiderophore and as Fe²⁺. *Plant J.* **45**: 335-346
- Jin C, You G, He Y, Tang C, Wu P, Zheng S** (2007) Iron deficiency-induced secretion of phenolics facilitates the reutilization of root apoplastic iron in red clover. *Plant Physiol.* **144**: 278-285
- Johnson HE, Broadhurst D, Goodacre R, Smith AR** (2003) Metabolic fingerprinting of salt-stressed tomatoes. *Phytochem.* **62**: 919-928
- Klatte M, Schuler M, Wirtz M, Fink-Straube C, Hell R, Bauer P** (2009) The analysis of *Arabidopsis* nicotianamine synthase mutants reveals functions for nicotianamine in seed iron loading and iron deficiency responses. *Plant Physiol.* **150**: 257-271
- Kobayashi T, Nishizawa N, Mori S** (2006) Molecular analysis of iron-deficient graminaceous plants, in: Barton L.L., Abadía J. (Eds.), *Iron Nutrition in Plants and Rhizospheric Microorganisms*, Springer, Dordrecht, Netherlands.
- Kobayashi T, Ogo Y, Itai RN, Nakanishi H, Takahashi M, Mori S, Nishizawa NK** (2007) The transcription factor IDEF1 regulates the response to and tolerance of iron deficiency in plants. *Proc. Natl. Acad. Sci. USA* **104**: 19150-19155
- Koike S, Inoue H, Mizuno D, Takahashi M, Nakanishi H, Mori S, Nishizawa N** (2004) OsYSL2 is a rice metal-nicotianamine transporter that is regulated by iron and expressed in the phloem. *Plant J.* **39**: 415-424
- Krishnan P, Kruger N, Ratcliffe R** (2005) Metabolite fingerprinting and profiling in plants using NMR. *J. Exp. Bot.* **56**: 255-265
- Krüger C, Berkowitz O, Stephan U, Hell R** (2002) A metal-binding member of the late embryogenesis abundant protein family transports iron in the phloem of *Ricinus communis* L. *J. Biol. Chem.* **277**: 25062-25069
- Küpper H, Mijovilovich A, Meyer-Klaucke W, Kroneck PMH** (2004) Tissue- and age-dependent differences in the complexation of cadmium and zinc in the cadmium/zinc hyperaccumulator *Thlaspi caerulescens* (Ganges ecotype) revealed by X-ray absorption spectroscopy. *Plant Physiol.* **134**: 748-757
- Laganowsky A, Gómez SM, Whitelegge JP, Nishio JN** (2009) Hydroponics on a chip: Analysis of the Fe deficient *Arabidopsis* thylakoid membrane proteome. *J. Proteom.* **72**: 397-415
- Lan P, Li W, Wen T-N, Shiau J-Y, Wu Y-C, Lin W-D, Schmidt W** (In Press) iTRAQ protein profile analysis of *Arabidopsis* roots reveals new aspects critical for Fe homeostasis. *Plant Physiol.* DOI: 10.1104/pp.110.169508
- Landsberg E** (1982) Transfer cell formation in the root epidermis: A prerequisite for Fe-efficiency? *J. Plant Nutr.* **5**: 415-432

- Landsberg E** (1986) Function of rhizodermal transfer cells in the Fe stress response mechanisms of *Capsicum annuum* L. *Plant Physiol.* **82**: 511-517
- Larbi A, Abadía A, Morales F, Abadía J** (2004) Fe resupply to Fe-deficient sugar beet plants leads to rapid changes in the violaxanthin cycle and other photosynthetic characteristics without significant de novo chlorophyll synthesis. *Photosynth. Res.* **79**: 59-69
- Larbi A, Morales F, Abadía J, Abadía A** (2003) Effects of branch solid Fe sulphate implants on xylem sap composition in field-grown peach and pear: changes in Fe, organic anions and pH. *J. Plant Physiol.* **160**: 1473-1481
- Li J, Wu X, Hao S, Wang X, Ling H** (2008) Proteomic response to iron deficiency in tomato root. *Proteomics* **8**: 2299-2311
- Li W, Schmidt W** (2010) A lysine-63-linked ubiquitin chain-forming conjugase, UBC13, promotes the developmental responses to iron deficiency in *Arabidopsis* roots. *Plant J.* **62**: 330-343
- López-Millán A, Morales F, Abadía A, Abadía J** (2001) Changes induced by Fe deficiency and Fe resupply in the organic acid metabolism of sugar beet (*Beta vulgaris*) leaves. *Physiol. Plant.* **112**: 31-38
- López-Millán A, Morales F, Andaluz S, Gogorcena Y, Abadía A, De Las Rivas J, Abadía J** (2000) Responses of sugar beet roots to iron deficiency. Changes in carbon assimilation and oxygen use. *Plant Physiol.* **124**: 885-897
- López-Millán A, Morales F, Gogorcena Y, Abadía A, Abadía J** (2001) Iron resupply-mediated deactivation of Fe-deficiency stress responses in roots of sugar beet. *Aust. J. Plant Physiol.* **28**: 171-180
- López-Millán A, Morales F, Gogorcena Y, Abadía A, Abadía J** (2009) Metabolic responses in iron deficient tomato plants. *J. Plant Physiol.* **166**: 375-384
- López-Millán AF, Morales F, Abadía A, Abadía J** (2000) Effects of iron deficiency on the composition of the leaf apoplastic fluid and xylem sap in sugar beet. Implications for iron and carbon transport. *Plant Physiol.* **124**: 873-884
- Marschner H** (1995) Mineral Nutrition of Higher Plants. Academic Press, London
- Marsili E, Baron DB, Shikhare ID, Coursolle D, Gralnick JA, Bond DR** (2008) *Shewanella* secretes flavins that mediate extracellular electron transfer. *Proc. Natl. Acad. Sci. USA* **105**: 3968-3973
- Meija J, Montes-Bayón M, Caruso J, Sanz-Medel A** (2006) Integrated mass spectrometry in (semi-) metal speciation and its potential in phytochemistry. *Trends Anal. Chem.* **25**: 44-51
- Mengel K, Planker R, Hoffmann B** (1994) Relationship between leaf apoplast pH and iron chlorosis of sunflower (*Helianthus annuus* L). *J. Plant Nutr.* **17**: 1053-1065
- Morales F, Grasa R, Abadía A, Abadía J** (1998) Iron chlorosis paradox in fruit trees. *J. Plant Nut.* **21**: 815-825
- Morrissey J, Baxter IR, Lee J, Li L, Lahner B, Grotz N, Kaplan J, Salt DE, Guerinot ML** (2009) The Ferroportin Metal Efflux proteins function in iron and cobalt homeostasis in *Arabidopsis*. *Plant Cell* **21**: 3326-3338
- Mukherjee I, Campbell N, Ash J, Connolly E** (2006) Expression profiling of the *Arabidopsis* ferric chelate reductase (FRO) gene family reveals differential regulation by iron and copper. *Planta* **223**: 1178-1190
- Murata Y, Ma J, Yamaji N, Ueno D, Nomoto K, Iwashita T** (2006) A specific transporter for iron(III)-phytosiderophore in barley roots. *Plant J.* **46**: 563-572
- Nozoye T, Nagasaka S, Kobayashi T, Takahashi M, Sato Y, Sato Y, Uozumi N, Nakanishi H, Nishizawa NK** (*In press*) Phytosiderophore efflux transporters are crucial for iron acquisition in graminaceous plants. *J. Biol. Chem.* DOI: 10.1074/jbc.M110.180026
- Ogo Y, Nakanishi Itai R, Nakanishi H, Kobayashi T, Takahashi M, Mori S, Nishizawa NK** (2007) The rice bHLH protein OsIRO2 is an essential regulator of the genes involved in Fe uptake under Fe-deficient conditions. *Plant J.* **51**: 366-377
- Pedas P, Ytting CK, Fuglsang AT, Jahn TP, Schjoerring JK, Husted S** (2008)

- Manganese efficiency in barley: identification and characterization of the metal ion transporter HvIRT1. *Plant Physiol.* **148**: 455-466
- Pich A, Scholz G, Stephan U** (1994) Iron-dependent changes of heavy -metals, nicotianamine, and citrate in different plant organs and in the xylem exudate of 2 tomato genotypes- Nicotianamine as a possible copper translocator. *Plant Soil* **165**: 189-196
- Plaxton W, Podesta F** (2006) The functional organization and control of plant respiration. *Crit. Rev. Plant Sci.* **25**: 159-198
- Punshon T, Guerinot ML, Lanzirotti A** (2009) Using synchrotron X-ray fluorescence microprobes in the study of metal homeostasis in plants. *Ann. Bot.* **103**: 665-672
- Rabotti G, De Nisi P, Zocchi G** (1995) Metabolic implications in the biochemical responses to iron deficiency in cucumber (*Cucumis sativus* L.) roots. *Plant Physiol.* **107**: 1195-1199
- Rellán-Álvarez R, Abadía J, Álvarez-Fernández A** (2008) Formation of metal-nicotianamine complexes as affected by pH, ligand exchange with citrate and metal exchange. A study by electrospray ionization time-of-flight mass spectrometry. *Rapid Commun. Mass Spectrom.* **22**: 1553-1562
- Robinson N, Procter C, Connolly E, Guerinot M** (1999) A ferric-chelate reductase for iron uptake from soils. *Nature* **397**: 694-697
- Rodríguez-Celma J, Lattanzio G, Grusak MA, Abadía A, Abadía J, López-Millán A-F** (Submitted) Root responses of *Medicago truncatula* plants grown in two different iron deficiency conditions: analysis of the root protein profile and the riboflavin biosynthesis pathway. *New Phytol.*
- Rogers E, Guerinot M** (2002) FRD3, a member of the multidrug and toxin efflux family, controls iron deficiency responses in *Arabidopsis*. *Plant Cell* **14**: 1787-1799
- Rombolà AD, Tagliavini M** (2006) Iron nutrition of fruit tree crops. In LL Barton, J Abadia, eds, Iron nutrition in plants and rhizospheric microorganisms. Springer, Dordrecht, Netherlands, pp 61-83
- Santi S, Schmidt W** (2009) Dissecting iron deficiency-induced proton extrusion in *Arabidopsis* roots. *New Phytol.* **183**: 1072-1084
- Sarret G, Saumitou-Laprade P, Bert V, Proux O, Hazemann J-L, Traverse A, Marcus MA, Manceau A** (2002) Forms of zinc accumulated in the hyperaccumulator *Arabidopsis halleri*. *Plant Physiol.* **130**: 1815-1826
- Scalbert A, Brennan L, Fiehn O, Hankemeier T, Kristal BS, Ommen B, Pujos-Guillot E, Verheij E, Wishart D, Wopereis S** (2009) Mass-spectrometry-based metabolomics: limitations and recommendations for future progress with particular focus on nutrition research. *Metabolomics* **5**: 435-458
- Schaaf G, Erenoglu B, von Wirén N** (2004) Physiological and biochemical characterization of metal-phytosiderophore transport in graminaceous species. *Soil Sci. Plant Nut.* **50**: 989-995
- Schagerlöff U, Wilson G, Hebert H, Al-Karadaghi S, Hägerhäll C** (2006) Transmembrane topology of FRO2, a ferric chelate reductase from *Arabidopsis thaliana*. *Plant Mol. Biol.* **62**: 215-221
- Schuler M, Lehmann M, Fink-Straube C, Bauer P** (2010) The interaction of NAS genes and FRD3 in the long-distance transport of iron in *Arabidopsis thaliana* 15th International Symposium on iron nutrition and interactions in plants, Budapest, Hungary
- Sijmons P, Bienfait H** (1983) Source of electrons for extracellular Fe(III) reduction in iron-deficient bean roots. *Physiol. Plant.* **59**: 409-415
- Stenchuk NN, Kutsiaba VI, Kshanovskaya BV, Fedorovich DV** (2001) Effect of the rib83 mutation on riboflavin synthesis and iron acquisition in the yeast *Pichia guilliermondii*. *Microbiology* **70**: 647-651
- Sumner L, Mendes P, Dixon R** (2003) Plant metabolomics: large-scale phytochemistry in the functional genomics era. *Phytochemistry* **62**: 817-836
- Susín S, Abian J, Sanchez-Baeza F, Peleato M, Abadía A, Gelpi E, Abadía J** (1993)

- Riboflavin 3'-Sulfate and 5'-Sulfate, 2 novel flavins accumulating in the roots of iron deficient sugar beet (*Beta vulgaris* L.). *J. Biol. Chem.* **268**: 20958-20965
- Szoboszlai N, Polgári Z, Mihucz VG, Záray G** (2009) Recent trends in total reflection X-ray fluorescence spectrometry for biological applications. *Anal. Chim. Acta* **633**: 1-18
- Takahashi M, Terada Y, Nakai I, Nakanishi H, Yoshimura E, Mori S, Nishizawa N** (2003) Role of nicotianamine in the intracellular delivery of metals and plant reproductive development. *Plant Cell* **15**: 1263-1280
- Terry N** (1980) Limiting factors in photosynthesis. I. Use of iron stress to control photochemical capacity *in vivo*. *Plant Physiol.* **65**: 114-120
- Terry N, Abadía J** (1986) Function of iron in chloroplasts. *J. Plant Nutr.* **9**: 609-646
- Thimm O, Essingmann B, Kloska S, Altmann T, Buckhout T** (2001) Response of *Arabidopsis* to iron deficiency stress as revealed by microarray analysis. *Plant Physiol.* **127**: 1030-1043
- Tiffin LO** (1966) Iron translocation. I. Plant culture exudate sampling iron-citrate analysis. *Plant Physiol.* **41**: 510-514
- Tiffin LO** (1966) Iron translocation. II. Citrate/iron ratios in plant stem exudates. *Plant Physiol.* **41**: 515-518.
- Tiffin LO, Brown JC** (1962) Iron chelates in soybean exudate. *Science* **135**: 311-313
- Timperio A, D'Amici G, Barta C, Loreto F, Zolla L** (2007) Proteomic, pigment composition, and organization of thylakoid membranes in iron-deficient spinach leaves. *J. Exp. Bot.* **58**: 3695-3710
- Vigani G, Maffi D, Zocchi G** (2009) Iron availability affects the function of mitochondria in cucumber roots. *New Phytol.* **182**: 127-136
- Vigani G, Zocchi G** (2009) The fate and the role of mitochondria in Fe-deficient roots of strategy I plants. *Plant Signal. Behav.* **4**: 375-379
- von Wirén N, Klair S, Bansal S, Briat J, Khodr H, Shioiri T, Leigh R, Hider R** (1999) Nicotianamine chelates both Fe-III and Fe-II. Implications for metal transport in plants. *Plant Physiol.* **119**: 1107-1114
- Vorwieger A, Gryczka C, Czihal A, Douchkov D, Tiedemann J, Mock H, Jakoby M, Weisshaar B, Saalbach I, Bäumllein H** (2007) Iron assimilation and transcription factor controlled synthesis of riboflavin in plants. *Planta* **226**: 147-158
- Worst D, M. Gerrits M, Vandenbroucke-Grauls C, Kusters J** (1998) *Helicobacter pylori* ribBA-mediated riboflavin production is involved in iron acquisition. *J. Bacteriol.* **180**: 1473-1479
- Yang TJW, Lin W-D, Schmidt W** (2010) Transcriptional profiling of the *Arabidopsis* iron deficiency response reveals conserved transition metal homeostasis networks. *Plant Physiol.* **152**: 2130-2141
- Yi Y, Guerinot M** (1996) Genetic evidence that induction of root Fe(III) chelate reductase activity is necessary for iron uptake under iron deficiency. *Plant J.* **10**: 835-844
- Yokosho K, Yamaji N, Ueno D, Mitani N, Ma J-F** (2009) OSFRDL1 is a citrate transporter required for efficient translocation of iron in rice. *Plant Physiol.* **149**: 297-305
- Yuan YX, Zhang J, Wang DW, Ling HQ** (2005) AtbHLH29 of *Arabidopsis thaliana* is a functional ortholog of tomato FER involved in controlling iron acquisition in strategy I plants. *Cell Res.* **15**: 613-621
- Zaharieva T, Gogorcena Y, Abadía J** (2004) Dynamics of metabolic responses to iron deficiency in sugar beet roots. *Plant Sci.* **166**: 1045-1050

OBJECTIVES/OBJETIVOS

Objectives

The general objectives of this Thesis are: i) to develop and apply new analytical methodologies for the determination of the Fe forms involved in long-distance Fe transport in plants, and ii) to study the metabolite profile of plants grown under Fe-deficiency conditions.

In order to achieve these general objectives the specific objectives are:

1. To study the formation of metal complexes with nicotianamine as affected by pH, ligand and metal exchange by means of electrospray time-of-flight mass spectrometry (ESI-TOFMS).
2. To develop a method for the determination of naturally occurring Fe complexes in xylem sap, using high performance liquid chromatography coupled to ESI-TOFMS and inductively coupled plasma mass spectrometry (HPLC-ESI-TOFMS and HPLC-ICP-MS, respectively).
3. To develop an HPLC-ESI-TOFMS method for the determination of organic acids in plant tissues.
4. To characterize the changes induced in the root metabolite profile in response to Fe deficiency and resupply, using gas chromatography coupled to mass spectrometry (GC-MS).
5. To characterize the changes induced in the metabolite profile of xylem sap and leaves of several plant species in response to Fe deficiency and resupply, using GC-MS.

Objetivos

Los objetivos generales de esta tesis doctoral son: a) desarrollar y aplicar nuevas metodologías analíticas que permitan la especiación química del Fe en los fluidos vegetales involucrados en el transporte a larga distancia de este elemento en plantas y b) estudiar el perfil de metabolitos de plantas cultivadas en condiciones de deficiencia de Fe.

Para alcanzar estos objetivos generales se plantean los siguientes objetivos específicos:

1. Estudiar el efecto del pH y las reacciones de intercambio del metal o el ligando sobre la formación de complejos metálicos con nicotianamina mediante espectrometría de masas (MS) con analizador de tiempo de vuelo (TOF) y fuente de electrospray (ESI).
2. Desarrollar un método que permita la determinación de complejos naturales de Fe en plantas involucrados en el transporte de este elemento *vía* xilema mediante cromatografía líquida de alta resolución (HPLC) acoplada a ESI-TOFMS y espectrometría de masas con fuente de plasma de acoplamiento inductivo (ICP-MS).
3. Desarrollar un método que permita la determinación de ácidos orgánicos en tejidos vegetales mediante HPLC-ES-TOFMS.
4. Caracterizar los cambios en el perfil de metabolitos que se producen en condiciones de deficiencia y reaporte de Fe en las raíces de las plantas mediante cromatografía de gases acoplada a espectrometría de masas (GC-MS).
5. Caracterizar los cambios en el perfil de metabolitos que se producen en condiciones de deficiencia y reaporte de Fe en la savia de xilema y las hojas de varias especies vegetales mediante GC-MS.

**FORMATION OF METAL-NICOTIANAMINE COMPLEXES AS AFFECTED BY PH,
LIGAND EXCHANGE WITH CITRATE AND METAL EXCHANGE. A STUDY BY
ELECTROSPRAY-TIME OF FLIGHT MASS SPECTROMETRY**

Rubén Rellán-Álvarez, Javier Abadía and Ana Álvarez-Fernández

Rapid Communications in Mass Spectrometry, 2008 22: 1553-1562

Department of Plant Nutrition, Aula Dei Experimental Station (CSIC), P.O. Box 202, 50080
Zaragoza, Spain.

**FORMATION OF METAL-NICOTIANAMINE COMPLEXES AS AFFECTED BY PH,
LIGAND EXCHANGE WITH CITRATE AND METAL EXCHANGE. A STUDY BY
ELECTROSPRAY-TIME OF FLIGHT MASS SPECTROMETRY**

Rubén Rellán-Álvarez, Javier Abadía and Ana Álvarez-Fernández

Department of Plant Nutrition, Aula Dei Experimental Station (CSIC), P.O. Box 202, 50080 Zaragoza, Spain.

Nicotianamine (NA) is considered as a key element in plant metal homeostasis. This non-proteinogenic amino acid has an optimal structure for chelation of metal ions, with six functional groups that allow octahedral coordination. The ability to chelate metals by NA is largely dependent on the pK of the resulting complex and the pH of the solution, with most metals being chelated at neutral or basic pH values. *In silico* calculations using pKa and pK values have predicted the occurrence of metal-NA complexes in plant fluids, but the use of soft ionization techniques (e.g. electrospray), together with high-resolution mass spectrometers (e.g. time of flight mass detector), can offer direct and metal-specific information on the speciation of NA in solution. We have used direct infusion electrospray-mass spectrometry (Time Of Flight) ESI-TOFMS to study the complexation of Mn, Fe(II), Fe(III), Ni, Cu by NA. The pH dependence of the metal-NA complexes in ESI/MS was compared to that predicted *in silico*. Possible exchange reactions that may occur between Fe-NA and other metal micronutrients as Zn and Cu, as well as between Fe-NA and citrate, another possible Fe ligand candidate in plants, were studied at pH 5.5 and 7.5, values typical of the plant xylem and phloem saps. Metal-NA complexes were generally observed in the ESI/MS experiments at a pH value approximately 1-2 units lower than that predicted *in silico*, and this difference could be only partially explained by the estimated error, approximately 0.3 pH units, associated to measuring pH in organic solvent-containing solutions. Iron-NA complexes are less likely to participate in ligand and metal exchange reactions at pH 7.5 than at pH 5.5. Results support that NA may be the ligand chelating Fe at pH values usually found in phloem sap, whereas in the xylem sap NA is not likely to be involved in Fe transport, conversely to what

occurs with other metals such as Cu and Ni. Some considerations that need to be addressed when studying metal complexes in plant compartments by ESI/MS are also discussed.

Introduction

Metals such as Mn, Fe, Ni, Cu or Zn are essential for plants, since they participate in numerous metabolic processes in different plant tissues and cell compartments. When these metals are in short supply, plants show deficiency symptoms such as growth reduction and reduced photosynthesis. However, when metals are in excess oxidative stress and other cellular disturbances occur, and plants develop toxicity symptoms (Hall, 2002). For these reasons, the processes involved in metal acquisition by roots and transport to the different plant organs must be tightly regulated, so that metals can be available where they are needed and in an appropriate chemical form. The tendency toward a relatively stable equilibrium between these interdependent mechanisms, maintained by physiological processes, is usually called metal homeostasis.

A key element in plant metal homeostasis is the non-proteinogenic amino acid nicotianamine (NA), first discovered by Noma *et al* (Noma *et al.*, 1971). Nicotianamine has an optimal structure for chelation of metal ions, with six functional groups that allow octahedral coordination, the distances between functional groups being optimal for the formation of chelate rings. Nicotianamine is known to chelate many metals, including Fe(II) and Fe(III) (Benes *et al.*, 1983; von Wiren *et al.*, 1999), Mn(II), Co(II), Ni(II), Cu(II) and Zn(II) (Anderegg and Ripperger, 1989; Stephan and Scholz, 1993). The NA stability constants (log K) of the metal-NA complexes with Fe(III), Cu(II), Ni(II), Zn(II), Fe(II) and Mn(II), are 20.6, 18.6, 16.1, 15.4, 12.8 and 8.8, respectively (Benes *et al.*, 1983; Anderegg and Ripperger, 1989; von Wiren *et al.*, 1999).

Nicotianamine is thought to be important in the speciation of soluble Fe in different plant compartments, (Hell and Stephan, 2003) because it is able to form stable complexes with both Fe(II) and Fe(III) at neutral and weakly alkaline pH values (Stephan et al., 1996). Although the Fe(III)-NA complex has a much higher stability constant, the Fe(II)-NA complex is also kinetically stable under aerobic conditions (von Wiren et al., 1999). Nicotianamine appears to be ubiquitous in higher plants and is present in all tissues (Scholz et al., 1992). For instance, NA concentrations are relatively increased in root tips of sunflower and barley in the regions of main uptake and radial transport of Fe (Stephan and Scholz, 1990). Also, both Fe-NA complexes constitute non-toxic Fe pools, because they are relatively poor Fenton reagents (von Wiren et al., 1999). In the NA-lacking tomato mutant *chloronerva*, enhanced activities of antioxidant enzymes (Herbik et al., 1996) and precipitation of Fe in vacuoles and mitochondria (Liu et al., 1998) do occur.

The possible roles of NA in long distance metal transport, both in the xylem and phloem compartments, is still being explored. Nicotianamine has been observed in the xylem at μM concentrations (Takahashi et al., 2003) although it does not seem to be absolutely necessary for xylem metal transport. For instance, in the NA-deficient tomato mutant *chloronerva*, Fe, Mn and Zn accumulate in old leaves (Pich et al., 1994). Instead, Fe is thought to be transported through the xylem complexed with citrate (Tiffin, 1966; Lopez-Millan et al., 2000). Recent findings support that the FRD3 protein transporter could import citrate into the root vasculature, and *frd3* mutants show symptoms of Fe deficiency that could be alleviated by external citrate supply (Durrett et al., 2007). In young leaves, Fe-ligand exchange (from citrate to NA) could occur during Fe transfer from xylem to phloem, and Fe-NA could pass through membranes by metal-NA complex specific transporters as suggested by Takahashi *et al* (Takahashi et al., 2003). Nicotianamine has been observed in the phloem, and could be involved in Fe phloem loading and unloading, although a 17 kD polypeptide has been proposed to be the Fe carrier in the phloem of *Ricinus* (Maas et al., 1988; Schmidke et al., 1999; Kruger et al., 2002). After the cloning of nicotianamine synthase (*NAS*) new tools are available to

modulate the concentrations of NA in different plant tissues (Herbik et al., 1999; Higuchi et al., 1999; Ling et al., 1999). Nicotianamine involvement in long distance transport is also supported by the fact that the protein OsYLS2, which can transport Fe(II)-NA and Mn(II)-NA complexes, is expressed in phloem companion cells of rice leaves (Koike et al., 2004). The protein ZmYS1, which transports both Fe(II)-NA (Roberts et al., 2004) and Fe(III)-NA, (Roberts et al., 2004; Schaaf et al., 2005) is able to rescue Fe-deficient yeast mutants and also transports Fe-NA complexes when expressed in *Xenopus* oocytes. In addition to its role in long-distance metal transport, NA might be involved in the regulation of inter-cellular metal transfer (Takahashi et al., 2003). Also, higher concentrations of NA are required for flower and seed development than for leaf development (Takahashi et al., 2003).

Nicotianamine can also form complexes with other metals apart from Fe. For instance, from *in silico* studies it has been proposed that Cu xylem transport could rely on complexation with NA (von Wiren et al., 1999). In fact, the Cu concentration in the xylem of NA-deficient tomato mutant *chloronerva* was enhanced by NA application, and a high supply of Cu resulted in higher NA concentration (Pich and Scholz, 1996). It seems also clear that NA is involved in Ni tolerance and hyper-accumulation. Vacchina *et al* (Vacchina et al., 2003) identified the Ni(II)-NA complex in the Ni hyper-accumulator species *Thlaspi caerulescens*. Also, a high *NAS* expression was found by microarray analysis in the hyper-accumulator species *Arabidopsis halleri* (Weber et al., 2004). Transgenic plants over-expressing *NAS* have been constructed and proved to be tolerant to high Ni concentrations, most likely due to the higher constitutive levels of NA (Douchkov et al., 2005; Kim et al., 2005; Pianelli et al., 2005).

Until now, a large part of the current knowledge on the role of metal-NA complexes in micronutrient plant nutrition has been gained using either indirect measurements or *in silico* calculations (von Wiren et al., 1999). Further investigation in this area should include direct determination of the possible metal-NA complexes, as suggested by Hider *et al* (Hider et al., 2004). Recent examples of this approach were the determination of the Ni(II)-NA complex in the Ni hyper-accumulator *T. caerulescens* by

mass spectrometry (Vacchina et al., 2003; Ouerdane et al., 2006), the identification of different metal-phytosiderophores by zwitterionic hydrophilic interaction liquid chromatography (ZIC-HILIC) coupled to ESI-MS (Xuan et al., 2006) and the characterization of Fe(II)/(III)-phytosiderophore complexes by direct infusion nano-ESI-Fourier transform ion cyclotron resonance MS (Weber et al., 2006).

The aim of our work was to study the of Mn(II), Fe(II), Fe(III), Ni(II), Cu(II), Zn(II) and Cd(II) complexation by NA, using ESI/TOF(MS) at different pH conditions and comparing the results with *in silico* estimations. Specifically, the formation of Fe(II)-NA and Fe(III)-NA complexes was analyzed in detail, by studying ligand exchange reactions with citrate as well as metal exchange reactions with Zn and Cu. These studies were carried out using typical xylem and phloem pH values, in an effort to get a better insight on the possible roles of NA in long distance metal transport in plants.

Experimental

Chemicals. All buffers and standard solutions were prepared with LC-MS grade water (Riedel-de Häen, Seelze, Germany). Ammonium bicarbonate (99.5%, Fluka), ammonium acetate (99.99%, Aldrich), leucine-enkephaline (Tyr-Gly-Gly-Phe-Leu, 98%, Sigma), methionine (99%, Sigma), citric acid (99%, Sigma), formic acid (50%, Fluka), acetonitrile and 2-propanol (in both cases LC-MS grade, Riedel-de Häen) were purchased from Sigma (St. Louis, MO, USA). Iron(II) chloride (98%, Aldrich), Ni(II) chloride (99.9%, Sigma) and Cd(II) chloride (98%, Sigma) were also purchased from Sigma. Manganese(II), Fe(III), Cu(II) and Zn(II) were Titrisol[®] metal standards (1 g of metal in 15% HCl, Merck, Darmstadt, Germany). Glutathione (99%) and nicotianamine (98%) were purchased from Calbiochem (San Diego, Ca) and T. Hasegawa Co., LTD. (Kawasaki, Japan), respectively.

Preparation of standard solutions. Solutions for tuning the mass spectrometer were (1) 10 mM LiOH, 0.2% (vol/vol) formic acid and 50% (vol/vol) 2-propanol, and (2) 1 μ M leucine-enkephaline, 20 μ M methionine, 5 μ M glutathione, 0.1% (vol/vol) formic acid and 50% (vol/vol) 2-propanol. Stock solutions of 100 mM ammonium acetate, 100 mM ammonium bicarbonate, 1 mM metal, 1 mM NA and 1 mM

citric acid were prepared by dissolving or diluting the starting products in water.

The ESI/TOF mass spectra of Mn(II)-NA, Fe(II)-NA, Fe(III)-NA, Ni(II)-NA, Cu(II)-NA, Zn(II)-NA and Cd(II)-NA were obtained by adding 1 mM NA solutions over 100 mM ammonium bicarbonate pH 7.1 and then adding the 1 mM metal standard. Just before ESI-TOFMS analysis, samples were diluted with 50% acetonitrile and the pH was measured again and if necessary readjusted with NH₄OH or HCl. A Biotrode[®] pH microelectrode with Idrolyte[®] electrolyte (Metrohm, Herisau, Switzerland), which allows measurements in the presence of organic solvents, was used. The final solution contained 50 μ M concentrations of both NA and metal. All possible precautions in the preparation of metal containing solutions were taken, specially with Fe(II) solutions, including N₂ bubbling, protection from light and immediate analysis to avoid oxidation of Fe(II).

In order to study the effects of pH on the formation of metal-NA complexes, solutions of Mn(II)-NA, Fe(II)-NA, Fe(III)-NA, Ni(II)-NA, Cu(II)-NA, Zn(II)-NA and Cd(II)-NA were prepared at different pH values (2.5 to 8.5) by adding 1 mM NA solutions over 100 mM ammonium acetate (when pH values were lower than 7.0) or ammonium bicarbonate (when pH was higher than 7.0), and then adding the 1 mM metal standard. Just before ESI-TOFMS analysis, samples were diluted with 50% acetonitrile and the pH was measured again. The final solution contained 50 μ M concentrations of both NA and metal.

Ligand exchange experiments were carried out with 50 μ M solutions of Fe(II)-NA, Fe(III)-NA and citric acid prepared in 50% acetonitrile. Metal exchange experiments were carried out with 50 μ M solutions of Fe(II)-NA, Cu(II) and Zn(II) prepared in 50% acetonitrile. Iron(II)-NA and Fe(III)-NA solutions were buffered at pH values 5.5 and 7.5 as described above.

ESI-TOFMS analysis. Analyses were carried out with a BioTOF[®] II (Bruker Daltonics, Billerica, MA, USA) coaxial multipass time of flight mass spectrometer (TOFMS) equipped with an Apollo electrospray ionization source (ESI). The maximum resolution of the mass spectrometer detector used is 10,000 FWHM (full width at half-maximum height).

BioTOF[®] II was operated with endplate and spray tip potentials of 2.8 kV and 3.3 kV,

respectively, in negative ion mode, and of 3.0 kV and 3.5 kV, respectively, in positive ion mode. Drying (N_2) and nebulizer gas (N_2) pressures were kept at 30 psi. The mass axis was calibrated using Li-formate adducts in negative ion mode and a mixture of 1 μ M leucine-enkephaline, 20 μ M methionine and 5 μ M glutathione in positive ion mode. Spectra were acquired in the mass/charge ratio (m/z) range of 100-700.

A syringe pump (Cole-Parmer Instrument, Vernon Hills, IL, USA) operated at 4 μ L/min was used to introduce in the ESI chamber the solutions containing metal-NA complexes at different pH values. For ligand exchange experiments, two syringe pumps operating at 4 μ L min^{-1} were used, the first containing 50 μ M Fe(II)-NA (or Fe(III)-NA) solution and the second containing 50 μ M citric acid. Both syringes were connected with a tee to the ESI chamber. The syringe containing Fe-NA was run until a stable $[M-H]^{-1}$ signal was obtained. Then, the syringe containing citric acid was switched on and both syringes were run until stabilization of the signal. For metal exchange experiments, the same set-up was used loading 50 μ M Fe(II)-NA in the first syringe and 50 μ M Cu(II) or Zn(II) in the second. A thorough mixing between the content of the two syringes was obtained by using a micro-static mixing PEEK[®] tee (internal swept volume 0.95 μ L; reference M-540A, Upchurch, Oak Harbor, WA, USA) that creates a turbulent flow. Then, the fluid was directed to the ESI chamber (at a 8 μ L/min flow) through PEEK[®] tubing (0.127 mm inner diameter, 250 mm in length; reference 1535, Upchurch). Therefore, the mixture was left to react for 0.5 min before entrance to the ESI chamber.

The system was controlled with the software package BioTOF (version 2.2, Bruker Daltonics). Data were processed with Data Analysis software (version 3.2, Bruker Daltonik GmbH, Bremen, Germany).

Speciation modelling. MINTEQA2 for Windows (Version 1.50, Allison Geoscience Consultants, Flowery Branch, GA and HydroGeoLogic, Inc., Herndon, VA, USA) was used to carry out ligand and metal speciation in solutions. All thermodynamic database equilibrium constants were determined in water. Input parameters were metal and ligand concentrations and pH values. NA protonation constants and stability constants for metal-NA complexes were taken from Benes *et al* (Benes et

al., 1983) and von Wirén *et al* (von Wiren et al., 1999). Citrate protonation constants and stability constants for metal-citrate complexes were taken from Martell and Smith (Martell AE, 1974).

Results and discussion

Electrospray ionization of NA and metal-NA complexes. Negative-mass spectra of NA and different metal-NA complex solutions at pH 7.1 are shown in Figs. 1 and 2. Nicotianamine showed a major peak corresponding to the monoisotopic $[M-H]^{-1}$ ion at an m/z value of 302.1 (Fig. 1A). For all metal-NA complexes analyzed, the only metal-NA species observed were single charged species with 1:1 metal:NA stoichiometry. Major peaks corresponding to the signal of the metal isotope $[M-H]^{-1}$ ions were observed at m/z values of 355.1 for ⁵⁵Mn(II)-NA (Fig. 1B), 356.1 for ⁵⁶Fe(II)-NA (Fig. 1C), 358.1 for ⁵⁸Ni(II)-NA (Fig. 1E), 363.1 for ⁶³Cu(II)-NA (Fig. 1F), 364.0 for ⁶⁴Zn(II)-NA (Fig. 1G), and 414.0 for ¹¹⁴Cd(II)-NA (Fig. 1H). Since Fe(III) forms a neutral charge complex with NA, the $[M-H]^{-1}$ ion (m/z 355.2) was poorly ionized when compared with the $[M-H]^{-1}$ ion of negatively charged divalent metal-NA complexes. Major peaks found in the mass spectrum of Fe(III)-NA (Fig. 1D) were at m/z values of 356.2 and 311.2, and could be assigned to the $[M-H]^{-1}$ and $[Fe(II)NA-H-CO_2]^{-1}$ ions of ⁵⁶Fe(II)-NA, respectively. The peak at m/z value of 356.2 indicates that the complex Fe(III)-NA undergoes a reduction to Fe(II)-NA that was apparent in all tested ionization conditions, reaching a minimum at a capillary exit voltage of 40 V (Fig. 1 in supplementary material). Although this reduction is not expected when considering the redox potentials (Neubert et al., 2002), redox reactions have been reported to occur in the electrospray process, with reduction being more likely in the negative mode (Blades et al., 1991). An alteration of the oxidation state of Fe-NA complexes was also found under nano-ESI conditions (Weber et al., 2006), although in that case it was possible to optimize ionization conditions to eliminate Fe oxidation state changes. The peak at m/z value of 311.2 indicates a reduction and concomitant decarboxylation of Fe(III)-NA. Metal reduction reactions followed by a ligand decarboxylation of metal complexes with the concomitant oxidation of amino (-N-) to imino N (-N=) have also been documented in the literature (Pecoraro et al., 1984). The signal attributed to the $[Fe(II)NA-H-$

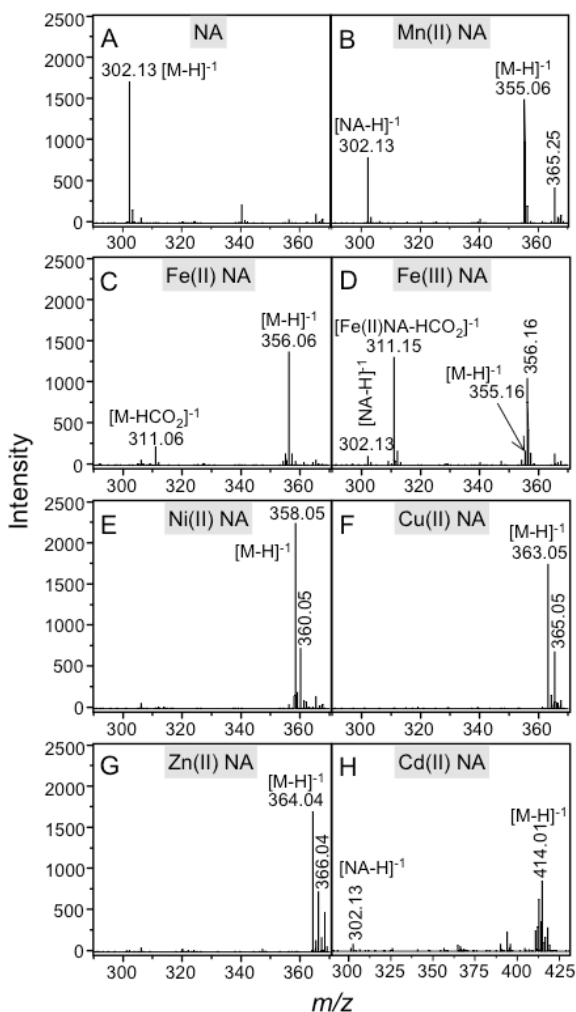


Figure 1. ESI-TOF mass spectra of nicotianamine (A) and the nicotianamine complexes with Mn(II) (B), Fe(II) (C), Fe(III) (D), Ni(II) (E), Cu(II) (F), Zn(II) (G), and Cd(II) (H), in negative ion mode. Data were acquired by injecting 50 mM solutions of each analyte in 50 mM ammonium acetate, pH 7.1, and 50% acetonitrile.

$\text{CO}_2\text{]}^{-1}$ ion was also found in the Fe(II)-NA spectrum (Fig. 1C), although with much lower intensity than in the case of Fe(III)-NA (Fig. 1D). Other minor signal at m/z 355.1 corresponding to the monoisotopic $[\text{M-H}]^{-1}$ ion of Fe(III)-NA was also found in the Fe(II)-NA spectrum (Fig. 1-2C). Oxidation of Fe(II)-species could occur during the ESI process and/or the solution preparation. However, oxidation reactions are unlikely to occur during ESI ionization in negative mode, whereas Fe(II)-species are easily oxidized by dissolved oxygen, light, etc during the solution preparation. Presence of Fe(III)-NA in Fe(II)-NA solutions was observed before

(Weber et al., 2006). A minor peak at m/z 302.1 corresponding to the monoisotopic $[\text{M-H}]^{-1}$ ion of NA was also found in Mn(II)-NA, suggesting that complexation of Mn with NA was not fully complete at the pH value of 7.1 used in this experiment. A minor signal at m/z 302.1 was also found in the MS spectra of Fe(III)-NA and Cd(II)-NA.

The negative mass spectra were zoomed close to the major signals (Fig. 2) to show in detail the isotopic signatures of the main $[\text{M-H}]^{-1}$ ions found. Observed isotopic signatures (Fig. 2 A-D) matched the theoretical ones (2a-2d). Metal isotopic signatures (insets in Fig. 2) were well preserved in metal-NA complexes, confirming the possibility to use isotopic signatures to identify metal-NA complexes in real samples.

Positive-mass spectra (not shown) showed major peaks at m/z values of 304.1, 357.1, 358.1, 360.1, 365.1, 366.1 and 416.0, corresponding to the $[\text{M+H}]^{+1}$ ions of NA, $^{55}\text{Mn(II)-NA}$, $^{56}\text{Fe(II)-NA}$, $^{58}\text{Ni(II)-NA}$, $^{63}\text{Cu(II)-NA}$, $^{64}\text{Zn(II)-NA}$ and $^{114}\text{Cd(II)-NA}$, respectively. The mass spectrum of Fe(III)-NA showed two major peaks at m/z values of 357.0, 358.0 and 313.0, corresponding to the $[\text{Fe(III)NA+H}]^{+1}$, $[\text{Fe(II)NA+2H}]^{+1}$ and $[\text{Fe(II)NA-CO}_2\text{+H}]^{+1}$ ions of Fe(II)-NA respectively.

The effect of capillary cone voltages (20-200 V) and drying gas temperatures (150, 200 and 250 reached a maximum intensity at approximately 90 V, and decreased sharply at higher voltage values. Cleaner spectra were obtained in negative than in positive mode, since in the latter case several unknown signals (artifacts or traces of impurities) with quite large intensities were observed. Signal intensities were not significantly different between both polarity modes, as it could be expected from the zwitterionic character of the NA molecule, which has carboxyl and amino positive mode, respectively. Polarity affected groups that can be easily ionized in negative and markedly Mn(II)-NA ionization, which was studied in negative ion mode, whereas in positive similar to that of other metal-NA complexes ion mode a poorer ionization was observed.

Therefore, the optimal operating conditions chosen included negative ion mode, 200° C drying gas temperature and 120 V capillary cone voltage, except for NA and Cu(II)-NA, where a voltage of 90 V was used. Under these conditions, Ni(II)-NA showed the highest the

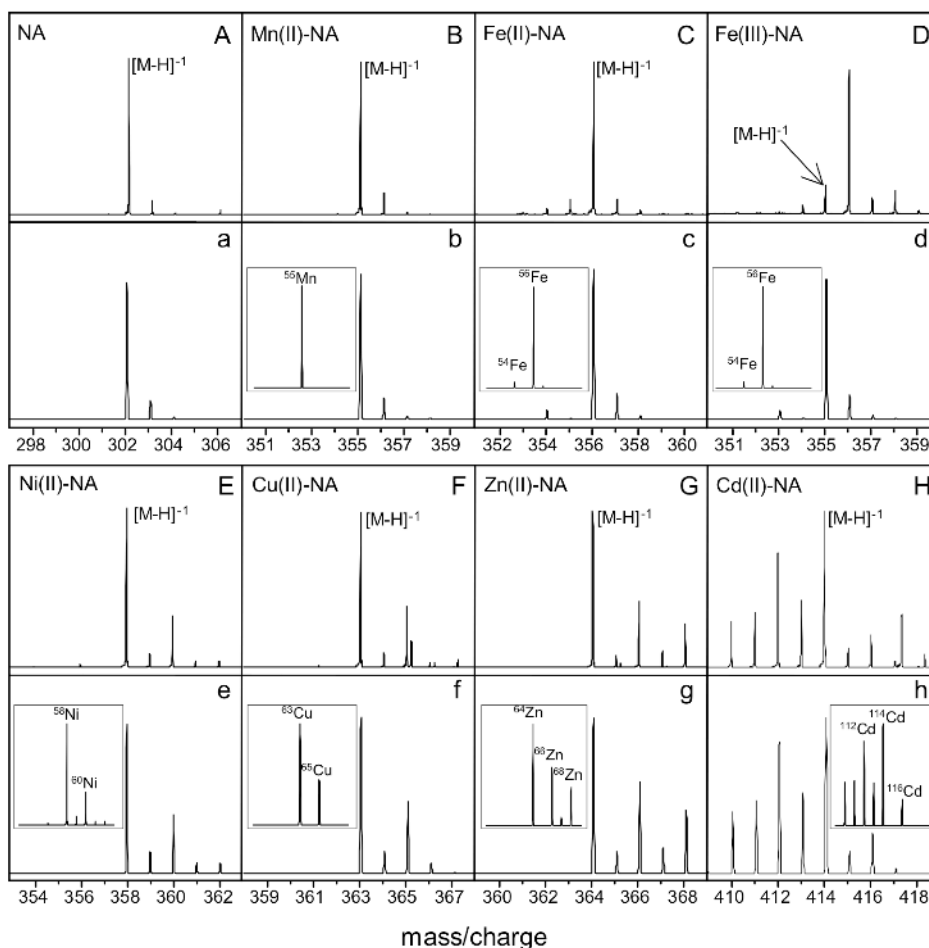


Figure 2. Experimental (upper case letters) and calculated (lower case) zoomed ESI-TOF mass spectra of nicotianamine (A, a) and the nicotianamine complexes with Mn(II) (B, b), Fe(II) (C, c), Fe(III) (D, d), Ni(II) (E, e), Cu(II) (F, f), Zn(II) (G, g), and Cd(II) (H, h) in negative ion mode. Experimental spectra are zoomed from those in Fig. 1. Insets in the calculated mass spectra show the theoretical isotopic distribution of the corresponding metal.

highest intensity. Since all these compounds are in low concentrations in real plant samples, highly sensitive MS devices would be required. In fact, the good ionization of the Ni(II)-NA complex, together with the use of plant Ni hyper-accumulators, could explain why this metal-NA complex has received more attention than others (Schaumloffel et al., 2003; Vacchina et al., 2003; Mari et al., 2006; Ouerdane et al., 2006). Theoretical and experimental m/z values for the most abundant isotopes of each compound described above are shown in Table I of supplementary material. Mass accuracy mean values, using external calibration, were approximately 15 ± 10 ppm (mean ± 3 SD) in negative mode and 13 ± 7 ppm in positive mode.

Effect of pH on metal-NA complexes. The pH dependence of metal-NA complexes was studied by ESI/MS in the pH range from approximately

2.5 to 8.5 (Fig. 3). Results shown are intensities corresponding to the most abundant ions of NA and metal-NA complexes (Fig. 3A-F). To assess the metal-NA complex pH dependence, both the NA and metal-NA complex signals must be used, because changes in the intensities of both signals with pH may be due either to metal-NA complex formation or to direct changes in ionization efficiency due to pH. Generally speaking, metal-NA complexes were scarcely formed at acidic pH values, partially formed around neutral values and completely formed at basic pH values, although some differences were efficiency of NA, which instead increased at high pH values (see Fig. II in supplementary material). With Mn(II)-NA, the signal corresponding to the complex appeared at a pH of approximately 6.2 and increased until pH 8.4 (Fig. 3A). In this pH range, the NA signal decreased until it was no

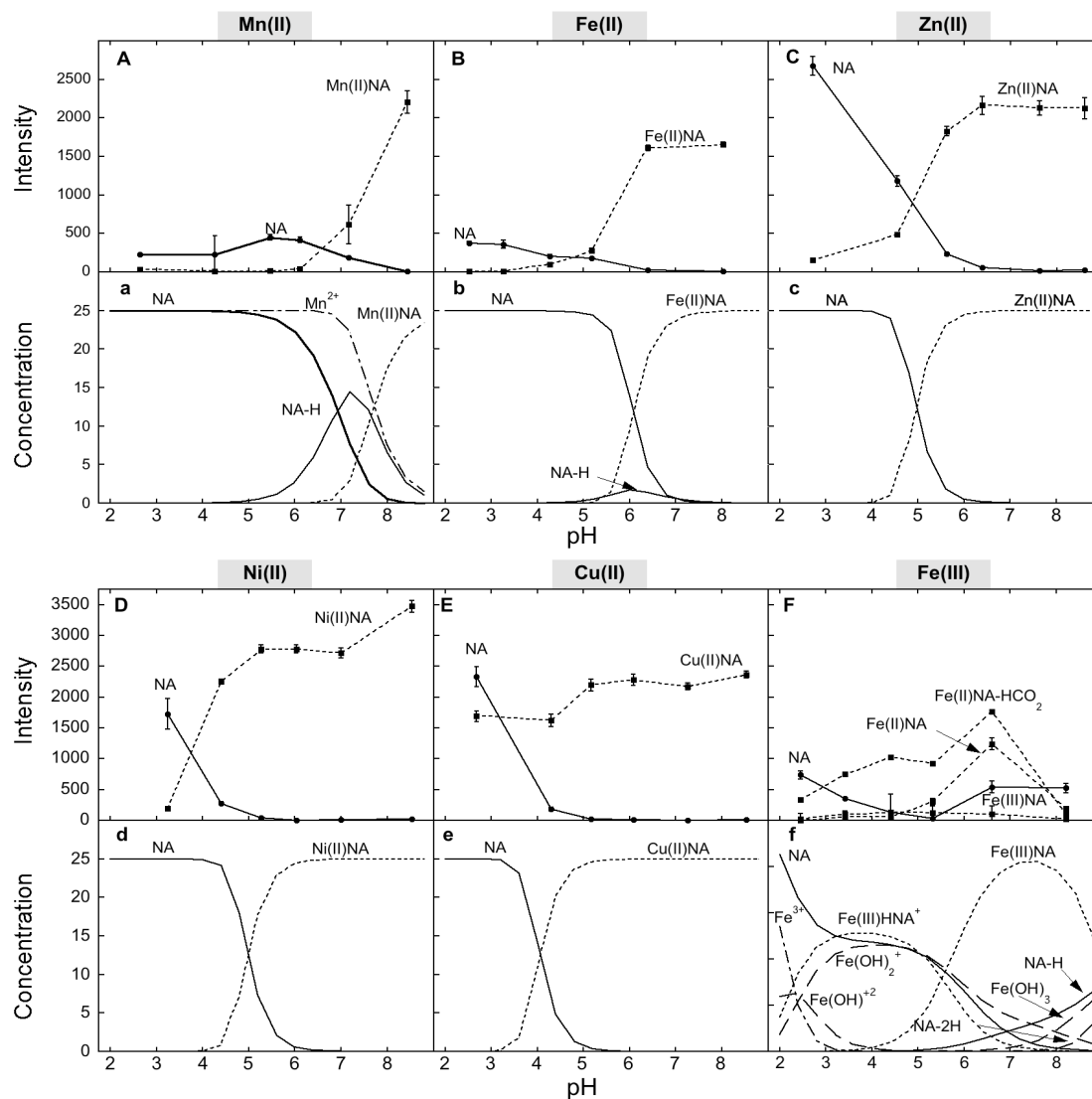


Figure 3. Software calculated (upper case letters) and experimental (lower case) pH dependences of the metal complexes of NA with Mn (A, a), Fe(II) (B, b), Zn(II) (C, c), Ni(II) (D, d), Cu(II) (E, e) and Fe(III) (F, f). Experimental values (means \pm SE, $n = 3$) show NA (solid line and circles) and metal-NA (dotted line and squares) major ion signal intensities obtained by ESI/MS analysis of a 50 μ M metal complex prepared by adding equimolar amounts of nicotianamine and metal chloride solutions, either in 100 mM ammonium acetate (pHs lower than 7) or 100 mM ammonium bicarbonate (pHs higher than 7). Samples were diluted with 50 % acetonitrile and pH was measured just before direct injection. *In silico* calculated values show the concentrations of the species NA (solid line) and metal-NA (dotted line) for NA and metal concentrations of 50 μ M. When non coincident with NA values, the concentration of free metal is also shown as dot-line-dot curve. Fe(III) hydroxides are shown as line-space curves.

longer observed, suggesting that at pH 8.4 all NA was present as Mn(II)-NA. With Cd(II)-NA, the signal was minor at low pH values, and increased markedly at pH values of 6.5 and above; at pH 8.0 the free NA signal was very small (Fig. III in supplementary material). The signals of Fe(II)-NA and Zn(II)-NA complexes were first

observed at pH values much lower than those found for Mn(II)-NA (Fig. 3B,C). The Fe(II)-NA and Zn(II)-NA signals sharply increased to pH values of approximately 6.2, whereas the NA signal decreased in the same pH range. At pH values above pH 6.2, metal-NA complex signal intensities did not change significantly and the

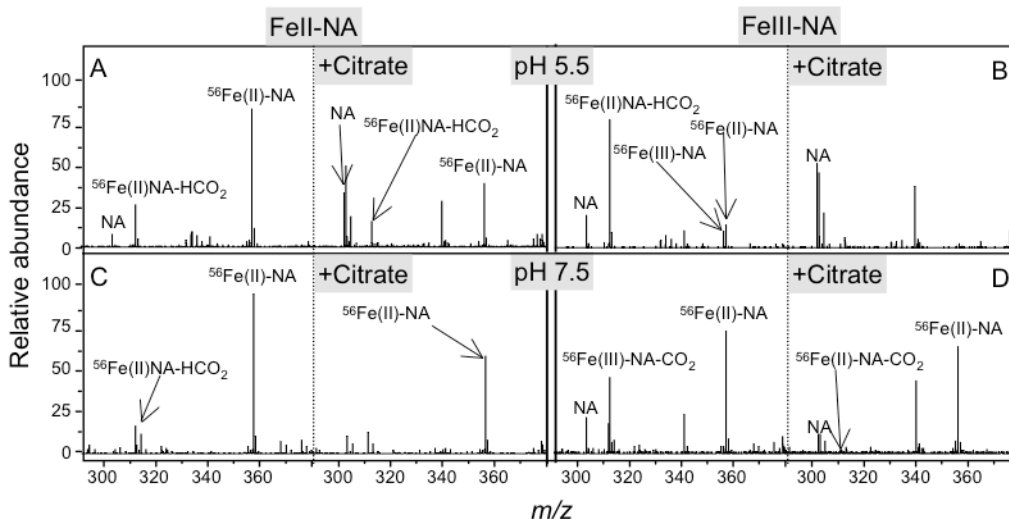


Figure 4. Ligand exchange reactions between Fe(II)-NA and citrate at pH 5.5 (A) and pH 7.5 (C), and between Fe(III)-NA and citrate at pH 5.5 (B) and pH 7.5 (D). Citrate and Fe-NA complex concentrations of the initial solutions were 50 μ M. Solutions were prepared in 100 mM ammonium acetate (pH 5.5) or ammonium bicarbonate (pH 7.5) and 50% acetonitrile.

NA signal was no longer observed. These data suggest that Fe(II)-NA and Zn(II)-NA complexes were completely formed at pH values of 6.2 or above. Ni(II)-NA and Cu(II)-NA signals were observed at pH values more acidic than those found for the other metal-NA complexes (Fig. 3D,E). In the case of Cu(II)-NA, large signals were observed even at pH values lower than 3.0 (Fig. 3E). In both cases no signal for NA was found at pH values of 5.2 or above, suggesting that metal-NA complexes were completely formed at these pH values. A positive effect on ionization at very high pH was found only in the case of Ni(II)-NA (Fig. 3D). In the case of Fe(III)-NA, a different pattern of metal-NA complex formation was found when compared with the rest of the metals (Fig. 3F). The NA signal disappeared at approximately pH 5.3, suggesting the total formation of the complex, and reappeared at higher pH values. This is possibly due to the formation of de-protonated NA (both NA and de-protonated NA give the same ion in MS spectra, see below). The two daughter signals of the Fe(III)-NA metal complex also increase its intensity until pH values close to 6.2, to decrease thereafter.

These experimental results can be compared with *in silico* simulations obtained with MINTEQA2 (Fig. 3a-f), which predict the equilibrium composition of aqueous solutions. However, some considerations should be made when comparing both approaches. First, *in silico* predictions are always done assuming that the

system has reached equilibrium, which is not likely to occur in the ESI/MS experiments. Moreover, the ESI process can induce equilibrium shifts in metal-ligand reactions (Wang and Agnes, 1999). Also, ESI/MS does not allow for the determination of some species predicted to occur by the *in silico* approach (i.e. Fe hydroxides), and some of the species predicted *in silico*, such as NA-H and NA, would give the same signal in the negative ion mode. Finally, all *in silico* predictions are done with stability and protonation constants calculated experimentally in aqueous solutions, whereas in ESI/MS experiments an organic solvent is generally needed to enhance the analyte signals, and this may affect the chemistry of the metal-NA complexes. Equilibrium constants used in the Minteqa2 thermodynamic database are determined always in water, and constants in other solvents or solvent mixtures are still rarely available due to the scarce knowledge of organic solvents physical properties (*e.g.* static dielectric constant). In the last years, the extensive use of organic solvent mixtures in chromatography has driven research in this area, and for instance static dielectric constants and density of acetonitrile mixtures at different temperatures and solvent concentrations have been only recently determined (Gagliardi et al., 2007). The use of both approaches led to similar conclusions, although ESI/MS data indicate that the metal-NA complexation processes do occur at lower pH values (1-2 units) than those estimated *in silico*.

For instance, Mn(II)-NA shows by ESI/MS a similar behaviour to that predicted *in silico*, although the signal of the Mn(II)-NA complex appeared at a pH value almost 1 unit lower than that predicted *in silico*. The same applies for Fe(II)-NA, although in this case the difference between the *in silico* predictions and the experimental values was even larger. In the case of Zn(II)-NA, Ni(II)-NA, Cu(II)-NA, the metal-NA complexes were predicted to occur only at pH values higher than of 4.0, 4.0 and 3.0, respectively, whereas all these compounds were seen by ESI/MS at lower pH values. In the case of Fe(III), the observed increase in the signal of free NA at neutral and basic pH could be due to the occurrence of the NA-H species, also predicted to occur *in silico*, which would give in ESI/MS the same signal than NA. No software simulation could be carried out for Cd(II)-NA, because the stability constant for this complex is not available.

These results indicate that the complex Fe(II)-NA could occur at the acidic pH values usually found in the xylem of the model plant species sugar beet, around 5.5 (Lopez-Millan et al., 2000), conversely to what is predicted *in silico*. The complexes Fe(III)-NA, Cu(II)-NA, Ni(II)-NA and Zn(II)-NA, would also occur at this pH, as seen by MS and predicted *in silico*. These data would support the role of NA in xylem transport of Fe(II), Fe(III), Cu(II), Ni(II) and Zn(II). A role for NA in the transport of Cu(II) and Ni(II) had already been proposed by other studies (Pich and Scholz, 1996; Mari et al., 2006). At more neutral and alkaline pH values, corresponding to the typical pHs found in the cytosol and phloem, NA would be able to complex all metals studied.

The results also show the importance of pH when establishing extraction, separation and determination methods for metal-NA complexes. To determine what are the metal species occurring in a specific plant cell compartment, the pH of that compartment should be kept as constant as possible throughout the whole extraction and determination processes. Lowering the pH could lead to the rupture of the metal-NA complexes, whereas using pH values significantly higher than those found in plant samples may lead to the formation of metal-complexes not occurring in the sample. One example of this would be the determination of Fe-NA complexes in xylem samples with an HPLC method buffered at neutral pH, which

could result in the formation of Fe(II)-NA complexes not present in the original sample.

Another issue is that organic solvent mixtures are usually employed when determining metal species with ESI/MS, and in these cases the pH values measured by using electrodes calibrated with aqueous buffers is not necessarily the true pH value. There are two possible ways of obtaining correct pH values with solvent/water mixtures. First, pH can be assessed by calibrating the pH electrode with buffers containing the organic solvent in question and then measuring the pH (s_pH) in the organic solvent-containing sample. A second option is to measure pH values after electrode calibration with the aqueous buffers (w_pH), and then calculate s_pH as ${}^w_pH - \partial$, with the coefficient ∂ being estimated by appropriate equations using the temperature value and the specific composition of the buffer (see for instance equation 12 in Gagliardi *et al.* (Gagliardi *et al.*, 2007) for acetonitrile/water buffers). In our case, using 50% acetonitrile in water and at 25 °C, the calculated s_pH values would be 0.3 pH units higher than the measured w_pH (for this particular buffer composition, ∂ has a negative value, see Gagliardi *et al.* (Gagliardi *et al.*, 2007.) This indicates that only part, but not all, of the pH discrepancy in metal-NA speciation between the experimental ESI/MS data and the *in silico* calculated values could be due to this issue. The pH difference issue should be taken into account in the development of chromatographic methods, especially if high concentrations of any organic solvent are being used. As an example, we have plotted the real pH of solvent mixture entering the column at different pH values in the method developed by Xuan *et al* (Xuan et al., 2006) (Fig. 4 in supplementary material). The percentage of acetonitrile at approximately 15 min (a retention time close to those of most metal complexes in that method) would be approximately 70%, leading to a ∂ value of approximately -0.7 units. Furthermore, the ∂ value at the beginning of the chromatographic run (in 90% acetonitrile) would be -1.9 pH units, so that metal complexes would be exposed to this pH value at the beginning of the chromatographic run.

Exchange reactions of Fe-NA complexes with metals and citrate. The signals of free NA and the metal-NA complexes (Fe(II)-NA, Fe(III)-NA, Cu(II)-NA and Zn(II)-NA) with the addition of

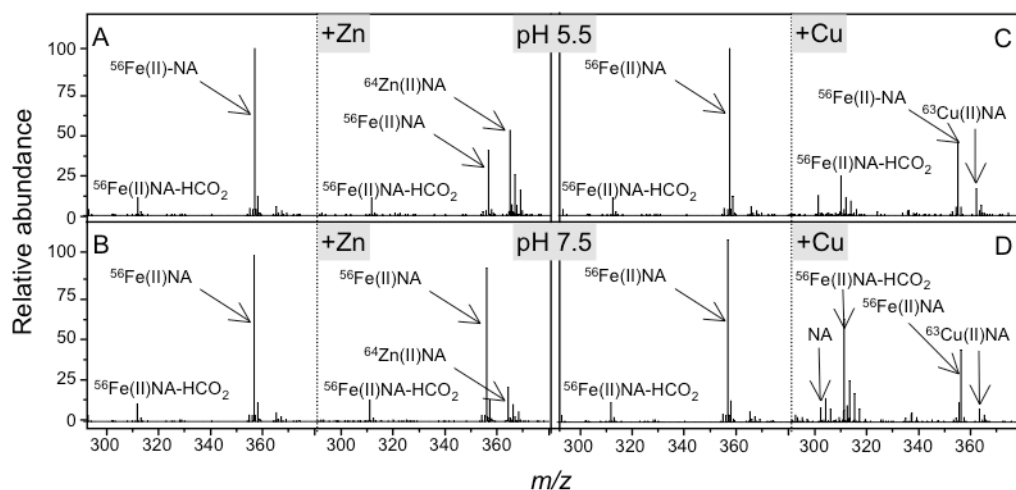


Figure 5. Metal exchange reactions between Fe(II)-NA and Zn(II) at pH 5.5 (A) and pH 7.5 (B), and between Fe(II)-NA and Cu(II) at pH 5.5 (C) and 7.5. Metal and Fe(II)-NA complex concentrations of the initial solutions were 50 μ M.

equimolar amounts of citrate, Cu or Zn, were measured. All reactions were done at two physiological relevant pH values, 5.5 as representative of xylem sap and 7.5 as representative of phloem sap.

The effect of citrate on the stability of the Fe-NA complexes was assayed at equimolar concentrations of citrate and Fe-NA. At pH 5.5, a major signal corresponding to the $[M-H]^{-1}$ ion of Fe(II)-NA can be seen in the ESI/MS spectrum (Fig. 4A, left panel), although minor signals for the $[M-H]^{-1}$ ion of free NA and the $[Fe(II)NA-HCO_2]^{-1}$ ion can also be observed. Once 50 μ M citrate is added, however, the Fe(II)-NA signal was reduced significantly and the free NA signal became approximately 4 times larger than that found in the absence of citrate (Fig. 4A, right panel). Assuming that Fe(II)-NA solutions can contain a certain amount of Fe(III)-NA produced during preparation, ligand exchange would take place with any Fe-NA complexes and not exclusively with Fe(II)-NA. *In silico* predictions indicate that the amount of Fe(II)-NA complex in these conditions would only account for a small percentage of total Fe, 1.4%, with Fe-citrate complexes accounting for 56% of total Fe, and the rest of Fe occurring as free Fe(II). No Fe-citrate complexes were observed by ESI/MS, but free citrate did show a very large signal at m/z 191 (out of the range shown in Fig. 4). Using larger concentrations of citrate produced a major inhibition in all signals, likely due to ionization interferences. With Fe(III)-NA, significant signals of the two daughter ions can be seen in

the ESI/MS spectrum at pH 5.5 (Fig. 4B, left panel), although the signal for free NA can also be observed. However, once citrate was added, the Fe(III)-NA signals almost disappeared and the NA signal became much larger than in the absence of citrate (Fig. 4C, right panel). Therefore, Fe(III)-NA seems to be more sensitive than Fe(II)-NA to the presence of citrate. Conversely, *in silico* predictions indicate that the amount of Fe(III) chelated by NA would be 33% of the total, with Fe-citrate complexes accounting for 56% of the total Fe, the rest of Fe occurring as Fe hydroxide. These results would support the current view that in the xylem, where quite large concentrations of citrate are usually present (up to the mM range),¹⁶ Fe-citrate complexes would be the major Fe species (von Wiren et al., 1999; Lopez-Millan et al., 2000). At pH 7.5, a large signal of the Fe(II)-NA complex can be seen in the ESI/MS spectrum (Fig. 4C, left panel), and no signal for free NA was observed. When citrate was added, the Fe(II)-NA complex signal was reduced but no signal of the free NA at m/z 302 was observed (Fig. 4C, right panel), suggesting that at this pH the Fe(II)-NA complex is still stable in the presence of 50 μ M citrate. Citrate ionization could negatively affect Fe(II)-NA and NA ionization, resulting in decreases in the intensities of the $[NA-H]^{-1}$ and $[Fe(III)NA-H]^{-1}$ ion signals. *In silico* predictions also indicate that the amount of Fe(II)-NA complex in these conditions would account for 94% of total Fe, with Fe-citrate complexes accounting for only 6% of total Fe. At pH 7.5, significant signals of

the two daughter ions of the Fe(III)-NA complex were seen in the ESI/MS spectrum (Fig. 4D, left panel), and the signal for free NA was also observed. Once citrate was added, one of the daughter signals (the $[\text{Fe(II)NA-HCO}_2]^{-1}$ ion) almost disappeared, whereas the other did not change much and the NA signal did not increase (Fig. 4D, right panel). This indicates that the Fe(III)-NA complex is less affected by citrate at pH 7.5 than at pH 5.5. *In silico* predictions indicated that the amount of Fe(III) chelated by NA would be 82% of the total, with Fe-citrate complexes being practically absent. It should be taken into account that the citrate:Fe ratios in sap could be much higher than 1:1 (in some cases as high as 2000:1) (Abadia et al., 2002), and therefore the real effects of citrate could be much more extreme than those found here. Metal exchange reactions between Fe(II)-NA, Zn(II) and Cu(II) were also studied. At pH 5.5, the only major signal found with Fe(II)-NA was the one corresponding to the $[\text{M-H}]^{-1}$ ion (Fig. 5A, left panel). After addition of Zn(II), a good signal for the Zn(II)-NA complex was observed, whereas the signal of the Fe(II)-NA complex was reduced to values lower than that of Zn(II)-NA (Fig. 5A, right panel), indicating a rapid metal exchange in agreement with the stability constant values of these complexes (15.4 for Zn(II) and 12.8 for Fe(II)). At pH 7.5 (Fig. 5B) the Fe(II)-NA complex seems to be quite stable in the presence of Zn(II), since only a small signal for the Zn(II)-NA complex was observed while the Fe(II)-NA signal was little decreased. *In silico* predictions, however, indicate that most of the NA should be chelating Zn(II) at both pH values. Possibly, the discrepancies between the observed speciation and the *in silico* predictions could be due to the kinetics of the exchange reaction. At pH 5.5, after the addition of Cu(II) to the Fe(II)-NA solution there was a large decrease of the Fe(II)-NA signal, although the signal of Cu(II)-NA was not very large (Fig. 5C). This supports the existence of metal exchange, as it could be expected from the values of the stability constants. The low intensity of the Cu(II)-NA complex can be explained by the voltage value used in the experiment (120 V), since the optimal voltage value found for the Cu(II) complex was 90V (Fig. I in supplementary material). Also, signals for free NA and the $[\text{M-H-CO}_2]^{-1}$ ion of Fe(II)-NA were observed. At pH 7.5 a similar behaviour was observed, although the peak at

m/z 311 corresponding to the $[\text{Fe(II)NA-H-CO}_2]^{-1}$ ion was larger than at pH 5.5 (Fig. 5D). *In silico* predictions indicate that most of the NA should be chelating Cu(II) at both pH values.

Conclusions

Results indicate that relatively small changes in pH and changes in the concentrations of citrate and metals can have significant effects in NA speciation in plant fluids such as xylem and phloem sap. In the xylem sap, NA is not likely to complex Fe due to exchange reactions with citrate and other metals, whereas it could chelate other metals such as Cu and Ni. In the phloem sap, NA could still be a good candidate to chelate Fe, specially in the Fe(II) form. Some metal-NA complexes, including Fe(II)-NA and Fe(III)-NA, were found by ESI/MS at lower pH values than those estimated *in silico*, and this effect could be only partially explained by the estimated size of the errors associated to measuring pH in organic solvent-containing solutions. Our work and recent examples of other researchers have shown the feasibility of ESI/MS to study metal-NA complexes within plant fluids, but some drawbacks inherent to the technique need to be addressed: namely, the need to maintain as much as possible the pH of the plant compartment under study through the whole extraction, separation and analysis process, the possible changes in metal-ligand complex chemistry and the difficulty to assess the true pH value in solutions with a considerable amount of organic solvent, and the possibility that metal redox reactions may occur in the ESI process. Our work has also shown that *in silico* predictions may fail to accurately speciate NA in non-equilibrium solutions such as plant fluids. It should also be mentioned that in real plant samples other metals such as Ca and ligands such as glutathione may affect the interpretations proposed here. But it would be unrealistic to analyze plant fluids by direct infusion ESI/MS due to matrix effects. To avoid matrix interferences a previous separation technique such as liquid chromatography is mandatory. Direct determination of metal-NA complexes in plant fluids may change the current knowledge on the role of NA in plant nutrition.

Acknowledgements

This work was funded by AGL2004-00194 and AGL2007-61948 grants from the Spanish Ministry of Education and Science (MEC; co-

financed with FEDER) to J.A. R.R-A. was supported by a FPI fellowship from the Spanish MEC. Acquisition of the HPLC-TOFMS system was co-financed with FEDER.

References

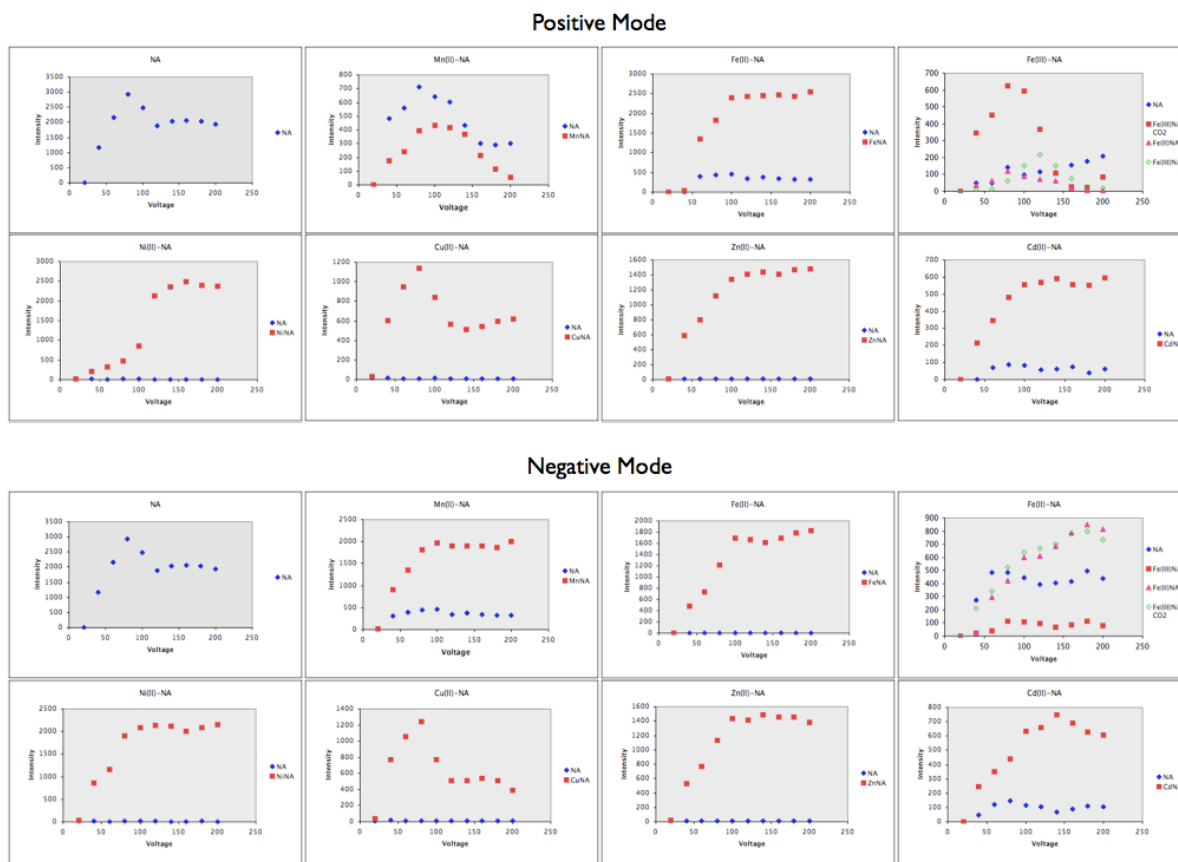
- Abadia J, Lopez-Millan A, Rombola A, Abadia A** (2002) Organic acids and Fe deficiency: a review. *Plant Soil* **241**: 75-86
- Anderegg G, Ripperger H** (1989) The normalizing factor for the tomato mutant *chloronerva*. 29. Correlation between metal-complex formation and biological activity of nicotianamine analogs. *J. Chem. Soc. Chem. Commun.* **14**: 647-650
- Benes I, Schreiber K, Ripperger H, Kircheiss A** (1983) On the normalizing factor for the tomato mutant *chloronerva*. 13. Metal complex formation by nicotianamine, a possible phytosiderophore. *Experientia* **39**: 261-262
- Blades AT, Ikonomou MG, Kebarle P** (1991) Mechanisms of electrospray-mass-spectrometry – Electrospray as an electrolysis cell. *Anal. Chem.* **63**: 2109-2114
- Douchkov D, Gryczka C, Stephan UW, Hell R, Baumlein H** (2005) Ectopic expression of nicotianamine synthase genes results in improved iron accumulation and increased nickel tolerance in transgenic tobacco. *Plant. Cell Environ.* **28**: 365-374
- Durrett TP, Gassmann W, Rogers EE** (2007) The FRD3-Mediated Efflux of Citrate into the Root Vasculature Is Necessary for Efficient Iron Translocation. *Plant Physiol.* **144**: 197-205
- Gagliardi LG, Castells CB, Rafols C, Roses M, Bosch E** (2007) delta Conversion parameter between pH scales ((s)(w)pH and (s)(s)pH) in acetonitrile/water mixtures at various compositions and temperatures. *Anal. Chem.* **79**: 3180-3187
- Gagliardi LG, Castells CB, Rafols C, Roses M, Bosch E** (2007) Static dielectric constants of acetonitrile/water mixtures at different temperatures and Debye-Huckel A and a(0)B parameters for activity coefficients. *J. Chem. Eng. Data* **52**: 1103-1107
- Hall JL** (2002) Cellular mechanisms for heavy metal detoxification and tolerance. *J. Exp. Bot* **53**: 1-11
- Hell R, Stephan UW** (2003) Iron uptake, trafficking and homeostasis in plants. *Planta* **216**: 541-551
- Herbik A, Giritch A, Horstmann C, Becker R, Balzer HJ, Baumlein H, Stephan UW** (1996) Iron and copper nutrition-dependent changes in protein expression in a tomato wild type and the nicotianamine-free mutant *chloronerva*. *Plant Physiol.* **111**: 533-540
- Herbik A, Koch G, Mock HP, Dushkov D, Czihal A, Thielmann J, Stephan UW, Baumlein H** (1999) Isolation, characterization and cDNA cloning of nicotianamine synthase from barley - A key enzyme for iron homeostasis in plants. *Eur. J. Biochem.* **265**: 231-239
- Hider RC, Yoshimura E, Khodr H, von Wiren N** (2004) Competition or complementation: the iron-chelating abilities of nicotianamine and phytosiderophores. *New Phytol.* **164**: 204-208
- Higuchi K, Suzuki K, Nakanishi H, Yamaguchi H, Nishizawa NK, Mori S** (1999) Cloning of nicotianamine synthase genes, novel genes involved in the biosynthesis of phytosiderophores. *Plant Physiol.* **119**: 471-479
- Kim S, Takahashi M, Higuchi K, Tsunoda K, Nakanishi H, Yoshimura E, Mori S, Nishizawa NK** (2005) Increased nicotianamine biosynthesis confers enhanced tolerance of high levels of metals, in particular nickel, to plants. *Plant Cell Physiol.* **46**: 1809-1818
- Koike S, Inoue H, Mizuno D, Takahashi M, Nakanishi H, Mori S, Nishizawa NK** (2004) OsYSL2 is a rice metal-nicotianamine transporter that is regulated by iron and expressed in the phloem. *Plant J.* **39**: 415-424
- Kruger C, Berkowitz O, Stephan UW, Hell R** (2002) A metal-binding member of the late embryogenesis abundant protein family transports iron in the phloem of *Ricinus communis* L. *J. Biol. Chem.* **277**: 25062-25069

- Ling HQ, Koch G, Baumlein H, Ganai MW** (1999) Map-based cloning of *chloronerva*, a gene involved in iron uptake of higher plants encoding nicotianamine synthase. *Proc. Natl. Acad. Sci. USA* **96**: 7098-7103
- Liu DH, Adler K, Stephan UW** (1998) Iron-containing particles accumulate in organelles and vacuoles of leaf and root cells in the nicotianamine-free tomato mutant *chloronerva*. *Protoplasma* **201**: 213-220
- Lopez-Millan AF, Morales F, Abadia A, Abadia J** (2000) Effects of iron deficiency on the composition of the leaf apoplastic fluid and xylem sap in sugar beet. Implications for iron and carbon transport. *Plant Physiol.* **124**: 873-884
- Maas FM, Vandewetering DAM, Vanbeusichem ML, Bienfait HF** (1988) Characterization of phloem iron and its possible role in the regulation of Fe-efficiency reactions. *Plant Physiol.* **87**: 167-171
- Mari S, Gendre D, Pianelli K, Ouerdane L, Lobinski R, Briat JF, Lebrun M, Czernic P** (2006) Root-to-shoot long-distance circulation of nicotianamine and nicotianamine-nickel chelates in the metal hyperaccumulator *Thlaspi caerulescens*. *J. Exp. Bot* **57**: 4111-4122
- Martell AE SR** (1974) Critical stability constants. Plenum, New York
- Neubert H, Hider RC, Cowan DA** (2002) Speciation of Fe(III)-chelate complexes by electrospray ionization ion trap and laser desorption/ionization Fourier transform ion cyclotron resonance mass spectrometry. *Rap. Commun. Mass Spectrom.* **16**: 1556-1561
- Noma M, Noguchi M, Tamaki E** (1971) New amino acid nicotianamine, from tobacco leaves. *Tetrahedron Lett.* **15**: 2017-2024
- Ouerdane L, Mari S, Czernic P, Lebrun M, Lobinski R** (2006) Speciation of non-covalent nickel species in plant tissue extracts by electrospray Q-TOFMS/MS after their isolation by 2D size exclusion-hydrophilic interaction LC (SEC-HILIC) monitored by ICP-MS. *J. Anal. Atom. Spectrom.* **21**: 676-683
- Pecoraro V, Bonadies JA, Marrese CA, Carrano CJ** (1984) Stepwise metal-assisted oxidative decarboxylation of Vanadium (V) ethylene bis (ortho-hydroxyphenyl)glycine) – Isolation of a possible intermediate. *J. Am. Chem. Soc.* **106**: 3360-3362
- Pianelli K, Mari S, Marques L, Lebrun M, Czernic P** (2005) Nicotianamine over-accumulation confers resistance to nickel in *Arabidopsis thaliana*. *Transgen. Res.* **14**: 739-748
- Pich A, Scholz G** (1996) Translocation of copper and other micronutrients in tomato plants (*Lycopersicon esculentum* Mill): Nicotianamine-stimulated copper transport in the xylem. *J. Exp. Bot.* **47**: 41-47
- Pich A, Scholz G, Stephan UW** (1994) Iron-dependent changes of heavy-metals, nicotianamine, and citrate in different plant organs and in the xylem exudate of 2 tomato genotypes - Nicotianamine as possible copper translocator. *Plant Soil* **165**: 189-196
- Roberts LA, Pierson AJ, Panaviene Z, Walker EL** (2004) Yellow stripe1. Expanded roles for the maize iron-phytosiderophore transporter. *Plant Physiol.* **135**: 112-120
- Schaaf G, Schikora A, Haberle J, Vert G, Ludewig U, Briat JF, Curie C, von Wiren N** (2005) A putative function for the Arabidopsis Fe-phytosiderophore transporter homolog AtYSL2 in Fe and Zn homeostasis. *Plant Cell Physiol.* **46**: 762-774
- Schaumloffel D, Ouerdane L, Bouyssiere B, Lobinski R** (2003) Speciation analysis of nickel in the latex of a hyperaccumulating tree *Sebertia acuminata* by HPLC and CZE with ICP MS and electrospray MS-MS detection. *J Anal. Atom. Spectrom.* **18**: 120-127
- Schmidke I, Kruger C, Frommichen R, Scholz G, Stephan UW** (1999) Phloem loading and transport characteristics of iron in interaction with plant-endogenous ligands in castor bean seedlings. *Physiol. Plant.* **106**: 82-89
- Scholz G, Becker R, Pich A, Stephan UW** (1992) Nicotianamine - A common constituent of Strategy I and Strategy II of iron acquisition by plants – A review. *J. Plant. Nutr.* **15**: 1647-1665

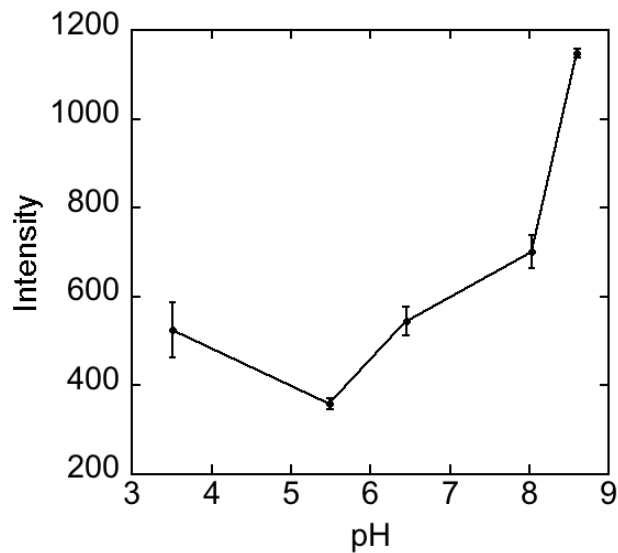
- Stephan UW, Schmidke I, Stephan VW, Scholz G** (1996) The nicotianamine molecule is made-to-measure for complexation of metal micronutrients in plants. *Biometals* **9**: 84-90
- Stephan UW, Scholz G** (1990) The normalizing factor for the tomato mutant *chloronerva*. 38. Nicotianamine, concentrations in iron sufficient and deficient sunflower and barley roots. *J Plant. Physiol.* **136**: 631-634
- Stephan UW, Scholz G** (1993) Nicotianamine – mediator of transport of iron and heavy metals in the phloem. *Physiol. Plant.* **88**: 522-529
- Takahashi M, Terada Y, Nakai I, Nakanishi H, Yoshimura E, Mori S, Nishizawa NK** (2003) Role of nicotianamine in the intracellular delivery of metals and plant reproductive development. *Plant Cell* **15**: 1263-1280
- Tiffin LO** (1966) Iron translocation. I. Plant culture exudate sampling iron-citrate analysis. *Plant Physiol.* **41**: 510-&
- Vacchina V, Mari S, Czernic P, Marques L, Pianelli K, Schaumlöffel D, Lebrun M, Lobinski R** (2003) Speciation of nickel in a hyperaccumulating plant by high-performance liquid chromatography-inductively coupled plasma mass spectrometry and electrospray MS/MS assisted by cloning using yeast complementation. *Anal. Chem.* **75**: 2740-2745
- von Wiren N, Klair S, Bansal S, Briat JF, Khodr H, Shioiri T, Leigh RA, Hider RC** (1999) Nicotianamine chelates both Fe-III and Fe-II. Implications for metal transport in plants. *Plant Physiol.* **119**: 1107-1114
- Wang HJ, Agnes GR** (1999) Kinetically labile equilibrium shifts induced by the electrospray process. *Anal. Chem.* **71**: 4166-4172
- Weber G, von Wiren N, Hayen H** (2006) Analysis of iron (II)/iron(III) phytosiderophore complexes by nano-electrospray ionization Fourier transform ion cyclotron resonance mass spectrometry. *Rap. Commun. Mass Spectrom.* **20**: 973-980
- Weber M, Harada E, Vess C, von Roepenack-Lahaye E, Clemens S** (2004) Comparative microarray analysis of *Arabidopsis thaliana* and *Arabidopsis halleri* roots identifies nicotianamine synthase, a ZIP transporter and other genes as potential metal hyperaccumulation factors. *Plant J.* **37**: 269-281
- Xuan Y, Scheuermann EB, Meda AR, Hayen H, von Wiren N, Weber G** (2006) Separation and identification of phytosiderophores and their metal complexes in plants by zwitterionic hydrophilic interaction liquid chromatography coupled to electrospray ionization mass spectrometry. *J. Chrom. A* **1136**: 73-81

SUPPLEMENTARY MATERIALS

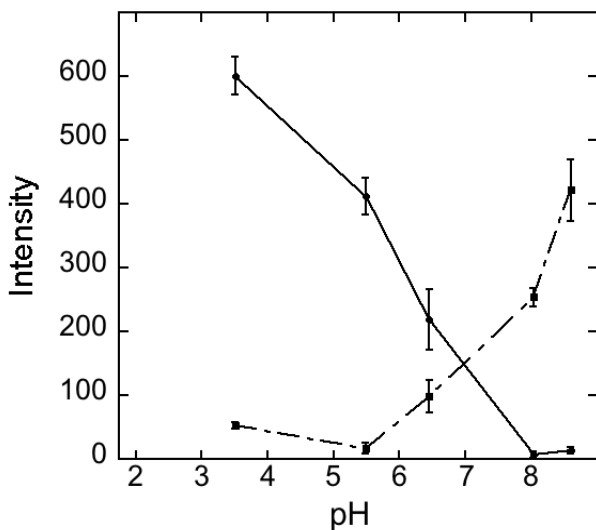
Supplementary Figure 1. Ionization of the different metal-NA complexes at between 20 and 200 V in negative and positive ion modes. Both modes were done at a drying gas temperature of 200 °C



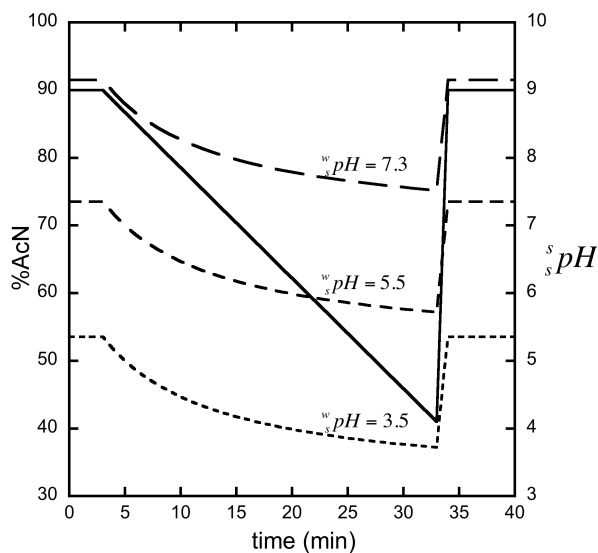
Supplementary Figure 2. ESI/MS pH dependence of NA. Capillary voltage used was 90 V. The rest of parameters were the same described in the text for the rest metal-NA complexes.



Supplementary Figure 3. ESI/MS pH dependence of Cd-NA. parameters were the same described in the text for the rest metal-NA complexes.



Supplementary Figure 4. pH corrected values of acetonitrile/water mixture in a typical HILIC chromatographic run. Values in the graphic correspond to the initial $s w pH$ values. pH axis is in the $s s pH$ scale. $s w pH$ values were transformed to $s s pH$ values with equation 1 after calculation of δ with equation 2.



**IDENTIFICATION OF A TRI-IRON(III), TRI-CITRATE COMPLEX IN THE XYLEM
SAP OF IRON-DEFICIENT TOMATO RESUPPLIED WITH IRON: NEW INSIGHTS
INTO PLANT IRON LONG-DISTANCE TRANSPORT**

**Rubén Rellán-Álvarez¹, Justo Giner-Martínez-Sierra², Jesús Orduna³, Irene Orera¹, José
Ángel Rodríguez-Castrillón², José Ignacio García-Alonso², Javier Abadía¹ and Ana Álvarez-
Fernández¹**

Plant & Cell Physiology, 2010 51: 91-102

¹Department of Plant Nutrition, Aula Dei Experimental Station, CSIC, P.O. Box 13034, E-50080 Zaragoza, Spain. ²Department of Physical and Analytical Chemistry, University of Oviedo, c/ Julian Clavería 8, E-33006 Oviedo, Spain, ³New Organic Materials Unit, Institute of Materials Science of Aragón, CSIC-University of Zaragoza, c/ Pedro Cerbuna 12, E-50009 Zaragoza, Spain.

IDENTIFICATION OF A TRI-IRON(III), TRI-CITRATE COMPLEX IN THE XYLEM SAP OF IRON-DEFICIENT TOMATO RESUPPLIED WITH IRON: NEW INSIGHTS INTO PLANT IRON LONG-DISTANCE TRANSPORT

Rubén Rellán-Álvarez¹, Justo Giner-Martínez-Sierra², Jesús Orduna³, Irene Orera¹, José Ángel Rodríguez-Castrillón², José Ignacio García-Alonso², Javier Abadía¹ and Ana Álvarez-Fernández¹

¹Department of Plant Nutrition, Aula Dei Experimental Station, CSIC, P.O. Box 13034, E-50080 Zaragoza, Spain. ²Department of Physical and Analytical Chemistry, University of Oviedo, c/ Julian Clavería 8, E-33006 Oviedo, Spain, ³New Organic Materials Unit, Institute of Materials Science of Aragón, CSIC-University of Zaragoza, c/ Pedro Cerbuna 12, E-50009 Zaragoza, Spain

The identification of the Fe transport forms in the plant xylem sap is crucial to understand long-distance Fe transport processes in plants. Previous studies have proposed that Fe may be transported as an Fe-citrate complex in plant xylem sap, but such a complex has never been detected. In this study we report the first direct and unequivocal identification of a natural Fe complex in plant xylem sap. A tri-Fe(III), tri-citrate complex (Fe₃Cit₃) was found in the xylem sap of Fe-deficient tomato (*Solanum lycopersicum* Mill. cv. 'Tres Cantos') resupplied with Fe, by using an integrated mass spectrometry approach based on exact molecular mass, isotopic signature and Fe determination and retention time. This complex has been modeled as having an oxo-bridged tri-Fe core. A second complex, a di-Fe(III), di-citrate complex was also detected in Fe-citrate standards along with Fe₃Cit₃, with the allocation of Fe between the two complexes depending on the Fe to citrate ratio. These results provide evidence for Fe-citrate complex xylem transport in plants. The consequences for the role of Fe to citrate ratio in long-distance transport of Fe in xylem are also discussed.

Introduction

The mechanisms of long-distance Fe transport in plants have remained elusive until now. In the case of the xylem sap, Fe is assumed to be transported as complexed forms, because free ionic forms (Fe(II) and Fe(III)) can be toxic and are also prone to undergo precipitation at the neutral or slightly acidic pH values typical of the xylem sap. Increases in carboxylate concentrations in plant xylem exudates with Fe deficiency were reported in several papers published in the 1960s by Brown and co-workers. Iron was first suggested to be transported bound

with malate (Tiffin and Brown 1962), but later citrate (Cit), which also increases markedly in stem exudates of many plant species when Fe-deficient (Brown 1966) and co-migrates with Fe during paper-electrophoresis (Clark et al. 1973; Tiffin 1966a, b, 1970), was considered the most likely candidate for Fe transport.

The identity of Fe-Cit complexes in the xylem sap has only been hypothesized by means of in silico calculations using total concentrations of possible Fe complexing agents (including carboxylates) and Fe, and the known stability constants of Fe-containing complexes, always assuming that chemical equilibrium was achieved. Using this approach, several Fe-Cit species were predicted to be the most abundant Fe-complexes in the xylem sap whereas other potential plant metal chelators such as nicotianamine (NA) were ruled out (Rellán-Álvarez et al. 2008; von Wirén et al. 1999) as possible xylem Fe carriers. NA function as an Fe chelator might be restricted to the cytoplasm and in Fe phloem loading (Curie et al. 2008). Citrate has been recently found to play a role in long-distance Fe transport by using molecular biology techniques. Xylem sap loading of Cit is seriously disrupted in two mutants, AtFRD3 (Durrett et al. 2007) and OsFRDL1 (Yokosho et al. 2009). These mutants display increased Fe-deficiency symptoms that have been associated to a decreased efficiency of Fe translocation into the root vasculature.

The Fe-Cit chemistry in aqueous solutions is very complex and a large number of chemical species may occur, depending on many factors (Gautier-Luneau et al. 2005; Pierre and Gautier-Luneau 2000; Spiro et al. 1967a; Spiro et al. 1967b). A direct proof of the presence of Fe-Cit complexes in xylem sap has not been obtained so far. Difficulties in detecting Fe-Cit species in xylem sap may arise because of different reasons.

First, both pH and Fe:Cit ratio values are known to affect markedly Fe-Cit speciation in standard aqueous solutions (Gautier-Luneau et al. 2005). Therefore, when analysis is carried out at pH values too acidic or basic (e.g., during High Performance Liquid Chromatography -HPLC-), the speciation of Fe-Cit complexes could change and species occurring in the original xylem sample may be no longer present after chromatography. Second, analytical techniques such as mass spectrometry (MS), which have been used successfully to identify other metal complexes in the xylem sap (Ouerdane et al. 2006; Xuan et al. 2006), usually involve ionization steps (with high temperatures and voltages) that may be too harsh for relatively labile compounds such as Fe-Cit complexes. Furthermore, in most plant species the total Fe concentration in the xylem sap is in the μM range, and consequently the concentrations of the possible Fe-Cit complexes are expected to be very low.

Molecular biology approaches have provided a breadth of information about metal, metal chelator and metal complex transporters (Briat et al. 2007; Kim and Guerinot 2007; Palmer and Guerinot 2009). However, the elucidation of the molecular identity of metal complexes in plant compartments is still one of the biggest challenges in plant metal transport (Hider et al. 2004). The molecular identification of metal complexes has been tackled by two different types of techniques. First, the use of highly selective and sensitive molecular and metal specific techniques such as integrated mass spectrometry (Meija et al. 2006) has been used (Ouerdane et al. 2006; Xuan et al. 2006), specially in plant fluids (e.g. xylem or phloem) where direct analysis can be carried out. Second, X-ray absorption spectroscopy -EXAFS and XANES (Küpper et al. 2004; Sarret et al. 2002) and synchrotron X-ray fluorescence (SXRF) (Punshon et al. 2009) techniques have been applied to study metal speciation in some plant materials. The combination of metal complex elucidation techniques and molecular biology approaches should give a better picture of plant metal transport.

In this study we have used HPLC coupled to Electrospray Time Of Flight Mass Spectrometry (HPLC-ESI-TOFMS) and Inductively Coupled Plasma Mass Spectrometry (HPLC-ICP-MS) to detect naturally occurring Fe-complexes in xylem

sap. Analysis conditions were kept as conservative as possible in order to maintain unaltered natural Fe species occurring in the xylem sap. With this approach we have successfully identified a tri-Fe(III), tri-citrate complex (Fe_3Cit_3) in the xylem sap of Fe-deficient tomato plants after short-term Fe resupply. This complex has been modeled as an oxo-bridged tri-Fe(III) tri-Cit complex. A second Fe-Cit complex, the binuclear Fe(III)-Cit species Fe_2Cit_2 , was only detected in Fe-Cit standard solutions along with the Fe_3Cit_3 complex, with the balance between the two complexes depending on the Fe:Cit ratio.

Results

Analysis of Fe-Cit standard solutions by integrated mass spectrometry. A method to separate and identify Fe-Cit complexes was developed by analyzing Fe-Cit solutions with Fe and Cit concentrations, Fe:Cit ratios and pH values typical of xylem sap (5.5), using HPLC and integrated mass spectrometry (ESI-TOFMS and ICP-MS). In all experiments, ESI-TOFMS spectra were searched for any molecular ion having the characteristic Fe isotopic signatures, including molecular ions previously detected by ESI-MS in high concentration Fe-Cit solutions (100 mM Fe:1 M Cit) (Gautier-Luneau et al. 2005). The four different Fe stable isotopes were determined in the HPLC-ICP-MS runs. The method to determine Fe-Cit complexes was designed by optimizing first the electrospray ionization conditions, and then developing appropriate HPLC separation conditions. Throughout this study we used ^{54}Fe , ^{57}Fe and ^{nat}Fe , the latter being Fe with the natural isotopic composition: 5.85, 91.75, 2.12 and 0.28% of ^{54}Fe , ^{56}Fe , ^{57}Fe and ^{58}Fe , respectively. Electrospray ionization conditions for Fe-Cit complexes were optimized to avoid in-source fragmentation using direct injection of a 1:10 ^{nat}Fe -Cit solution (100 μM ^{nat}Fe). Optimal ESI values for capillary exit, skimmer 1, and hexapole RF voltages were -57.1, -39.1 and 145.2 V, respectively. These values correspond to softer ESI conditions than those usually applied to low molecular weight analytes (in the 100-600 m/z range). In all conditions tested, citrate gave a strong signal at the $[\text{CitH}]^-$ mass-to-charge ratio (m/z) of 191.0 (Supplementary Fig. 1A and B; see inset for isotopic signature). With these soft conditions, a 10-fold increase in ionization efficiency was

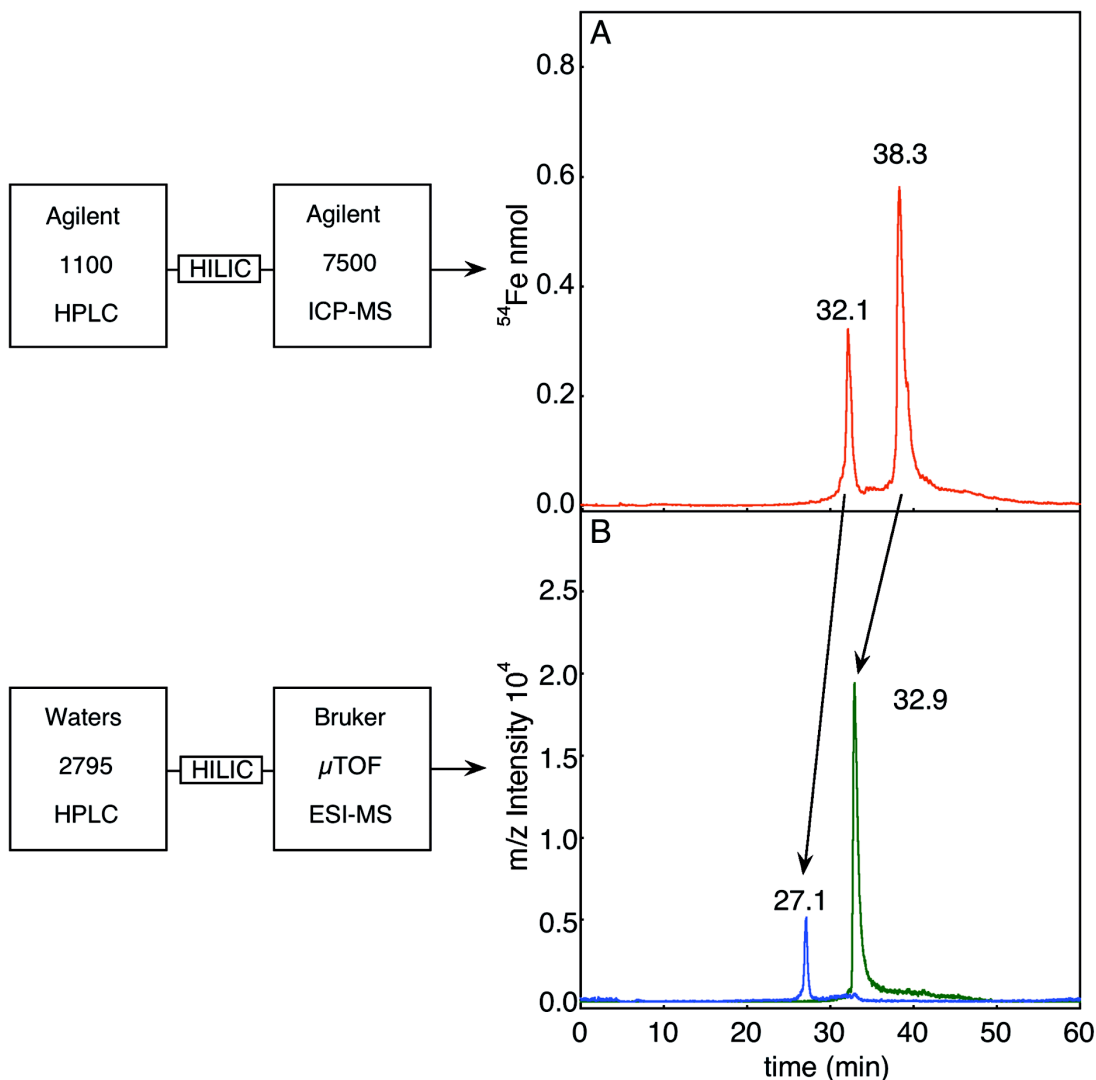


Figure 1. HPLC-ICP-MS (A) and HPLC-ESI-TOFMS (B) chromatograms of a ^{54}Fe -Cit standard solution (Fe:Cit ratio 1:10, $100\ \mu\text{M}$ ^{54}Fe , pH 5.5, in 50% mobile phase B) showing peaks corresponding to Fe complexes. HPLC-ESI-TOFMS traces (B) are the sum of molecular ions at m/z values 241.93 and 484.87 (± 0.05 ; blue line) and 363.40 and 372.40 (± 0.05 ; green line).

achieved for a m/z 366.4 signal that showed the characteristic isotopic signature of a double charged, 3 Fe atom-containing molecular ion. This signal can be assigned to the $[\text{Fe}(\text{III})_3\text{Cit}_3\text{H}]^{2-}$ molecular ion (Supplementary Fig. 1A and B; see inset for isotopic signature). Furthermore, a second molecular ion with the characteristic isotopic signature of a double charged, 3 Fe atom-containing molecular ion was detected at m/z 375.4 (Supplementary Fig. 1B; see inset for isotopic signature). This signal can be assigned to the $[\text{Fe}(\text{III})_3\text{OCit}_3\text{H}_3]^{2-}$ ion. The 9 m/z difference with $[\text{Fe}(\text{III})_3\text{Cit}_3\text{H}]^{2-}$ was assigned to correspond to a labile ligand such as aquo OH_2 , hydroxo OH , or oxo O^{2-} (Gautier-Luneau et al. 2005). Both Fe-Cit molecular ions were

previously reported to occur at neutral pH values and at similar Fe:Cit ratios (Gautier-Luneau et al. 2005). The relative intensities of the different peaks did not match those found by Gautier-Luneau et al. (2005), probably due to differences in MS devices and solution pH values (at least one pH unit of difference). Conversely, signals at m/z 300.4 and 271.9 appeared under standard ESI conditions (Supplementary Fig. 1A) but they were significantly reduced after ESI optimization (Supplementary Fig. 1B), suggesting that they may correspond to in-source fragmentation products (mainly due to decarboxylation processes, very common in these kind of compounds) of the Fe_3Cit_3 produced at higher voltage values.

HPLC separation conditions were also optimized to obtain a good separation of the Fe-Cit complexes from other matrix components (*e.g.* Cit) that could interfere in the ESI process. The range of HPLC options available was limited, since: i) both Cit and Fe-Cit complexes are compounds with a high polarity; ii) it is mandatory to maintain during chromatography xylem sap typical pH values, and iii) the method must be suitable for ESI-TOFMS and ICP-MS detection. Different approaches, including several column types, elution programs and eluents – acetonitrile and methanol- were tested. The best results were obtained with a zwitterionic hydrophilic interaction column (ZIC®-HILIC, Sequant, Sweden), previously used to separate polar Fe-compounds such as Fe(II)-NA, Fe(III)-deoxymugineic acid (Fe(III)-DMA) and others (Xuan et al. 2006). Two parallel systems, a HPLC-ICP-MS and a HPLC-ESI-TOFMS, were used to gain knowledge about atomic and molecular identity, respectively. Experiments were carried out with ^{54}Fe -Cit and also with ^{nat}Fe -Cit.

HPLC-ICP-MS experiments were carried out using ^{54}Fe -Cit solutions (100 μM ^{54}Fe :1 mM Cit) to avoid ^{nat}Fe background from the HPLC system, which could be significant when determining very low concentrations of Fe by ICP-MS. Iron-54 molar flow chromatograms showed only two well defined Fe peaks at 32.1 and 38.3 min (Fig. 1A) that were also observed using UV detection (Supplementary Fig. 2A). Using ESI-TOFMS detection, only four molecular ions with characteristic ^{54}Fe isotopic signatures (see below for identification) were found in the chromatogram, two of them at 27.1 min (241.9 and 484.9 m/z) and two more at 32.9 min (363.4 and 372.4 m/z) (Fig. 1B), and an UV signal was also found for these peaks (Supplementary Fig. 2B). The 5-min differences in retention time between HPLC-ESI-TOFMS and HPLC-ICP-MS analyses are due to the different HPLC devices used (Waters and Agilent, respectively), as judged by the shift in UV detection traces (Supplementary Fig. 2). A 5 mM Cit solution was also injected and no Fe-Cit complexes were found in the HPLC-ESI-TOFMS chromatogram, indicating that complexes found were not formed *de novo* during the chromatographic run. With this HPLC method a complete separation of Fe-Cit complexes from Cit was reached, since Cit eluted as a broad peak at 5-9 min (m/z trace at

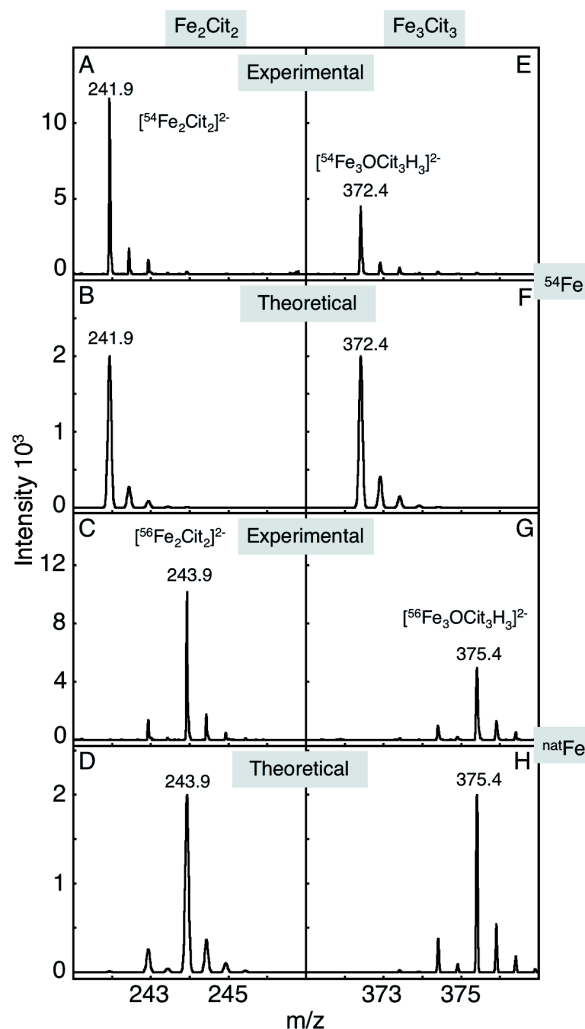


Figure 2. Experimental (A, C, E and G) and theoretical (B, D, F and H) isotopic signatures of the molecular ions associated to Fe_2Cit_2 and Fe_3Cit_3 , $[\text{Fe}_2\text{Cit}_2]^{2-}$ and $[\text{Fe}_3\text{OCit}_3\text{H}_3]^{2-}$, respectively. Experimental data are zoomed ESI-TOF mass spectra of the Fe_2Cit_2 and Fe_3Cit_3 chromatographic peaks found when using ^{54}Fe (A, E) and ^{nat}Fe (C, G).

191.1, not included in Fig. 1B; Supplementary Fig. 3A). Other Fe-complexes putatively occurring in plant tissues, such as Fe(III)-NA and Fe(III)-DMA, elute at retention times lower than 20 min (Supplementary Fig. 3B and C).

Identification of an Fe_2Cit_2 complex in Fe-citrate standard solutions. When using ^{54}Fe -Cit, the Fe peak at 27.1 min in HPLC-ESI-TOFMS showed signals at m/z 241.9 and 484.9 (Fig. 1B), with Fe isotopic signatures characteristic of 2 ^{54}Fe atom-containing molecular ions, the first double charged (Fig. 2A, Table I) and the second single charged (Supplementary Fig. 4A). Based on these exact mass and isotopic pattern data, the

Table I. Experimental ESI-TOFMS molecular ion data and parameters used to identify the molecular formulae of the Fe-Cit complexes in standard solutions and tomato xylem sap.

Measured m/z	$^{56}\text{Fe}/^{54}\text{Fe}$ (Fe atoms) ^a	Charge ^b	Molecular formula	Calculated m/z	Error m/z (ppm)	SigmaFit TM value	Molecular ion
Standard solutions							
241.9362	-	-2	$^{54}\text{Fe}_2\text{C}_{12}\text{H}_8\text{O}_{14}$	241.9359	2.1	0.0234	$[\text{}^{54}\text{Fe}_2\text{Cit}_2]^{2-}$
484.8781	-	-1	$^{54}\text{Fe}_2\text{C}_{12}\text{H}_9\text{O}_{14}$	484.8790	1.8	0.0157	$[\text{}^{54}\text{Fe}_2\text{Cit}_2\text{H}]^-$
372.4119	-	-2	$^{54}\text{Fe}_3\text{C}_{18}\text{H}_{13}\text{O}_{21}$	372.4127	2.3	0.0273	$[\text{}^{54}\text{Fe}_3\text{Cit}_3\text{H}]^{2-}$
363.4068	-	-2	$^{54}\text{Fe}_3\text{C}_{18}\text{H}_{15}\text{O}_{22}$	363.4074	1.4	0.0106	$[\text{}^{54}\text{Fe}_3\text{OCit}_3\text{H}_3]^{2-}$
243.9311	7.4 (2)	-2	$\text{}^{\text{nat}}\text{Fe}_2\text{C}_{12}\text{H}_8\text{O}_{14}$	243.9311	1.7	0.0165	$[\text{}^{\text{nat}}\text{Fe}_2\text{Cit}_2]^{2-}$
488.8705	7.1 (2)	-1	$\text{}^{\text{nat}}\text{Fe}_2\text{C}_{12}\text{H}_9\text{O}_{14}$	488.8696	2.6	0.0214	$[\text{}^{\text{nat}}\text{Fe}_2\text{Cit}_2\text{H}]^-$
375.4047	5.2 (3)	-2	$\text{}^{\text{nat}}\text{Fe}_3\text{C}_{18}\text{H}_{15}\text{O}_{22}$	375.4057	1.7	0.0284	$[\text{}^{\text{nat}}\text{Fe}_3\text{OCit}_3\text{H}_3]^{2-}$
366.3994	5.2 (3)	-2	$\text{}^{\text{nat}}\text{Fe}_3\text{C}_{18}\text{H}_{13}\text{O}_{21}$	366.4004	2.0	0.0294	$[\text{}^{\text{nat}}\text{Fe}_3\text{Cit}_3\text{H}]^{2-}$
Xylem sap							
372.4097	-	-2	$^{54}\text{Fe}_3\text{C}_{18}\text{H}_{15}\text{O}_{22}$	372.4057	8.2	0.0283	$[\text{}^{54}\text{Fe}_3\text{OCit}_3\text{H}_3]^{2-}$
375.4045	5.56 (3)	-2	$\text{}^{\text{nat}}\text{Fe}_3\text{C}_{18}\text{H}_{15}\text{O}_{22}$	375.4057	6.8	0.0197	$[\text{}^{\text{nat}}\text{Fe}_3\text{OCit}_3\text{H}_3]^{2-}$

Sigma FitTM algorithm (Ojanperä et al. 2006) proposed $^{54}\text{Fe}_2\text{C}_{12}\text{H}_8\text{O}_{14}$ and $^{54}\text{Fe}_2\text{C}_{12}\text{H}_9\text{O}_{14}$ as the most accurate formulae, corresponding to the 2 Fe-, 2 Cit- molecular ions $[\text{}^{54}\text{Fe}(\text{III})_2\text{Cit}_2]^{2-}$ and $[\text{}^{54}\text{Fe}(\text{III})_2\text{Cit}_2\text{H}]^-$, respectively (Table I); these molecular ions were previously found in concentrated Fe-Cit standards (Gautier-Luneau et al. 2005). The fit of the experimental and theoretical isotopic signatures of the $[\text{}^{54}\text{Fe}(\text{III})_2\text{Cit}_2]^{2-}$ molecular ion at m/z 241.9 is shown in Figs. 2A and B, respectively. A good fit was also found for the ion $[\text{}^{54}\text{Fe}(\text{III})_2\text{Cit}_2\text{H}]^-$ at m/z 484.9 (Supplementary Fig. 4A and B).

Further confirmation of the molecular identity of the Fe_2Cit_2 complex was obtained analyzing $\text{}^{\text{nat}}\text{Fe}$ -Cit standard solutions by HPLC-ESI-TOFMS, taking advantage of the characteristic $\text{}^{\text{nat}}\text{Fe}$ isotopic signature. The Fe peak at 27.1 min in HPLC-ESI-TOFMS showed signals at m/z 243.9 and 488.9, characteristic of 2 $\text{}^{\text{nat}}\text{Fe}$ atom-containing molecular ions, the first double charged and the second single charged (Fig. 2C, Supplementary Fig. 4C and Table I). The differences in m/z values found using ^{54}Fe and $\text{}^{\text{nat}}\text{Fe}$ (92% ^{56}Fe) were those expected for 2 Fe atom-containing molecular ions (2 and 4 m/z difference for a double and a single charged ion, respectively). The Sigma FitTM algorithm (Ojanperä et al. 2006) proposed $\text{}^{\text{nat}}\text{Fe}_2\text{C}_{12}\text{H}_{18}\text{O}_{14}$ and $\text{}^{\text{nat}}\text{Fe}_2\text{C}_{12}\text{H}_9\text{O}_{14}$ as the most accurate formulae corresponding to the molecular ions $[\text{}^{\text{nat}}\text{Fe}_2\text{Cit}_2]^{2-}$ and $[\text{}^{\text{nat}}\text{Fe}_2\text{Cit}_2\text{H}]^-$ (Table I). The fit of the experimental and theoretical isotopic signatures of the $[\text{}^{\text{nat}}\text{Fe}_2\text{Cit}_2]^{2-}$ molecular ion (for the ^{56}Fe signal at m/z 243.9) is shown in Figs. 2C and D, respectively. A good fit was also found for the molecular ion $[\text{}^{\text{nat}}\text{Fe}_2\text{Cit}_2\text{H}]^-$ (for the ^{56}Fe signal at

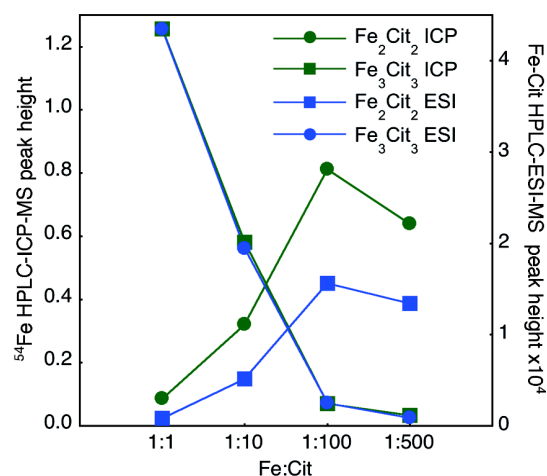


Figure 3. Effect of the Fe:Cit ratio on the Fe_2Cit_2 and Fe_3Cit_3 balance. Data are chromatographic peak maximum heights obtained with ICP-MS and ESI-TOFMS detection. ^{54}Fe -Cit standard solutions with Fe:Cit ratios of 1:1, 1:10, 1:100 and 1:500 (at $100 \mu\text{M}$ ^{54}Fe , pH 5.5 in 50% mobile phase B) were used.

m/z 488.9 m/z; Supplementary Fig. 4C and D).

Identification of an Fe_3Cit_3 complex in Fe-citrate standard solutions. The Fe peak at 32.9 min in HPLC-ESI-TOFMS analysis of ^{54}Fe -Cit solutions (Fig. 1B) showed signals at m/z 372.4 and 363.4, with isotopic signatures characteristic of 3 ^{54}Fe atom-containing molecular ions, both of them double charged (Fig. 2E, Supplementary Fig. 4E and Table I). The algorithm proposed $^{54}\text{Fe}_3\text{C}_{18}\text{H}_{15}\text{O}_{22}$ and $^{54}\text{Fe}_3\text{C}_{18}\text{H}_{13}\text{O}_{21}$ as the most accurate formulae, corresponding to the 3 Fe-, 3 Cit- molecular ions $[\text{}^{54}\text{Fe}_3\text{OCit}_3\text{H}_3]^{2-}$ and $[\text{}^{54}\text{Fe}_3\text{Cit}_3\text{H}]^{2-}$ (Table I). The fit of the experimental and theoretical isotopic signatures

Table II. Xylem sap pH, Fe and citrate concentrations, Fe:Cit ratios and Fe_3Cit_3 and Fe_2Cit_2 complexes (in % of the chromatographically eluted Fe), in Fe-sufficient (+Fe), Fe-deficient (-Fe) and Fe-deficient tomato plants resupplied with Fe-*o,o*EDDHA for 12 hours (Fe-resupplied). Data are means \pm SE of at least three independent samples.

Fe status	Fe in solution (μM)	pH	Fe (μM)	Cit (μM)	Fe:Cit	Fe_3Cit_3 (%)	Fe_2Cit_2 (%)
+Fe	45	5.8 \pm 0.1	19.9 \pm 2.6	11.6 \pm 6.6	1:0.6	bld ^a	bld
-Fe	0 + HCO_3^-	5.8 \pm 0.0	5.4 \pm 4.4	165 \pm 9.2	1:31	bld	bld
Fe-resupplied	(0 + HCO_3^-) + 45	5.5 \pm 0.1	121.0 \pm 13.7	172.2 \pm 12.6	1:1.4	71% ^b	bld

Data are means \pm SE of at least three independent samples.

^abld: below detection limit.

^bSince only 25 % of the total injected Fe was eluted from the column, this percentage corresponds to 16 % of the total injected Fe.

of the $[\text{}^{54}\text{Fe}_3\text{OCit}_3\text{H}_3]^{2-}$ molecular ion at m/z 372.4 is shown in Figs. 2E and F, respectively. The same occurs with the ion $[\text{}^{54}\text{Fe}_3\text{Cit}_3\text{H}]^{2-}$ at m/z 363.5 (Supplementary Fig. 4E and F).

Further confirmation of the molecular identity of the Fe_3Cit_3 complex was obtained analyzing $^{\text{nat}}\text{Fe}$ -Cit standard solutions. The peak at 32.9 min shows signals at m/z 375.4 and 366.4, characteristic of 3 $^{\text{nat}}\text{Fe}$ atom-containing molecular ions (Fig. 2G and Table I); these values were 3 m/z higher than those found using ^{54}Fe . The algorithm proposed $^{\text{nat}}\text{Fe}_3\text{C}_{18}\text{H}_{15}\text{O}_{22}$ and $^{\text{nat}}\text{Fe}_3\text{C}_{18}\text{H}_{13}\text{O}_{21}$ and as the most accurate formulae, corresponding to the 3 Fe-, 3 Cit- molecular ions $[\text{}^{\text{nat}}\text{Fe}_3\text{OCit}_3\text{H}_3]^{2-}$ and $[\text{}^{\text{nat}}\text{Fe}_3\text{Cit}_3\text{H}]^{2-}$ (Table I). The fit of the experimental and theoretical isotopic signatures of the $[\text{}^{\text{nat}}\text{Fe}_3\text{OCit}_3\text{H}_3]^{2-}$ molecular ion (for the ^{56}Fe signal at m/z 375.4) is shown in Figs. 2G and H, respectively. A good fit was also found for the ion $[\text{}^{\text{nat}}\text{Fe}_3\text{Cit}_3\text{H}]^{2-}$ (for the ^{56}Fe signal at 366.4 m/z ; Supplementary Fig. 4G and H).

Iron to citrate ratios drive the balance between Fe_2Cit_2 and Fe_3Cit_3 in standard solutions. To assess the influence of the Fe:Cit ratio on the balance of Fe-Cit complexes, standard solutions with Fe:Cit ratios 1:1, 1:10, 1:100 and 1:500 (at 100 μM Fe) were analyzed by HPLC-ESI-TOFMS and HPLC-ICP-MS, always at the typical pH value of the xylem sap. Both detection systems show that high Fe:Cit ratios favor the formation of Fe_3Cit_3 , whereas lower Fe:Cit ratios lead to the formation of Fe_2Cit_2 (Fig. 3). With Fe:Cit ratios higher than 1:10, Fe_3Cit_3 would account for more than 75% of the total complexed Fe, whereas with Fe:Cit ratios lower than 1:75, Fe_2Cit_2 would account for more than 75% of the total. In the range between these ratios, both complexes would be present. In all cases, no other Fe-containing peaks different

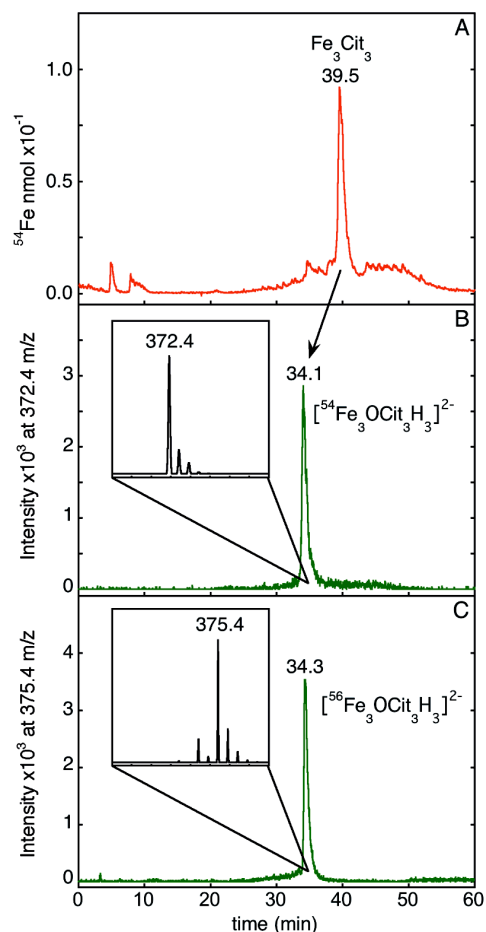


Figure 4. HPLC-ICP-MS (A) and HPLC-ESI-TOFMS (B and C) typical chromatograms of xylem sap samples from Fe-deficient, 12-h Fe-resupplied tomato plants, showing the peak corresponding to the Fe_3Cit_3 complex. Plants were resupplied with $^{54}\text{Fe-}o,o\text{EDDHA}$ (A and B) or $^{\text{nat}}\text{Fe-}o,o\text{EDDHA}$ (C). HPLC-ESI-TOFMS traces were extracted at m/z values 372.40 and 375.40 (± 0.05), corresponding to $[\text{}^{54}\text{Fe}_3\text{OCit}_3\text{H}_3]^{2-}$ and $[\text{}^{56}\text{Fe}_3\text{OCit}_3\text{H}_3]^{2-}$. Isotopic signatures of both molecular ions are shown in insets in (B) and (C).

from Fe_2Cit_2 and Fe_3Cit_3 were found by HPLC-ICP-MS or HPLC-ESI-TOFMS (Supplementary Fig. 5).

Quantification of Fe-Cit complexes in Fe-citrate standard solutions. We attempted to quantify the amount of Fe associated to the Fe-Cit complexes found in ^{54}Fe -Cit solutions by using HPLC-ICP-MS ^{54}Fe molar flow chromatograms. The sum of the Fe-Cit complexes Fe_2Cit_2 and Fe_3Cit_3 accounted for approximately 60% ($n=4$) of the total injected Fe. However, only 67% of the Fe was eluted from the HPLC. Therefore, the Fe contained in the Fe_2Cit_2 and Fe_3Cit_3 peaks accounted for 91% of the eluted Fe. When the analysis was carried out with longer run times a broad Fe peak eluted approximately at 70 min, indicating that at least an additional Fe form either occurred in the original sample or was formed from Fe-Cit complexes during the LC-run. The UV-visible spectra of this peak suggests that it may correspond to Fe-oxyhydroxides.

The Fe_3Cit_3 complex is present in the xylem sap of Fe-deficient tomato plants resupplied with Fe. We analyzed xylem sap to look for the presence of possible Fe-Cit complexes by the optimized methodology described above. We used xylem of Fe-sufficient, Fe-deficient and Fe-deficient plants resupplied with Fe-*o,o*EDDHA for 6, 12 and 24 h, where Fe concentrations were 19.9 ± 2.6 , 5.4 ± 4.4 , 42.9 ± 3.7 , 121.0 ± 13.7 and 43.5 ± 9.1 μM ($n=4$), respectively (Table II). The xylem sap of plants resupplied for 12 h was chosen for further studies, since they have the highest concentrations of Fe. These xylem sap samples showed a major ^{54}Fe peak in HPLC-ICP-MS at 39.5 min (Fig. 4A). When using HPLC-ESI-TOFMS, an Fe peak eluted at 34.1 min and showed signals at m/z 372.4 or 375.4 when the Fe source was ^{54}Fe -*o,o*EDDHA or ^{nat}Fe -*o,o*EDDHA, respectively (Fig. 4B and C). The retention time difference between HPLC-ICP-MS and HPLC-ESI-TOFMS was due to the use of Different HPLC systems as explained above. Based on these exact mass and the isotopic pattern data (see insets of Fig. 4B and C), the algorithm proposed $\text{Fe}_3\text{C}_{18}\text{H}_{15}\text{O}_{22}$ as the more accurate molecular formula (Table I; ^{56}Fe signal m/z error 6.8 ppm and SigmaFit™ value 0.0197), corresponding to the Fe_3Cit_3 molecular ion $[\text{Fe}_3\text{O}(\text{Cit})_3\text{H}_3]^{2-}$ also found in the Fe-Cit standard (Figs. 1 and 2). The approximately 1-min difference in retention time for Fe_3Cit_3 between

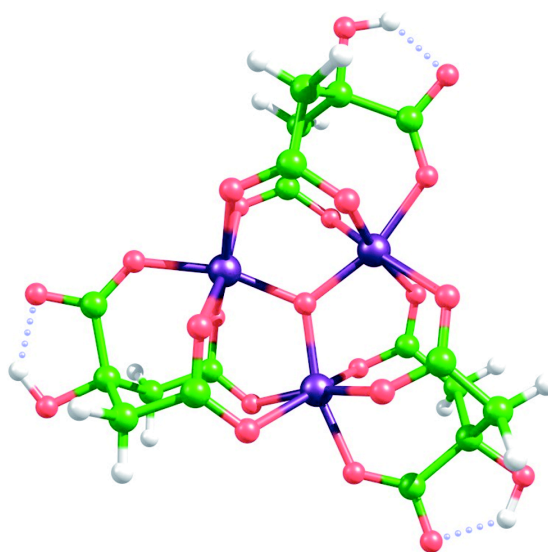


Figure 5. Proposed structure for the Fe_3Cit_3 found in plant xylem as an oxo-bridged tri-iron-citrate complex. Iron, oxygen, carbon and hydrogen atoms are shown in purple, red, green and white, respectively.

xylem sap samples (Fig. 4) and standards (Fig. 1) in both HPLC systems was likely due to matrix effects. It should be noted that although the Fe_3Cit_3 complex was detected in standard solution as a mixture of two ions $[\text{Fe}_3\text{Cit}_3\text{H}]^{2-}$ and $[\text{Fe}_3\text{OCit}_3\text{H}_3]^{2-}$, in xylem sap only the latter was found. No other Fe-containing molecular ions, including Fe-NA, were found in the whole HPLC-ESI-TOFMS run using these HPLC conditions. However, using a HPLC-ESI-TOFMS method designed for Fe-*o,o*EDDHA analysis (Orera et al. 2009) a very low concentration of this Fe chelate (0.3 ± 0.1 μM ; $n=4$) was found. The Fe_3Cit_3 complex was also found in xylem sap of Fe-deficient plants resupplied with Fe-EDTA for 12 h, as well as in those of plants resupplied with Fe-*o,o*EDDHA for 6 and 24 h (data not shown). However, no Fe-containing compounds could be detected in the xylem of Fe-deficient and Fe-sufficient plants.

We also attempted to quantify the amount of Fe associated to the Fe_3Cit_3 complex found in the xylem of the ^{54}Fe -*o,o*EDDHA 12h-resupplied plants by using HPLC-ICP-MS ^{54}Fe molar flow chromatograms ($n=3$). In these xylem samples more than 95% of the total Fe was ^{54}Fe . Only 25% of the injected Fe eluted from the column. The $^{54}\text{Fe}_3\text{Cit}_3$ peak accounted for the 71% of the eluted Fe and 16% of the injected Fe (Table II).

Method sensitivity for the Fe_3Cit_3 complex. The sensitivity of the HPLC-ESI-TOFMS and

HPLC-ICP-MS methods for the detection of the Fe_3Cit_3 complex in xylem sap can be estimated from the signal to noise ratios (s/n). Limits of detection and quantification are usually considered as the analyte concentrations giving s/n of 3 and 10, respectively. S/n found in xylem sap samples with total Fe concentrations of approximately $40 \mu\text{M}$ were 12 and 6 in HPLC-ESI-TOFMS and HPLC-ICP-MS, respectively. Therefore, in xylem sap with Fe: Cit ratios favouring the formation of Fe_3Cit_3 (lower than 1:10; Fig. 3), an Fe concentration of approximately $25\text{-}30 \mu\text{M}$ will be needed for the Fe_3Cit_3 complex to be detected.

Molecular modeling of the Fe_3Cit_3 complex: an oxo-bridged tri-Fe(III) core complex. Molecular modeling of the Fe_3Cit_3 complex was carried out using the information gained from the molecular identification in xylem sap samples of Fe-deficient plants resupplied with Fe and on the basis of the known basic structure of Fe(III) carboxylates (Lippard 1988). The complex Fe_3Cit_3 has a molecular mass of 750.83 Da , a molecular formula of $\text{Fe}_3\text{C}_{18}\text{H}_{15}\text{O}_{22}$, is composed by 3 Cit molecules, 3 Fe atoms and 1 O atom and has two negative charges. The complex was modeled using Density Functional Theory (DFT), that has become the standard method for quantum chemical modeling of transition metals including those of biological relevance ((Deeth et al. 2009) and references therein), as a trinuclear Fe(III) oxo-bridged complex (Fig. 5, Supplementary Fig 5). The 3 Fe atoms form an equilateral triangle with an O atom in the center bridging all of them. All Fe atoms have a slightly distorted octahedral configuration. In each of the 3 Cit molecules, both distal carboxylate groups are bound to 2 Fe atoms. The 4 O atoms of the Cit distal carboxylate groups (2 from each Cit molecule) are in the same plane of the Fe atom they complex. The 2 remaining positions of the Fe atom are occupied by the central carboxylate group of a Cit molecule and the O of the oxo-bridged 3-Fe center. This compact molecular geometry is further stabilized by the formation of hydrogen bonds between the hydroxyl groups and the free O atoms in the central carboxylates. Until now, 6 Fe-Cit complexes (3 mononuclear and 2 dinuclear found in concentrated standard solutions, plus a nonanuclear one) have been isolated and structurally characterized in solid state ((Gautier-Luneau et al. 2005) and references therein), and

none of them has a central μ_3 -oxygen coordinated to three Fe atoms. The Fe_2Cit_2 complex found only in Fe-Cit standard solutions was also modeled (see Supplementary Figures 7 and 8 and Supplementary Table III) according to the known structural characteristics found in solid state by Gautier-Luneau et al. (2005) and references therein.

Discussion

We report here the first direct and unequivocal identification of a natural Fe complex in plant xylem sap, Fe_3Cit_3 . The complex was modeled as having an oxo-bridged tri-Fe(III) core. This is the first time that an Fe-Cit complex has been identified in biological systems. The Fe_3Cit_3 complex was identified using an integrated mass spectrometry approach, based on exact molecular mass, isotopic signature, Fe content and retention time. This complex was not predicted to occur in previous *in silico* xylem speciation studies (López-Millán et al. 2000, 2001). A second Fe-Cit complex, Fe_2Cit_2 , was also found along with Fe_3Cit_3 in standard solutions at xylem typical pH values, with their respective abundances being tuned by the Fe: Cit ratio. The detection of Fe_3Cit_3 in the xylem sap was made possible by the use of: i) pH values similar to those of the xylem sap throughout the analysis, ii) a zwitterionic hydrophilic interaction column that allows for the separation of Cit and Fe-Cit complexes, iii) high resolution detection techniques such as ICP-MS and ESI-TOFMS, and iv) stable Fe isotopes for identification and quantification purposes.

The changes in Fe: Cit ratios in standard solutions drive the balance between the Fe_2Cit_2 and Fe_3Cit_3 complexes, with ratios above 1:10 favoring the formation of Fe_3Cit_3 and ratios below 1:75 favoring the formation of Fe_2Cit_2 (Fig. 3). In the xylem sap of Fe-deficient tomato plants resupplied with Fe for 12 h, where the Fe: Cit ratio was approximately 1:1 (Table II), the only complex observed was Fe_3Cit_3 . The xylem sap Fe: Cit ratios in Fe-sufficient and Fe-deficient plants were approximately 1:1 and 1:30, and therefore the expected Fe-Cit complexes would be Fe_3Cit_3 and a mixture of the Fe_2Cit_2 and Fe_3Cit_3 complexes, respectively. However, no Fe-Cit complexes could be detected by HPLC-ESI-TOFMS or HPLC-ICP-MS in the xylem of these plants, likely because concentrations were below the limit of detection, estimated in approximately $25\text{-}30 \mu\text{M}$ Fe-Cit. In fact, xylem total Fe

concentrations were approximately 20 and 5 μM in Fe-sufficient and Fe-deficient plants, respectively, much lower than the 43-121 μM found in Fe-deficient plants resupplied with Fe where the complex was detected. Limits of detection (LODs) for these Fe-Cit complexes are considerably higher than that reported, also in xylem sap and with similar analytical techniques, for the synthetic Fe chelate Fe(III)-*o,o*EDDHA, which is below 1 μM (Orera et al. 2009). This supports that further analytical efforts should be done to improve the LODs for the determination of Fe-Cit complexes in plant fluids, taking into account that Fe-Cit complexes could be very sensitive to the external conditions and may decompose during chromatography. Also, since the potential occurrence of other Fe-compounds along with Fe-Cit complexes could explain the mass balance results found in both standard solutions or xylem sap, further analytical efforts should be done to completely speciate Fe in xylem sap.

The finding that at least an Fe-Cit complex, Fe_3Cit_3 , participates in long-distance xylem Fe transport in plants is in line with what is known to occur in other organisms. In humans most of the Fe is usually chelated by transferrin, but the serum of patients with Fe overload disorders may have up to 10 μM Fe not bound to transferrin (at pH 7.4, with 100 μM Cit and an Fe:Cit ratio of 1:10) (Evans et al. 2008). This Fe fraction was proposed to consist in a mixture of oligomeric, dimeric and possibly monomeric Fe species, using a different approach from that used here. The Fe:Cit ratio in serum has also been proposed to control the balance between Fe-Cit species, with Fe:Cit ratios higher than 1:10 leading to oligomeric and polymeric Fe species and lower than 1:100 leading to monomeric and dimeric Fe species (Evans et al. 2008). This framework is similar to the one we propose here for plant xylem sap, with high Fe:Cit ratios leading to Fe_3Cit_3 and low ratios leading to Fe_2Cit_2 . In the bacterial plasma membrane a Fe_2Cit_2 complex is thought to be transported by the coordinated action of FecABCDE proteins (Mahren et al. 2005) where Fe_2Cit_2 binds to FecA in the outer membrane and initiates two independent processes, Fe-Cit transport into the periplasm and transcriptional induction of the fecABCDE genes (Yue et al. 2003). Fe-Cit transport by proteins of the CitMHS family has also been recently described in bacteria (Lensbauer et al. 2008).

The idea that Fe could be transported in the plant xylem by organic acids was first suggested many years ago (Rogers 1932), based on the ability of Fe to form stable complexes with organic acids and on the increase in these carboxylates with Fe-deficiency (see Abadía et al. (2002) for a review). Pioneering studies by Brown and co-workers proposed that Fe and Cit were associated in some way, in different plant species, from the co-migration of Fe and Cit during electrophoresis and the increase in xylem Cit concentration with Fe deficiency (Brown and Tiffin 1965; Clark et al. 1973; Tiffin 1966a, b, 1970). The first *in silico* xylem Fe speciation studies also suggested a major role for Cit in the complexation of Fe in tomato and soybean (Mullins et al. 1986; White et al. 1981a; White et al. 1981b). More recently, *in silico* studies incorporating the stability constants of other possible Fe chelators (e.g. NA), also support that Cit, rather than NA, could play a major role in Fe xylem transport (López-Millán et al. 2000, 2001; Rellán-Álvarez et al. 2008; von Wirén et al. 1999), and this was also supported by ESI-TOFMS direct determination of Fe-NA complexes in standard solutions containing Fe, NA and Cit at typical xylem pH values (Rellán-Álvarez et al. 2008). We have reviewed previous studies reporting xylem Fe and Cit concentrations to explore the likelihood of finding the Fe-Cit complexes in xylem sap (Supplementary Table I). Within a given plant species, Fe:Cit ratios were generally higher in Fe-sufficient than in Fe-deficient plants, and when plants were resupplied with Fe even higher Fe:Cit ratios were found (Supplementary Table I). A comparison of these Fe:Cit ratios with the threshold values proposed in this study with standard solutions (1:10 for $\geq 75\%$ Fe_3Cit_3 and 1:75 for $\geq 75\%$ Fe_2Cit_2) suggest that the Fe_3Cit_3 complex may occur in a wide range of species regardless of Fe-nutrition status. On the other hand, the Fe_2Cit_2 complex may be prevalent in xylem sap samples with Cit concentrations in the mM range, such as those of some Fe-deficient plant species (Supplementary Table I).

Recent molecular evidence also supports that Cit may be involved in long distance Fe transport. Two *A. thaliana* and rice mutants with altered root vasculature Cit transporters show decreases in the xylem sap concentrations of Fe and Cit, increased Fe deficiency symptoms and Fe accumulation in the root (Durrett et al. 2007; Yokosho et al. 2009). Changes found in Fe and

Cit concentrations do not support that changes in Fe-Cit speciation may occur, since Fe_3Cit_3 would be expected to occur both in the wild type and mutant genotypes of both species (Supplementary Table I). The phenotype of these mutants could result from a hampered Fe xylem transport, and/or from the decrease in xylem C transport itself, that may in turn impair the ability of the mutant plants to elicit root responses to Fe deficiency. Carbon fixation in roots by phosphoenolpyruvate carboxylase and export in the xylem has been proposed to play a role in the plant responses when leaf C fixation is decreased by Fe deficiency (López-Millán et al. 2000; Zocchi et al. 2007).

The central oxo-bridged tri-Fe(III) core bridged by citrate ligands of the Fe_3Cit_3 complex proposed here to occur in the xylem sap is structurally related to the active sites of numerous polyiron-oxo proteins (Tshuva and Lippard 2004). Di-Fe sites are found in a functionally diverse class of proteins which are activated by oxygen binding and catalyze hydroxylation, desaturation, and epoxidation reactions on a variety of alkyl and aryl substrates. A di-Fe site in ribonucleotide reductase, which participates in DNA biosynthesis, is responsible for the formation of organic radicals, whereas ferritins are important for Fe oxidation, storage and transport (see (Tshuva and Lippard 2004) and references therein). This is the first time that a small molecule containing an oxo-bridged tri-Fe center is reported in a biological system. We may speculate that the oxy-bridge structure may confer redox properties to this plant Fe transport form. In fact, the lowest unoccupied molecular orbital of the complex, obtained by DFT calculations, displays an energy of 1.5 eV, which is rather low for a dianionic species and supports that the reduction of this trinuclear species could be feasible.

The finding of this negatively double charged, relatively large (750.83 Da) Fe_3Cit_3 complex opens new possibilities to re-examine the long-distance transport of Fe in the plant xylem. Very little is still known on the mechanisms of Fe xylem unloading, although it is accepted that a direct flow of Fe could occur through plasmodesmata into xylem parenchyma cells, and a second mechanism could proceed to the leaf mesophyll apoplast (Kim and Guerinot 2007; Palmer and Guerinot 2009). The molecular size of Fe_3Cit_3 , 1.1 x 0.4 nm, would permit the direct

passage through plasmodesmata, that usually allows trafficking of molecules smaller than 2 nm. Once in the xylem parenchyma cytoplasm, the prevailing pH change would favor ligand exchange reactions with NA, leading to the formation of Fe-NA complexes (Rellán-Álvarez et al. 2008; von Wirén et al. 1999). Xylem Fe unloading can also proceed directly to the apoplast, where the Fe_3Cit_3 complex is also likely to occur (considering the apoplast chemical composition (Kim and Guerinot 2007; Palmer and Guerinot 2009) and will probably function as a suitable substrate for the mesophyll cell leaf plasma membrane Fe(III) chelate reductase. As mentioned above this complex is likely to have redox activity, and the oxo-bridge may play a role in the interaction with the reductase enzyme. In fact, low Fe:Cit ratios -favoring the presence of Fe_3Cit_3 - seem to be optimal for leaf plasma membrane Fe(III)-chelate reductase activity, since 20-fold increases were observed when Fe:Cit ratios increased from 1:500 to 1:5 (González-Vallejo et al. 1999). Also, the complex may be a natural substrate of the root Fe(III)-chelate reductase, since it is known that root Cit excretion occurs in many plant species under Fe deficiency (Abadía et al. 2002).

Experimental

Plant culture. Tomato (*Solanum lycopersicum* Mill. cv. 'Tres Cantos') plants were grown in a growth chamber with a photosynthetic photon flux density of $350 \mu\text{mol m}^{-2} \text{s}^{-1}$ photosynthetically active radiation, and a 16/8 h photoperiod, 23/18 °C day/night temperature regime. Seeds were germinated and grown in vermiculite for two weeks. Seedlings were grown for an additional two-week period in half-strength Hoagland nutrient solution with $45 \mu\text{M}$ $^{nat}\text{Fe(III)}$ -ethylenediamine-tetraacetic acid (EDTA), and then transplanted to 10 L plastic buckets (18 plants per bucket) containing half-strength Hoagland nutrient solution, pH 5.5, with either 0 (Fe-deficient plants) or $45 \mu\text{M}$ Fe(III)-EDTA (Fe-sufficient plants). Throughout this study we use ^{nat}Fe to refer to Fe with the natural isotopic composition: 5.85, 91.75, 2.12 and 0.28% of ^{54}Fe , ^{56}Fe , ^{57}Fe and ^{58}Fe , respectively. After 10 days, Fe-deficient plants were resupplied with Fe by transfer to nutrient solution with Fe ($45 \mu\text{M}$ of either $^{nat}\text{Fe(III)}$ -ethylenediamine-N-N'-bis(o-hydroxyphenylacetic) acid (*o,o*EDDHA),

$^{54}\text{Fe(III)-}o,o\text{EDDHA}$ or $^{\text{nat}}\text{Fe(III)-EDTA}$). Iron-54 was purchased as Fe_2O_3 (98% Fe, 95% ^{54}Fe ; Cambridge Isotope Labs, Andover, MA). Xylem was sampled from Fe-deficient, Fe-sufficient and Fe-deficient plants resupplied with Fe for 6, 12 and 24 h.

Xylem sap sampling. Tomato xylem sap was sampled using the detopping technique (López-Millán et al. 2009). Plant shoots were cut just below the first true leaf using a razor blade, and xylem sap was left to exude. The sap of the first 5 min was discarded to avoid contamination, the surface was washed with distilled water and blotted dry, and sap was then directly collected for 20 min using a micro-pipet and maintained in Eppendorf tubes kept on ice. Immediately after sample collection, the pH of the samples was measured with a Biotrode[®] pH microelectrode with Idrolyte[®] electrolyte (Metrohm, Herisau, Switzerland), tested for cytosolic contamination as indicated below and kept frozen at $-80\text{ }^\circ\text{C}$ until further analysis. All samples were assessed for cytosolic contamination using c-mdh (EC 1.1.1.37) as a cytosolic contamination marker (López-Millán et al. 2000), and no contamination was found. Before analysis, samples were thawed and diluted two-fold with 10 mM ammonium acetate in methanol at pH 6.8. The actual pH value of this organic mixture is estimated to be 5.5 (Canals et al. 2001). Then, samples were vortexed, centrifuged at 12000g for 2 min and the supernatant immediately analyzed.

Fe-Cit standard solutions preparation. Iron-Cit standard solutions at different Fe: Cit ratios were prepared by adding the appropriate amounts of Fe ($^{\text{nat}}\text{Fe}$ or ^{54}Fe) to Cit solutions prepared in 10 mM ammonium acetate at pH 5.5. Fe-Cit solutions were gently vortexed, diluted two-fold with 10 mM ammonium acetate in methanol at pH 6.8 and immediately analyzed. The pH value of this organic mixture is estimated to be 5.5 (Canals et al. 2001).

Analysis of Fe-complexes by high-performance liquid chromatography coupled to electrospray ionization mass spectrometry. Chromatographic separation was performed on a modified Alliance 2795 HPLC system (Waters, Milford, MA). The fluidics system, with the exception of the pump head, was built with PEEK[™], and a Ti needle was used to minimize metal contamination. Different HPLC conditions were tested, including several column types, elution programs and organic solvents

(acetonitrile and methanol). Final HPLC analysis conditions were as follows. The autosampler was kept at $4\text{ }^\circ\text{C}$ and the column compartment temperature was set at $30\text{ }^\circ\text{C}$. Injection volume was $20\text{ }\mu\text{L}$, and a ZIC[®]-pHILIC, $150 \times 2.1\text{ mm}$, $5\text{ }\mu\text{m}$ column (Sequant, Umea, Sweden) was used with a flow rate of $100\text{ }\mu\text{L min}^{-1}$. The mobile phase was built using two eluents: A (10 mM ammonium acetate in water at pH 5.5) and B (10 mM ammonium acetate in methanol at pH 6.8). All mobile phase chemicals were HPLC-MS grade (Riedel-de Haën, Seelze, Germany). For separation, an initial equilibration time of 80% B and 20% A (from min 0 to 5) was followed by a linear gradient from 80 to 20% B (from min 5 to 20). This mobile phase composition was held for 15 min, then changed linearly to the initial conditions for 10 min, and kept as such for another 15 min. Total run time per sample was 1 h. The pH values during the HPLC-run ranged from 5.3 to 6.2 depending on organic mixture composition of the mobile phase (Canals et al. 2001). Injections of 5 mM Cit ($20\text{ }\mu\text{L}$) were carried out between samples to minimize Fe cross-contamination.

High-resolution mass spectrometry analysis was carried out with a micrOTOF II ESI-TOFMS apparatus (Bruker Daltonics GmbH, Bremen, Germany) in the 50-1000 m/z range. The micrOTOF II was operated in negative mode at 3000 and -500 V capillary and end-plate voltages, respectively. After optimization, capillary exit, skimmer 1 and hexapole RF voltages were set at -57.1 , -39.1 and 145.2 V , respectively. Nebulizer gas (N_2) pressure was kept at 2.0 bar and drying gas (N_2) flow was set at 8.0 L min^{-1} with a temperature of $180\text{ }^\circ\text{C}$. Mass calibration was carried out with 10 mM Li-formate solution using a syringe pump (Cole-Parmer Instruments, Vernon Hills, IL). In each HPLC run mass calibration was carried out by on-line injection of $20\text{ }\mu\text{L}$ of Li-formate at minute 2. Molecular formulae were assigned based on i) exact molecular mass, with errors below 10 ppm, and ii) the SigmaFit[™] algorithm, with a threshold tolerance value of 0.03 SigmaFit[™] values (Ojanperä et al. 2006). Appropriate isotopic abundances were used for the calculations. The system was controlled with the software packages MicrOTOF Control v.2.2 and HyStar v.3.2 (Bruker Daltonics). Data were processed with Data Analysis v.3.4 software (Bruker Daltonics).

Analysis of Fe and Fe-complexes by inductively coupled plasma mass spectrometry. ICP-MS analysis was carried out with a Q-ICP-MS instrument (7500ce, Agilent Technologies, Tokyo, Japan). The instrument was fitted with an octapole collision cell system located between the ion lenses and a quadrupole MS analyzer for removal of polyatomic interferences. In this study He was used as a collision gas. In addition, O₂ (7%) was added to the plasma by an additional mass flow controller to remove C excess, and to prevent it from condensing on the interface and ion lenses due to the high organic content of the mobile phase during HPLC separation (Woods and Fryer 2007). Platinum interface cones were used to allow the addition of O₂. The Q-ICP-MS instrument was operated with a RF power of 1500 W and cooling, sample and make-up gas flows of 15, 0.9 and 0.2 L min⁻¹, respectively. The collision cell was operated with a He gas flow of 4.2 mL min⁻¹ and octapole bias and QP bias voltages of -18.0 and -16.0 V, respectively. The torch position and ion lens voltage settings were optimized daily for maximum sensitivity with a 1 ng g⁻¹ Li, Co, Y, Tl and Ce mixture in 1% (w/w) HNO₃ solution. A solution of 1% (w/w) HNO₃ was also used to check the background level caused by polyatomic Ar interferences. The possible contribution of isobaric interferences of ⁵⁴Cr and ⁵⁸Ni in the determination of the ⁵⁴Fe and ⁵⁸Fe isotopes was corrected mathematically by measuring the ion signals at masses 52 for Cr and 60 for Ni and assuming natural abundances reported by IUPAC (De Laeter et al. 2003). Mass bias correction was carried out by measuring the isotope ratios of the ^{nat}Fe standard and calculating the mass bias factor (K) with an exponential model (Rodríguez-Castrillón et al. 2008). The ICP-MS instrument was controlled with the software packages ICP-MS ChemStation v.B.03.04 and ICP-MS Chromatographic v.B.03.04 (Agilent Technologies).

For the ICP-MS analysis of ⁵⁴Fe-citrate complexes in standard solutions and xylem sap samples, a chromatographic separation was performed on an Agilent 1100 chromatographic system (Agilent Technologies) using the method described for HPLC-ESI-TOFMS analysis. Iron-54 and ^{nat}Fe quantification was carried out by post-column isotope dilution analysis (IDA) (Rodríguez-González et al. 2005) with a 20 ng g⁻¹ ⁵⁷Fe in EDTA solution continuously introduced at

0.10 g min⁻¹ through a T piece connected to the end of the column and before the plasma entrance. Iron-57 was purchased as Fe₂O₃ (98% Fe, 95% ⁵⁷Fe; Cambridge Isotope Labs). The ICP-MS intensity chromatograms (counts s⁻¹) were converted into Fe molar flow chromatograms (⁵⁴Fe nmol min⁻¹) using the isotope pattern deconvolution (IPD) equations described elsewhere (González Iglesias et al. 2009; Rodríguez-Castrillón et al. 2008). Accurate isotope abundances of the ⁵⁷Fe and ⁵⁴Fe enriched solutions were determined by direct ICP-MS injections and used for these calculations. Isotope abundances (% ⁵⁴Fe, ⁵⁶Fe, ⁵⁷Fe and ⁵⁸Fe) were 0.14, 4.74, 94.63 and 0.49 in ⁵⁷Fe enriched solutions and 99.67, 0.25, 0.01 and 0.06 in ⁵⁴Fe enriched solutions.

Total ⁵⁴Fe and ^{nat}Fe determinations in xylem sap samples were carried out by direct ICP-MS injections and IDA, spiking known amounts of the characterized ⁵⁷Fe-enriched solution into the samples acidulated with HNO₃. Also, the mathematical IPD procedure described elsewhere (González Iglesias et al. 2009; Rodríguez-Castrillón et al. 2008) was used.

Other determinations. Citrate was analyzed by HPLC (Waters Alliance 2795) using a Supelcogel H 250x4.6mm column. Analyses were performed isocratically at a flow rate of 200 μL min⁻¹ and at a temperature of 30 °C. The mobile phase was 0.1 % formic acid. Detection was performed by ESI-TOFMS (micrOTOF II, Bruker Daltonics) at 191.0 m/z. Quantification was carried out by external calibration with internal standardization (with ¹³C4-L-malic acid, Cambridge Isotope Laboratories). The Fe(III)-chelate of ethylenediamine-N,N'-bis(*o*-hydroxyphenylacetic) acid (*o,o*EDDHA) was determined as described elsewhere (Orera et al. 2009).

Iron-citrate complex molecular modeling. All theoretical calculations were performed by using the Gaussian 03 program (Frisch et al. 2003). The molecular geometry of (Fe₃OCit₃)²⁻ was optimized assuming C_{3h} symmetry. The chemistry model used consisted in the Becke's three-parameter exchange functional combined with the LYP correlation functional (B3LYP) (Becke 1993) and the LanL2DZ basis set as indicated in the Gaussian 03 program (Frisch et al. 2003). In order to achieve the convergence of the wavefunction, an initial guess was obtained using the same chemistry model on the closed

shell (Fe₃OCit₃)²⁻ species.

Funding

This work was supported by the Spanish Ministry of Science and Innovation (grant numbers AGL2006-1416, AGL2007-61948 and CTQ2006-05722, co-financed with FEDER); the European Commission (Thematic Priority 5– Food Quality and Safety, 6th Framework RTD Programme, grant number FP6-FOOD–CT-2006-016279) and the Aragón Government (groups A03 and E39). Acquisition of the HPLC-TOFMS apparatus was cofinanced with FEDER. RR-A, JG-M-S, IO and JAR-C were supported by FPI-MICINN, FICYT-MICINN, CONAID-DGA and FPU-MICINN grants respectively.

Acknowledgements

We thank Ade Calviño and Aurora Poc (Aula Dei Experimental Station-CSIC, Zaragoza, Spain) for growing the plants, Jiang Feng Ma (Research Institute for Bioresources, Okayama University, Kurashiki, Japan) for the kind supply of DMA and Ana Flor López-Millán (Aula Dei Experimental Station-CSIC, Zaragoza, Spain) for critically reviewing the manuscript and helpful suggestions.

References

- Abadía J, López-Millán AF, Rombolá A, Abadía A** (2002) Organic acids and Fe deficiency: a review. *Plant Soil* **241**: 75-86
- Becke AD** (1993) A new mixing of Hartree-Fock and local density-functional theories. *J Chem Phys* **98**: 1372-1377
- Briat JF, Curie C, Gaymard F** (2007) Iron utilization and metabolism in plants. *Curr Opin Plant Biol* **10**: 276-282
- Brown J** (1966) Fe and Ca uptake as related to root-sap and stem-exudate citrate in soybeans. *Physiol Plantarum* **19**: 968-976
- Brown JC, Tiffin LO** (1965) Iron stress as related to the iron and citrate occurring in stem exudate. *Plant Physiol* **40**: 395-400
- Canals I, Oumada FZ, Rosés M, Bosch E** (2001) Retention of ionizable compounds on HPLC. 6. pH measurements with the glass electrode in methanol-water mixtures. *J Chrom A* **911**: 191-202
- Clark RB, Tiffin LO, Brown JC** (1973) Organic-acids and iron translocation in

maize genotypes. *Plant Physiol* **52**: 147-150

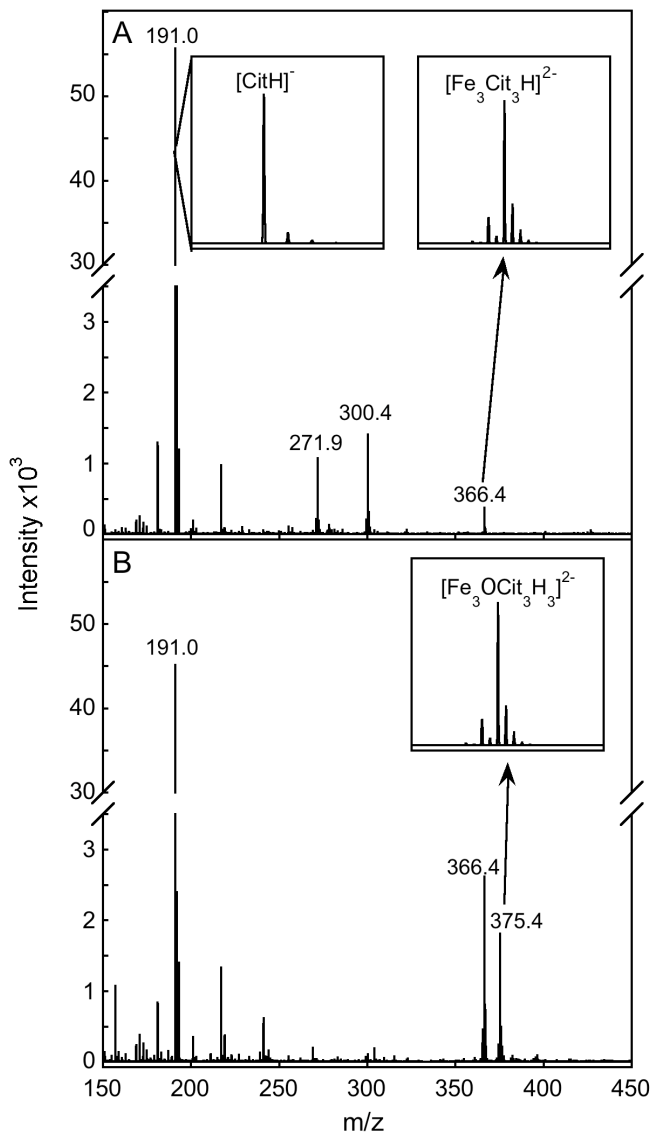
- De Laeter J, Böhlke J, De Bièvre P, Hidaka H, Peiser H, Rosman K, Taylor P** (2003) Atomic weights of the elements: review 2000. *Pure Appl Chem* **75**: 683-800
- Deeth R, Anastasi A, Diedrich C, Randell K** (2009) Molecular modelling for transition metal complexes: dealing with d-electron effects. *Coord Chem Rev* **253**: 795-816
- Durrett TP, Gassmann W, Rogers EE** (2007) The FRD3-mediated efflux of citrate into the root vasculature is necessary for efficient iron translocation. *Plant Physiol* **144**: 197-205
- Evans RW, Rafique R, Zarea A, Rapisarda C, Cammack R, Evans PJ, Porter JB, Hider RC** (2008) Nature of non-transferrin-bound iron: studies on iron citrate complexes and thalassemic sera. *J Biol Inorg Chem* **13**: 57-74
- Frisch MJ** (2003) Gaussian 03, Revision B.05. Gaussian, Inc, Pittsburgh, PA
- Gautier-Luneau I, Merle C, Phanon D, Lebrun C, Biaso F, Serratrice G, Pierre JL** (2005) New trends in the chemistry of iron(III) citrate complexes: Correlations between X-ray structures and solution species probed by electrospray mass spectrometry and kinetics of iron uptake from citrate by iron chelators. *Chem Europ J* **11**: 2207-2219
- González Iglesias H, Fernández Sánchez ML, Rodríguez-Castrillón JA, García-Alonso JI, Sastre JL, Sanz-Medel A** (2009) Enriched stable isotopes and isotope pattern deconvolution for quantitative speciation of endogenous and exogenous selenium in rat urine by HPLC-ICP-MS. *J Anal Atom Spectrom* **24**: 460-468
- González-Vallejo E, González-Reyes J, Abadía A, López-Millán A, Yunta F, Lucena J, Abadía J** (1999) Reduction of ferric chelates by leaf plasma membrane preparations from Fe-deficient and Fe-sufficient sugar beet. *Aust J Plant Physiol* **26**: 601-611
- Hider RC, Yoshimura E, Khodr H, von Wiren N** (2004) Competition or complementation: the iron-chelating

- abilities of nicotianamine and phytosiderophores. *New Phytol* **164**: 204-208
- Larbi A, Morales F, Abadía J, Abadía A** (2003) Effects of branch solid Fe sulphate implants on xylem sap composition in field-grown peach and pear: changes in Fe, organic anions and pH. *J Plant Physiol* **160**: 1473-1481
- Lensbauer J, Patel A, Sirianni J, Doyle R** (2008) Functional characterization and metal ion specificity of the metal-citrate complex transporter from *Streptomyces coelicolor*. *J Bacteriol* **190**: 5616-5623
- Lippard SJ** (1988) Oxo-bridged polyiron centers in biology and chemistry. *Angew Chem Int. Edit* **27**: 344-361
- López-Millán A, Morales F, Gogorcena Y, Abadía A, Abadía J** (2009) Metabolic responses in iron deficient tomato plants. *J Plant Physiol* **166**: 375-384
- López-Millán AF, Morales F, Abadía A, Abadía J** (2000) Effects of iron deficiency on the composition of the leaf apoplastic fluid and xylem sap in sugar beet. Implications for iron and carbon transport. *Plant Physiol* **124**: 873-884
- López-Millán AF, Morales F, Abadía A, Abadía J** (2001) Iron deficiency-associated changes in the composition of the leaf apoplastic fluid from field-grown pear (*Pyrus communis* L.) trees. *J Exp Bot* **52**: 1489-1498
- Mahren S, Schnell H, Braun V** (2005) Occurrence and regulation of the ferric citrate transport system in *Escherichia coli* B, *Klebsiella pneumoniae*, *Enterobacter aerogenes*, and *Photobacterium luminescens*. *Arch Microbiol* **184**: 175-186
- Meija J, Montes-Bayón M, Caruso J, Sanz-Medel A** (2006) Integrated mass spectrometry in (semi-) metal speciation and its potential in phytochemistry. *Trends Anal Chem* **25**: 44-51
- Mullins GL, Sommers LE, Housley TL** (1986) Metal speciation in xylem and phloem exudates. *Plant Soil* **16**: 377-391
- Nikolic M, Römheld V** (1999) Mechanism of Fe uptake by the leaf symplast: is Fe inactivation in leaf a cause of Fe deficiency chlorosis? *Plant Soil* **215**: 229-237
- Ojanperä S, Pelander A, Pelzing M, Krebs I, Vuori E, Ojanperä I** (2006) Isotopic pattern and accurate mass determination in urine drug screening by liquid chromatography/time-of-flight mass spectrometry. *Rapid Commun Mass Spectrom* **20**: 1161-1167
- Orera I, Abadía A, Abadía J, Álvarez-Fernández A** (2009) Determination of *o,o*EDDHA -a xenobiotic chelating agent used in Fe fertilizers- in plant tissues by liquid chromatography/electrospray mass spectrometry: overcoming matrix effects. *Rapid Commun Mass Spectrom* **23**: 1694-1702
- Ouerdane L, Mari S, Czernic P, Lebrun M, Lobinski R** (2006) Speciation of non-covalent nickel species in plant tissue extracts by electrospray Q-TOFMS/MS after their isolation by 2D size exclusion-hydrophilic interaction LC (SEC-HILIC) monitored by ICP-MS. *J Anal Atom Spectrom* **21**: 676-683
- Palmer C, Guerinot ML** (2009) Facing the challenges of Cu, Fe and Zn homeostasis in plants. *Nat Chem Biol* **5**: 333-340
- Pierre JL, Gautier-Luneau I** (2000) Iron and citric acid: a fuzzy chemistry of ubiquitous biological relevance. *Biometals* **13**: 91-96
- Rellán-Álvarez R, Abadía J, Álvarez-Fernández A** (2008) Formation of metal-nicotianamine complexes as affected by pH, ligand exchange with citrate and metal exchange. A study by electrospray ionization time-of-flight mass spectrometry. *Rapid Commun Mass Spectrom* **22**: 1553-1562
- Rodríguez-Castrillón JA, Moldován M, Encinar JR** (2008) Isotope pattern deconvolution for internal mass bias correction in the characterisation of isotopically enriched spikes. *J Anal Atom Spectrom* **23**: 318-324
- Rodríguez-González P, Marchante-Gayón J, García Alonso J, Sanz-Medel A** (2005) Isotope dilution analysis for elemental speciation: a tutorial review. *Spectrochim Acta B* **60**: 151-207
- Rogers C** (1932) Factors affecting the distribution of iron in plants. *Plant Physiology* **7**: 227-252
- Spiro T, Bates G, Saltman P** (1967a) Hydrolytic

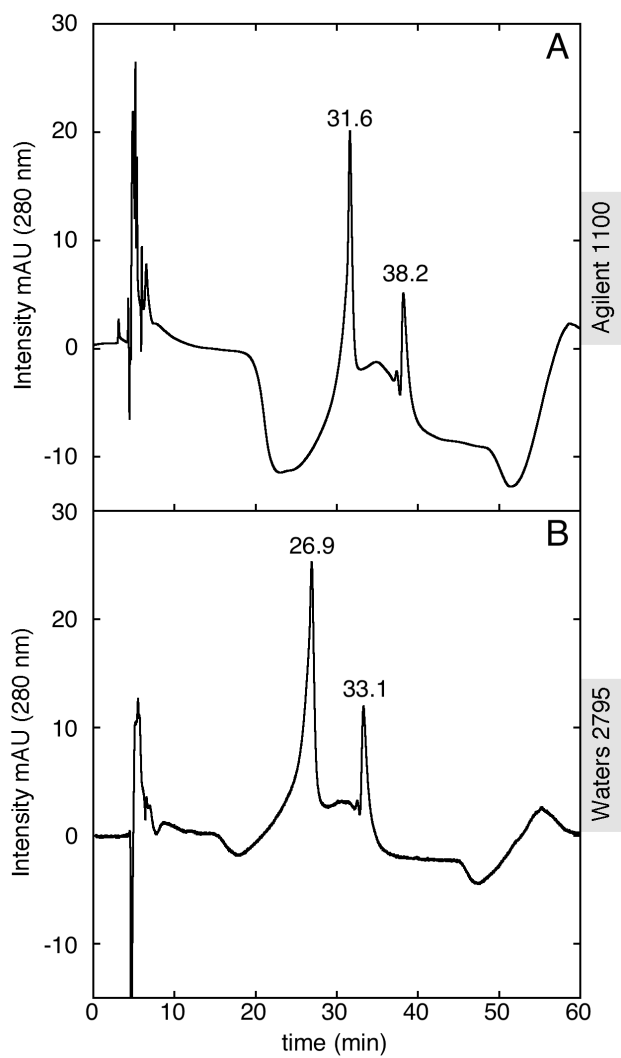
- polymerization of ferric citrate. II. Influence of excess citrate. *J Am Chem Soc* **89**: 5559-5562
- Spiro T, Pape L, Saltman P** (1967b) Hydrolytic polymerization of ferric citrate. I. Chemistry of the polymer. *J Am Chem Soc* **89**: 5555-5559
- Tiffin LO** (1966a) Iron translocation.I. Plant culture exudate sampling iron-citrate analysis. *Plant Physiol* **41**: 510-514
- Tiffin LO** (1966b) Iron translocation.II. Citrate/iron ratios in plant stem exudates. *Plant Physiol* **41**: 515-518
- Tiffin LO** (1970) Translocation of iron citrate and phosphorus in xylem exudate of soybean. *Plant Physiol* **45**: 280-283
- Tiffin LO, Brown JC** (1962) Iron chelates in soybean exudate. *Science* **135**: 311-313
- Tshuva E, Lippard S** (2004) Synthetic models for non-heme carboxylate-bridged diiron metalloproteins: Strategies and tactics. *Chem Rev* **104**: 987-1012
- von Wirén N, Klair S, Bansal S, Briat JF, Khodr H, Shioiri T, Leigh RA, Hider RC** (1999) Nicotianamine chelates both FeIII and FeII. Implications for metal transport in plants *Plant Physiol* **119**: 1107-1114
- White MC, Baker FD, Chaney RL, Decker AM** (1981a) Metal complexation in xylem fluid: II. Theoretical equilibrium and computational computer program. *Plant Physiol* **67**: 301-310
- White MC, Decker AM, Chaney RL** (1981b) Metal complexation in xylem fluid: I. Chemical composition of tomato and soybean exudate. *Plant Physiol* **67**: 292-300
- Woods GD, Fryer FI** (2007) Direct elemental analysis of biodiesel by inductively coupled plasma-mass spectrometry. *Anal Bioanal Chem* **389**: 753-761
- Xuan Y, Scheuermann EB, Meda AR, Hayen H, von Wirén N, Weber G** (2006) Separation and identification of phytosiderophores and their metal complexes in plants by zwitterionic hydrophilic interaction liquid chromatography coupled to electrospray ionization mass spectrometry. *J Chrom A* **1136**: 73-81
- Yokosho K, Yamaji N, Ueno D, Mitani N, Ma JF** (2009) OsFRDL1 is a citrate transporter required for efficient translocation of iron in rice. *Plant Physiol* **149**: 297-305
- Yue WW, Grizot S, Buchanan S** (2003) Structural evidence for iron-free citrate and ferric citrate binding to the TonB-dependent outer membrane transporter FecA. *J Mol Biol* **332**: 353-368
- Zocchi G, De Nisi P, Dell'Orto M, Espen L, Gallina PM** (2007) Iron deficiency differently affects metabolic responses in soybean roots. *J Exp Bot* **58**: 993-1000

SUPPLEMENTARY MATERIALS

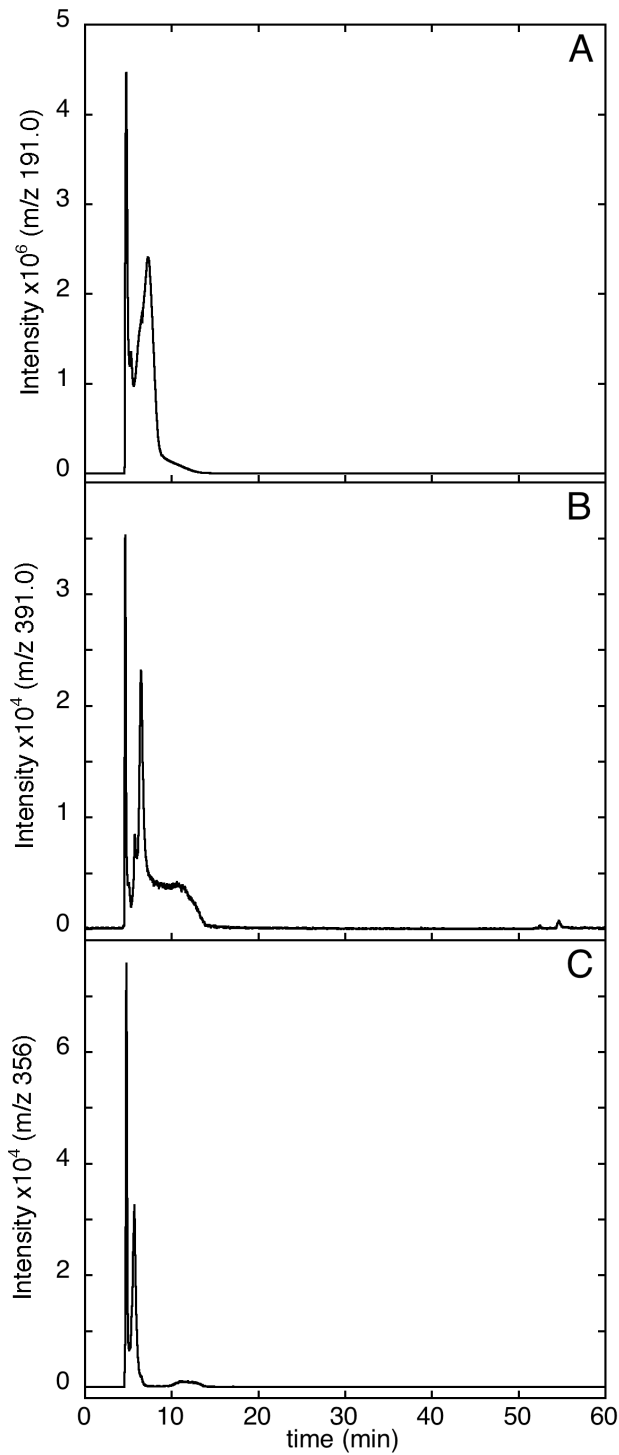
Supplementary Figure 1. ESI-TOFMS mass spectra of a ^{nat}Fe -Cit standard solution (Fe:Cit ratio 1:10, $100\ \mu\text{M}$ ^{nat}Fe , pH 5.5, in 50% mobile phase B) before (A) and after electrospray ionization optimization (B). Isotopic signatures of the $[\text{CitH}]^-$, $[\text{Fe}_3\text{Cit}_3\text{H}]^{2-}$ and $[\text{Fe}_3\text{OCit}_3\text{H}_3]^{2-}$ molecular ions are shown in the panel insets.



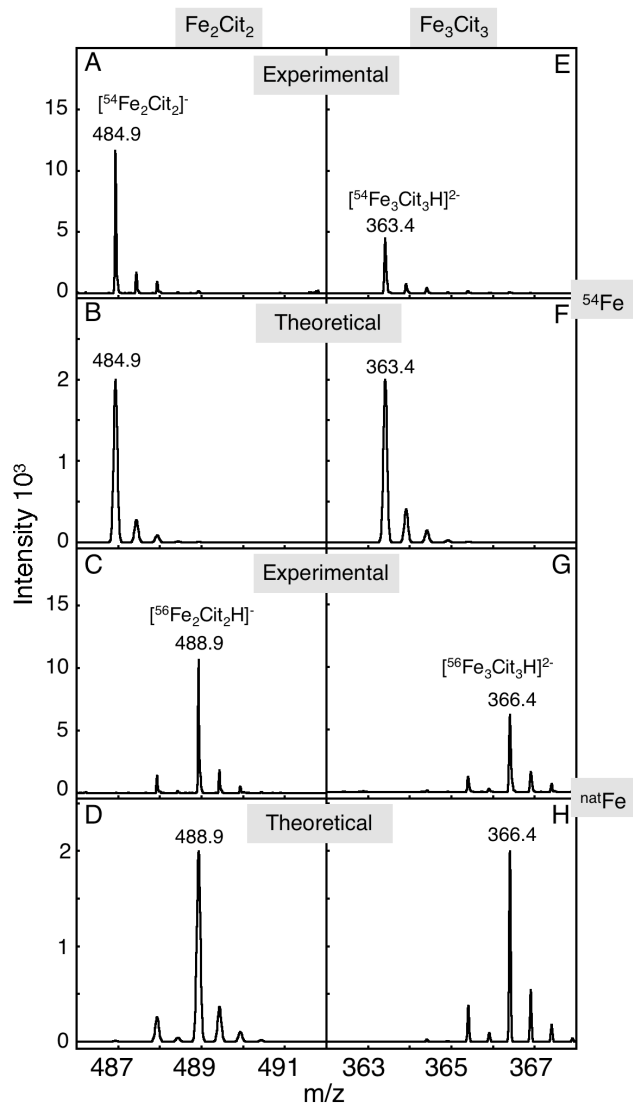
Supplementary Figure 2. HPLC-UV chromatograms obtained with Agilent 1100 (A) and Waters 2795 (B) HPLC systems of an Fe-Cit standard solution (Fe:Cit ratio 1:10, 100 μ M Fe, pH 5.5 diluted in 50% mobile phase B) showing peaks corresponding to Fe_2Cit_2 and Fe_3Cit_3 complexes.



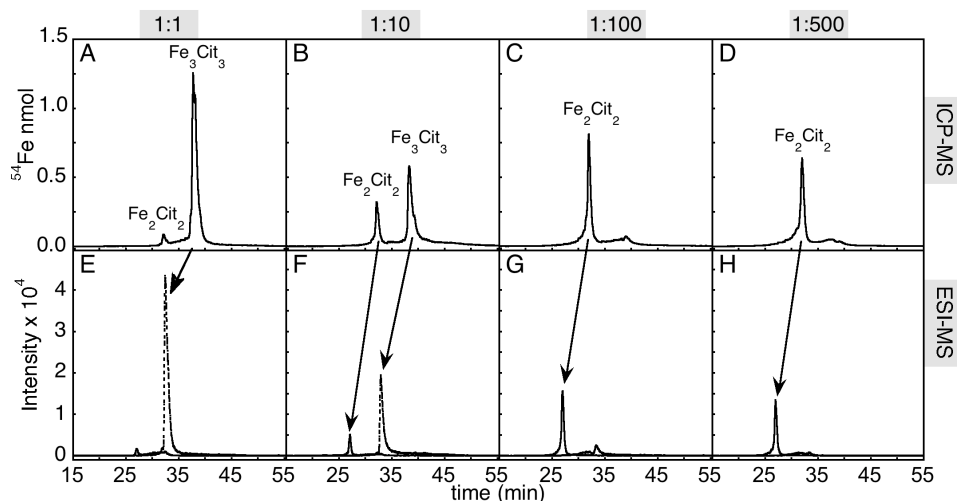
Supplementary Figure 3. HPLC-ESI-TOFMS chromatograms of 5 mM citrate (A), 100 μ M Fe(III)-NA (B) and 100 μ M Fe(III)-DMA (C) standard solutions. Chromatograms show the [CitH]⁻ (A), [Fe(III)-NA+Cl]⁻ (B) and [Fe(III)-DMA]⁻ (C) ions at m/z values 191.0, 391.0 and 356.0 (\pm 0.1), respectively.



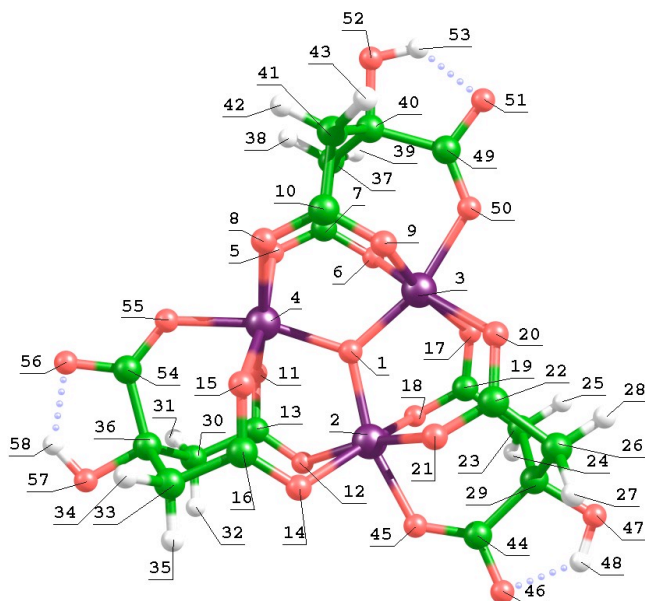
Supplementary Figure 4. Experimental (A, C, E and G) and theoretical (B, D, F and H) isotopic signatures of the molecular ions associated to Fe_2Cit_2 and Fe_3Cit_3 , $[\text{Fe}_2\text{Cit}_2\text{H}]^-$ and $[\text{Fe}_3\text{Cit}_3\text{H}]^{2-}$, respectively. Experimental data are zoomed ESI-TOF mass spectra of the Fe_2Cit_2 and Fe_3Cit_3 chromatographic peaks found when using ^{54}Fe (A, E) and ^{nat}Fe (C, G).



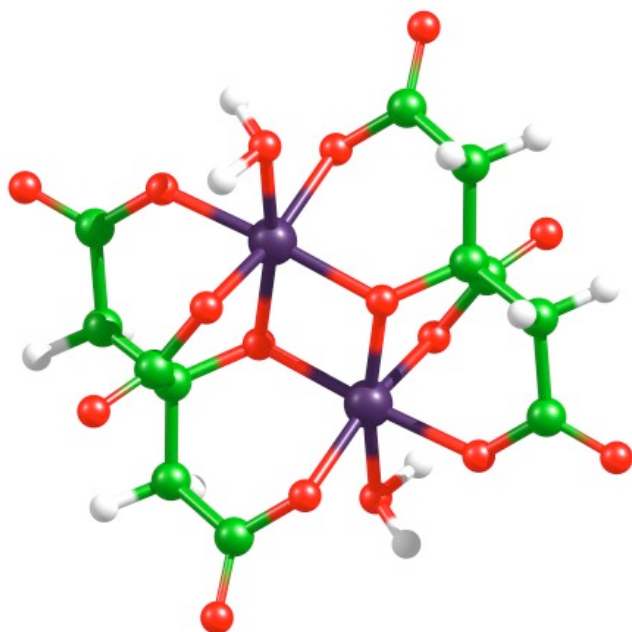
Supplementary Figure 5. Effect of the Fe:Cit ratio on the Fe_2Cit_2 and Fe_3Cit_3 balance, HPLC-ICP-MS (A-D) and HPLC-ESI-TOFMS (E-H) chromatograms of ^{54}Fe -Cit standard solutions with Fe:Cit ratios 1:1, 1:10, 1:100 and 1:500 ($100\ \mu\text{M}\ ^{54}\text{Fe}$, pH 5.5 in 50% mobile phase B) showing peaks corresponding to Fe_2Cit_2 and Fe_3Cit_3 complexes. HPLC-ESI-TOFMS traces were extracted at m/z values 241.93 and 484.87 (± 0.05), corresponding to $[\text{Fe}_2\text{Cit}_2]^{2-}$ and $[\text{Fe}_2\text{Cit}_2\text{H}]^-$, respectively, (for Fe_2Cit_2 , solid line) and 363.40 and 372.40 (± 0.05), corresponding to $[\text{Fe}_3\text{Cit}_3\text{H}]^{2-}$ and $[\text{Fe}_3\text{OCit}_3\text{H}_3]^{2-}$, respectively, (for Fe_3Cit_3 , dotted line).



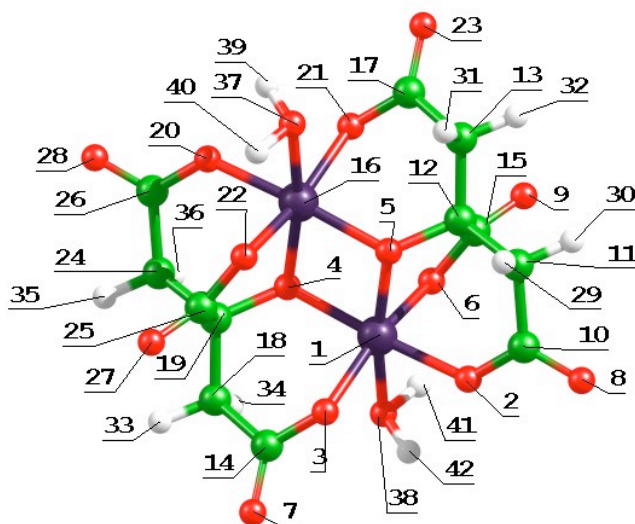
Supplementary Figure 6. Proposed structure for the Fe_3Cit_3 indicating the center numbers (See atom coordinates in Supplementary Table I). Iron, oxygen, carbon and hydrogen atoms are shown in purple, red, green and white, respectively.



Supplementary Figure 7. Proposed structure for the Fe_2Cit_2 complex. Iron, oxygen, carbon and hydrogen atoms are shown in purple, red, green and white, respectively.



Supplementary Figure 8. Proposed structure for the Fe_2Cit_2 indicating the center numbers (See atom coordinates in Supplementary Table III). Iron, oxygen, carbon and hydrogen atoms are shown in purple, red, green and white, respectively.



Supplementary Table I. Xylem sap pH, Fe and citrate concentrations, and Fe:Cit ratios found in previous studies under different Fe status. The most likely Fe-Cit forms are indicated with ● symbols.

	Fe status ^a	Fe in solution (μM) ^b	pH	Fe (μM)	Cit (μM)	Fe:Cit	$\text{Fe}_3\text{Cit}_3^c$	$\text{Fe}_2\text{Cit}_2^c$
Sunflower (Tiffin, 1966)	+Fe	10 + 10	-	2	30	1:15	●	●
	-Fe/+Fe	0.01 + 10	-	31	890	1:29	●	●
Sunflower (Tiffin, 1966)	-Fe	1 + 1	-	8	200	1:25	●	●
	-Fe/+Fe	1 + 50	-	465	460	1:1.0	●	
Tomato (Tiffin, 1966)	-Fe	1 + 2	-	28	72	1:2.6	●	
	-Fe/+Fe	1 + 10	-	131	135	1:1.0	●	
Soybean (Tiffin, 1966)	-Fe	1 + 0.5	-	10	400	1:40	●	●
	-Fe/+Fe	1 + 10	-	290	710	1:2.5	●	
Soybean (Tiffin, 1970)	-Fe	1 + 2.5	-	34	120	1:3.6	●	
<i>Zea mays</i> L WF9 (Clark et al., 1973)	-Fe	18 + 0	-	57	120	1:2	●	
<i>Zea mays</i> L ys1/ys2 (Clark et al., 1973)	-Fe		-	9	430	1:48	●	●
Soybean (White et al., 1981)	+Fe	10	6.1	6	1700	1:283		●
Tomato (White et al., 1981)	+Fe		6.4	7	300	1:43	●	●
Faba bean (Nikolic and Römheld, 1999)	+Fe	100	5.5	12	100	1:8	●	
	-Fe	2	5.5	4	2600	1:650		●
	-Fe	1 + HCO_3^-	5.5	3	2300	1:767		●
Sugar beet (López-Millán et al., 2000)	+Fe	45	6.0	6	200	1:36	●	●
	-Fe	0 + HCO_3^-	5.7	2	4700	1:2474		●
Pear trees (Larbi et al., 2003)	-Fe	field-grown	6.8	3	780	1:260		●
	-		6.5	4	470	1:118		●
	Fe/+Fe		6.6	2	250	1:125		●
Peach trees (Larbi et al., 2003)	-Fe		6.4	5	40	1:8	●	
	Fe/+Fe							
<i>A. thaliana</i> WT (Durrett et al., 2007)	+Fe	100	-	11	90	1:8	●	
<i>A. thaliana frd3-1</i> (Durrett et al., 2007)	+Fe		-	5	55	1:11	●	●
<i>O. sativa</i> WT (Yokosho et al., 2009)	-Fe	2	-	6	185	1:31	●	●
	+Fe	10	-	13	135	1:10	●	●
<i>O. sativa FRDL1 KO</i> (Yokosho et al., 2009)	-Fe	2	-	5	80	1:16	●	●
	+Fe	10	-	9	55	1:65	●	●

Supplementary Table II. Atom coordinates of the Fe₃Cit₃ complex. The center numbers are indicated in Supplementary Fig. 6. All values are expressed in Amstrongs.

Center number	Atomic number	Coordinates		
		X	Y	Z
1	8	0.000000	0.000000	0.000000
2	26	1.910259	0.007702	0.000000
3	26	-0.948460	-1.658184	0.000000
4	26	-0.961800	1.650482	0.000000
5	8	-2.478861	1.197270	1.251661
6	8	-1.916080	-0.994839	1.526843
7	6	-2.789751	-0.038554	1.417397
8	8	-2.478861	1.197270	-1.251661
9	8	-1.916080	-0.994839	-1.526843
10	6	-2.789751	-0.038554	-1.417397
11	8	0.096485	2.156794	1.526843
12	8	2.276297	1.548122	1.251661
13	6	1.361487	2.435272	1.417397
14	8	2.276297	1.548122	-1.251661
15	8	0.096485	2.156794	-1.526843
16	6	1.361487	2.435272	-1.417397
17	8	0.202565	-2.745392	1.251661
18	8	1.819596	-1.161955	1.526843
19	6	1.428264	-2.396718	1.417397
20	8	0.202565	-2.745392	-1.251661
21	8	1.819596	-1.161955	-1.526843
22	6	1.428264	-2.396718	-1.417397
23	6	2.561794	-3.405276	1.309731
24	1	3.240187	-3.292325	2.161717
25	1	2.181368	-4.430083	1.274604
26	6	2.561794	-3.405276	-1.309731
27	1	3.240187	-3.292325	-2.161717
28	1	2.181368	-4.430083	-1.274604
29	6	3.411223	-3.161585	0.000000
30	6	1.668158	3.921217	1.309731
31	1	1.231144	4.452247	2.161717
32	1	2.745881	4.104162	1.274604
33	6	1.668158	3.921217	-1.309731
34	1	1.231144	4.452247	-2.161717
35	1	2.745881	4.104162	-1.274604
36	6	1.032402	4.534998	0.000000
37	6	-4.229952	-0.515941	1.309731
38	1	-4.927249	0.325922	1.274604
39	1	-4.471331	-1.159922	2.161717
40	6	-4.443624	-1.373413	0.000000
41	6	-4.229952	-0.515941	-1.309731
42	1	-4.927249	0.325922	-1.274604
43	1	-4.471331	-1.159922	-2.161717
44	6	4.288980	-1.772224	0.000000
45	8	3.822713	-0.553188	0.000000
46	8	5.545710	-2.022058	0.000000
47	8	4.404176	-4.226855	0.000000
48	1	5.277408	-3.731650	0.000000
49	6	-3.679281	-2.828253	0.000000
50	8	-2.390431	-3.033973	0.000000
51	8	-4.524009	-3.791697	0.000000
52	8	-5.862652	-1.700701	0.000000
53	1	-5.870407	-2.704545	0.000000
54	6	-0.609699	4.600477	0.000000
55	8	-1.432282	3.587160	0.000000
56	8	-1.021702	5.813755	0.000000
57	8	1.458476	5.927556	0.000000
58	1	0.592999	6.436194	0.000000

**LOW MOLECULAR WEIGHT ORGANIC ACID DETERMINATION IN PLANT TISSUE
EXTRACTS BY LIQUID CHROMATOGRAPHY– ELECTROSPRAY TIME-OF-FLIGHT
MASS SPECTROMETRY**

**¹*Rubén Rellán-Álvarez, ^{1,2}*Sara López-Gomollón, ¹Javier Abadía and ¹Ana Álvarez
Fernández**

Submitted to Journal of Agriculture and Food Chemistry

¹Department of Plant Nutrition, Aula Dei Experimental Station (CSIC), P.O. Box 13034, E-50080
Zaragoza, Spain²Present address: School of Biological Sciences, University of East Anglia,
Norwich NR4 7TJ, UK*These authors contributed equally to the paper.

LOW MOLECULAR WEIGHT ORGANIC ACID DETERMINATION IN PLANT TISSUE EXTRACTS BY LIQUID CHROMATOGRAPHY-ELECTROSPRAY TIME-OF-FLIGHT MASS SPECTROMETRY

^{1,*}Rubén Rellán-Álvarez, ^{1,2,*}Sara López-Gomollón, ¹Javier Abadía and ¹Ana Álvarez-Fernández

¹Department of Plant Nutrition, Aula Dei Experimental Station (CSIC), P.O. Box 13034, E-50080 Zaragoza, Spain, ²Present address: School of Biological Sciences, University of East Anglia, Norwich NR4 7TJ, UK. *These authors contributed equally to the paper.

A fast, sensitive and reproducible liquid chromatography-electrospray ionization time of flight mass spectrometry method HPLC-ESI-TOFMS has been developed for the direct and simultaneous determination of organic acids in different plant tissue extracts and exudates. This method permits the simultaneous determination and quantification of several organic acids (oxalic, cis-aconitic, 2-oxoglutaric, citric, malic, quinic, ascorbic, shikimic, succinic and fumaric acids) in less than 15 min. Quantification is accomplished using ¹³C labelled malic and succinic acids as internal standards. Limits of detection were 255 pmol for oxalic acid, 1.16 pmol for cis-aconitic acid, 0.13 pmol for 2-oxoglutaric acid, 1.27 pmol for citric acid, 0.05 pmol for malic acid, 0.85 pmol for quinic acid, 24.9 pmol for ascorbic acid. 1.0 pmol for shikimic acid, 0.42 pmol for succinic acid and 10.8 pmol for fumaric acid. The intraday repeatability values were approximately 0.06 and 1.63 % for retention time and peak area, respectively. The interday repeatability values were about 0.14 and 4.37 % respectively for retention time and peak area. The recoveries obtained for oxalic, 2-oxoglutaric and ascorbic acids were below 90% probably due to potential interferences in the matrix or degradation. For the rest of them, analyte recoveries varied between 92 and 110 %. Due to the importance of organic acids in cellular metabolism and oxidative stress response, this method may be applied for qualitative and quantitative analysis of plant tissue extracts to obtain useful information about the cellular status or response to a specific environmental situation.

Introduction

Low molecular weight organic acids are involved in essential pathways in plant metabolism and catabolism. For instance, citrate, malate, succinate, fumarate and 2-oxoglutarate are

carboxylate intermediates in the Krebs cycle, the central energy-producing pathway of the cell. This metabolic route not only provides reducing power to the cell, but also supplies important precursors for the synthesis of other biomolecules (Buchanan et al., 2000; McCleskey et al., 2002). 2-oxoglutarate is also a key metabolite for proper balancing of the carbon/nitrogen metabolism (Labboun et al., 2009), whereas shikimic acid is a precursor for aromatic amino acids, flavonoids, alkaloids and lignin (Herrmann, 1995), and ascorbate takes part in cellular redox control and antioxidative activities (Smirnoff, 1996). Oxalate, malate and citrate are also involved in metal detoxification (Ma, 2000) and/or transport (Rellán-Álvarez et al., 2010). Organic acids also play important roles in the metabolic response and adaptation of plants to different micronutrient stresses such as Fe (Abadía et al., 2002) and P deficiencies (Vance et al., 2003). Furthermore, organic acids determine the organoleptic properties of fruit juices and other fresh produces (Saavedra and Barbas, 2003).

Many methods have been developed for the determination of carboxylates in a wide range of matrices, including plant tissues (Li et al., 2003; Pérez-Ruíz et al., 2004; Arnetoli et al., 2008; Erro et al., 2009). Some of these methods tackle the direct determination of organic acids in sample extracts without any previous separation step. For instance, enzymatic assays using UV-Vis detection have been used for the determination of some organic acids; however, these techniques usually target a specific compound and cannot be used to determine the whole range of carboxylates in the sample (McCleskey et al., 2002; Rassam and Laing, 2005). Most of the methods used nowadays combine a first separation step and a second detection one. Commonly used separation techniques are capillary zone electrophoresis and high-performance liquid chromatography (HPLC), and the detection technique most often

used is UV-Vis spectrophotometry. However, UV-Vis has a poor specificity, due to the fact that many compounds present in the complex sample extract matrices, including carboxylates and others, can have similar spectra (Zhanguo and Jiuru, 2002). Due to the relatively low UV-Vis extinction coefficient of organic acids, derivatization has been used to improve sensitivity (Rivasseau et al., 2006).

Recently, mass spectrometry (MS) detection-based techniques have been used, coupled to gas chromatography (GC) and HPLC. Mass spectrometry detection provides major advantages over UV-Vis for the determination of carboxylates in complex matrices that contain a large number of interfering compounds. First, selectivity is highly improved, especially in the case of high-resolution MS detection techniques such as Time-Of-Flight (TOFMS); the good mass accuracy provided by high-resolution MS allows for unambiguous elucidation of the molecular formulae of small analytes such as carboxylates. This technique has been used for the determination of carboxylates in different plant tissues and exudates (Avula et al., 2009; Jaitz et al., 2010). Furthermore, sensitivity is also frequently improved in MS detection as compared to UV-Vis, as recently shown for shikimic acid (Avula et al., 2009). Derivatization has been used to further improve chromatographic separation of carboxylates and MS ionization efficiency, leading to sensitivity and selectivity increases (Santa et al., 2009; Jaitz et al., 2010). Also, derivatization with isotope labelled tags has been recently used in metabolome analysis with a focus on profiling carboxylic acid-containing metabolites (Guo and Li, 2010). When mass resolution is not sufficient, the occurrence of isobaric compounds such as citric and quinic acids (both having MW 192.1) can make necessary either a previous separation of these compounds or the use of selected reaction monitoring (SRM) MS² techniques. For instance, SRM has been used to determine carboxylates by quadrupole ion trap MS in different plant species and tissues (Erro et al., 2009) and by triple quadrupole MS in natural waters (Bylund et al., 2007).

Although some recent methods do not use MS internal standards (Chen et al., 2008; Avula et al., 2009; Fernández-Fernández and López-Martínez, 2010), the use of such standards is mandatory to assure the reproducibility and

accuracy of any HPLC-ESI-MS analysis when using complex sample matrices (Rellán-Álvarez et al., 2006; Orera et al., 2009). This is due to the nature of the ionization process required to couple the HPLC and MS devices, since analyte ionization efficiency is strongly affected by co-eluting compounds and can also change during day-to-day operation. Compounds used as internal standards should have chemical characteristics as close as possible to those of the analytes, and for this reason stable isotope-labelled compounds are commonly used. For instance, D-labelled succinic acid (Erro et al., 2009) and ¹³C-labelled oxalic and citric acids (Jaitz et al., 2010) have been recently used as internal standards in HPLC-ESI-MS analysis of carboxylates in different plant materials.

In this study, we have developed and validated a new HPLC-ESI-MS method for the direct determination of organic acids in plant tissue extracts and fluids. The method does not include a derivatization step, and is based on an isocratic HPLC separation and a high-resolution TOFMS detection, using ¹³C-labelled malic and succinic acids as internal standards. For many of the carboxylates analysed the sensitivity of the method is better than that of other recent HPLC-MS based methods for carboxylate determination. The method has been applied to determine several carboxylates in different plant tissue extracts and fluids (root and leaf extracts, xylem sap and orange juice).

Materials and Methods

Reagents. Oxalic and 2-oxoglutaric acids were purchased from Fluka (Sigma-Aldrich, St. Louis, MO, USA); cis-aconitic, malic, quinic, shikimic and fumaric acids were purchased from Sigma-Aldrich; succinic acid was purchased from Merck (Darmstadt, Germany); citric and ascorbic acids were purchased from Riedel-de Hën (Seelze, Germany). Two ¹³C-labelled organic acids were used as internal standards: [¹³C₄]malic acid (¹³C-malic) and [1,4-¹³C₂]succinic acid (¹³C-succinic); both were purchased from Cambridge Isotope Laboratories (Andover, MA, USA). All solvents, extraction buffers and standard solutions were prepared with analytical-grade type I water (Milli-Q Synthesis, Millipore, Bedford, MA, USA). Formic acid was purchased from Fluka, and meta-phosphoric acid was purchased from Sigma-Aldrich.

Standard solutions. Stock solutions containing 10 mM oxalic (M_m 126.1), cis-aconitic (M_m 174.1), 2-oxoglutaric (M_m 146.1), citric (M_m 192.1), malic (M_m 134.1), quinic (M_m 192.2), ascorbic (M_m 176.1), shikimic (M_m 174.1), succinic (M_m 118.1) and fumaric (M_m 116.1) acids, and the internal standards ^{13}C -malic acid (M_m 137.1) and ^{13}C -succinic acid (M_m 120.1) were prepared in 0.1% (v/v) formic acid. Aliquots of each stock were conserved at $-20\text{ }^\circ\text{C}$ until analysis.

Plant material. Different plant materials were used: commercial orange juice, xylem of tomato (*Solanum lycopersicum* L.) and leaves of sugar beet (*Beta vulgaris* L.) were chosen to cover a wide range of analytes, analyte concentrations and matrix composition. Plants were grown in a controlled-environment growth chamber (16 h light/8 h dark photoperiod, 24°C day/ 20°C night).

Sample extraction. Commercial orange juice was diluted (1/20) with 1 mL of cold 4% (w/v) meta-phosphoric acid (MPA). Tomato xylem sap was diluted 1/5 with 1 mL of cold 4% MPA. The internal standards ^{13}C -malic (200 nmol) and ^{13}C -succinic acids (200 nmol) were added at the moment of sample dilution. Samples were extracted by vortexing for 3 min, centrifuged at 15000g for 5 min at 4°C , and supernatants were collected and then filtered through $0.22\text{-}\mu\text{m}$ polyvinylidene fluoride (PVDF) membranes. The filtered sample was taken to a final volume of 2 mL with 0.1% (v/v) formic acid and analysed immediately. Leaves of *B. vulgaris* were frozen in liquid N_2 and ground with mortar and pestle; 100 mg of dry powder were supplemented with ^{13}C -malic and ^{13}C -succinic acids (200 nmol each) and homogenized with a Restch MM301 ball mill (Restch, Düsseldorf, Germany) for 3 min with 1 mL of cold 4% MPA. Homogenates were centrifuged at 15000g for 20 min at 4°C , supernatants were collected and the pellets were extracted again by vortexing with 4% MPA for 3 min; after centrifugation at 15000g for 5 min at 4°C , both supernatants were pooled and then filtered through $0.22\text{-}\mu\text{m}$ PVDF membranes. The filtered sample was taken to a final volume of 2 mL with 0.1% (v/v) formic acid and analysed immediately. Extracts were carried out with five replications.

HPLC-ESI-TOFMS analysis. Analyses were carried out with a with a microTOF II ESI-TOFMS apparatus (Bruker Daltoniks, Bremen, Germany) coupled to a Waters Alliance 2795

HPLC system (Waters, Milford, MA, USA). To optimize the MS signal, direct injection of 10 μM solution of all standards prepared in 0.1% (v/v) formic acid were carried out using a syringe pump (Cole-Parmer Instrument, Vernon Hills, IL, USA) operated at $180\text{ }\mu\text{l}\cdot\text{min}^{-1}$. All analyses were done in negative mode. Drying and nebulizer gas (N_2) were kept at 1.6 psi and $8.0\text{ L}\cdot\text{min}^{-1}$. The mass axis was calibrated using Li-formate adducts ((10mM LiOH, 0.2% (v/v) formic acid and 50% (v/v) 2-propanol). Spectra were acquired in the mass/charge ratio (m/z) range of 80-300. HPLC-ESI-TOFMS analyses were carried out by injection of $20\text{-}\mu\text{l}$ aliquots of standard solutions and sample extracts in a Supelcogel H 250 x 4.6mm anion exchange column packed with a matrix of sulphonated polystyrene/divinylbenzene (Sigma). Autosampler and column temperatures were $6\text{ }^\circ\text{C}$ and $30\text{ }^\circ\text{C}$, respectively, and samples were eluted at a flow rate of $200\text{ }\mu\text{l}\cdot\text{min}^{-1}$. A 20 min isocratic separation was carried out with a mobile phase built with 0.1% formic acid and 5% isopropanol in milliQ water. The system was controlled with the software packages microTOF control 1.2 and HyStar 3.0 (Bruker Daltoniks). Data were processed with Data Analysis 3.4 software (Bruker Daltoniks). The Sigma Fit™ (Bruker Daltoniks) algorithm was used for molecular formula determination (Ojanperä et al., 2006). Validation was carried out using calibration curves corrected with the internal standards ^{13}C -malic and ^{13}C -succinic acids, to account for possible losses during sample extraction and also for possible variations in electrospray ionization. ^{13}C -malic acid (100 μM) was used for the quantification of oxalic, cis-aconitic, 2-oxoglutaric, citric, malic, quinic and ascorbic acids, and ^{13}C -succinic acid (100 μM) was used for the quantification of shikimic, succinic and fumaric acids. Limits of detection (LOD; signal/noise (S/N) ratio of 3) and quantification (LOQ; S/N ratio of 10), intra- and inter-day repeatability, and analyte recovery were assessed using standard techniques. Recovery assays were carried out for oxalic, cis-aconitic, 2-oxoglutaric, citric, malic, quinic, ascorbic, shikimic, succinic and fumaric acids. Plant samples for recovery assays were spiked with 200 nmol of each organic acid and extracted as described above.

Results and Discussion

HPLC-ESI-TOFMS analysis. Direct infusion of a 10 μM standard solution of all organic acids prepared in 0.1 % formic acid was used to optimize ionization parameters. Optimal parameter voltage values, leading to maximum signal intensity for most of the organic acids were (in V): -500 for end plate offset, 3000 for capillary, -82.1 for capillary exit, -41.4 for skimmer 1, and 80.0 for hexapole RF. Using direct infusion and negative mode, individual carboxylate standard solutions (10 μM) gave major $[\text{M}-\text{H}]^{-1}$ ions at m/z values of 89.03 (oxalic acid), 173.11 (cis-aconitic acid) 173.15 (shikimic acid), 145.11 (oxoglutaric acid), 191.12 (citric acid) 191.17 (quinic acid), 133.09 (malic acid), 175.12 (ascorbic acid), 117.09, (succinic acid), 115.07 (fumaric acid), 137.09 (^{13}C -malic acid) and 119.07 (^{13}C -succinic acid).

The chromatographic separation of the different organic acids is shown in Fig. 1. All the peaks obtained were sharp, and a good separation was obtained for all organic acids used, except for the pairs succinic/shikimic and quinic/ascorbic acids, which showed partial overlapping. The rest of the organic acids had a near baseline separation. The two isobaric couples *-i.e.*, with near identical m/z values- citric and quinic acids (with m/z 191.12 and 191.17, respectively), and cis-aconitic and shikimic acids (with m/z 173.11 and 173.15, respectively), were well separated in the chromatographic run (Fig. 1). The two internal standards co-eluted with the corresponding unlabelled compounds (Fig. 1). Analysis time for

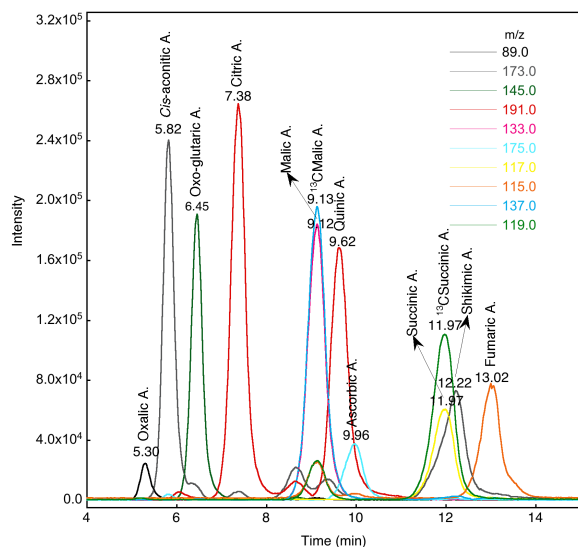


Figure 1. Chromatograms of a mixture of organic acid standards. Concentration of all organic acids (including the internal standards) was 100 μM .

all compounds analysed was approximately 15 min.

Validation of the HPLC-ESI-TOFMS method. Standard solutions of the different carboxylates were prepared in the extraction solution for validation of the method. Calibration curves were corrected with the internal standards, and intra-day-inter-day repeatability and LOD and LOQ values were obtained. Calibration curves in the 0.1-1000 μM range, obtained for the different organic acids, are shown in Supplementary Fig. 1; all correlation coefficients (R^2) obtained were higher than 0.992. Different ranges of linearity were observed for the organic acids analysed, with the best results being obtained for cis-aconitic, 2-oxoglutaric, malic and succinic acids, with linearity ranges from (0.15-0.25) to 1000 μM . In the cases of oxalic, citric, ascorbic and fumaric acids, linearity ranges were from (0.14-17) to 500 μM . The shorter linearity ranges corresponded to quinic and shikimic acids, from 0.18 to 70 and from 0.38 to 100 μM , respectively. The concentration of most of the analysed organic acids is usually within the linear ranges found in plant tissues (Fiehn et al., 2000; Gout et al., 2001).

Limits of detection and LOQ values, defined as the analyte amount that gives a S/N ratio of 3 and 10, respectively, are shown in Table I. LOD values were between 0.13 (2-oxoglutaric acid) and 255 pmol (oxalic acid), respectively, while LOQs values ranged between 2.8 (citric acid) and 337 pmol (oxalic acid), respectively. For most of the organic acids measured, LODs and LOQs were below 2 and 5 pmol, respectively (Table 1), and method sensitivity is similar or better to that of previous HPLC-MS methods (Bylund et al., 2007; Chen et al., 2008; Erro et al., 2009; Jaitz et al., 2010); see Supplementary

Table I. LODs and LOQs for the organic acids using the LC-ESI/MS TOF method

Organic Acid	LOD		LOQ	
	μM	pmol	μM	pmol
Oxalic acid	12.8	255	16.9	337
Cis-aconitic acid	0.058	1.16	0.245	4.91
2-oxoglutaric acid	0.007	0.13	0.208	4.15
Citric acid	0.063	1.27	0.140	2.80
Malic acid	0.003	0.05	0.162	3.24
Quinic acid	0.043	0.85	0.184	3.68
Ascorbic acid	1.25	24.9	2.42	48.3
Shikimic acid	0.050	1.00	0.367	7.35
Succinic acid	0.021	0.42	0.158	3.15
Fumaric acid	0.540	10.8	1.87	37.5

Table 1).

The intra-day repeatability was assessed by injecting a 100 μM standard of all carboxylates and internal standards in 10 consecutive chromatographic runs; the variation in retention time and peak area was analysed for each organic acid is shown in Table II. The inter-day repeatability was assessed by analysing the same standard during five consecutive days. The relative standard deviation (RSD) for peak retention time was always lower than 0.2% in the intraday test and 0.4% in the inter-day test. The RSD for peak area was in the range of 0.5 to

2.8% in the intraday test; in the inter-day test, the RSD was in the range of 1 to 4%, except for ascorbic acid (RSD: 20%), a compound that is known to be very labile and easily degraded with time.

In the case of slight shifts in retention time, when using the TOFMS detection proposed here the identity of any given peak can be confirmed from the molecular formula determination derived from the isotopic pattern information in combination with the Sigma Fit™ (Bruker Daltoniks) algorithm (Ojanperä et al., 2006).

Table II. Intra-day (n=10) and inter-day (n=5) repeatability of the LC-ESI-TOFMS method. A 100- μM standard solution of all organic acids including internal standards was used.

		Intra-day			Inter-day		
		Mean	SD	RSD (%)	Mean	SD	RSD (%)
Oxalic acid	RT	5.36	0.01	0.15	5.35	0.01	0.22
	A_S/A_{IS}	0.06	0.00	1.56	0.05	0.00	3.70
Cis-aconitic acid	RT	5.87	0.00	0.08	5.87	0.00	0.06
	A_S/A_{IS}	1.15	0.02	1.47	1.04	0.03	3.19
2-oxoglutaric acid	RT	6.48	0.00	0.04	6.47	0.00	0.07
	A_S/A_{IS}	0.61	0.01	2.28	0.66	0.01	2.27
Citric acid	RT	7.42	0.00	0.04	7.41	0.01	0.13
	A_S/A_{IS}	1.74	0.03	1.62	1.73	0.02	0.99
Malic acid	RT	9.18	0.00	0.04	9.17	0.01	0.11
	A_S/A_{IS}	0.82	0.02	2.32	0.85	0.02	2.91
Quinic acid	RT	9.64	0.00	0.05	9.64	0.01	0.08
	A_S/A_{IS}	1.06	0.01	0.84	0.88	0.04	4.14
Ascorbic acid	RT	9.99	0.01	0.06	9.97	0.04	0.35
	A_S/A_{IS}	0.22	0.01	2.74	0.25	0.05	19.18
Shikimic acid	RT	12.21	0.00	0.03	12.20	0.01	0.10
	A_S/A_{IS}	1.08	0.02	1.92	1.08	0.05	4.41
Succinic acid	RT	12.02	0.01	0.05	12.01	0.01	0.10
	A_S/A_{IS}	0.53	0.00	0.52	0.51	0.01	1.36
Fumaric acid	RT	13.21	0.01	0.06	13.20	0.02	0.16
	A_S/A_{IS}	0.73	0.01	1.11	0.72	0.01	1.52

RT: retention time; As: area of standard's peak; AIS: area of internal standard's peak.

Recovery assays. Recovery assays were carried out for all organic acids in sugar beet leaf extracts, tomato xylem and orange juice, by spiking samples with known amounts of analyte standards and isotope-labelled internal standards. Recovery was calculated by dividing the amount of analyte found in the spiked sample by the sum of the amount originally found in the sample plus the amount spiked. Good analyte recoveries were found (in the range 92-110%; 99% average value) for cis-aconitic, citric, malic, quinic, succinic, shikimic and fumaric acids. However, the recovery values for oxalic, oxo-glutaric and ascorbic acids were lower, with average values

of 64, 60 and 61%, respectively (Table III). Compounds present in plant tissues or saps, such as metals, flavonoids, amino acids and sugars, can significantly affect ascorbic acid measurements (Clydesdale et al., 1991). Ascorbate is oxidized by light and air and it is only detectable by ESI-MS when in reduced state, so that recovery may be increased by protecting samples during extraction by using a cold chamber and a green safe-light (Rellán-Álvarez et al., 2006). Regarding the low recovery of oxalic acid in tomato xylem and orange juice, some studies suggest that pH and Ca^{2+} have a great impact in oxalic solubility, leading to the

formation of insoluble precipitates that interfere with its quantification (Rassam and Laing, 2005); however, oxalic acid recovery in sugar beet leaves is good. In the cases of succinic and malic acids, where isotope-labelled compounds were used as internal standards, recoveries were 96-104% in all tissues tested. Therefore, it seems likely that results could be improved by using the corresponding isotope-labelled internal standard for each analyte, although a compromise between the number of expensive internal standards and total analysis costs is needed; the rationale is that a given internal standard may provide coverage for carboxylates eluting within a range of retention times. Therefore, the use of one additional ^{13}C -labelled organic, eluting close to oxalic and 2-oxoglutaric acids) would lead to

improved recoveries for these carboxylates. Also, regarding internal standards we have preferred using ^{13}C -labelled internal standards over D-labelled ones (Erro et al., 2009) because when using the latter compounds, proton exchange reactions with the extraction media and/or mobile phase can easily occur (Chavez-Eng et al., 2002). The method explained in this study has been already applied for the determination of organic acids in peach roots (Jiménez et al. *In press*) and roots, xylem sap and leaves of sugar beet (Sagardoy et al., *In press*).

Conclusions

An HPLC-ESI-TOFMS method has been developed and validated to determine

Table III. Recoveries obtained for the different organic acids in tomato xylem sap, sugar beet leaf extracts and commercial orange juice. All values with the exception of recovery are expressed in pmol. Results are means \pm SE. (n=5)

Organic Acid	Sample	Sample amount	Amount added	Amount found	Recovery (%)
Oxalic acid	Sugar beet leaf	29991 \pm 832.1	1780.7 \pm 9.3	33722.9 \pm 431.0	107.8 \pm 3.6
	Tomato xylem	549.9 \pm 8.0	2045.7 \pm 15.1	1204.1 \pm 23.1	46.5 \pm 1.0
	Orange juice	243.3 \pm 0.0	2046.9 \pm 21.8	888.9 \pm 20.1	38.9 \pm 1.0
Cis-aconitic acid	Sugar beet leaf	9.4 \pm 0.3	1935.4 \pm 8.3	1925.5 \pm 25.7	99.2 \pm 1.7
	Tomato xylem	80.2 \pm 0.0	2043.8 \pm 11.3	2179.4 \pm 41.2	102.8 \pm 2.3
	Orange juice	0 \pm 0.0	1422.9 \pm 7.8	925.5 \pm 17.8	95.8 \pm 2.0
2-oxoglutaric acid	Sugar beet leaf	7.6 \pm 0.0	1924.8 \pm 3.3	1279.8 \pm 17.6	66.2 \pm 0.9
	Tomato xylem	77.7 \pm 0.8	1961.5 \pm 12.1	1400.6 \pm 30.0	68.8 \pm 1.8
	Orange juice	26.7 \pm 0.5	1952.8 \pm 16.5	868.3 \pm 7.4	43.9 \pm 0.7
Citric acid	Sugar beet leaf	2076.3 \pm 61.5	2275.0 \pm 5.5	4329.9 \pm 17.5	100.0 \pm 1.8
	Tomato xylem	1078.8 \pm 6.3	1999.3 \pm 17.3	3367.5 \pm 51.0	109.6 \pm 2.2
	Orange juice	12426.7 \pm 257.0	1751.0 \pm 25.4	13667.7 \pm 75.6	96.7 \pm 1.5
Malic acid	Sugar beet leaf	1260.1 \pm 37.7	1948.9 \pm 5.7	3381.9 \pm 26.9	104.0 \pm 1.4
	Tomato xylem	1730.4 \pm 10.5	1825.1 \pm 15.3	3574.7 \pm 28.4	100.6 \pm 1.0
	Orange juice	3087.5 \pm 25.3	1879.9 \pm 14.8	5016.4 \pm 20.5	101.0 \pm 0.5
Quinic acid	Sugar beet leaf	0 \pm 0.0	1841.7 \pm 2.1	1757.6 \pm 6.8	98.0 \pm 0.4
	Tomato xylem	0 \pm 0.0	1487.3 \pm 10.8	1367.3 \pm 26.7	96.7 \pm 2.4
	Orange juice	252.9 \pm 1.9	1769.9 \pm 17.5	1982.9 \pm 11.9	98.2 \pm 1.4
Ascorbic acid	Sugar beet leaf	296.6 \pm 9.1	1968.2 \pm 6.6	486.2 \pm 9.0	21.5 \pm 0.4
	Tomato xylem	459.1 \pm 0.0	2196.7 \pm 14.4	2266.3 \pm 41.5	85.5 \pm 1.9
	Orange juice	913.7 \pm 8.2	2178.5 \pm 17.1	2362.6 \pm 23.4	76.4 \pm 0.5
Shikimic acid	Sugar beet leaf	0 \pm 0.0	1811.5 \pm 6.4	1830.1 \pm 11.2	103.2 \pm 0.8
	Tomato xylem	47.5 \pm 0.0	1660.6 \pm 24.4	1652.7 \pm 21.2	97.4 \pm 2.5
	Orange juice	47.5 \pm 0.0	1641.8 \pm 33.1	1545.7 \pm 16.7	91.9 \pm 1.9
Succinic acid	Sugar beet leaf	159.3 \pm 4.8	1806.5 \pm 7.3	1973.0 \pm 14.7	100.4 \pm 0.6
	Tomato xylem	64.7 \pm 0.6	1697.2 \pm 18.3	1698.1 \pm 30.0	96.8 \pm 2.5
	Orange juice	59.2 \pm 7.1	1690.2 \pm 26.0	1676.9 \pm 11.5	96.4 \pm 2.5
Fumaric acid	Sugar beet leaf	0 \pm 0.0	2162.3 \pm 6.8	1989.4 \pm 12.7	93.2 \pm 0.5
	Tomato xylem	0 \pm 0.0	2148.8 \pm 31.6	1999.4 \pm 34.6	94.8 \pm 3.1
	Orange juice	0 \pm 0.0	2142.8 \pm 45.5	1969.9 \pm 12.8	93.5 \pm 2.7

simultaneously ten different low molecular weight carboxylates in plant tissue samples. Carboxylate analysis is carried out following a rapid and easy extraction procedure, and neither sample pre-purification nor derivatization time-consuming steps are necessary. The method is based on a separation with anion exchange HPLC, followed by ionization of the sample by electrospray and analyte detection with a TOFMS device using two ^{13}C isotope-labelled internal standards. The method is highly selective, with the identification of carboxylates being unequivocal, based both in retention time and exact molecular mass. This method allows for the simultaneous and accurate determination of carboxylates in a variety of plant tissues and extracts, such as orange juice, leaf and root extracts and xylem sap, with an overall sensitivity better than that offered by currently available HPLC-ESI-MS methods.

Acknowledgements

This study was supported by the Spanish Ministry of Science and Innovation (MICINN; projects AGL2007-61948 and AGL2009-09018, co-financed with FEDER), the European Commission (Thematic Priority 5–Food Quality and Safety, 6th Framework RTD Programme, Contract no. FP6-FOOD–CT-2006-016279), the trilateral Project Hot Iron (ERA-NET Plant Genome Research KKBE; MICINN EUI2008-03618), and the Aragón Government (group A03). R.R.-A. and S.L.-G. were supported by a FPI-MCINN fellowship and a CSIC Grant (I3P-2005) from the I3P programme, co-financed by the European Social Fund, respectively. Acquisition of the HPLC-TOFMS apparatus was co-financed with FEDER.

References

- Abadía J, López-Millán AF, Rombolá A, Abadía A** (2002) Organic acids and Fe deficiency: a review. *Plant Soil* **241**: 75-86
- Arnetoli M, Montegrossi G, Buccianti A, Gonnelli C** (2008) Determination of organic acids in plants of *Silene paradoxa* L. by HPLC. *J. Ag. Food Chem.* **56**: 789-795
- Avula B, Wang Y, Smillie T, Khan I** (2009) Determination of shikimic acid in fruits of illicium species and various other

plant samples by LC–UV and LC–ESI–MS. *Chromatographia* **69**: 307-314

- Buchanan BB, Gruissem W, Jones RR** (2000) *Biochemistry and Molecular Biology of Plants*. American Society of Plant Physiologists, Rockville, Maryland
- Bylund D, Norstrom SH, Essen SA, Lundstrom US** (2007) Analysis of low molecular mass organic acids in natural waters by ion exclusion chromatography tandem mass spectrometry. *J. Chromatogr.* **1176**: 89-93
- Chavez-Eng CM, Constanzer ML, Matuszewski BK** (2002) High-performance liquid chromatographic-tandem mass spectrometric evaluation and determination of stable isotope labeled analogs of rofecoxib in human plasma samples from oral bioavailability studies. *J. Chrom. B* **767**: 117-129
- Chen Z, Kim K-R, Owens G, Naidu R** (2008) Determination of carboxylic acids from plant root exudates by ion exclusion chromatography with ESI-MS. *Chromatographia* **67**: 113-117
- Clydesdale FM, Ho CT, Lee CY, Mondy NI, Shewfelt RL** (1991) The effects of postharvest treatment and chemical interactions on the bioavailability of ascorbic acid, thiamin, vitamin A, carotenoids, and minerals. *Crit. Rev. Food Sci. Nutr.* **30**: 599-638
- Erro J, Zamarreño AM, Yvin J-C, García-Mina JM** (2009) Determination of organic acids in tissues and exudates of maize, lupin and chickpea by high-performance liquid chromatography-tandem mass spectrometry. *J. Ag. Food Chem.* **57**: 4004-4010
- Fernández-Fernández R, López-Martínez J** (2010) Simple LC–MS determination of citric and malic acids in fruits and vegetables. *Chromatographia* **72**: 55-62
- Guo K, Li L** (2010) High-performance isotope labeling for profiling carboxylic acid-containing metabolites in biofluids by mass spectrometry. *Anal. Chem.* **82**: 8789-8793
- Herrmann KM** (1995) The shikimate pathway as an entry to aromatic secondary metabolism. *Plant Physiol.* **107**: 7-12
- Jaitz L, Mueller B, Koellensperger G, Huber D, Oburger E, Puschenreiter M, Hann**

- S (2010) LC-MS analysis of low molecular weight organic acids derived from root exudation. *Anal. Bioanal. Chem.* **10.1007/s00216-010-4090-0**
- Jiménez S, Ollat N, Deborde C, Maucourt M, Rellán-Álvarez R, Moreno MÁ, Gogorcena Y** (*In Press*) Metabolic response in roots of *Prunus* rootstocks submitted to iron chlorosis. *J. Plant Physiol.* DOI: 10.1016/j.jplph.2010.08.010
- Labboun S, Terc-Laforgue T, Roscher A, Bedu M, Restivo FM, Velanis CN, Skopelitis DS, Moshou PN, Roubelakis-Angelakis KA, Suzuki A, Hirel B** (2009) Resolving the role of plant glutamate dehydrogenase. I. in vivo real time nuclear magnetic resonance spectroscopy experiments. *Plant Cell Physiol.* **50**: 1761-1773
- Li C, Pang X, Zhang F** (2003) Comparison on responses of different phosphorus-efficient wheat varieties to phosphorus-deficiency stress. *Act. Bot. Sinica* **45**: 936-943
- Ma JF** (2000) Role of organic acids in detoxification of aluminum in higher plants. *Plant Cell Physiol.* **41**: 383-390
- McCleskey SC, Metzger A, Simmons CS, Anslyn EV** (2002) Competitive indicator methods for the analysis of citrate using colorimetric assays. *Tetrahedron* **58**: 621-628
- Ojanperä S, Pelander A, Pelzing M, Krebs I, Vuori E, Ojanperä I** (2006) Isotopic pattern and accurate mass determination in urine drug screening by liquid chromatography/time-of-flight mass spectrometry. *Rapid Commun. Mass Sp.* **20**: 1161-1167
- Orera I, Abadía A, Abadía J, Álvarez-Fernández A** (2009) Determination of *o,o*EDDHA - a xenobiotic chelating agent used in Fe fertilizers - in plant tissues by liquid chromatography/electrospray mass spectrometry: overcoming matrix effects. *Rapid Commun. Mass Sp.* **23**: 1694-1702
- Pérez-Ruiz T, Martínez-Lozano C, Tomas V, Martín J** (2004) High-performance liquid chromatographic separation and quantification of citric, lactic, malic, oxalic and tartaric acids using a post-column photochemical reaction and chemiluminescence detection. *J. Chromatogr.* **1026**: 57-64
- Rassam M, Laing W** (2005) Variation in ascorbic acid and oxalate levels in the fruit of *Actinidia chinensis* tissues and genotypes. *J. Ag. Food Chem.* **53**: 2322-2326
- Rellán-Álvarez R, Giner-Martínez-Sierra J, Orduna J, Orera I, Rodríguez-Castrillón JA, García-Alonso JI, Abadía J, Álvarez-Fernández A** (2010) Identification of a tri-iron(III), tri-citrate complex in the xylem sap of iron-deficient tomato resupplied with iron: new insights into plant iron long-distance transport. *Plant Cell Physiol.* **51**: 91-102
- Rellán-Álvarez R, Hernández LE, Abadía J, Álvarez-Fernández A** (2006) Direct and simultaneous determination of reduced and oxidized glutathione and homogluthathione by liquid chromatography-electrospray/mass spectrometry in plant tissue extracts. *Anal. Biochem.* **356**: 254-264
- Rivasseau C, Boisson AM, Mongelard G, Couram G, Bastien O, Bligny R** (2006) Rapid analysis of organic acids in plant extracts by capillary electrophoresis with indirect UV detection: directed metabolic analyses during metal stress. *J. Chromatogr.* **1129**: 283-290
- Saavedra L, Barbas C** (2003) Validated capillary electrophoresis method for small-anions measurement in wines. *Electrophoresis* **24**: 2235-2243
- Sagardoy R, Morales F, Rellán-Álvarez R, Abadía A, Abadía J, López-Millán A-F** (*In press*) Carboxylate metabolism in sugar beet plants grown with excess Zn. *J. Plant Physiol.* DOI: /10.1016/j.jplph.2010.10.012
- Santa T, Al-Dirbashi OY, Yoshikado T, Fukushima T, Imai K** (2009) Synthesis of benzofurazan derivatization reagents for short chain carboxylic acids in liquid chromatography/electrospray ionization-tandem mass spectrometry (LC/ESI-MS/MS). *Biomed. Chromatogr.* **23**: 443-446

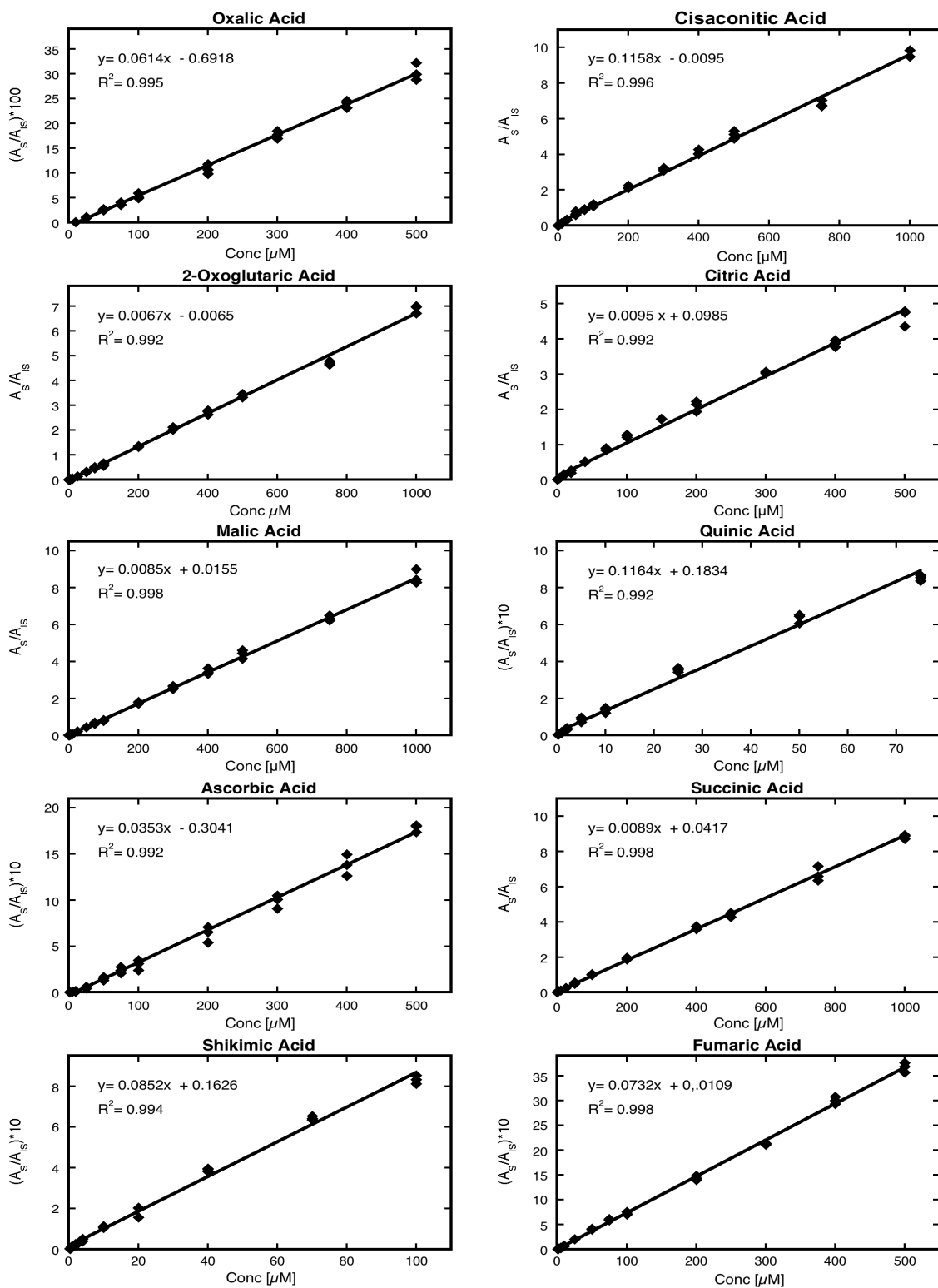
- Smirnoff N** (1996) The function and metabolism of ascorbic acid in plants. *Ann. Bot.* **78**: 661-669
- Vance CP, Uhde-Stone C, Allan DL** (2003) Phosphorus acquisition and use: Critical adaptations by plants for securing a nonrenewable resource. *New Phytol.* **157**: 423-447
- Zhanguo C, Jiuru L** (2002) Simultaneous and direct determination of oxalic acid, tartaric acid, malic acid, vitamin C, citric acid, and succinic acid in *Fructus mume* by reversed-phase high-performance liquid chromatography. *J. Chrom. Sc.* **40**: 35-39

SUPPLEMENTARY MATERIALS

Supplementary Table 1. Comparison of LODs with those of other published HPLC-ESI-MS methods. All LODs are shown in pmol. (n.a.: not analysed). LODs lower and higher than those of this method are marked in red and green, respectively.

Organic Acid	This study	(Bylund, 2007)	(Chen, 2008)	(Avula, 2009)	(Erro, 2009)	(Jaitz, 2010)	(Fernández, 2010)
Internal Standard	✓	-	-	-	✓ (D-labelled)	✓	-
Derivatization	-	-	-	-	-	✓	-
Oxalic	255	20	10	n.a.	5,000	1.6	n.a.
Cis-aconic	1.16	0.1	1.72	n.a.	86	0.2	n.a.
2-oxoglutaric	0.13	0.5	n.a.	n.a.	n.a.	n.a.	n.a.
Citric	1.27	0.2	1.56	n.a.	310	0.1	4600
Malic	0.05	0.1	n.a.	n.a.	220	1	9600
Quinic	0.85	n.a.	n.a.	n.a.	n.a.	n.a.	n.a.
Ascorbic	24.9	n.a.	n.a.	n.a.	n.a.	n.a.	n.a.
Shikimic	1.00	5	n.a.	1.69	n.a.	n.a.	n.a.
Succinic	0.42	0.5	2.54	n.a.	762	1.5	n.a.
Fumaric	10.8	5	n.a.	n.a.	1292	4.7	n.a.

Supplementary Figure 1. Calibration curves of oxalic, cisaconitic, 2-oxoglutaric, citric, malic, quinic, ascorbic, succinic, shikimic and fumaric acid obtained by analyzing a mixture of standards by the LC-ESI/ TOF MS method.



**CHANGES IN THE PROTEOMIC AND METABOLIC PROFILES OF *BETA VULGARIS*
ROOT TIPS IN RESPONSE TO IRON DEFICIENCY AND RESUPPLY**

**Ruben Rellán-Álvarez¹, Sofía Andaluz¹, Jorge Rodríguez-Celma¹, Gert Wohlgenuth²,
Graziano Zocchi³, Ana Álvarez-Fernández¹, Oliver Fiehn², Ana-Flor López-Millán¹, Javier
Abadía¹**

BMC Plant Biology, 2010 10: 120

¹Department of Plant Nutrition, Aula Dei Experimental Station, CSIC, P.O. Box 13034, E-50080 Zaragoza, Spain. ²Genome Center, University of California Davis, CA 95616, USA ³Dipartimento di Produzione Vegetale, Sez. Biochimica e Fisiologia delle Piante, Università di Milano, Via Celoria 2, I-20133 Milano, Italy.

CHANGES IN THE PROTEOMIC AND METABOLIC PROFILES OF BETA VULGARIS ROOT TIPS IN RESPONSE TO IRON DEFICIENCY AND RESUPPLY

Rellán-Álvarez R^{*1}, Andaluz S^{*1}, Rodríguez-Celma J¹, Wohlgemuth G², Zocchi G³, Álvarez-Fernández A¹, Fiehn O², López-Millán AF¹, Abadía J¹

¹Department of Plant Nutrition, Aula Dei Experimental Station, CSIC, P.O. Box 13034, E-50080 Zaragoza, Spain. ²Genome Center, University of California Davis, CA 95616, USA ³Dipartimento di Produzione Vegetale, Sez. Biochimica e Fisiologia delle Piante, Università di Milano, Via Celoria 2, I-20133 Milano, Italy. *These authors contributed equally to the paper

Background

Plants grown under iron deficiency show different morphological, biochemical and physiological changes. These changes include, among others, the elicitation of different strategies to improve the acquisition of Fe from the rhizosphere, the adjustment of Fe homeostasis processes and a reorganization of carbohydrate metabolism. The application of modern techniques that allow the simultaneous and untargeted analysis of multiple proteins and metabolites can provide insight into multiple processes taking place in plants under Fe deficiency. The objective of this study was to characterize the changes induced in the root tip proteome and metabolome of sugar beet plants in response to Fe deficiency and resupply.

Results

Root tip extract proteome maps were obtained by 2-D isoelectric focusing polyacrylamide gel electrophoresis, and approximately 140 spots were detected. Iron deficiency resulted in changes in the relative amounts of 61 polypeptides, and 22 of them were identified by mass spectrometry (MS). Metabolites in root tip extracts were analyzed by gas chromatography-MS, and more than 300 metabolites were resolved. Out of 77 identified metabolites, 26 changed significantly with Fe deficiency. Iron deficiency induced increases in the relative amounts of proteins and metabolites associated to glycolysis, tri-carboxylic acid cycle and anaerobic respiration, confirming previous studies. Furthermore, a protein not present in Fe-sufficient roots, dimethyl-8-ribityllumazine (DMRL) synthase, was present in high amounts in root tips from Fe-deficient sugar beet plants and also gene transcript levels were higher in Fe-deficient root tips. Also, a marked increase in the relative amounts of the raffinose family of oligosaccharides (RFOs)

was observed in Fe-deficient plants, and a further increase in these compounds occurred upon short term Fe resupply.

Conclusions

The increases in DMRL synthase and in RFO sugars were the major changes induced by Fe deficiency and resupply in root tips of sugar beet plants. Flavin synthesis could be involved in Fe uptake, whereas RFO sugars could be involved in the alleviation of oxidative stress, C trafficking or cell signalling. Our data also confirm the increase in proteins and metabolites related to carbohydrate metabolism and TCA cycle pathways.

Background

Two different strategies of Fe uptake have been described in plants. The so-called chelation strategy (or Strategy II), which is mainly found in graminaceous plants, is based on the excretion of phytosideropores (PS) to the rhizosphere. Phytosideropores rapidly chelate Fe(III), to form Fe(III)-PS chelates that are subsequently transported into the root cells through a specific transporter. The so-called reduction strategy (or Strategy I) relies on the coordinated action of a membrane bound Fe reductase, that reduces Fe(III) to Fe(II) [1], an Fe(II) uptake transporter [2] and an H⁺-ATPase that lowers the pH of the rhizosphere [3], is mainly used by non graminaceous plants, including *Beta vulgaris*. The reduction strategy includes root morphological, physiological and biochemical changes that lead to an increased capacity for Fe uptake. Morphological changes include root tip swelling, development of transfer cells and an increase in the number of lateral roots, leading to an increase in the root surface in contact with the medium [4].

Some plants are able to accumulate and/or release both reducing and chelating substances, such as phenolics and flavins, which may have a role in Fe acquisition [5, 6]. Iron has been shown

to down-regulate riboflavin (Rbfl) synthesis in flavinogenic yeast strains and some bacteria [7, 8]. In plants, Rbfl and derivatives are accumulated and/or excreted in Fe-deficient roots and could act as a redox bridge for electron transport to the Fe(III) reductase [9]. Moreover, FRO2 belongs to a superfamily of flavocytochrome oxidoreductases [1], and a recent study confirmed that the FRO2 protein contains FAD sequence motifs on the inside of the membrane [10]. Also, a connection between Fe deficiency perception and Rbfl excretion has been described to occur through basic helix-loop-helix (bHLH) transcription factors in *Arabidopsis thaliana* [11].

At the metabolic level, increases in the activity of phosphoenolpyruvate carboxylase (PEPC) and several enzymes of the glycolytic pathway and the tricarboxylic acid (TCA) cycle have been found in different plant species grown under Fe deficiency [12, 13]. Transcriptomic [14] and proteomic studies in Fe deficient plants [15-17] have also reported increases in root transcript and protein abundances, respectively, of enzymes related to the glycolytic and TCA cycle pathways, among others. Iron deficiency also induces an accumulation of organic acids, mainly malate and citrate, in roots [12]. The induction of C metabolism in roots of Fe-deficient plants would not only provide a source of reducing power, protons and ATP for the Fe(III) reductase and H⁺-ATPase enzymes, but also lead to an anaplerotic root C fixation [18, 19]. Carbon accumulated in roots is exported in the form of organic acids *via* xylem [18, 20, 21] to leaves [22], which have otherwise drastically reduced photosynthetic rates when Fe-deficient. The higher energy requirements in Fe-deficient root cells are tackled by increasing mitochondrial oxidative processes, and roots from Fe-deficient plants show enhanced respiratory activities and higher O₂ consumption rates [9, 23]. On the other hand, the mitochondrial respiratory chain is strongly affected under Fe-deficient conditions [23, 24], since some of its components are Fe-containing enzymes. Iron deficiency leads to an enhancement of different ROS detoxification strategies [25]. Furthermore, an increase in anaerobic metabolism has also been described in Fe-deficient roots [9], probably as a strategy to oxidize all the reducing power generated by glycolysis and TCA cycle that can not be easily oxidized in the respiratory chain. When

resupplied with Fe, Fe-deficient plants reorganize its metabolism by readjusting metabolic cycles and changing root morphology towards those typical of Fe-sufficient plants [21, 26].

The most common approach used to study Fe deficiency in roots is to analyze only a small number of genes, proteins and/or metabolites. A more comprehensive knowledge of the processes taking place in Fe-deficient roots has been recently provided by the application of modern techniques allowing for the simultaneous and untargeted analysis of multiple genes or proteins [14-17]. The aim of this work was to characterize the changes induced in the root tip proteome and metabolome of sugar beet plants in response to Fe deficiency and resupply, in order to provide a holistic view of the metabolic processes occurring in plants under different Fe status.

Results

IEF-PAGE electrophoresis. The polypeptide pattern of root tip extracts was obtained by 2-D IEF-SDS PAGE electrophoresis. Real scans of typical 2-D gels are shown in Figure 1; an average number of 141 and 148 polypeptides were detected in Fe-sufficient and Fe-deficient plants, respectively (Figure 1A and B). The total number of spots detected was relatively low when compared to other proteomic studies [16, 17]. Several causes may account for this discrepancy, including i) protein extraction method and amount of protein loaded in the gels, ii) gel size, iii) pI range and iv) sensitivity of the staining method. Averaged 2-D polypeptide maps were obtained using gels of three independent preparations, each from a different batch of plants (gels obtained with different root tip extract preparations isolated from different batches of plants were very similar; data not shown). To better describe polypeptide changes we built a composite averaged virtual map containing all spots present in both Fe-deficient and control root tip extracts (Figure 1C and D). Iron deficiency caused 2-fold increases in 29 spots (yellow marks in Figure 1C, $p < 0.10$ student T-test) and 2-fold decreases in signal intensity in 13 spots (green marks in Figure 1C, $p < 0.10$ student T-test). Furthermore, 6 spots were only detected in Fe-sufficient plant samples (blue marks in Figure 1C) and 13 spots were only detected in Fe-deficient plants (red marks in Figure 1C). All polypeptides in the composite averaged map are depicted again in Figure 1D, to

permit annotation of those polypeptides where identification was achieved by MALDI TOF (marked by squares in Figure 1D). These polypeptides were labeled from *a* to *v* as described in Figure 1D, and homologies found are described in detail in Table 1.

From the 29 spots that showed increases in signal in root tip extracts of Fe-deficient as compared to Fe-sufficient controls, the 20 more abundant were excised and analyzed by MALDI MS. Since the sugar beet genome has not been sequenced yet and few sequences are available in the databases, identification was performed by homology searches with proteins from other plant species. From the 20 spots analyzed, 14 proteins were identified (proteins labeled *a* to *n* in Figure 1D and Table 1). These include proteins related to glycolysis such as fructose 1,6-bisphosphate aldolase (spot *a*), triose-phosphate isomerase (spot *b*), 3-phosphoglycerate kinase (spot *c*) and enolase (spots *d* and *e*, respectively). Three spots gave significant matches to malate dehydrogenase (MDH; spots *f-h*), and two more polypeptides presented homology with α and β subunits from F1 ATP synthase (spots *i* and *j*). Other proteins increasing in root tip extracts from Fe-deficient sugar beet plants as compared to the controls were fructokinase (spot *k*) and formate dehydrogenase (spot *l*). Also, one spot gave significant matches to a cytosolic peptidase At1g79210/YUP8H12R_1 (spot *m*). Spot *n* gave significant match to a glycine rich protein, which possibly has a role in RNA transcription or processing during stress conditions.

From the 13 new spots detected *de novo* in proteome maps from root tip extracts of Fe-deficient plants (Figure 1C), the 6 more abundant were excised and analyzed by MALDI-MS, resulting in only 2 positive matches (spots *o* and *p* in Figure 1D and Supplementary Table 1). These significant matches were found for glyceraldehyde 3-phosphate dehydrogenase (GADPH; spot *o*) and DMRL (spot *p*). Changes in the amount of DMRL as well as *DMRL* gene expression and flavin analysis were further studied using root tip extracts of Fe-sufficient, Fe-deficient and Fe-resupplied sugar beet plants (see below).

From the 13 spots showing a decrease in signal intensity in root tip extracts from Fe-deficient plants as compared to controls (Figure 1C), 3 were identified by MALDI-MS. Spots *q* and *r* (Figure 1D, Table 1) gave a significant match to

nucleoside diphosphate kinase I and to oxalate oxidase-like germin, respectively. Spot *s* presented homology with the At4g27270 protein (Figure 1D) whose molecular function is to interact selectively with FMN, and also presents oxidoreductase activity.

From the 6 spots not detected in root tip extracts from Fe-deficient plants as compared to the controls (Figure 1C), 3 were identified by MALDI-MS (spots *t-v* in Figure 1D and Supplementary Table 1). Proteins matched were oxalate oxidase (spot *t*), peroxidase (spot *u*) and caffeoyl CoA O-methyltransferase (spot *v*).

DMRL synthase gene expression analysis. To identify a putative DMRL synthase cDNA in *B. vulgaris*, primers were designed based on DMRL synthase sequence from the closely related specie *S. oleracea* ([AF147203.1](#)). A PCR product of approximately 675 bp was amplified, purified and sequenced (Supplementary Figure 1A). The translated amino acid sequence for the DMRL synthase putative ORF had 224 aminoacids, a predicted MW of 23.7 kDa and a pI of 8.26. The predicted protein displayed 90% identity at the amino acid level with *S. oleracea* DMRL ([AAD44808.1](#)), and homologies with other known DMRLs sequences included in the alignment analysis ranged from 50 to 56% (Supplementary Figure 1B). Thus, we have assigned the name BvDMRL to the corresponding DMRL synthase gene of *B. vulgaris*, and the sequence has been deposited in GenBank as accession [GQ375163](#). Transcriptional regulation by Fe status of the BvDMRL gene was assessed by semi-quantitative RT-PCR. BvDMRL transcript abundance was much higher in root tips from Fe-deficient as compared to control plants (Figure 2A). The expression of BvDMRL was drastically reduced 24 h after Fe-resupply to Fe-deficient plants (Figure 2A) but it was still higher than that observed in Fe-sufficient root tips. However, transcript abundance in root tips sampled 72 h after Fe-resupply, which showed two different zones (white -WZ- and yellow -YZ-, see [26]), had a low expression level, similar to that measured in Fe-sufficient plants (Figure 2A).

DMRL synthase protein analysis Real scans of the 2-D gel zone where DMRL synthase protein is located (16 kDa, pI 6.6) are shown in Figure 2B. The DMRL synthase protein was detected not only in Fe-deficient root tip extracts but also in extracts of root tip YZ

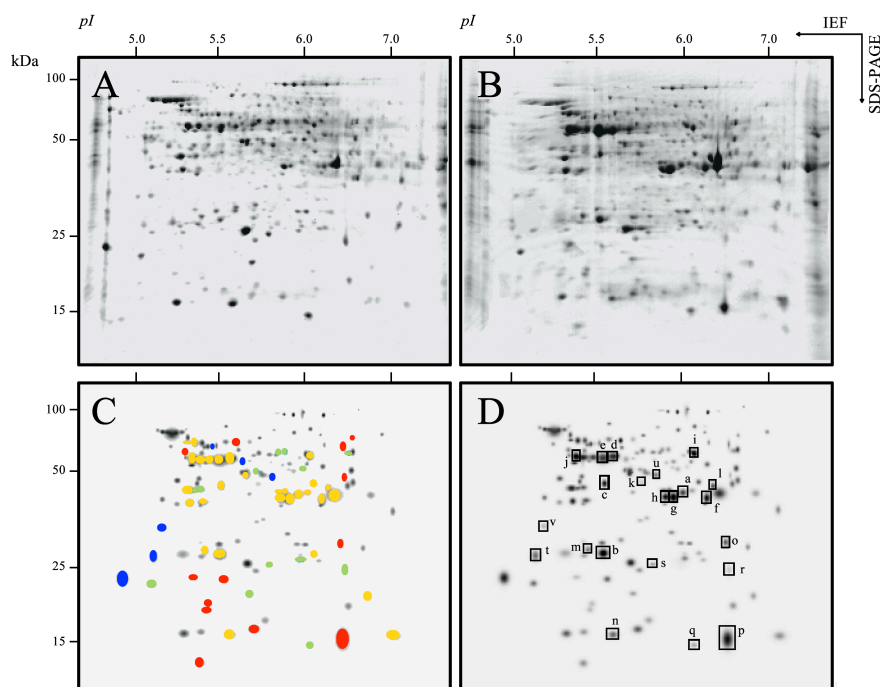


Figure 1 - 2-D IEF-SDS PAGE proteome maps of root tips from Fe-sufficient and Fe-deficient *Beta vulgaris* plants. Proteins were separated in the first dimension in linear (pH 5-8) IPG gel strips and in the second dimension in 12% acrylamide vertical gels. Scans of real typical gels of root tips from Fe-sufficient and Fe-deficient plants are shown in A and B, respectively. Virtual composite images, showing all polypeptides present in root tips from Fe-deficient and Fe-sufficient plants are shown in panels C and D. Statistical significance was assessed with a t-test ($p < 0.10$), and a 2-fold change in spot intensity between treatments was used as a threshold. Only spots that fit both criteria are marked in panel C; spots whose intensities decrease or disappear completely with Fe deficiency were labelled with green and blue marks, respectively, and those increasing with Fe deficiency or only present in Fe-deficient gels were labelled with yellow and red marks, respectively C. In panel D, polypeptides that had significant homologies with proteins in the databases (using MALDI MS and MASCOT) are marked by squares and labelled. Homologies are described in detail in Table 1.

from plants resupplied with Fe for 24 and 72 h (Figure 2B). Conversely, DMRL synthase was not detected in extracts of the new WZ of root tips from plants 72 h after Fe resupply, or in Fe-sufficient root tip extracts (Figure 2B).

Flavin concentrations. Since DMRL synthase is one of the key enzymes in flavin synthesis, we also examined flavin concentrations in root tip extracts from Fe-sufficient, Fe-deficient and Fe-resupplied plants by HPLC. Riboflavin, FAD and Rbfl sulphates were found in Fe-deficient and Fe-resupplied root tip YZ extracts. Riboflavin sulphates and Rbfl account for 98% and 2% of the total flavin concentration, respectively, and only traces of FAD were found. Rbfl sulphate concentrations were 319, 384 and 488 nmol g^{-1} FW in the root YZ of Fe-deficient plants and 24 h and 72 h Fe-resupplied plants, respectively (Figure 2C). Riboflavin concentration ranged from 1.1- to 2.3 nmol g^{-1} FW in root YZ (Figure

2D). Only traces of these compounds were present either in controls or in the WZ of 72 h Fe-resupplied plants.

Metabolite Analyses. Changes induced by Fe-deficiency and Fe-resupply in the root tip metabolome were evaluated by non-biased GC-MS metabolite profiling. A total of 326 metabolites were present in at least 80% of the samples of at least one treatment, and 77 of them were identified. Partial least square analysis shows a good separation between +Fe and -Fe root tips (Figure 3). Iron-deficient samples were closer to the 24 h and 72 h YZ samples than to the 72 h WZ ones. On the other hand, the 72 h WZ samples were closer to the +Fe samples than to the -Fe ones. Iron deficiency and/or resupply caused significant changes ($p < 0.05$) in the levels of 62 out of the 77 identified metabolites. Metabolite level data were normalized to the mean response of the +Fe treatment; response

Table 1. Proteins identified by MALDI-MS in 2-D IEF-SDS PAGE gels

Spot	Th. MW	Th. pI	Exp. MW	Exp. pI	Score ^(1,2)	Accession #	Homology	Species
Increased proteins in Fe-deficiency								
<i>a</i>	39	7.6	42	5.9	76 ¹	T48396	fructose 1,6-bisphosphate aldolase	<i>A. Thaliana</i>
<i>b</i>	27	5.5	35	5.4	143 ¹	gil556171	triose-phosphate isomerase	<i>C. japonica</i>
<i>c</i>	31	4.9	45	5.4	103 ¹	gil28172909	cytosolic 3-phosphoglycerate kinase	<i>T. Aestivum</i>
<i>d</i>	49	5.6	59	5.5	188 ¹	gil1087071	enolase	<i>M. crystallinum</i>
<i>e</i>	49	5.6	58	5.4	123 ¹	T12341	enolase	<i>L. sativa</i>
<i>f</i>	36	5.9	40	6.2	140 ¹	CAB61618	malate dehydrogenase	<i>B. vulgaris</i>
<i>g</i>	36	5.9	40	5.8	77 ¹	CAB61618	malate dehydrogenase	<i>B. vulgaris</i>
<i>h</i>	22	7.6	40	6.0	124 ¹	gil48375044	malate dehydrogenase	<i>N. tabacum</i>
<i>i</i>	55	6.0	60	6.0	185 ¹	O78692	F1 ATPase α subunit	<i>B. vulgaris</i>
<i>j</i>	49	5.1	58	5.3	170 ¹	gil4388533	F1 ATPase β subunit	<i>S. bicolor</i>
<i>k</i>	36	5.2	49	5.5	299 ¹	gil1052973	fructokinase	<i>B. vulgaris</i>
<i>l</i>	41	6.5	44	6.3	102 ¹	gil38636526	formate dehydrogenase	<i>Q. robur</i>
<i>m</i>	26	5.5	35	5.4	113 ¹	gil21689609	At1g79210/YUP8H12R_1	<i>A. thaliana</i>
<i>n</i>	17	5.9	17	5.5	116 ²	gil16301	glycine rich protein	<i>A. thaliana</i>
New spots in Fe-deficiency								
<i>o</i>	37	7.1	36	6.6	101 ¹	gil19566	glyceraldehyde 3-phosphate DH	<i>M. quinquepeta</i>
<i>p</i>	23	8.7	16	6.6	65 ²	Q9XH32	DMRL synthase	<i>S. oleracea</i>
Decreased spots in Fe-deficiency								
<i>q</i>	16	6.3	15	6.4	166 ¹	gil3309053	nucleoside diphosphate kinase I	<i>M. crystallinum</i>
<i>r</i>	23	6.4	30	6.8	217 ¹	gil11496133	oxalate oxidase-like germin 171	<i>B. vulgaris</i>
<i>s</i>	22	6.1	32	5.7	188 ¹	gil34365651	At4g27270	<i>A. thaliana</i>
Missing spots in Fe-deficiency								
<i>t</i>	23	6.4	34	5.7	217 ¹	gil11496133	oxalate oxidase-like germin 171	<i>B. vulgaris</i>
<i>u</i>	9	6.0	49	5.7	49 ²	gil2956703	peroxidase	<i>S. oleracea</i>
<i>v</i>	29	5.1	38	5.3	69 ²	gil5101868	caffeoyl CoA O-methyltransferase	<i>Z. Mays</i>

Scores (equal to $-10 \cdot \log P$, P being the probability that the observed match is a random event) are based on: ⁽¹⁾MS1 Peptide mass fingerprint data, with protein scores >76 being statistically significant ($p < 0.05$), and ⁽²⁾MS2 ion sequencing data, with individual ion scores >40 indicating identity or extensive homology ($p < 0.05$). In both cases, protein scores are derived from ion scores as a non-probabilistic basis for ranking protein hits. Proteins are separated in different groups depending on whether they increased, decreased, appeared (new) or disappeared (missing) when compared to control plants.

ratios, defined as the level in a given treatment divided by the level in the +Fe control, are indicated in bold in Table 2. Iron deficiency caused significant changes in the response ratios of 26 metabolites. Large (>4 -fold) increases were found for some organic acids (citric, and aconitic acid), some sugars (sucrose, myo-inositol and those of the raffinose family of oligosaccharides - RFOs-, namely galactinol and raffinose), nicotianamine and 2-amino adipic acid. The response ratio of oxalic acid decreased markedly in -Fe conditions, whereas those of other aminoacids, N compounds, lipid metabolites and others did not show large (>4 -fold) changes when compared to the Fe-sufficient controls. Twenty-four hours after Fe-resupply, there was a dramatic coordinated increase in the root tip response ratios of galactinol, raffinose, lactobionic acid, cellobiose and nicotianamine

when compared to those found in Fe-deficient roots, whereas the response ratios of sucrose, myo-inositol, citrate and malate decreased. Seventy-two hours after Fe resupply, the response ratios of galactinol, raffinose, cellobiose, nicotianamine and many other compounds had decreased in the YZ areas, whereas in the WZ the response ratio was very low. The response ratio of many of the lipids increased moderately in all Fe resupplied samples. Metabolites in the coenzyme, glycolysis, oxidative stress, pentose-phosphate pathway and signaling categories did not show large response ratio changes with Fe resupply.

Regarding the unknown metabolites, significant changes (at $p < 0.01$, with response ratios >4) were found for 46 of the 269 metabolites with Fe deficiency and/or resupply

(Supplementary Table 1). BinBase metabolite ID 211891 showed the largest response ratio (18, 146 and 70-fold, for -Fe, 24 h and 72 h YZ, respectively). The response of this metabolite to Fe status was very similar to that found for the RFOs, and in fact its mass spectra and retention index show a good similarity in BinBase to those of other disaccharides such as leucrose, suggesting that it could be a RFO related compound (see 211891 mass spectra in BinBase).

Raffinose and galactinol concentrations

The concentrations of raffinose and galactinol in root tips were determined by HPLC-MS. Raffinose concentrations were 35.1, 50.4, 35.4, 80.8 and 4.2 nmol g FW⁻¹ in the -Fe, 24h, 72h WZ, 72h YZ and +Fe tissues, respectively. Galactinol concentrations were 75.6, 39.8, 16.1, 37.1 and 7.6 nmol g FW⁻¹ in the -Fe, 24h, 72h WZ, 72h YZ and +Fe tissues, respectively.

Discussion

The changes induced by Fe deficiency in the root tip proteome and metabolome from sugar beet plants grown in hydroponics have been studied. More than 140 proteins (Figure 1) and 300 metabolites (Table 2 and Supplementary Table 1) were resolved in sugar beet root tip extracts. Iron deficiency resulted in significant and higher than 2-fold changes in the relative amounts of 61 polypeptides, and 22 of them were identified. Out of 77 identified metabolites, 26 changed significantly with Fe deficiency. In general, our results are in agreement with previous transcriptomic [14], proteomic [15-17] and enzymatic [19] studies on Fe-deficient roots. Our data confirm the increases previously found in proteins and metabolites related to carbohydrate metabolism and TCA cycle pathways [9, 13, 27]. Two major changes induced by Fe deficiency in roots are described in this study for the first time: the increase in DMRL synthase protein concentration and gene expression, and the increase in RFO sugars.

The largest change found in the proteome map of root tip extracts from sugar beet plants grown in Fe deficiency conditions corresponded to DMRL synthase, which was detected *de novo* in Fe-deficient root tips, and is the protein with the highest concentration in these gels (spot *p* in Figure 1D). This enzyme catalyses the fourth step of Rbfl biosynthesis, and Rbfl is the precursor of Rbfl sulphates, FMN and FAD, the last one being a cofactor for the root plasma membrane Fe

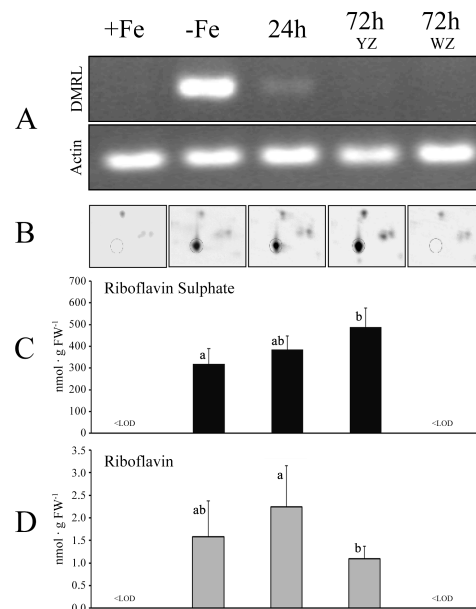


Figure 2 - DMRL and flavin analysis. Semi-quantitative RT-PCR analysis of the BvDMRL and actin gene transcripts (A), zoom scans of typical gels containing the BvDMRL protein (B) and Rbfl sulphate (C) and Rbfl (D) concentrations in sugar beet root tips from Fe sufficient (+Fe), Fe-deficient (-Fe), 24 Fe-resupplied, 72 h Fe-resupplied YZ and 72 h Fe-resupplied WZ. Letters in (C) and (D) indicate significant differences (n=6, p<0.05, Duncan test).

reductase [10]. The expression of *BvDMRL* decreased drastically 24 h after the addition of Fe to Fe-deficient plants, whereas DMRL synthase protein abundance and Rbfl and Rbfl sulphate concentrations did not change significantly with Fe-resupply in the YZ of root tips (Figure 2), suggesting that the turnover of this protein is slow. Accumulation in Fe-deficient roots of flavin compounds, including Rbfl and Rbfl 3'- and 5'-sulphate is a characteristic response of sugar beet and other plant species [6]. The exact role of flavins in Fe deficiency is unknown, and it has been hypothesized, based on the similar location of flavin accumulation and Fe reduction and on the fact that the Fe reductase is a flavin-containing protein, that free flavin accumulation may be an integral part of the Fe-reducing system in roots from Strategy I plants [9, 28]. On the other hand, these compounds are secreted to the growth media at low pH [6] and, assuming high concentrations at the secretion site, they could mediate extracellular electron transfer between

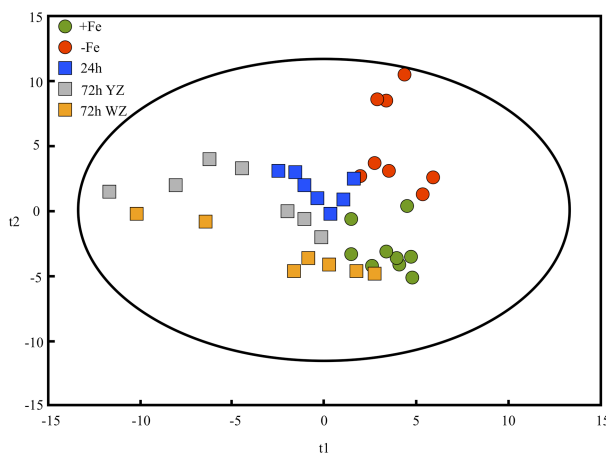


Figure 3. Partial Least Square (PLS) analysis, showing the score scatter plot of PLS vector 1 (t1) vs. PLS vector 2 (t2) of identified metabolites in sugar beet root tips from Fe sufficient (+Fe, green circles), Fe-deficient (-Fe, red circles), 24 Fe-resupplied (24h, blue squares), 72 h Fe-resupplied YZ (72 h YZ, grey squares) and 72 h Fe-resupplied WZ (72 h WZ, orange squares).

soil Fe deposits and root Fe reductase as it has been described for flavin phosphates secreted by some bacteria [29]. Moreover, excreted flavins could also act as a plant-generated signal that could influence rhizosphere microbial populations, indirectly affecting Fe availability [11].

A major change in carbohydrate metabolism was the large increase in RFO compounds (34- to 16-fold changes in the response ratios of galactinol and raffinose, respectively; Table 2) that occurs in roots with Fe-deficiency. This increase was higher than that found for sucrose (5-fold). The total concentrations of raffinose and galactinol were also determined by HPLC-MS, and concentrations of both compounds in the 35-80 nmol g FW⁻¹ range were found in Fe-deficient and Fe-resupplied root tips (equivalent to approximately 50 μ M), whereas concentrations in the +Fe treatment were one order of magnitude lower (see Results Section). The sum of the raffinose and galactinol concentrations in the -Fe, 24h, 72hWZ, 72hYZ and +Fe tissues was 13.9, 7.4, 2.2, 5.1 and 0.6% of the total sucrose, respectively, supporting the relevance of the RFOs changes with Fe status. RFOs have diverse roles in plants, including transport and storage of C [30] and acting as compatible solutes for protection in abiotic stresses [31, 32]. Other explanation for the large increase in the relative

amounts of RFOs could be the ability to function as antioxidants [33, 34]; galactinol and raffinose have hydroxyl radical scavenging activities similar to other soluble antioxidants such as glutathione and ascorbic acid [33]. Since ROS damage and ROS detoxification strategies have been observed in Fe-deficient roots [25, 35], the increase in RFO concentration could help to alleviate ROS damage produced under Fe deficiency. Moderate increases in sugars commonly found in cell walls such as cellobiose, xyloic acid and arabinose, which may indicate cell wall modifications, were measured in sugar beet Fe-deficient root tips. Changes in cell wall metabolism have been also described in Fe-deficient tomato roots [16]. On the other hand, it has been described that cell wall damage generates oligosaccharides that can act as signalling molecules in stresses such as wounding [36]. The increase in RFOs could act as a long distance Fe-deficiency signal via phloem sap transport. This is the first description of RFOs accumulation in plants under Fe deficiency, and the physiological implications of this increase deserve further consideration.

Most of the proteins found to be up-accumulated in sugar beet root tips by Fe deficiency were identified as carbohydrate catabolism enzymes, including 5 of the 10 glycolytic pathway enzymes (fructose 1,6-bisphosphate aldolase, triosephosphate isomerase, glyceraldehyde 3-phosphate dehydrogenase, 3-phosphoglycerate kinase and enolase), one of the citric acid cycle (MDH) and fructokinase. Increases in the activities and concentrations of several glycolytic enzymes in root extracts with Fe deficiency have been previously found, including fructose 1,6-bisphosphate aldolase, enolase, triosephosphate isomerase and GADPH [15, 16, 37-39]. Also, increases in the activities and concentrations of several enzymes of the citric acid cycle with Fe deficiency have been previously reported in root extracts, including MDH [9, 16, 38]. Results are also in agreement with microarray gene analysis in Fe-deficient *A. thaliana* roots [14]. Increases in the amount of PEPC have been found at the protein level [16, 40, 41], but this enzyme, with a molecular mass of 110 kDa, was not in the range (apparent molecular mass 10-100 kDa) used in our 2-D gels. Up-regulation of carbohydrate catabolism in roots of plants grown in Fe deficient conditions is probably a result of an

Table 2. Identified metabolite response ratios of the different treatments vs. +Fe

#	metabolites	-Fe	24h	72hYZ	72hWZ	<i>A. thaliana</i> KEGG pathway number
Aminoacid and Nitrogen Metabolism						
1	nicotianamine	7.9	11.8	2.9	2.1	
2	2-aminoadipic acid	6.4	3.5	12.3	11.2	0300, 1100, 0310
3	2-hydroxyglutaric acid	3.8	4.1	2.3	1.3	0650
4	citrulline	3.6	1.4	2.9	1.7	0330, 1100
5	lysine	3.0	2.2	2.5	-1.2	0300, 1100, 0310, 0780, 0960, 0310
6	serine	2.4	1.7	1.8	-1.8	0970, 1100, 0260, 0600, 0460, 0271, 0272, 0920, 0680
7	hydroxylamine	1.1	2.0	4.2	3.2	0910
8	urea	1.0	1.0	2.5	6.2	0330, 1100, 0230, 0240
9	arginine + ornithine	2.2	1.1	1.6	0.0	0330, 1100, 0970
10	aspartic acid	1.0	1.3	1.4	1.1	0970, 1100, 0260, 0760, 0710, 0300, 0910, 0252, 0460, 0410, 0330, 0770
11	glutamic acid	1.1	1.0	1.2	-1.0	0970, 1100, 0480, 0860, 0650, 0251, 0340, 0330
12	glycine	-1.3	-1.3	1.3	-1.5	0970, 1100, 0260, 0480, 0730, 0310, 0230, 0120, 0460, 0860, 0680
13	phenylalanine	1.2	-1.1	1.2	-1.1	0970, 1100, 0400, 0966, 0960, 0360, 0940
14	tyrosine	2.1	-1.2	1.3	-1.3	0970, 1100, 0950, 0730, 0960, 0350, 0940, 0966
15	putrescine	-1.1	-1.8	-1.3	-1.3	1100, 0960, 0480
16	ornithine	1.6	-1.2	1.2	-1.0	1100, 0330, 0480
17	tryptophan	1.0	-1.9	-1.2	-2.4	1100, 0970, 0380, 0901, 0400, 0966
18	oxoproline	-1.3	-1.9	-1.1	-1.2	0330
19	valine	1.2	1.0	1.4	-2.2	0970, 0901, 0400, 0966, 0380, 1100
20	asparagine	-1.0	-1.8	-1.2	-2.4	1100, 0970, 0910, 0252, 0460
21	alanine	-1.4	1.7	1.5	-3.4	1100, 0970, 0252, 0710, 0450, 0430, 0272, 0720
22	glutamine	-1.6	-4.5	-2.5	-3.8	1100, 0970, 0910, 0251, 0240, 0230
Carbohydrate metabolism						
23	galactinol	33.7	86.2	23.2	7.6	0052
24	raffinose	16.3	59.7	9.7	9.9	0052
25	sucrose	4.7	2.3	1.9	2.2	0052, 1100, 0500
26	lactobionic acid	3.3	10.9	4.8	3.2	
27	N-acetyl-D-mannosamine	2.1	1.5	2.0	1.6	1100, 0530
28	arabinose	2.1	1.4	2.2	1.4	
29	xylonic acid	2.0	1.6	2.2	1.4	
30	inulobiose	2.0	3.4	2.3	2.1	
31	cellobiose	5.1	8.0	4.7	2.2	0500
32	mannitol	-1.3	1.6	3.1	1.4	0052, 1100, 0053, 4070, 0562
33	xylitol	1.1	1.3	2.1	1.4	1100, 0040
34	fructose	-1.8	-1.7	1.9	-1.3	0052, 1100, 0051, 0500
35	suberyl glycine	1.1	-2.0	-1.1	-2.6	
Co-enzymes and alkaloid biosynthesis						
36	ribitol	5.6	5.4	2.9	2.0	1100, 0040, 0740
37	pantothenic acid	1.7	2.0	2.2	1.4	1100, 0410, 0770
38	nicotinic acid	-1.3	1.3	2.6	1.8	1100, 0760, 0960
Glycolysis						
39	glucose-1-phosphate	1.4	2.7	2.5	1.7	0052, 1100, 0010, 0500, 0040, 0520
40	glucose	1.1	-3.9	1.8	-2.4	0052, 1100, 0010, 0500, 0030, 0901

41	fructose-6-phosphate	-1.1	-1.3	1.2	1.2	0710, 1100, 0040, 0680, 0530
42	glucose-6-phosphate 2	-1.3	-1.6	1.2	-1.1	0500, 1100, 0562
43	3-phosphoglycerate	-1.9	-1.3	1.5	1.2	0561, 0260, 0010, 0710, 0630, 1100
Glyoxylate and dicarboxylate metabolism						
44	glyceric acid	3.4	1.3	1.5	1.7	0561, 0260, 0030, 0630, 1100
45	glycolic acid	2.9	2.0	3.1	3.6	0630, 1100, 0361
46	oxalic acid	-10.9	-5.2	-3.6	1.5	0630, 1100
Lipid metabolism						
47	behenic acid	1.9	1.9	2.8	3.3	1040
48	γ hexaric acid	1.6	3.8	3.2	1.7	
49	stearic acid	-1.2	2.8	4.1	3.3	0061, 1040
50	glycerol	-1.2	2.2	3.9	3.8	
51	cerotic acid	-1.1	2.0	3.8	2.9	
52	myristic acid	1.0	2.1	3.7	2.7	0061
53	palmitic acid	-1.2	1.9	3.4	2.7	0061, 1040, 1100, 0062, 0071
54	phosphoethanolamine	1.7	1.7	1.5	1.7	0600, 0260, 1100, 0564
55	lauric acid	-1.1	2.1	3.5	2.3	0061
56	capric acid	-1.1	1.4	3.1	2.1	0061
57	pentadecanoic acid	1.0	1.2	2.9	3.0	
58	pelargonic acid	-1.2	1.1	2.5	1.8	
59	linoleic acid	-1.4	1.2	2.3	2.4	1040, 1100
60	glycerol-α-phosphate	-1.0	1.0	1.5	1.5	
Oxidative stress						
61	threonic acid	3.7	1.6	1.2	1.7	
62	dehydroascorbate	3.3	1.4	2.8	1.4	
63	2-hydroxypentanoic acid	-1.2	1.5	3.5	1.9	0982
64	1,2,4-benzenetriol	1.5	3.0	4.5	4.6	1100, 0361, 0362, 0627
65	γ pentonic acid	1.6	-1.4	-1.1	-1.8	
Pentose phosphate pathway						
66	ribose	1.5	1.7	1.6	1.9	1100, 0030
67	gluconic acid	1.6	1.7	2.5	1.6	1100, 0030, 0710, 0230
Signaling						
68	myoinositol	5.3	2.2	3.3	2.4	
69	GABA	1.8	4.4	4.5	1.5	1100, 0251, 0410, 0650
70	inositol-monophosphate	-1.2	1.7	2.3	2.2	4070, 0562
TCA Cycle						
71	aconitic acid	4.5	5.4	5.3	1.8	1100, 0020, 0720, 0630
72	citric acid	21.1	16.2	10.3	1.5	1100, 0020, 0720, 0630, 0251, 0252
73	malate	3.3	2.6	2.6	1.8	1100, 0020, 0720, 0630, 0251, 0252, 0710, 0620
74	succinic acid	1.4	1.5	3.7	2.2	1100, 0020, 0720, 0630, 0251, 0252, 0350, 0650, 0632, 0361, 0190, 0640
Others						
75	acetohydroxamic acid	1.1	-1.6	5.0	3.7	
76	phosphoric acid	-1.3	-4.6	-1.5	3.8	1100, 0190, 0195, 0550
77	adenosine-5-monophosphate	-1.3	-1.2	1.3	1.1	1100, 0230, 0908

When the response ratio (level in a given treatment divided by the level in the +Fe treatment) was lower than 1 the inverse was taken and the sign changed. Values indicated in bold represent a t-test significance of $p < 0.05$. The last column shows *A. thaliana* KEGG pathway numbers where the metabolite is predicted to be involved; all KEGG pathway numbers are hyper-linked to the corresponding KEGG website.

increased demand of energy and reducing power in roots needed to sustain the increased activity of H⁺-ATPase and Fe reductase [14, 16, 19]. Also, two spots corresponding to different subunits of F1 ATP synthase increased in 2-D gels from Fe deficient root tips, further supporting the higher energy requirement in these roots. Moreover, our results show an increase in the amount of formate dehydrogenase, an enzyme related to the anaerobic respiration, in Fe-deficient roots, confirming the results of enzyme [9] and transcriptional [14] analysis. Anaerobic respiration is an alternative pathway for energy production when oxidative phosphorylation is impaired.

Metabolite studies revealed large increases in organic acids, including a 20-fold citric acid increase. These increases in TCA cycle organic acids with Fe deficiency are coupled with increases in glycolysis [9, 16] and root C fixation by PEPC [40, 41], and provide an anaplerotic, non-autotrophic (*via* xylem) C source for leaves which have otherwise reduced photosynthetic rates [18, 22]. Malate and citrate could also be pumped from the cytosol to the mitochondria via a di-tricarboxylate carrier (DTC) where they would allow a higher turnover of reducing equivalents [23]. A significant decrease (-10.9) in oxalic acid concentration was observed in Fe deficient root tips, and similar decreases (ca. 10 times) have been reported in Fe-deficient tomato roots [13]. The implications of oxalate concentration decreases with Fe deficiency are still not known, since the role of oxalic acid in plants is quite different from that of the other organic acids, and for a long time it has been considered as a toxin or a metabolic end product [42]. Regarding N and amino-acid compounds, a large increase (8-fold) was measured for nicotianamine, which has been described to play a role in cytosolic Fe availability [43, 44].

A comprehensive representation of the metabolomic and proteomic changes taking place in root tips under Fe deficiency and resupply is shown in Figure 4. Red and yellow symbols indicate major and moderate increases in metabolites (squares) and proteins (circles) compared to the Fe-sufficient controls. Blue and green symbols indicate major and moderate decreases in metabolites (squares) and proteins (circles) compared to the controls. Besides the major increases in RFOs and DMRL, Fe deficiency induced significant changes in root tip

metabolism, mainly associated to increases in carbohydrate catabolism, glycolysis and TCA cycle and to a lesser extent in aminoacid and nitrogen metabolism (Figure 4). Similar changes were observed in the 24 and 72h YZ Fe-resupplied roots, whereas the WZ of 72 h Fe-resupplied plants did not show major changes when compared to +Fe plants (Figure 4). On the other hand, the relative amount of lipid metabolism compounds did not change markedly in Fe-deficient roots, whereas Fe resupply caused a moderate increase in this type of metabolites (Figure 4).

Conclusions

The proteomic and metabolic profiles of root tips from sugar beet plants were affected by Fe deficiency and resupply. Changes in the glycolysis and TCA cycle metabolites and proteins confirmed previous studies. Two novel and major findings were the increase in i) DMRL synthase protein concentration and gene expression, and ii) some RFO sugars (raffinose and galactinol). These new findings give new perspectives to the knowledge of Fe deficiency.

Materials and Methods

Plant Material. Sugar beet (*Beta vulgaris* L. “Monohil” and “Orbis” from Hilleshög, Landskröna, Sweden and Syngenta, Madrid, Spain, respectively) was grown as described elsewhere [26]. “Monohil” was always used, with the exception of raffinose and galactinol analysis, that was carried out with “Orbis”. After seed germination in vermiculite and 2 weeks in half-strength Hoagland’s nutrient solution with 45 µM Fe(III)-EDTA, plants were transferred into 20-L plastic buckets (four plants per bucket) containing half-strength Hoagland’s nutrient solution with either 0 or 45 µM Fe(III)-EDTA. The pH of the Fe-free nutrient solution was buffered at approximately 7.7 by adding 1 mM NaOH and 1 g L⁻¹ of CaCO₃. In the Fe resupply experiments, plants grown for 10 d in the absence of Fe were transferred to 20-L plastic buckets containing half-strength Hoagland’s nutrient solution, pH 5.5, with 45 µM Fe(III)-EDTA. The root subapical region from Fe-sufficient plants (+Fe), Fe-deficient plants (-Fe), Fe-deficient plants resupplied with Fe for 24 h (24h) and Fe-deficient plants resupplied with Fe for 72 h (72h) were collected with a razor blade and immediately frozen in liquid N₂. The specific

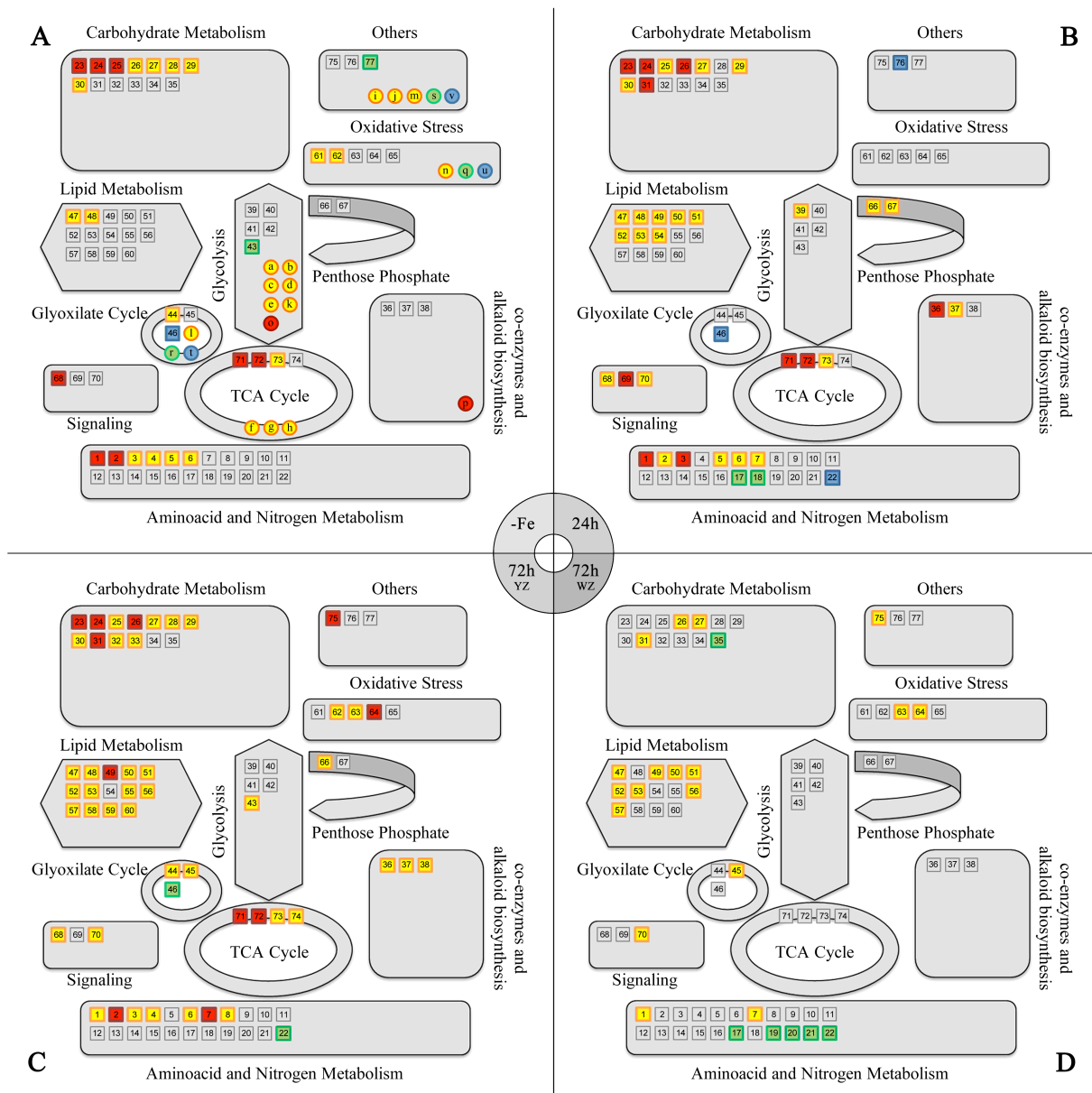


Figure 4 - Changes in metabolic pathways as affected by Fe status

Pathways related to metabolites and proteins were integrated according to the KEGG database. Statistical t-student tests were performed to both protein and metabolite data to show statistically relevant changes between samples. Red squares indicate metabolites showing significant, marked (more than 4-fold) up-accumulation compared to the controls, and yellow ones mean significant, moderate (less than 4-fold) up-accumulation. Blue squares mean significant, marked (more than 4-fold) down-accumulation, and green ones mean significant moderate (less than 4-fold) down-accumulation. The same colour code was used with proteins, represented by circles. Red circles are proteins detected only in Fe-deficient gels, and yellow ones mean significantly up-accumulated proteins using a 2-fold threshold. Decreased (at least 50%) and missing proteins in the Fe-deficient treatment were represented in green and blue respectively. Each number or letter corresponds to those showed in the corresponding protein and metabolite tables (Table 1 and 2 respectively). Panels correspond to root tip extracts from plants Fe-deficient (A), 24 h after Fe resupply (B), and 72 h after Fe resupply (YZ in panel C and WZ in panel D).

regions of root sampled were: in the case of +Fe, -Fe and 24 h plants, the first 10 mm from the root

apex (+Fe roots were thin and white, whereas -Fe and 24 h roots were swollen and yellow); in the

case of 72 h Fe resupplied roots two zones were sampled separately, the first 5 mm from the root apex, where a new white zone had developed (72h WZ), and the next 5 mm, comprising the still swollen and yellow root zone (72h WZ). Samples were taken at approximately 4 h after light onset in the growth chamber.

Protein extraction and analysis. Protein extracts were obtained as described elsewhere [45] and protein concentration was measured with RC DC Protein Assay (Bio-Rad, Hercules, CA, USA). A first dimension isoelectric focusing (IEF) separation was carried out on ReadyStrip IPG Strips (BioRad), using a linear pI gradient 5-8. Strips were loaded in a PROTEAN IEF Cell (BioRad) and focused at 20 °C, for a total of 14000 V.h. For the second dimension polyacrylamide gel electrophoresis (SDS-PAGE), IPG strips were placed onto 12% SDS-PAGE gels to separate proteins between 10 and 100 kDa. Proteins were stained with Coomassie-Blue R-250 (Sigma, Barcelona, Spain) and results analyzed with the PDQuest 8.0 software (BioRad) [46]. Gels were made from independent root tip preparations from three different batches of plants. In-gel digestion, sample preparation, MALDI TOF-TOF peptide mass fingerprint and database searching was carried out as described in detail elsewhere [46]. Statistical significance was tested with a t-Student test ($p < 0.10$). A 2-fold change in spot signal intensity between treatments was taken as a threshold.

Metabolite extraction, analysis, data processing and statistical analysis. Metabolite extraction and analysis was carried out as described previously [47]. Root tips (ca. 50 mg FW) from eight different replicates per treatment (one plant each) were used. After metabolite extraction and derivatization, samples (1 μ L) were injected randomly in split-less mode with a cold injection system (Gerstel, Mülheim an der Ruhr, Germany) and analyzed by GC (Agilent 6890 San Jose, CA, USA) using a Rtx 5Sil MS column (30 m x 0.25 mm, 0.25 μ m film thickness) and an integrated guard column (Restek, Bellefonte, PA, USA). The GC was connected to a Leco Pegasus IV time of flight mass spectrometer controlled with Leco ChromaTOF software v.2.32 (Leco, St. Joseph, MI, USA). Initial peak detection and mass spectra deconvolution were performed with Leco Chroma-TOF software v.2.25. GC-MS chromatograms were processed as described

previously [47]. Further analysis after deconvolution was done using the semi-automated workflow in the UC Davis Genome Center metabolomics laboratory [48]. Metabolite data were normalized using FW and the sum of all metabolite heights in a single run to account for small FW and GC injection variations [47]. Statistical analysis, including i) breakdown one-way ANOVA univariate statistics ($p < 0.05$), ii) multivariate analysis supervised partial least square (PLS) and iii) unsupervised principal component analysis (PCA; data not shown) were carried out with Statistica software (v.8.0. StatSoft, Inc.). A 4-fold change in signal intensity between treatments was taken as a threshold for discussion.

DMRLs gene identification and expression analysis. To identify putative dimethyl-8-ribityllumazine (DMRL) gene sequences in sugar beet, searches were performed with TBLASTX [49] using previously identified DMRL synthase sequences from *A. thaliana* ([AF148649.1](#)), *Nicotiana tabacum* ([AF422802.1](#)) and *Spinacia oleracea* ([AF147203.1](#)). Since the search gave no hits in *B. vulgaris*, primers were designed based on the DMRL synthase sequence from *S. oleracea* ([AF147203.1](#)), the closest phylogenetically related species. Primers used to amplify the complete cDNA sequence were f-ATGGCTTCATTTGCAGCTTCT and r-TTAGGCCTTCAAATGATGTTC. Total RNA from Fe-deficient root tips was isolated using the RNeasy Plant Mini kit (Qiagen, GmbH, Hilden, Germany) according to the manufacturer's instructions. The concentrations of RNAs were assessed by UV-Vis. The structural integrity of the RNAs was checked with non-denaturing agarose gel and ethidium bromide staining. A sample aliquot containing 3 μ g total RNA was subjected to reverse transcription with 25 μ g mL⁻¹ oligo (dT) primer, 0.05 mM dNTP mix and 1 unit of Superscript II Reverse Transcriptase (Invitrogen, Carlsbad, USA) in a final volume of 20 μ L. PCR reactions were carried out with 2 μ L of resulting cDNA solution, using 0.5 μ M of the specific primers, 75 mM Tris HCl pH 9.0, 1.5 mM MgCl₂, 50 mM KCl, 20 mM (NH₄)₂SO₄, 200 μ M dNTP's and 0.5 units DNA polymerase (Biotools, Madrid, Spain). PCR cycling conditions were as follows: 95 °C for 5 min, 30 cycles consisting of 95 °C for 45 s, 55 °C for 45 s and 70 °C for 1 min, and a final period of 10 min at 70 °C. The PCR product was purified with the

QIAquick gel extraction kit (Quiagen) and sequenced (CNIO, Madrid, Spain). The nucleotide sequence was translated, MW and pI predicted by using the ExPASy server tools [50], and multiple-sequence alignments done with ClustalIW v.2 [51]. Expression of the DMRL gene in *B. vulgaris* root tips was analyzed by semi-quantitative RT-PCR. One plant per treatment was used to extract RNA, and two different batches of plants were analyzed. RNA extraction and RT-PCR reactions were carried out as described above. Amplified products from 15 μ l of PCR reaction were visualized on 1% TBE agarose gel containing ethidium bromide. Bands were photographed using the Quantity One 4.5.1 Chemdoc EQ Software system (Bio-Rad). Actin (DQ866829.1) was used as housekeeping gene. Primers used to amplify the actin sequence were: f-GGCAAACAGGGAAAAGATGA and r-ACGACCAGCAAGATCCAAAC. RT-PCR reactions were carried twice for each sample set.

Flavin analysis. Root material (ca. 100 mg FW) was frozen in liquid N₂ and ground in a mortar with 0.1 M ammonium acetate, pH 6.1. Extracts were centrifuged for 5 min at 14000 g and the supernatant stored at -80 °C until analysis. Flavins were determined by HPLC as described by Susín et al. [6]. Six samples per treatment from 3 independent batches of plants were used for measurements.

Raffinose and galactinol analysis. Root tips (ca. 100 mg) from 3 different plants per treatment were extracted with 80% EtOH as described elsewhere [52]. After ethanol evaporation, extracts were resuspended in AcN-H₂O and analyzed by LC-ESI-MS as described in [53] with some modifications. Chromatographic separation was performed on an Alliance 2795 HPLC system (Waters, Mildford, MA, USA). The autosampler was kept at 4°C and the column compartment temperature was set at 25°C. Injection volume was 10 μ l, and a ZIC-pHILIC, 150 \times 2.1 mm, 5 μ m column (Sequant, Umea, Sweden) was used with a flow rate of 200 μ l min⁻¹. The mobile phase was built using two eluents: A (5 mM ammonium acetate in 0.1 % formic acid at pH 4) and B (AcN 0.1% Formic acid). All mobile phase chemicals were LC-MS grade (Riedel-de Haen, Seelze, Germany). For separation, the initial solvent composition 90% B and 10% A was taken to 10% B and 90% with a 19 min linear gradient. Then, the mobile phase

returned to initial conditions in 1 min and these conditions were kept for another 10 min, to allow column equilibration. Total run time per sample was 30 min. MS analysis was carried out with a micrOTOF II ESI-TOFMS apparatus (Bruker Daltonics GmbH, Bremen, Germany) in the 50–1000 m/z range. The micrOTOF II was operated in negative mode at 3000 and -500V capillary and end-plate voltages, respectively. Capillary exit, skimmer 1 and hexapole RF voltages were set at -82.1, -41.4 and 80.0 V, respectively. Nebulizer gas (N₂) pressure was kept at 2.0 bar and drying gas (N₂) flow was set at 8.0 liter min⁻¹ with a temperature of 180°C. Mass calibration was carried out with 10 mM Li-formate solution using a syringe pump (Cole-Parmer Instruments, Vernon Hills, IL, USA). The system was controlled with the software packages MicrOTOF Control v.2.2 and HyStar v.3.2 (Bruker Daltonics). Data were processed with Data Analysis v.3.4 software (Bruker Daltonics).

Authors' contributions

SA and AFLM carried out the proteomic, genetic and flavin studies. RRA carried out the metabolomic studies. JRC prepared some of the figures and analyzed proteomics data. GW and OF prepared and analyzed metabolomics data. AAF and GZ analyzed critically the results. RRA, SA, AFLM, AAF and JA wrote the manuscript. All authors read and approved the final manuscript.

Acknowledgements

SA and RRA were supported by FPI fellowships from the Spanish Ministry of Science and Innovation (MICINN). JRC was supported by an I3P-CSIC predoctoral fellowship. Work supported by the Spanish MICINN (projects AGL2004-00194 and AGL2007-61948, co-financed with FEDER), the Spain-Italy Integrated Action HI2007-0228, the European Commission (Thematic Priority 5–Food Quality and Safety, 6th Framework RTD Programme, Contract no. FP6-FOOD–CT-2006-016279), and the Aragón Government (group A03). We appreciate the help of Ade Calviño, Aurora Poc and Giuseppe Lattanzio (EEAD) for excellent assistance in growing and sampling the plants.

1. Robinson N, Procter C, Connolly E, Guerinot ML: **A ferric-chelate reductase for iron uptake from soils.** *Nature* 1999, **397**:694-697.

2. Eide D, Brodenius M, Fett J, Guerinot M: **A novel iron-regulated metal transporter from plants identified by functional expression in yeast.** *Proc Natl Acad Sci USA* 1996, **93**:5624-5628.
3. Santi S, Schmidt W: **Dissecting iron deficiency-induced proton extrusion in *Arabidopsis* roots.** *New Phytol* 2009, **183**:1072-1084.
4. Landsberg E: **Transfer cell formation in the root epidermis: A prerequisite for Fe-efficiency?** *J Plant Nut* 1982, **5**:415-432.
5. Jin CW, You GY, He YF, Tang C, Wu P, Zheng SJ: **Iron deficiency-induced secretion of phenolics facilitates the reutilization of root apoplastic iron in red clover.** *Plant Physiol* 2007, **144**:278-285.
6. Susín S, Abian J, Peleato M, Sanchez-Baeza F, Abadía A, Gelpi E, Abadía J: **Flavin excretion from roots of iron-deficient sugar beet (*Beta vulgaris* L.).** *Planta* 1994, **193**:514-519.
7. Worst D, M. Gerrits M, Vandenbroucke-Grauls C, Kusters J: ***Helicobacter pylori* ribBA-mediated riboflavin production is involved in iron acquisition.** *J Bacteriol* 1998, **180**:1473-1479.
8. Stenchuk NN, Kutsiaba VI, Kshanovskaya BV, Fedorovich DV: **Effect of the rib83 mutation on riboflavin synthesis and iron acquisition in the yeast *Pichia guilliermondii*.** *Microbiol* 2001, **70**:647-651.
9. López-Millán A, Morales F, Andaluz S, Gogorcena Y, Abadía A, De Las Rivas J, Abadía J: **Responses of sugar beet roots to iron deficiency. Changes in carbon assimilation and oxygen use.** *Plant Physiol* 2000, **124**:885-897.
10. Schagerlöf U, Wilson G, Hebert H, Al-Karadaghi S, Hägerhäll C: **Transmembrane topology of FRO2, a ferric chelate reductase from *Arabidopsis thaliana*.** *Plant Mol Biol* 2006, **62**:215-221.
11. Vorwieger A, Gryczka C, Czihal A, Douchkov D, Tiedemann J, Mock H, Jakoby M, Weisshaar B, Saalbach I, Bäumlein H: **Iron assimilation and transcription factor controlled synthesis of riboflavin in plants.** *Planta* 2007, **226**:147-158.
12. Abadía J, López-Millán AF, Rombolá A, Abadía A: **Organic acids and Fe deficiency: a review.** *Plant Soil* 2000, **241**:75-86.
13. López-Millán A, Morales F, Gogorcena Y, Abadía A, Abadía J: **Metabolic responses in iron deficient tomato plants.** *J Plant Physiol* 2009, **166**:375-384.
14. Thimm O, Essingmann B, Kloska S, Altmann T, Buckhout T: **Response of *Arabidopsis* to iron deficiency stress as revealed by microarray analysis.** *Plant Physiol* 2001, **397**:417-426.
15. Herbik A, Giritch A, Horstmann C, Becker R, Balzer H, Baumlein H, Stephan U: **Iron and copper nutrition-dependent changes in protein expression in a tomato wild type and the nicotianamine-free mutant *chloronerva*.** *Plant Physiol* 1996, **111**:533-540.
16. Li J, Wu X, Hao S, Wang X, Ling H: **Proteomic response to iron deficiency in tomato root.** *Proteomics* 2008, **397**:2299-2311.
17. Brumbarova T, Matros A, Mock H-P, Bauer P: **A proteomic study showing differential regulation of stress, redox regulation and peroxidase proteins by iron supply and the transcription factor FER.** *Plant J* 2008, **54**:321-334.
18. López-Millán AF, Morales F, Abadía A, Abadía J: **Effects of iron deficiency on the composition of the leaf apoplastic fluid and xylem sap in sugar beet. Implications for iron and carbon transport.** *Plant Physiol* 2000, **124**:873-884.
19. Zocchi G, De Nisi P, Dell'Orto M, Espen L, Gallina PM: **Iron deficiency differently affects metabolic responses in soybean roots.** *J Exp Bot* 2007, **58**:993-1000.
20. Bialzyck J, Lechowski L: **Absorption of HCO₃⁻ by roots and its effect on carbon metabolism of tomato.** *J Plant Nutr* 1999, **15**:293-312.
21. Larbi A, Morales F, Abadía A, Abadía J: **Changes in iron and organic acid concentrations in xylem sap and**

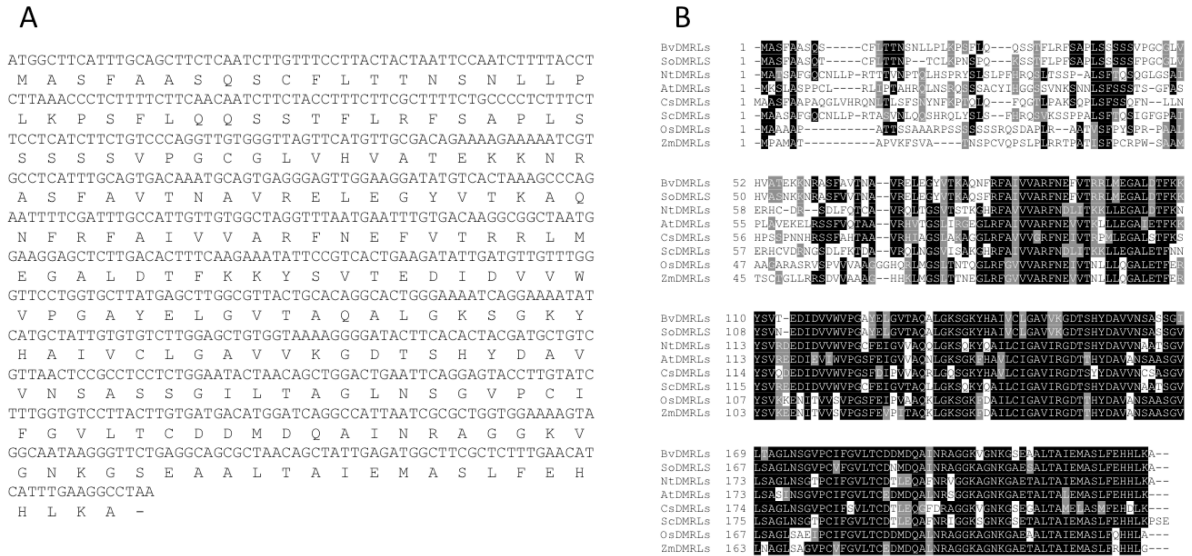
- apoplastic fluid of iron-deficient *Beta vulgaris* plants in response to iron resupply. *J Plant Physiol* 2010, **167**:255-260.
22. López-Millán AF, Morales F, Abadía A, Abadía J: **Changes induced by Fe deficiency and Fe resupply in the organic acid metabolism of sugar beet (*Beta vulgaris*) leaves.** *Physiol Plant* 2001, **112**:31-38.
 23. Vigani G, Maffi D, Zocchi G: **Iron availability affects the function of mitochondria in cucumber roots.** *New Phytol* 2009, **182**:127-136.
 24. Vigani G, Zocchi G: **The fate and the role of mitochondria in Fe-deficient roots of strategy I plants.** *Plant Signal Behav* 2009, **4**:375-379.
 25. Zaharieva TB, Abadía J: **Iron deficiency enhances the level of ascorbate, glutathione and related enzymes in sugar beet roots.** *Protoplasma* 2004, **221**:269-275.
 26. López-Millán A, Morales F, Gogorcena Y, Abadía A, Abadía J: **Iron resupply-mediated deactivation of Fe-deficiency stress responses in roots of sugar beet.** *Aust J Plant Physiol* 2001, **28**:171-180.
 27. Zocchi G: **Metabolic changes in iron stressed dicotyledoneous plants.** In *Iron Nutrition in Plants and Rhizospheric Microorganisms*. Edited by LL Barton, J Abadía. Dordrecht, The Netherlands: Springer; 2006:437-448.
 28. Cakmak I, Van e Wetering D, Marschner H, Bienfait H: **Involvement of superoxide radical in extracellular ferric reduction by iron-deficient bean roots.** *Plant Physiol* 1987, **85**:310-314.
 29. Marsili E, Baron DB, Shikhare ID, Coursolle D, Gralnick JA, Bond DR: ***Shewanella* secretes flavins that mediate extracellular electron transfer.** *Proc Natl Acad Sci USA* 2008, **105**:3968-3973.
 30. McCaskill A, Turgeon R: **Phloem loading in *Verbascum phoeniceum* L. depends on the synthesis of raffinose-family oligosaccharides.** *Proc Natl Acad Sci USA* 2007, **104**:19619-19624.
 31. Bachmann M, Matile P, Keller F: **Metabolism of the raffinose family of oligosaccharides in leaves of *Ajuga reptans* L. (Cold acclimation, translocation, and sink to source transition: Discovery of chain elongation enzyme).** *Plant Physiol* 1994, **105**:1335-1345.
 32. Taji T, Ohsumi C, Iuchi S, Seki M, Kasuga M, Kobayashi M, Yamaguchi-Shinozaki K, Shinozaki K: **Important roles of drought- and cold-inducible genes for galactinol synthase in stress tolerance in *Arabidopsis thaliana*.** *Plant J* 2002, **29**:417-426.
 33. Nishizawa A, Yabuta Y, Shigeoka S: **Galactinol and raffinose constitute a novel function to protect plants from oxidative damage.** *Plant Physiol* 2008, **147**:1251-1263.
 34. Van den Enden W, Valluru R: **Sucrose, sucrosyl oligosaccharides, and oxidative stress: scavenging and salvaging?** *J Exp Bot* 2009, **6**:9-18.
 35. M'sheli W, Dell'Orto M, Donnini S, De Nisi P, Zocchi G, Abdelly C, Gharsalli M: **Variability of metabolic responses and antioxidant defence in two lines of *Medicago ciliaris* to Fe deficiency.** *Plant Soil* 2009, **320**:219-230.
 36. John M, Röhrig H, Schmidt J, Walden R, Schell J: **Cell signalling by oligosaccharides.** *Trends Plant Sc* 1997, **2**:111-115.
 37. Vigani G, Zocchi G, Sijmons P, Bienfait H: **Source of electrons for extracellular Fe(III) reduction in iron-deficient bean roots.** *Physiol Plant* 1983, **59**:409-415.
 38. Rabotti G, De Nisi P, Zocchi G: **Metabolic implications in the biochemical responses to iron deficiency in cucumber (*Cucumis sativus* L.) roots.** *Plant Physiol* 1995, **107**:1195-1199.
 39. Espen L, Dell'Orto M, De Nisi P, Zocchi G: **Metabolic responses in cucumber (*Cucumis sativus* L.) roots under Fe-deficiency: a ³¹P-nuclear magnetic resonance in-vivo study.** *Planta* 2000, **210**:985-992.
 40. De Nisi P, Zocchi G: **Phosphoenolpyruvate carboxylase in cucumber (*Cucumis sativus* L.) roots under iron deficiency: activity and kinetic characterization.** *J Exp Bot* 2000, **51**:1903-1909.

41. Andaluz S, López-Millán A, Peleato M, Abadía J, Abadía A: **Increases in phosphoenolpyruvate carboxylase activity in iron-deficient sugar beet roots: Analysis of spatial localization and post-translational modification.** *Plant Soil* 2002, **241**:43-48.
42. Franceschi VR, Nakata PA: **Calcium oxalate in plants: Formation and function.** *Ann Rev Plant Biol* 2005, **56**:41-71.
43. von Wirén N, Klair S, Bansal S, Briat J, Khodr H, Shioiri T, Leigh R, Hider R: **Nicotianamine chelates both Fe-III and Fe-II. Implications for metal transport in plants.** *Plant Physiol* 1996, **119**:1107-1114.
44. Rellán-Álvarez R, Abadía J, Álvarez-Fernández A: **Formation of metal-nicotianamine complexes as affected by pH, ligand exchange with citrate and metal exchange. A study by electrospray ionization time-of-flight mass spectrometry.** *Rapid Commun Mass Spectrom* 2008, **22**:1553-1562.
45. Meyer I, Grosset J, Chartier Y, Cleyet-Marel J: **Preparation by two-dimensional electrophoresis of proteins for antibody production: antibody against proteins whose synthesis is reduced by auxin in tobacco mesophyll protoplasts.** *Electrophoresis* 1988, **9**:704-712.
46. Andaluz S, López-Millán A-F, De las Rivas J, Aro E-M, Abadía J, Abadía A: **Proteomic profiles of thylakoid membranes and changes in response to iron deficiency.** *Photosynt Res* 2006, **89**:141-155.
47. Fiehn O, Wohlgemuth G, Scholz M, Kind T, Lee DY, Lu Y, Moon S, Nikolau B: **Quality control for plant metabolomics: reporting MSI-compliant studies.** *Plant J* 2008, **53**:691-704.
48. Fiehn O, Wohlgemuth G, Scholz M R: **Setup and annotation of metabolomic experiments by integrating biological and mass spectrometric metadata.** *Data Integrat Life Sci Proc* 2005, **3615**:224-239.
49. Altschul S, Lipman D: **Protein database searches for multiple alignments.** *Proc Natl Acad Sci USA* 1990, **87**:5509-5513.
50. Gasteiger E, Hoogland C, Gattiker A, Duvaud S, Wilkins MR, Appel RD, Bairoch A: **Protein identification and analysis tools on the ExPASy server.** In *The Proteomics Protocols Handbook*. Edited by Walker JM. Totowa, NJ: Humana Press; 2005:571-607.
51. Larkin M, Blackshields G, Brown N, Chenna R, McGettigan P, McWilliam H: **Clustal W and clustal X version 2.0.** *Meth Biochem Anal* 2007, **23**:2947-2948.
52. Jiménez S, Gogorcena Y, Hévin C, Rombolà A, Ollat N: **Nitrogen nutrition influences some biochemical responses to iron deficiency in tolerant and sensitive genotypes of Vitis.** *Plant Soil* 2007, **290**:343-355.
53. Antonio C, Larson T, Gilday A, Graham I, Bergström E, Thomas-Oates J: **Hydrophilic interaction chromatography/electrospray mass spectrometry analysis of carbohydrate-related metabolites from Arabidopsis thaliana leaf tissue.** *Rapid Commun Mass Spectrom* 2008, **22**: 1399-1407.

SUPPLEMENTARY MATERIALS

Supplementary Figure 1. DMRL synthase sequence and alignment.

DMRL synthase sequence (A) in *Beta vulgaris* (GQ375163) and alignment (B) of DMRL synthase protein from *Beta vulgaris* (Bv) and *Spinacia oleracea* (So; [AAD44808.1](#)), *Nicotiana tabacum* (Nt; [AAQ04061.1](#)), *Arabidopsis thaliana* (At; [AAD44810.1](#)), *Cucumis sativus* (Cs; [ABZ88150.1](#)), *Solanum chacoense* (Sc; [ACB32230.1](#)) and *Oryza sativa* (Os; [ACS94980.1](#)) and *Zea mays* (Zm)



Supplementary Table 1 - Unknown metabolite response ratios of the different treatments vs. +Fe

List of unknown metabolites with response ratios (level in a given treatment divided by the level in the +Fe treatment) higher than 4 and a t-test significance of $P < 0.01$ (indicated in bold). When the ratios were lower than 1 the inverse was taken and the sign changed.

BinBase Metabolite ID	-Fe	24 h	72 h YZ	72 h WZ
199205	6.3	13.1	4.3	2.3
199242	2.3	7.5	7.1	3.1
200421	-1.9	2.7	6.8	-1.3
200463	2.7	2.5	4.8	1.5
200523	2.7	4.6	3.3	2.7
200624	-3.0	-6.1	-1.5	2.0
200844	2.7	4.8	5.1	2.7
200925	-7.4	-2.0	1.0	2.2
201005	-1.7	-5.9	-2.5	-6.3
202178	3.8	5.8	3.4	2.1
202293	8.2	21.7	6.7	2.7
202808	2.6	6.7	3.5	2.1
203241	1.4	1.7	4.0	2.2
207227	4.2	6.7	6.5	2.3
208770	1.7	2.6	4.0	4.0
211890	1.8	3.9	7.6	2.6
211891	17.6	145.9	69.5	6.3
211991	32.5	5.1	4.4	2.0
212373	4.8	7.9	2.0	2.4
212672	37.5	7.7	3.1	1.7
217840	-8.1	-4.1	-1.2	-1.4
217841	1.1	1.3	4.5	1.8
218550	1.4	2.2	4.2	4.1
218596	1.4	2.1	4.6	4.6
218761	3.4	6.7	3.9	1.9
218766	1.2	2.4	4.9	2.0
218767	1.6	3.9	7.0	2.8
218769	4.5	41.7	5.0	6.0
218771	6.6	6.6	6.2	2.1
218773	1.2	4.0	8.3	4.1
218798	1.5	10.1	8.3	4.0
218824	2.1	-1.7	4.8	11.3
218829	3.1	3.3	2.8	6.1
218832	1.3	-1.5	-1.2	4.1
218834	3.1	3.8	9.7	5.1
218847	1.4	2.3	4.2	4.3
218852	2.7	3.6	9.7	5.4
218867	4.9	8.7	10.0	9.1
218986	-3.6	-5.3	-1.2	1.3
218993	-4.1	-6.9	-1.4	-1.3
218995	-1.1	1.8	4.1	2.3
219171	5.1	9.3	4.9	1.8
219181	2.0	2.1	4.3	1.5
219185	3.2	5.4	3.1	1.3
219513	4.2	11.0	3.8	2.1
220143	1.0	1.7	4.5	1.7

**METABOLITE PROFILES CHANGES IN THE XYLEM SAP AND LEAVES OF
STRATEGY I PLANTS IN RESPONSE TO IRON DEFICIENCY AND IRON RESUPPLY**

**Rubén Rellán-Álvarez¹, Hamdi El Jendoubi¹, Martin Scholz², Gert Wohlgemuth²,
Anunciacion Abadía¹, Oliver Fiehn², Javier Abadía¹, Ana Álvarez Fernández¹**

Submitted to Plant Cell and Environment

¹Department of Plant Nutrition, Aula Dei Experimental Station, CSIC, P.O. Box 13034, E-50080 Zaragoza, Spain. ²Genome Center, University of California Davis, CA 95616, USA

METABOLITE PROFILES CHANGES IN THE XYLEM SAP AND LEAVES OF STRATEGY I PLANTS IN RESPONSE TO IRON DEFICIENCY AND IRON RESUPPLY

¹Rubén Rellán-Álvarez, ¹Hamdi El Jendoubi, ²Martin Scholz, ²Gert Wohlgenuth, ¹Anunciacion Abadía, ²Oliver Fiehn, ¹Javier Abadía and ¹Ana Álvarez Fernández

¹Department of Plant Nutrition, Aula Dei Experimental Station (CSIC), P.O. Box 13034, E-50080 Zaragoza, Spain ²Genome Center, University of California Davis, CA 95616, USA

Iron deficient plants do not synthesize enough chlorophyll to maintain normal photosynthetic rates. Therefore, under Fe-deficiency C fixation through photosynthesis is impaired and plants need to readjust their metabolism to cope with this C shortage. This metabolic adaptation to Fe deficiency includes increases of organic acid concentration in all plant tissues, in the activities of different enzymes of the pentose phosphate pathway and TCA cycle such as phosphoenolpyruvate carboxylase (PEPC) activity and in the anaerobic metabolism. All these metabolic adaptations have been well characterized in Fe-deficient roots of different species, using both biochemical and -omic approaches. However, Fe deficiency induced metabolic changes in leaves and xylem sap have been less studied. In this work we have characterized the metabolite profile changes induced by Fe-deficiency in leaves and xylem sap of several strategy I plant species. The short-term effect of Fe-resupply in the metabolite xylem sap profile of Fe-deficient tomato plants was also evaluated. We have identified between 60 to 90 metabolites in the different tissues studied. The most relevant changes found were the large increase of organic acids in xylem sap and leaves and of free aminoacids in leaves. Xylem sap analysis of Fe-deficient tomato plants resupplied with Fe (24h) showed a fast re-adaptation to control conditions. A good correlation between aminoacids and carboxylates of the TCA cycle indicate that anaplerotic reactions using aminoacids as C source may occur in Fe-deficient sugar beet leaves.

Introduction

Iron is an essential micronutrient for plants because it is a component of different proteins involved in processes such as photosynthesis, respiration and others (Marschner, 1995). In calcareous and alkaline soils Fe is mainly found as poorly soluble oxides and/or hydroxides, and therefore the amount of Fe available to plants is

very low. Since 30% of cultivated plants are grown in calcareous soils, Fe deficiency is a major problem for crop productivity (Hansen et al., 2006; Rombolà and Tagliavini, 2006).

Upon sensing Fe shortage, many plant species, with the exception of grasses, boost different mechanisms included in the so-called reduction strategy (Strategy I) to maximize Fe mobilization and uptake from the soil (Abadía et al., 20011, *In press*). This strategy is based on the reduction of rhizospheric Fe by means of an Fe reductase enzyme (FRO; (Robinson et al., 1999), and the subsequent cell Fe uptake by an Fe(II) transporter (IRT; (Eide et al., 1996). Iron solubilization in the rhizosphere is enhanced by an H⁺-ATPase that is up-regulated with Fe-deficiency (Santi and Schmidt, 2009). Grasses use a distinct strategy called chelation strategy (Strategy II) that relies on the synthesis and excretion of phytosiderophores (PS) to the rhizosphere where they chelate Fe(III) (Abadía et al., 20011, *In press*) the Fe(III)-PS complexes are then taken up by YSL-type transporters (Curie et al., 2009).

Plant adaptation to Fe shortage involves different metabolic changes occurring at the root, xylem and leaf level. In roots, there are increases in the activities of phosphoenolpyruvate carboxylase (PEPC) (Andaluz et al., 2002) and several enzymes of the glycolytic pathway and the tricarboxylic acid (TCA) cycle (Herbik et al., 1996; Brumbarova et al., 2008; Li et al., 2008). The increased activity of PEPC leads to an accumulation of organic acids (Abadía et al., 2002), that may play important roles in the transport of Fe and C (López-Millán et al., 2000) *via* xylem to the leaf. Organic acid concentrations in xylem sap and leaf apoplastic fluid are markedly increased in several Strategy I plant species with Fe deficiency (López-Millán et al., 2000; López-Millán et al., 2001; Larbi et al., 2003; Jiménez et al., 2007; López-Millán et al., 2009). At the leaf level, the most characteristic Fe-deficiency symptom is the greenish-yellow colour of young leaves, caused by decreases in the amount of the light-harvesting pigments,

pecially chlorophyll (Chl), causing a relative enrichment in carotenoids (Abadía, 1992; Larbi et al., 2004; Timperio et al., 2007). Iron deficiency-induced leaf chlorosis leads to reduced photosynthetic efficiency and electron transport, with less C being fixed *via* photosynthesis (Abadía, 1992; Larbi et al., 2006). Whereas most of these metabolic changes have been revealed by physiological and biochemical studies, the recent application of ‘-omic’ techniques, that allow for the simultaneous and untargeted determination of a large amount of compounds, has complemented previous studies by providing new information. Iron deficiency studies have been recently published involving the use of transcriptomic (Thimm et al., 2001; Buhtz et al., 2010; Yang et al., 2010), proteomic (Herbik et al., 1996; Andaluz et al., 2006; Timperio et al., 2007; Brumbarova et al., 2008; Li et al., 2008; Laganowsky et al., 2009; Donnini et al., 2010; Lan et al., 2010; Li and Schmidt, 2010; Rellán-Álvarez et al., 2010; Rodríguez-Celma et al., 2011, *Submitted*) and metabolomic studies (Rellán-Álvarez et al., 2010), with focus on whole plants, roots and thylakoid membranes. Iron resupply either to leaves or to roots leads to a de-activation of some root Fe acquisition mechanisms, including FRO and IRT (López-Millán et al., 2001; Enomoto et al., 2007; Abadía et al., 20011, *In press*). Regarding metabolic changes, root PEPC activity, organic acid concentrations and the whole metabolite profile reach control levels within a few days after Fe-resupply (Rellán-Álvarez et al., 2010; Abadía et al., 20011, *In press*). Also, Fe resupply leads to increases in chlorophyll concentrations and photosynthetic rates within few days or weeks (Larbi et al., 2003; Larbi et al., 2004; Timperio et al., 2007), as well as to decreases in the concentration of organic acids in the whole plant (López-Millán et al., 2001; López-Millán et al., 2001). Xylem sap and leaf apoplastic carboxylate concentrations were markedly reduced after Fe resupply in Fe-deficient sugar beet (Larbi et al., 2010) and fruit trees (Larbi et al., 2003).

The aim of this study was to characterize the metabolite profile of the xylem sap and leaves of different Strategy I plant species in response to Fe deficiency. Metabolite profiles obtained using gas chromatography mass spectrometry (GC-MS) were obtained from xylem sap and leaves of tomato, lupine, peach and sugar beet plants grown in Fe-sufficient and Fe-deficient

conditions. Also, short-term effects (6-24 h) of Fe resupply on the xylem sap metabolite profiles of Fe-deficient tomato plants were studied.

Materials and Methods

Plant Material. Xylem sap and leaves were obtained from four different Strategy I plant species grown in controlled and field conditions and with different Fe-nutrition status. Tomato (*Lycopersicon esculentum* L. cv. ‘Tres Cantos’), lupine (*Lupinus albus* cv. ‘Multolupa’) and sugar beet (*Beta vulgaris* L. ‘Orbis’) plants were grown in a growth chamber with a photosynthetic photon flux density at leaf height of 350 $\mu\text{mol m}^{-2} \text{s}^{-1}$ photosynthetic active radiation and a 16 h-22 °C/8 h-19 °C, day/night regime. Seeds were germinated and grown in vermiculite for 2 weeks. Seedlings were grown for 3 more weeks in half-strength Hoagland nutrient solution with 45 μM Fe-EDTA. Then, seedlings were transplanted to plastic buckets containing half-strength Hoagland nutrient solution with either 0 (-Fe) or 45 μM Fe(III)-EDTA (+Fe). The pH of the Fe-free nutrient solutions was buffered at approximately 7.7 by adding 1 mM NaOH and 1 g L^{-1} of CaCO_3 . This treatment simulates conditions usually found in the field that lead to Fe deficiency (Susín et al., 1996). After growth for 14 days in these conditions, xylem sap (lupine and tomato) and young, fully developed leaves (tomato and sugar beet) were sampled 4 h after light onset from 6-8 plants per treatment (Fig. 1A-C, E-G). Also, a set of Fe-deficient tomato plants were resupplied (at 4 h after light onset) with Fe (45 μM Fe(III)-EDTA in the nutrient solution). Xylem sap samples were taken from Fe-deficient and Fe-deficient, Fe-resupplied plants at 6, 12, 18 and 24 h after Fe-resupply, from 6-8 plants per treatment and sampling time. Leaves were washed with distilled water, discs were taken using a cork borer with a surface of 0.50 cm^2 , immediately frozen in liquid N_2 and stored at -80 °C until metabolite extraction.

Fourteen year-old peach trees (*Prunus persica* (L.) Batsch, cv. ‘Catherina’ grafted on ‘GF677’) grown on a flood-irrigated calcareous soil (*Typical xerofluvent*, clay-loamy texture, with 31% total CaCO_3 , 10% active CaCO_3 , 7 mg kg^{-1} DTPA-extractable Fe, 2% organic matter and pH 8.0 in water) were used. The orchard was located in Peñaflores (Zaragoza, Spain), had a frame of 2.5 \times 6 m, and was appropriately maintained in terms of nutrition, pruning and pest and disease control.

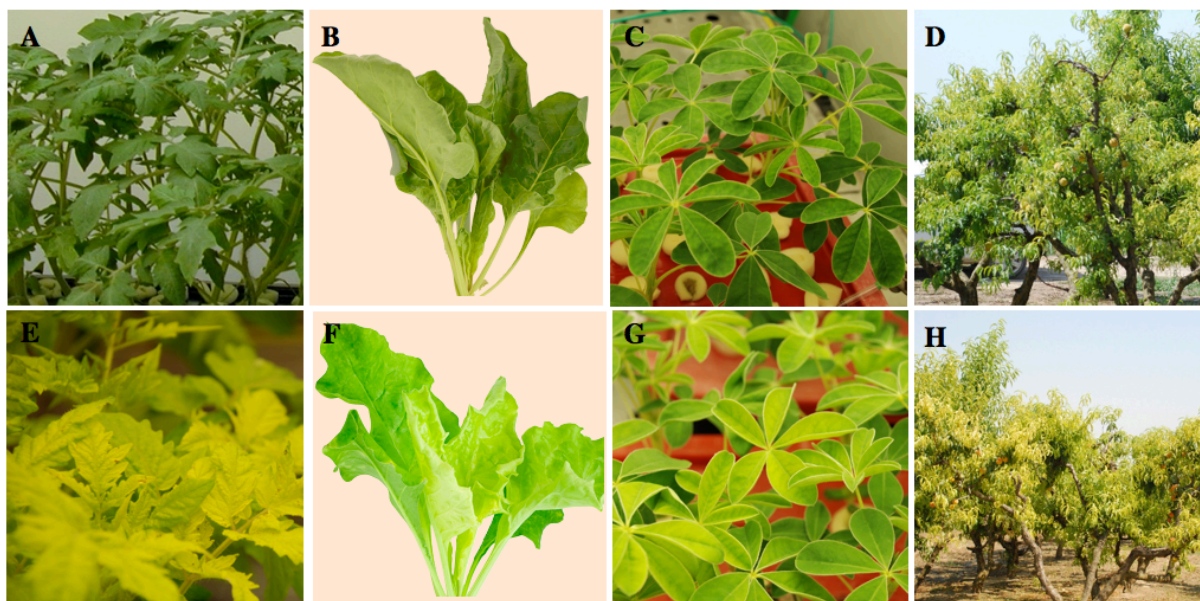


Figure 1. Plants grown in Fe-sufficient (upper row) and Fe-deficient (lower row) conditions. Xylem sap and/or leaf samples of tomato (A, E), sugar beet (B, F), lupine (C, G) and peach (D, H) were taken from plants and analyzed by gas chromatography-mass spectrometry to study metabolite changes induced by Fe deficiency.

Some trees did not receive any Fe fertilization for 2 years prior to the beginning of the trial. Tree Fe status was monitored by estimating leaf Chl concentration with a hand-held Chl meter (SPAD-502, Minolta Corp., Ramsey, NJ) in the 3rd-4th leaves from the shoot tip. All SPAD data presented were measured at sampling time. Five trees were selected and grouped into two classes: 3 trees with no chlorosis symptoms in the springtime season but with a slight chlorosis at the sampling time (control trees, +Fe; SPAD 18-32) and 2 trees with severe Fe-deficiency symptoms (-Fe; SPAD 9-17, Fig. 1 D, H). Seven current year branches (25-30 cm in length) were taken from each tree in July 2008 between 7:00 and 8:00 AM (solar time). Leaf discs from the 3rd-4th leaf from the branch tip were sampled in the field as described above (see below). Then, sampled branches were protected with a wet paper towel and immediately brought to the laboratory for xylem sampling (see below).

Xylem sap sampling. Xylem sap from tomato and lupine plants was collected by de-topping the plants 3-4 cm above the cotyledons (López-Millán et al., 2009). Stumps were allowed to bleed for 2-3 minutes, the first drops of sap were discarded, the cut surface was wiped out with paper tissue, cleaned with distilled water and blotted dry. Then, xylem sap was collected with a micro-pipette for 20 min in Eppendorf tubes kept

on ice. Extraction of peach xylem sap from branches was made as described elsewhere (Larbi et al., 2003) with some modifications. The cutting was devoid of the basal bark (3-4 cm), washed with distilled water and placed in a Schölander chamber with the distal end, including leaves, inside the pressure chamber. Then, pressure was increased progressively from 5 to 22 bar (higher pressure values resulted in cytosolic contamination). The first few drops of sap were discarded to avoid contamination, and xylem sap was collected for 4 min in Eppendorf tubes kept on ice. Cytosolic malate dehydrogenase c-mdh (EC 1.1.1.37) was used as xylem sap cytosolic contamination marker (López-Millán et al., 2000) in all cases.

Metabolite extraction and derivatization. Metabolite extraction was carried out as previously described for xylem sap (Fiehn, 2003) and leaves (Fiehn et al., 2008). The dried extracts were derivatized as described elsewhere (Fiehn et al., 2008).

Metabolite analysis by gas chromatography - mass spectrometry and data processing. Derivatized samples (1 μ L) were injected randomly in split-less mode with a cold injection system (Gerstel, Mülheim an der Ruhr, Germany) and analyzed by a GC device (Agilent 6890, San Jose, CA, USA) using a Rtx 5Sil MS column (30 m x 0.25 mm, 0.25 μ m film thickness) and an

integrated guard column (Restek, Bellefonte, PA, USA). The GC was connected to a Leco Pegasus IV time-of-flight mass spectrometer (TOFMS) controlled with Leco ChromaTOF software v.2.32 (Leco, St. Joseph, MI, USA). Peak detection and mass spectra deconvolution were performed with Leco Chroma-TOF software v.2.25. GC-MS chromatograms were processed as described previously (Fiehn et al., 2008). Metabolite data were normalized using the sum of all metabolite peak heights in a single run to account for small GC injection variations. The resulting data were multiplied by a constant factor in order to obtain values without decimal figures. Data were analyzed to check for possible correlation between peak height values and peak variance, and since a positive correlation was found a log₁₀ transformation of the data was carried out to avoid the variance-mean dependence (Chich et al., 2007).

Statistical analysis. Statistical analysis of the normalized log₁₀ transformed data was carried out with Statistica software (v.9.0. StatSoft, Inc., Tulsa, OK, USA). Six to eight biological replicas per tissue, plant species and Fe treatments were used.

Iron determination. Iron was determined by graphite furnace atomic absorption spectrometry (Varian SpectrAA with Zeeman correction). Each sample was analyzed in triplicate with 6 biological replicates.

Results

After metabolite peak processing, normalization and log₁₀ transformation, xylem sap and leaf metabolite data were subjected to different types of analysis. A first glimpse of the metabolite increases and decreases occurring with Fe deficiency was obtained from 1-factor analysis of variance (ANOVA) of the metabolite data for each tissue and specie. Mean response ratios, defined as the level in the Fe deficiency treatment divided by the level in the Fe-sufficient controls. Then, the clustering of the Fe-deficient and control samples, as well as the metabolites responsible of the separation between both samples, were studied using multivariate analysis (supervised partial least square, PLS). Using the same techniques, the effects of Fe resupply in the xylem sap metabolite composition of Fe-deficient tomato plants were analyzed. Also, mean response ratios for each metabolite were compared using Duncan's test at $p < 0.05$ in

order to find significant differences due to the Fe-resupply time. Finally, the correlations between different metabolites were analyzed to look for possible reactions that may be relevant in Fe deficiency.

Xylem sap metabolite profile changes in response to Fe deficiency. The xylem sap from tomato, lupine and peach Fe-deficient and control plants was analyzed by GC-MS. In each species, only those metabolites present in at least 80% of either the Fe-deficient or the control samples were selected for further analysis. From a total of 253, 233 and 251 metabolites detected in tomato, lupine and peach, respectively, 77, 83, and 77 metabolites were identified. The levels of several identified metabolites changed significantly (at $p < 0.05$) in response to Fe deficiency. For this group of metabolites, those with a mean response ratio above 2.0 (41, 19 and 6 for tomato, lupine and peach, respectively) are shown in Table 1. The highest increases were found for the TCA cycle carboxylates aconitate and succinate in tomato and lupine, and citrate, malate and oxoglutarate in tomato only. However, the only metabolite that increased (>2-fold) in peach was nicotianamine. Most metabolites decreased with Fe deficiency, and the largest decreases were found for polyamines such as putrescine (8- to 12-fold) and spermidine (2- to 7-fold) in tomato and lupine. Aminoacids such as glycine, tyrosine and alanine also decreased (2- to 4-fold) in both tomato and lupine, whereas others decreased (2- 5-fold) only in lupine (β -alanine, tryptophan and oxoproline) or tomato (lysine, leucine, isoleucine, valine and serine). Decreases were also found for carbohydrates such as glucose-6-P and myoinositol in both tomato and lupine and 3-phosphoglyceraldehyde in both lupine and peach, whereas other carbohydrates only decreased in tomato (arabinose, inulobiose, fructose, galactinol and sucrose), lupine (trehalose) or peach (gluconate).

Cluster analysis of the metabolite profile of Fe-deficient and Fe-sufficient xylem sap samples. Score scatter plots obtained by Partial Least Squares Analysis (PLS) were drawn for the metabolite profiles of each species, including both the identified and the unidentified compounds (Fig. 2A-C). Iron-deficient and control, Fe-sufficient samples were clearly separated in clusters in the three species studied. However, the separation between the Fe-deficient and Fe-sufficient samples was more obvious in

Table 1. Xylem sap extracts identified metabolite response ratios of Fe deficient (-Fe) vs. Fe-sufficient controls (+Fe). When the response ratio (level in the -Fe treatment divided by the level in the +Fe treatment) was lower than 1 the inverse was taken and the sign changed. Only changes >2 and with t-test significance of p<0.05 are shown. Numbers on the left correspond to those indicated inside the different metabolite symbols in Fig. 5.

#	Lupine	#	Peach	#	Tomato			
<i>Aminoacid and Nitrogen Metabolism</i>								
38	maleic acid	2.5	45	nicotianamine	2.4	57	suberyl glycine	7.1
60	shikimic acid	-2.0	8	benzoic acid	-2.3	68	tryptophan	6.4
42	spermidine	-2.0	10	butane-2,3-diol	-2.4	31	hydroxyglutaric acid	4.6
70	tyrosine	-2.1				38	maleic acid	4.0
7	glycine	-2.1				6	asparagine	2.5
68	tryptophan	-2.2				59	serine	-2.0
3	alanine	-2.4				3	alanine	-2.3
48	oxoproline	-2.5				50	phenylalanine	-2.8
9	beta alanine	-2.6				71	urea	-2.9
52	putrescine	-7.6				72	valine	-3.0
						70	tyrosine	-3.1
						40	methionine	-3.1
						34	isoleucine	-3.2
						66	threonine	-3.6
						26	glycine	-3.8
						35	leucine	-3.9
						53	quinic acid	-4.2
						60	shikimic acid	-4.3
						36	lysine	-5.1
						61	spermidine	-6.7
						52	putrescine	-11.8
<i>TCA cycle</i>								
2	aconitic acid	2.6				47	oxoglutaric acid	91
62	succinic acid	2.4				39	malic acid	6.2
						11	citric acid	5.7
						62	succinic acid	4.7
						2	aconitic acid	2.8
<i>Carbohydrate Metabolism</i>								
67	trehalose	-2.3	22	gluconic acid	-2.1	16	N-acetyl-D-mannosamine	-2.6
						63	sucrose	-2.7
						73	xylose	-3.8
						21	galacturonic acid	-4.1
						24	glucuronic a	-4.2
						19	galactinol	-4.7
						14	fructose	-5.2
						33	inulobiose	-5.2
						5	arabinose	-7.5
<i>Glycolysis and Pentose Phosphate Metabolism</i>								
49	PGA	-2.5	49	PGA	-3.9	23	glucose-6-P	-2.3
20	galactose-6-P	-4.6				37	lyxytol	-2.3
23	glucose-6-P	-5.0				56	ribose	-4.3
<i>Others</i>								
28	guanosine	-2.4	1	2-deoxyerythritol	-2.1	15	myo-inositol	-2.5
18	GABA	-2.7				54	ribitol	-4.1
41	myoinositol	-3.9				18	GABA	-4.4

tomato and lupine than in peach. In fact, the separation explained by the first vector (v1) was 53, 38 and 13% in tomato, lupine, and peach, respectively. The Fe-deficient and Fe-sufficient cluster separation is associated to the metabolites with the highest contribution (X-weights) to v1. In tomato, the metabolites with the highest positive X-weights were carboxylates of the TCA

cycle such as oxoglutaric, malic 2-hydroxyglutaric, citric, succinic and aconitate whereas those with the highest negative X-weights were aminoacids, other N related compounds (spermidine, putrescine, glycine, shikimic acid and lysine) and carbohydrates (arabinose, galacturonic acid, xylose and inulobiose) (Supplementary Table 1). A similar

pattern was found in lupine, where metabolites with the highest positive X-weights were carboxylates such as succinate, aconitate, fumarate, maleate, oxoglutarate and malate, whereas the metabolites with the highest negative X-weights were aminoacids like tryptophan, tyrosine, β -alanine and oxoproline (Supplementary Table 1). In peach, the metabolites with the highest positive X-weights were carbohydrates (glucose, arabitol and sucrose) and glycolysis related compounds (ribose and gluconate), whereas the metabolites with highest negative X-weights were aminoacids and other N related metabolites (2-hydroxyglutarate, proline, phenylalanine), carbohydrates (galactinol, galactonic acid and

threonine) and some carboxylates such as fumarate.

Leaf metabolite profile changes in response to Fe deficiency. From a total of 238, 128 and 375 metabolites detected (present in at least 80% of either Fe-deficient or Fe-sufficient plants in each species), 65, 82, and 92 metabolites were identified in leaf extracts of tomato, sugar beet and peach, respectively. The levels of several identified metabolites changed significantly (at $p < 0.05$) in response to Fe deficiency. For this group of metabolites, those with a mean response ratio above 2.0 (21, 34 and 4 in tomato, sugar beet and peach, respectively) are shown in Table 2. Most of the metabolites increased with Fe deficiency, with the largest increases found (2- to

Table 2. Leaf extracts identified metabolite response ratios of Fe deficient (-Fe) vs. Fe-sufficient controls (+Fe). When the response ratio (level in the -Fe treatment divided by the level in the +Fe treatment) was lower than 1 the inverse was taken and the sign changed. Only changes >2 and with t-test significance of $p < 0.05$ are shown. Numbers on the left correspond to those indicated inside the different metabolite symbols in Fig. 5.

#	Sugar beet	#	Peach	#	Tomato			
<i>Aminoacid and Nitrogen Metabolism</i>								
26	glutamine	32.8	62	s- glycine	5.9	70	tyrosine	4.2
59	serine	19.6	6	asparagine	4.3	12	ethanolamine	3.8
34	isoleucine	13.7	34	isoleucine	2.0	38	maleic acid	2.1
72	valine	8.9				68	tryptophan	2.1
48	oxoproline	8.0				35	leucine	2
35	leucine	8.0				26	glutamine	-2.2
38	maleic acid	7.7				7	aspartic acid	-2.6
27	glycine	6.8				29	homoserine	-5.7
70	tyrosine	6.1				32	hydroxylamine	-13.6
66	threonine	6.0						
69	tyramine	4.6						
25	glutamic acid	3.5						
3	alanine	2.5						
52	putrescine	-2.9						
<i>TCA cycle</i>								
11	citric acid	13.7				62	succinic acid	2.8
62	succinic acid	12.2						
16	fumaric acid	2.9						
<i>Carbohydrate Metabolism</i>								
43	N-acetyl-D-hexosamine	5.8	22	gluconic acid	-2.4	64	threitol	6.5
74	lactobionic acid	3.5				54	ribonic acid	4.1
44	N-acetyl-D-mannosamine	3.2				43	N-acetyl-D-hexosamine	3.8
75	xylonic acid	3.2				19	galactinol	2.5
76	arabitol	3.1				44	N-acetyl-D-mannosamine	2.1
21	erythronic acid	2.9				15	fucose + rhamnose	2
73	xylose	2.9				58	saccharic acid	-4.0
28	xylitol	2.2						
<i>Glycolysis and Pentose Phosphate Metabolism</i>								
49	PGA	-12.4				23	glucose-6-P	-2.0
<i>Others</i>								
17	g-tocopherol	17.3				51	phytol	-2.3
13	FAD	2.9				30	hydroxycarbamate	-8.0
4	alpha-tocopherol	2.7						
65	threonic acid	2.6						
42	myristic acid	2.1						
51	phytol	-3.9						
46	oxalic acid	-5.5						

33-fold change) for aminoacids and N related compounds: isoleucine in sugar beet and peach, glutamine, serine, valine, oxoproline, leucine, glycine, tyrosine, threonine, glutamate and alanine in sugar beet, tyrosine, ethanolamine, tryptophan and leucine in tomato, and suberyl glycine and asparagine in peach. Other increases were only found in tomato and/or sugar beet: TCA cycle carboxylates (citrate, succinate and fumarate) with 3- to 14-fold changes, and carbohydrates (*e.g.*, N-acetyl-D-hexosamine and N-acetyl-D-mannosamine) with 2- to 6-fold changes. A few metabolites decreased with Fe deficiency, most of them in tomato, including aminoacids and N related compounds (hydroxylamine, homoserine, aspartate and glutamine) and other metabolites such as hydroxycarbamate. Other compounds that decreased were phytol and oxalate in sugar beet and gluconate in peach.

Cluster analysis of the metabolite profile of Fe-deficient and Fe-sufficient leaf samples. Score scatter plots obtained by PLS analysis for the leaf metabolite profiles of each species, including both identified and non-identified compounds, are shown in Fig. 2. Iron-deficient and Fe-sufficient samples are in separated clusters in the three species (Fig. 2D-F), especially in tomato and sugar beet. The separation explained by the first vector (v1) was 35, 33 and 14% in tomato,

sugar beet and peach, respectively. In tomato, the metabolites with the highest positive X-weights are mainly aminoacids and N related compounds (hydroxylamine, homoserine, citrulline, aspartate, cyclohexylamine and glutamine), whereas among the metabolites with highest negative X-weights we found carbohydrates (fucose + rhamnose, N-acetyl-D-hexosamine, N-acetyl-D-mannosamine and myo-inositol), and aminoacids and other N related compounds (tyrosine, 2-isopropylmalate, leucine and glutamate) (Supplementary Table 1). In sugar beet, the metabolites with the highest positive X-weights were mainly 3 types of compounds: carboxylates (succinate and citrate) carbohydrates (lactobionic acid, xylitol, N-acetyl-D-hexosamine and N-acetyl-D-mannosamine) and aminoacids (oxoproline, serine and threonine) (Supplementary Table 1). In sugar beet, metabolites with the highest negative X-weights were glycolysis and pentose phosphate pathway related compounds (PGA, fructose 6-P and glucose 6-P), and aminoacids and other N related compounds (putrescine and aspartate) (Supplementary Table 1). In the case of peach, metabolites with the highest positive X-weights included aminoacids and N related compounds (*e.g.*, isoleucine, asparagine, serine, phenylalanine, or threonine), whereas among the

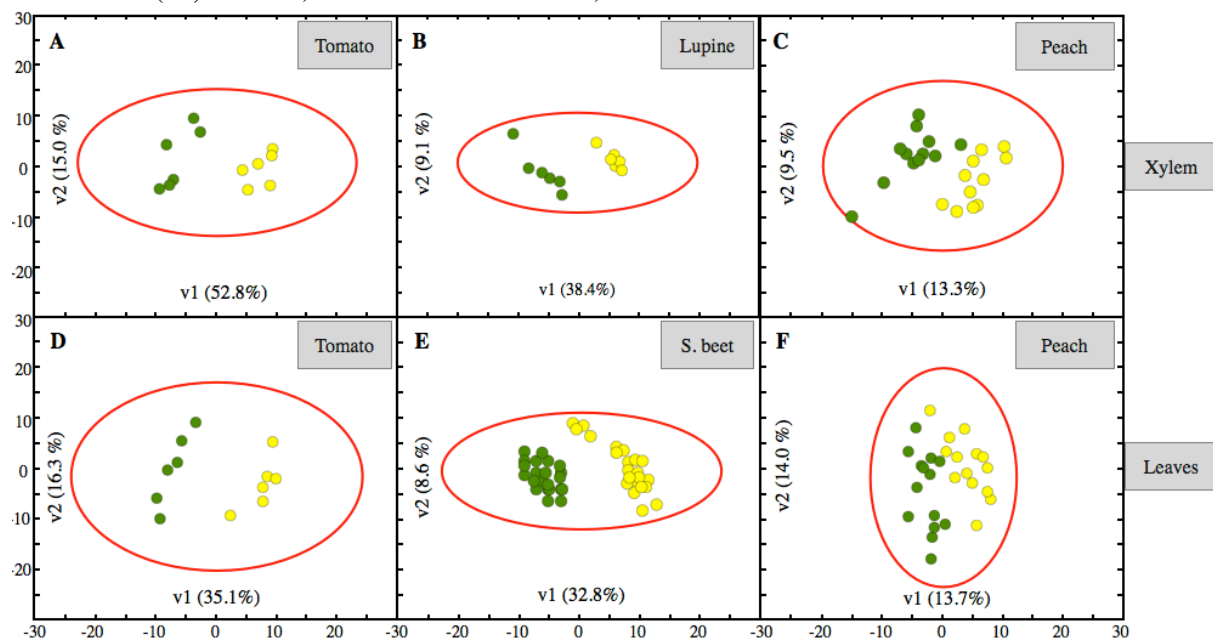


Figure 2. Score scatter plot of detected metabolites. Partial Least Square (PLS) analysis, showing the score scatter plot of PLS vector 1 (v1) vs. PLS vector 2 (v2) of detected metabolites in the different tissues from control (green circles) and Fe-deficient (yellow circles) The percentage of variability explained by each vector is also indicated.

metabolites with highest negative X-weights we found carbohydrates (erythronic acid and erythrose) and glycolysis and pentose phosphate pathway related compounds such as gluconate and PGA.

Metabolite correlations between metabolites involved in anaplerotic reactions. Since one of the main response of Fe deficiency is the increase of anaplerotic reactions such as PEPC, we explored the possible occurrence of other anaplerotic reactions occurring in leaf samples of the three species by looking at the correlations between aminoacids and the TCA cycle carboxylates (Fig. 3A). Positive correlations between the levels of aminoacids and carboxylates were found in Fe-sufficient samples, whereas the correlations were negative in Fe-deficient samples. As an example, the relationships between i) aspartate vs. citrate, ii) glutamate vs. oxoglutarate and iii) tyrosine vs. fumarate in Fe-deficient and Fe-sufficient sugar beet samples are shown in Fig. 3B, C and D, respectively. Similar correlations were found for the pair aspartate/citrate in tomato and peach leaves, although the in the latter case it was much less obvious.

Metabolite profile changes and sample cluster analysis of Fe-deficient tomato plants xylem sap in response to Fe-resupply. The xylem sap Fe concentrations of Fe-sufficient, Fe-deficient and Fe-deficient resupplied tomato plants collected at 6, 12, 18 and 24 h after Fe-resupply were 20 ± 3 , 5 ± 4 , 74 ± 4 , 177 ± 15 , 156 ± 19 and 66 ± 3 μM ($n=6$), respectively. Iron concentrations in the xylem sap of Fe-sufficient plants remained constant at all sampling times (Supplementary Fig. 1). The changes in the tomato xylem sap metabolite profile were investigated at 6, 12, 18 and 24 hours after Fe resupply with $45 \mu\text{M}$ Fe-EDTA. From a total of 253 detected compounds (present in at least 80% of the samples of at least one treatment) 77 were identified. From these metabolites, the mean response ratios of 44 (in Fe-deficient plants), 47, 26, 25 and 10 of them (at 6, 12, 18 and 24 h after Fe resupply, respectively) changed significantly ($p < 0.05$) when compared to the xylem of Fe-sufficient plants sampled at the same sampling time points (Supplementary Table 2). The largest increases at 6 h after Fe-resupply were for TCA cycle metabolites (alpha-ketoglutarate, citrate, malate, fumarate and aconitate, with response ratios of 123, 30, 12, 7

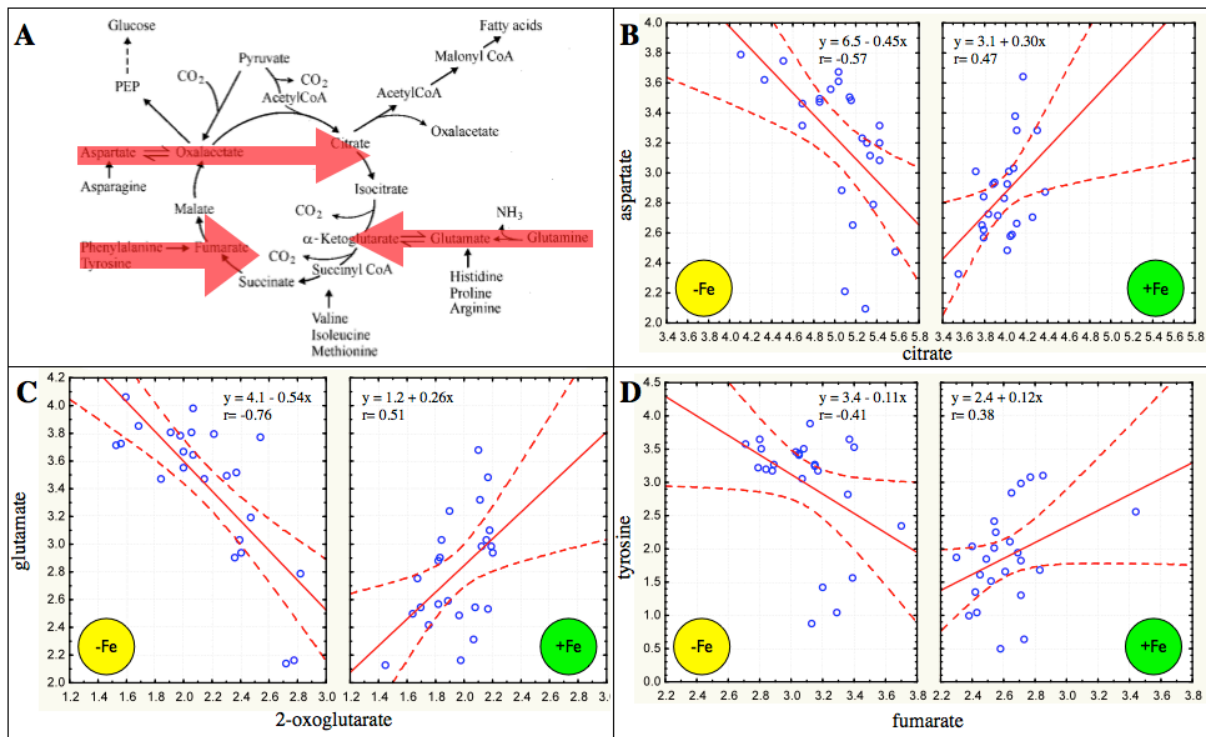


Figure 3. Metabolite correlations. TCA cycle with anaplerotic reactions that use aminoacids as C source shown with red arrows (A). Metabolite correlations between citric and aspartic acid (B); oxoglutaric and glutamic acid (C); fumaric and tyrosine (D).

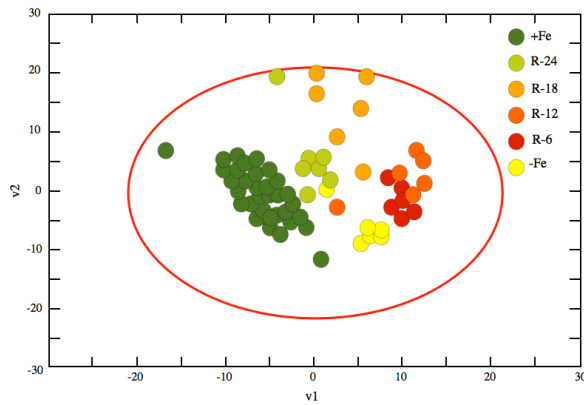


Figure 4. Score scatter plot of detected xylem-metabolites for the tomato resupply experiment. Partial Least Square (PLS) analysis, showing the score scatter plot of PLS vector 1 (v1) vs. PLS vector 2 (v2) of identified metabolites in the Fe treatments: control (+Fe), Fe-deficient (-Fe) and Fe-deficient after 6 (R-6), 12 (R-12), 18 (R-18) and 24 (R-24) hours of Fe resupply.

and 5, respectively) and some aminoacids and other N related compounds (maleate, tryptophan, aspartate and 2-hydroxyglutarate, with response ratios of 19, 7, 6 and 6, respectively). At the following sampling times, the response ratios for all these metabolites decreased, and 24 h after Fe-resupply only two of the metabolites (aconitate and citrate) showed significant differences when compared with the control values. Most of the metabolites that decreased with Fe deficiency were still affected at a similar level 6 h after Fe resupply, including some aminoacids and N related compounds (*e.g.* isoleucine, leucine, putrescine, tyrosine, valine) and carbohydrates (*e.g.* arabinose, fructose, inulobiose and glucose). After this time point, less metabolites remained affected, with 17, 12 and 6 the total showing negative response ratios in the samples taken 12, 18, and 24 h after Fe-resupply, respectively. Sample clusters were also separated but at a lesser extent, indicating a rapid adaptation of the xylem sap metabolite profile to control values.

Discussion

We have studied the effects of Fe deficiency on the metabolite profiles of xylem sap and leaves of several Strategy I plant species using GC-MS analysis. Iron deficiency led to important alterations in the metabolite profile of both xylem sap and leaves of three of the species analyzed, sugar beet, tomato and lupin, whereas peach tree showed less marked changes (Fig. 5). TCA cycle

metabolites were increased both in xylem sap and leaves. On the other hand, carbohydrates and aminoacids and N metabolism compounds decreased in xylem sap and increased in leaves. In sugar beet leaves, significant correlations were found between selected pairs of aminoacids and TCA cycle metabolites involved in known anaplerotic reactions, and the sign of these correlations was affected by Fe status. In tomato, the xylem sap metabolite profile of Fe-deficient plants was similar to that of Fe-sufficient plants after one day of Fe-resupply.

The most relevant changes in the xylem sap metabolite profile induced by Fe-deficiency were the increases in carboxylates of the TCA cycle (Table 1; Fig. 5). This is a typical effect of Fe-deficiency (Abadía et al., 2002), and for example 24-, 17- and 20-fold citrate increases have been reported to occur in xylem sap of Fe-deficient sugar beet (López-Millán et al., 2000), tomato (López-Millán et al., 2009) and peach tree plants (Larbi et al., 2010), respectively. This has been attributed to an increase in the activities of PEPC and TCA cycle enzymes induced by Fe deficiency in roots (De Nisi and Zocchi, 2000; López-Millán et al., 2000; Ollat et al., 2003). On the other hand, TCA cycle carboxylates (mainly citrate) can also function as a xylem sap Fe carrier (Rellán-Álvarez et al., 2010), and mutant plants not able to transport sufficient citrate to the xylem sap show Fe-deficiency like symptoms (Durrett et al., 2007; Yokosho et al., 2009). Whether these Fe-deficiency symptoms are caused by a decreased C transport to the shoots or the inability of these mutants to effectively chelate Fe with citrate is still an open question (Abadía et al., 2011). Unlike TCA cycle carboxylates, aminoacids and other N related compounds and carbohydrates in the xylem sap decreased in response to Fe deficiency (Fig. 5). There is no data, to the best of our knowledge, reporting aminoacid values in the xylem sap of Fe-deficient plants. However, the total concentration of aminoacids increased with Fe deficiency in the apoplastic fluid of sugar beet plants (López-Millán et al., 2000). Among the N related compounds, the largest decreases in xylem sap correspond to putrescine and spermidine, and this could be associated with the aminoacid decreases since the concentration of these amines is correlated with those of aminoacids (Mattoo et al., 2010). Xylem sap carbohydrate decreases in response to Fe-

deficiency are not in accordance to previous results found in sugar beet (López-Millán et al., 2000). It should be taken into account that carbohydrates are not expected to occur in the xylem and they may be the result of contamination and/or transfer with the phloem.

Most of the changes found in tomato and lupine xylem sap metabolite profile did not occur in peach. This could be explained by the fact that peach trees used as controls at the beginning of the growth-season (Fe-sufficient) became slightly chlorotic (leaf SPAD values close to those of Fe-deficient peach trees; see Material and Methods section) at the sampling time. However, a significant metabolite related with Fe transport, nicotianamine, increased (2-fold) in peach xylem sap with Fe deficiency. This could be due to the possible distinct role of NA in peach and other fruit tree species grown in the field, where the xylem sap pH is in the range 6.5-7.5 (Larbi et al., 2003), in comparison with the xylem sap pH of other species, which is usually around 5.5. *In vitro* chelation experiments (Rellán-Álvarez et al., 2008) indicate that NA would be able to chelate Fe at pH 7.5, whereas at pH 5.5 Fe-citrate would still be the main xylem sap Fe form (Rellán-Álvarez et al., 2010).

Iron-resupply to Fe-deficient tomato plants induced progressive changes with time (0-24 h) in the xylem sap metabolite profile (Fig. 4). After 24 h of Fe-resupply, the xylem sap metabolite profiles were already more closely related with those of the Fe-sufficient plants than with those of the Fe-deficient plants (Fig. 4). However, all resupplied plants still had similar leaf chlorosis levels than those of Fe-deficient plants (Fig. 1), whereas xylem sap Fe concentrations reached a clear peak between 12 and 18 h after resupply. In fact, a lag-phase between the increases of leaf Fe concentrations and chlorophyll occurring after Fe-resupply has been previously described (Nishio and Terry, 1983; Thoiron et al., 1997; López-Millán et al., 2001; Larbi et al., 2004). Another significant change induced by Fe-resupply was a dramatic increase in the TCA cycle metabolites in the xylem sap between 6 and 12 h after Fe-resupply, with concentrations reaching higher values than those of Fe-deficient plants. After 24 h of Fe-resupply, the levels of these metabolites were similar to those of Fe-sufficient plants, suggesting that the anaplerotic root C supply occurring in Fe-deficient plants ceased within this time. This is in agreement with

a 65% decrease of the root PEPC activity reported in sugar beet Fe-deficient plants after 24h of Fe-resupply (Abadía et al., 20011, *In press*). The metabolite levels of carbohydrates and the aminoacids and N related compounds, also altered by Fe-deficiency, changed progressively towards Fe-sufficient values.

In leaves, the most relevant change induced by Fe-deficiency was an increase in the TCA cycle metabolites, in agreement with previous data (López-Millán et al., 2001, 2001; Abadía et al., 2002). This is in line with the high levels of carboxylates coming from the roots *via* xylem sap. The high concentration of organic acids in leaves cannot be the result of increased TCA cycle and PEPC enzyme activities did not change with Fe deficiency in sugar beet, pear trees and tomato (López-Millán et al., 2001, 2001; López-Millán et al., 2009).

Aminoacid leaf levels also increased with Fe-deficiency. Chlorosis induced by several factors (including Fe deficiency) has been reported to increase leaf aminoacid concentrations and decrease the total protein content in several species (DeKock and Morrison, 1958). Iron deficiency induces decreases in root nitrite reductase (5-fold, Rodríguez-Celma et al., 2011, *Submitted*), xylem nitrate transport (2.6-fold, López-Millán et al., 2000) and aminoacid xylem transport (Fig. 5, Table 1), so the increases in leaf aminoacid levels should be the result of processes occurring within the leaves. In roots, increased levels of aminoacids were found in Fe-deficient sugar beet plants (Rellán-Álvarez et al., 2010), and an increase in protein turnover has been recently described in *Cucumis sativus* Fe-deficient roots (Donnini et al., 2010). This suggest that the increase of free aminoacids found in leaves maybe be the result of proteolysis processes such as those occurring in roots. Proteolysis could occur in old leaves (still green and therefore with normal photosynthetic rates) rather than in young leaves and the resulting free aminoacids would be remobilized *via* phloem to the young leaves. The same mechanism occurs senescent plants, in fact is estimated that as much as 43% of the amino acids in young leaves (youngest leaf 7) would be supplied by N partitioning *via* upflow of amino acids through the phloem (Jeschke and Pate, 1991). The leaf-levels of N carrier molecules such as glutamine, glutamic and asparagine were largely increased in response to Fe deficiency (Table 2), whereas

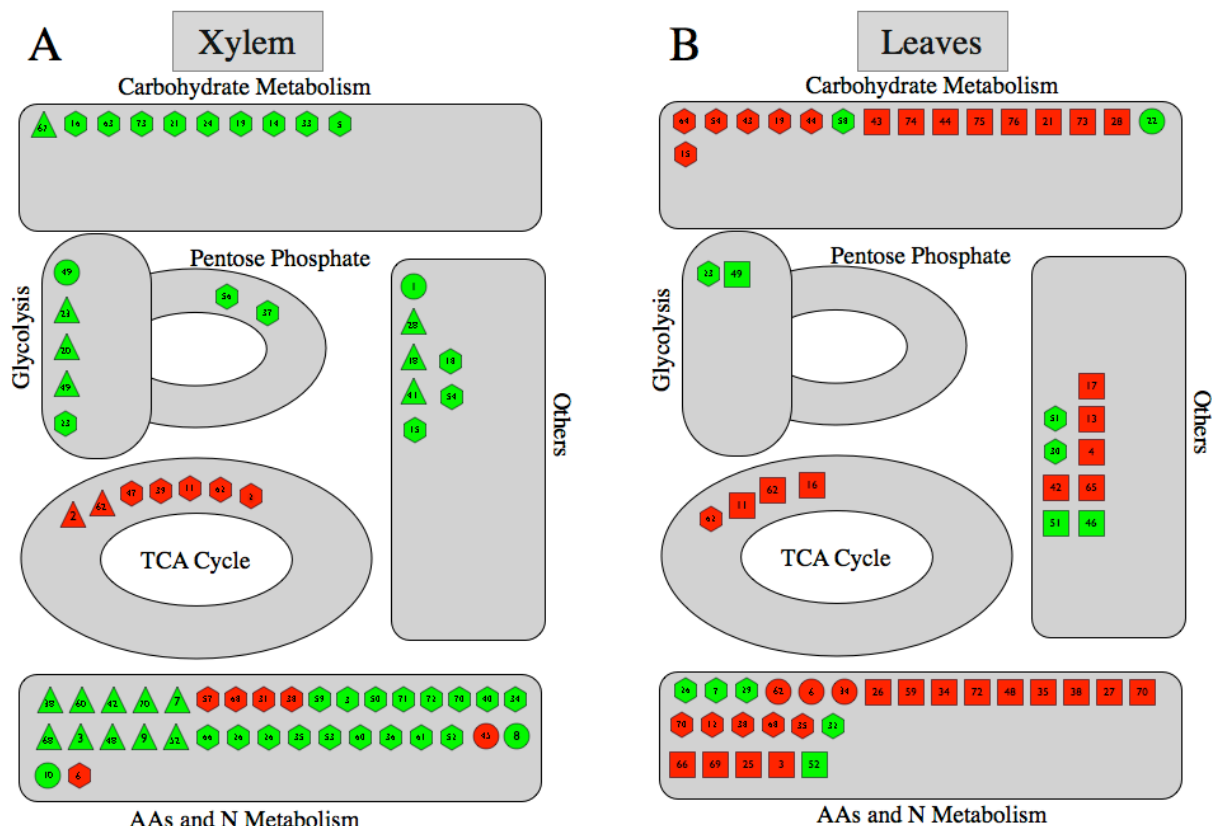


Figure 5. Changes in metabolites of xylem sap (A) and leaves (B) as affected by Fe chlorosis. Pathways related to metabolites and proteins were integrated according to the KEGG database. Statistical t-student tests were performed and only metabolite data to show statistically relevant changes (increases or decreases) between samples. Red and green indicate significant ($p > 0.01$) increases or decreases respectively. Triangles, circles, squares and octogone symbols correspond to lupine, peach, sugar beet and tomato samples, respectively.

other N compound such as the polyamines spermidine and putrescine were found to decrease in xylem sap and leaves. One of the enzymes (S-adenosyl-L-methionine synthetase) involved in the biosynthesis of these polyamines was also found to decrease in *Medicago truncatula* Fe-deficient roots (Rodríguez-Celma et al., 2011, Submitted).

As indicated above, Fe chlorotic leaves are in need of C skeletons, because of the markedly reduced photosynthetic rates. Iron-deficient plants may fix C anaplerotically in the roots and translocate it to the leaves *via* xylem sap to maintain basic metabolic processes such as respiration (López-Millán et al., 2000; López-Millán et al., 2000). There are other anaplerotic reactions that can occur using aminoacids as a C source (Owen et al., 2002). High correlations between selected pairs of aminoacids and TCA cycle metabolites involved in anaplerotic reactions were found in sugar beet leaves (Fig.

3), and these correlations were positive in Fe-sufficient plants and negative in Fe-deficient ones (the increase of TCA carboxylates is correlated with a decrease of aminoacids). This may suggest that the increased aminoacid levels could generate carboxylates, and consequently C and reducing power through the reactions described in Figure 3. Chlorotic plants would face a “cellular effort” (Donnini et al., 2010) similar to what occurs in mammal cells that degrade their muscle proteins to fulfill their energetic requirements once the glycogen reserves are depleted if no carbohydrates are ingested. As indicated above, the source for free aminoacids in young leaves seems to be the old leaves. An open question that needs to be addressed is if the anaplerotic reactions occur in the young chlorotic leaves or if they occur in old leaves and both free aminoacids and carboxylates are translocated to *via* phloem to the young leaves.

We are currently designing new experiments to test

Conclusions

The main changes in the metabolite profile of xylem sap in response to Fe deficiency were an increase in TCA cycle metabolites and a decrease in aminoacids and carbohydrates. The xylem sap metabolite profile of Fe-deficient tomato plants becomes similar to that of Fe-sufficient controls one day after Fe resupply. In Fe-deficient leaves, the main changes in the metabolite profile were the increases in TCA cycle metabolites, aminoacids and carbohydrates. High correlations between aminoacids and TCA cycle metabolites levels suggest that some anaplerotic reactions using aminoacids as a C source may occur in *Beta vulgaris* leaves in response to Fe deficiency.

Acknowledgements

This study was supported by the Spanish Ministry of Science and Innovation (MICINN; projects AGL2007-61948 and AGL2009-09018, co-financed with FEDER), the trilateral Project Hot Iron (ERA-NET Plant Genome Research KKBE; MICINN EUI2008-03618), the Spanish National Research Council (PA1000990, International Promotion Programme 2007) and the Aragón Government (group A03). R.R.-A. and H.E.-J. were supported by MICINN-FPI grants.

References

Abadía J (1992) Leaf responses to iron nutrition - A review. *J. Plant Nutr.* **15**: 1699-1713

Abadía J, López-Millán A-F, Rombolà AD, Abadía A (2002) Organic acids and Fe deficiency: a review. *Plant Soil* **241**: 75-86

Abadía J, Vázquez S, Rellán-Álvarez R, El Jendoubi H, Abadía A, Álvarez-Fernández A, López-Millán A-F (2011, *In press*) Towards a knowledge-based correction of iron chlorosis. *Plant Physiol. Biochem.*

Andaluz S, López-Millán A, Peleato M, Abadía J, Abadía A (2002) Increases in phosphoenolpyruvate carboxylase activity in iron-deficient sugar beet roots: Analysis of spatial localization and post-translational modification. *Plant Soil* **241**: 43-48

Andaluz S, López-Millán A, Rivas J, Aro E, Abadía J, Abadía A (2006) Proteomic profiles of thylakoid membranes and changes in response to iron deficiency. *Photosynt.Res.* **89**: 141-155

Brumbarova T, Matros A, Mock HP, Bauer P (2008) A proteomic study showing differential regulation of stress, redox regulation and peroxidase proteins by iron supply and the transcription factor FER. *Plant J.* **54**: 321-334

Buhtz A, Pieritz J, Springer F, Kehr J (2010) Phloem small RNAs, nutrient stress responses, and systemic mobility. *BMC Plant Biol.* **10**: 64

Chich J-F, David O, Villers F, Schaeffer B, Lutowski D, Huet S (2007) Statistics for proteomics: experimental design and 2-DE differential analysis. *J. Chromatogr. B* **849**: 261-272

Curie C, Cassin G, Couch D, Divol F, Higuchi K, Le Jean M, Misson J, Schikora A, Czernic P, Mari S (2009) Metal movement within the plant: contribution of nicotianamine and yellow stripe 1-like transporters. *Ann. Bot.* **103**: 1-11

De Nisi P, Zocchi G (2000) Phosphoenolpyruvate carboxylase in cucumber (*Cucumis sativus* L.) roots under iron deficiency: activity and kinetic characterization. *J. Exp. Bot.* **51**: 1903-1909

DeKock P, Morrison R (1958) The metabolism of chlorotic leaves. 1. Amino acids. *Biochem. J.* **70**: 266-272

Donnini S, Bhakti P, Negri AS, Vignani G, Espen L, Zocchi G (2010) Proteomic characterization of iron deficiency response in *Cucumis sativus* L. roots. *BMC Plant Biol.* **10**: 268

Durrett TP, Gassmann W, Rogers EE (2007) The FRD3-Mediated efflux of citrate into the root vasculature is necessary for efficient iron translocation. *Plant Physiol.* **144**: 197-205

Eide D, Brodenius M, Fett J, Guerinot M (1996) A novel iron-regulated metal transporter from plants identified by functional expression in yeast. *Proc. Natl. Acad. Sci. USA* **93**: 5624-5628

Enomoto Y, Hodoshima H, Shimada H, Shoji K, Yoshihara T, Goto F (2007) Long-distance signals positively regulate the

- expression of iron uptake genes in tobacco roots. *Planta* **227**: 81-89
- Fiehn O** (2003) Metabolic networks of *Cucurbita maxima* phloem. *Phytochemistry* **62**: 875-886
- Fiehn O, Wohlgemuth G, Scholz M, Kind T, Lee DY, Lu Y, Moon S, Nikolau B** (2008) Quality control for plant metabolomics: reporting MSI-compliant studies. *Plant J.* **53**: 691-704
- Hansen N, Hopkins B, Ellsworth J, Jolley V** (2006) Iron nutrition in field crops. In LL Barton, J Abadía, eds, *Iron Nutrition in Plants and Rhizospheric Microorganisms*. Springer, Dordrecht, Netherlands, pp 23-59
- Herbik A, Giritch A, Horstmann C, Becker R, Balzer H, Baumlein H, Stephan U** (1996) Iron and copper nutrition-dependent changes in protein expression in a tomato wild type and the nicotianamine-free mutant chloronerva. *Plant Physiol.* **111**: 533-540
- Jeschke WD, Pate JS** (1991) Modelling of the partitioning, assimilation and storage of nitrate within root and shoot organs of castor bean (*Ricinus communis* L.). *J. Exp. Bot.* **42**: 1091-1103
- Jiménez S, Gogorcena Y, Hevin C, Rombolà AD, Ollat N** (2007) Nitrogen nutrition influences some biochemical responses to iron deficiency in tolerant and sensitive genotypes of *Vitis*. *Plant Soil* **290**: 343-355
- Laganowsky A, Gómez SM, Whitelegge JP, Nishio JN** (2009) Hydroponics on a chip: Analysis of the Fe deficient *Arabidopsis* thylakoid membrane proteome. *J. Proteom.* **72**: 397-415
- Lan P, Li W, Wen T-N, Shiau J-Y, Wu Y-C, Lin W-D, Schmidt W** (In Press) iTRAQ protein profile analysis of *Arabidopsis* roots reveals new aspects critical for Fe homeostasis. *Plant Physiol.* DOI: 10.1104/pp.110.169508
- Larbi A, Abadía A, Abadía J, Morales F** (2006) Down co-regulation of light absorption, photochemistry, and carboxylation in Fe-deficient plants growing in different environments. *Photosynt. Res.* **89**: 113-126
- Larbi A, Abadía A, Morales F, Abadía J** (2004) Fe resupply to Fe-deficient sugar beet plants leads to rapid changes in the violaxanthin cycle and other photosynthetic characteristics without significant de novo chlorophyll synthesis. *Photosynt. Res.* **79**: 59-69
- Larbi A, Morales F, Abadía A, Abadía J** (2010) Changes in iron and organic acid concentrations in xylem sap and apoplastic fluid of iron-deficient *Beta vulgaris* plants in response to iron resupply. *J. Plant Physiol.* **167**: 255-260
- Larbi A, Morales F, Abadía J, Abadía A** (2003) Effects of branch solid Fe sulphate implants on xylem sap composition in field-grown peach and pear: changes in Fe, organic anions and pH. *J. Plant Physiol.* **160**: 1473-1481
- Li J, Wu X, Hao S, Wang X, Ling H** (2008) Proteomic response to iron deficiency in tomato root. *Proteomics* **8**: 2299-2311
- Li W, Schmidt W** (2010) A lysine-63-linked ubiquitin chain-forming conjugase, UBC13, promotes the developmental responses to iron deficiency in *Arabidopsis* roots. *Plant J.* **62**: 330-343
- López-Millán A, Morales F, Abadía A, Abadía J** (2001) Changes induced by Fe deficiency and Fe resupply in the organic acid metabolism of sugar beet (*Beta vulgaris*) leaves. *Physiol. Plant.* **112**: 31-38
- López-Millán A, Morales F, Abadía A, Abadía J** (2001) Iron deficiency-associated changes in the composition of the leaf apoplastic fluid from field-grown pear (*Pyrus communis* L.) trees. *J. Exp. Bot.* **52**: 1489-1498
- López-Millán A, Morales F, Andaluz S, Gogorcena Y, Abadía A, De Las Rivas J, Abadía J** (2000) Responses of sugar beet roots to iron deficiency. Changes in carbon assimilation and oxygen use. *Plant Physiol.* **124**: 885-897
- López-Millán A, Morales F, Gogorcena Y, Abadía A, Abadía J** (2001) Iron resupply-mediated deactivation of Fe-deficiency stress responses in roots of sugar beet. *Aust. J. Plant Physiol.* **28**: 171-180
- López-Millán A, Morales F, Gogorcena Y, Abadía A, Abadía J** (2009) Metabolic responses in iron deficient tomato plants. *J. Plant Physiol.* **166**: 375-384

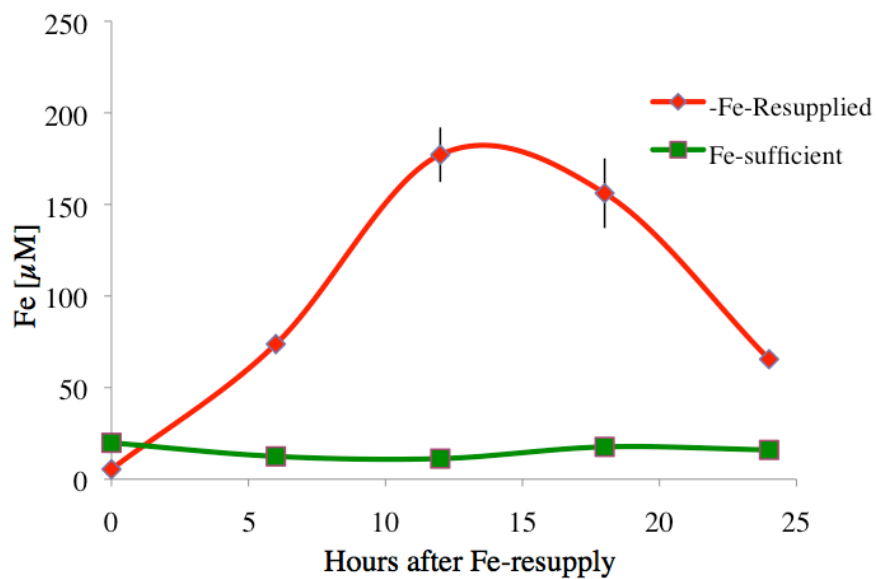
- López-Millán AF, Morales F, Abadía A, Abadía J** (2000) Effects of iron deficiency on the composition of the leaf apoplastic fluid and xylem sap in sugar beet. Implications for iron and carbon transport. *Plant Physiol.* **124**: 873-884
- Marschner H** (1995) Mineral Nutrition of Higher Plants. Academic Press, London
- Mattoo AK, Minocha SC, Minocha R, Handa AK** (2010) Polyamines and cellular metabolism in plants: transgenic approaches reveal different responses to diamine putrescine versus higher polyamines spermidine and spermine. *Amino Acids* **38**: 405-413
- Nishio J, Terry N** (1983) Iron nutrition-mediated chloroplast development. *Plant Physiol.* **71**: 688-691
- Ollat N, Laborde W, Neveux M, Diakou-Verdin P, Renaud C, Moing A** (2003) Organic acid metabolism in roots of various grapevine (*Vitis*) rootstocks submitted to iron deficiency and bicarbonate nutrition. *J. Plant Nutr.* **26**: 2165-2176
- Owen OE, Kalhan SC, Hanson RW** (2002) The key role of anaplerosis and cataplerosis for citric acid cycle function. *J. Biol. Chem.* **277**: 30409-30412
- Rellán-Álvarez R, Abadía J, Álvarez-Fernández A** (2008) Formation of metal-nicotianamine complexes as affected by pH, ligand exchange with citrate and metal exchange. A study by electrospray ionization time-of-flight mass spectrometry. *Rapid Commun. Mass Spectrom.* **22**: 1553-1562
- Rellán-Álvarez R, Andaluz S, Rodríguez-Celma J, Wohlgenuth G, Zocchi G, Álvarez-Fernández A, Fiehn O, López-Millán A, Abadía J** (2010) Changes in the proteomic and metabolic profiles of *Beta vulgaris* root tips in response to iron deficiency and resupply. *BMC Plant Biol.* **10**: 120
- Rellán-Álvarez R, Giner-Martínez-Sierra J, Orduna J, Orera I, Rodríguez-Castrillón JA, García-Alonso JI, Abadía J, Álvarez-Fernández A** (2010) Identification of a tri-iron(III), tri-citrate complex in the xylem sap of iron-deficient tomato resupplied with iron: new insights into plant iron long-distance transport. *Plant Cell Physiol.* **51**: 91-102
- Robinson N, Procter C, Connolly E, Guerinot M** (1999) A ferric-chelate reductase for iron uptake from soils. *Nature* **397**: 694-697
- Rodríguez-Celma J, Lattanzio G, Grusak MA, Abadía A, Abadía J, López-Millán A-F** (2011) Root responses of *Medicago truncatula* plants grown in two different iron deficiency conditions: analysis of the root protein profile and the riboflavin biosynthesis pathway. *New Phytol.* Submitted
- Rombolà AD, Tagliavini M** (2006) Iron nutrition of fruit tree crops. In LL Barton, J Abadía, eds, Iron nutrition in plants and rhizospheric microorganisms. Springer, Dordrecht, Netherlands, pp 61-83
- Santi S, Schmidt W** (2009) Dissecting iron deficiency-induced proton extrusion in *Arabidopsis* roots. *New Phytol.* **183**: 1072-1084
- Susín S, Abadía A, GonzálezReyes J, Lucena J, Abadía J** (1996) The pH requirement for in vivo activity of the iron deficiency-induced "Turbo" ferric chelate reductase - A comparison of the iron-deficiency-induced iron reductase activities of intact plants and isolated plasma membrane fractions in sugar beet. *Plant Physiol.* **110**: 111-123
- Thimm O, Essingmann B, Kloska S, Altmann T, Buckhout T** (2001) Response of *Arabidopsis* to iron deficiency stress as revealed by microarray analysis. *Plant Physiol.* **127**: 1030-1043
- Thoirion S, Pascal N, Briat J** (1997) Impact of iron deficiency and iron re-supply during the early stages of vegetative development in maize (*Zea mays* L.). *Plant Cell Environ.* **20**: 1051-1060
- Timperio A, D'Amici G, Barta C, Loreto F, Zolla L** (2007) Proteomic, pigment composition, and organization of thylakoid membranes in iron-deficient spinach leaves. *J Exp Bot* **58**: 3695-3710
- Yang TJW, Lin WD, Schmidt W** (2010) Transcriptional profiling of the *Arabidopsis* iron deficiency response reveals conserved transition metal homeostasis networks. *Plant Physiol.* **152**: 2130-2141

Yokosho K, Yamaji N, Ueno D, Mitani N, Ma J-F (2009) OSFRDL1 is a citrate transporter required for efficient

translocation of iron in rice. *Plant Physiol.* **149:** 297-305

SUPPLEMENTARY MATERIAL

Supplementary Figure 1. Iron concentrations (μM) in Fe-sufficient and Fe-deficient plants resupplied with Fe ($45 \mu\text{M}$ Fe-EDTA) and sampled at different times alter Fe resupply. Fe-resupply was done at 11:00 AM, 3 hours alter light onset.



Supplementary Table 1: Metabolites X-weights after PLS analysis.

Xylem											
Lupine				Peach				Tomato			
Positive		Negative		Positive		Negative		Positive		Negative	
metabolite	value	metabolite	value	metabolite	value	metabolite	value	metabolite	value	metabolite	value
succinic a.	0.1568	Tryptophan	-0.1720	2-deoxyerythritol	0.1442	pipecolic a.	-0.2592	oxoglutaric a.	0.1574	arabinose	-0.1545
ribose	0.1491	tyrosine	-0.1626	glucose	0.1323	hydroxyglutaric a.	-0.2503	malate	0.1538	putrescine	-0.1545
aconitic a.	0.1469	beta alanine	-0.1607	ribose	0.1316	ketoisocaproic a.	-0.2248	2-hydroxyglutaric a.	0.1498	spermidine	-0.1523
galacturonic a.	0.1393	Oxoproline	-0.1556	ribonic a.	0.1186	galactinol	-0.1970	citric a.	0.1493	galacturonic a.	-0.1508
2-hydroxyglutaric a.	0.1341	Inositol	-0.1530	arabitol	0.1087	citramalic a.	-0.1965	succinic a.	0.1468	GABA	-0.1503
fumaric a.	0.1234	lysine	-0.1528	sucrose	0.1031	Proline	-0.1954	tryptophan	0.1437	glycine	-0.1490
maleic a.	0.1224	Sucrose	-0.1526	chlorogenic a.	0.1030	fumaric a.	-0.1909	aconitic a.	0.1421	xylose	-0.1472
arabinose	0.1156	Glucose	-0.1477	glycerol	0.0926	galactonic a.	-0.1843	suberyl glycine	0.1353	inulobiose	-0.1457
oxoglutaric a.	0.1135	Spermidine	-0.1474	gluconic a.	0.0887	Phenylalanine	-0.1787	maleic a.	0.1200	shikimic a.	-0.1443
malic a.	0.1098	galactose	-0.1466	N-ac-D-hexosamine	0.0819	threonine	-0.1775	beta alanine	0.1049	lysine	-0.1444
Leaves											
Sugar beet											
Positive		Negative		Positive		Negative		Positive		Negative	
metabolite	value	metabolite	value	metabolite	value	metabolite	value	metabolite	value	metabolite	value
succinic a.	0.1757	phytol	-0.1676	suberyl glycine	0.2941	glyceric a.	-0.2503	hydroxylamine	0.1859	fuco + rhamno	-0.1809
lactobionic a.	0.1726	oxalic a.	-0.1469	isoleucine	0.2839	erythronic a.	-0.2136	homoserine	0.1768	tyrosine	-0.1781
xylytol	0.1724	PGA	-0.1385	asparagine	0.2834	erythrose	-0.1922	saccharic a.	0.1670	succinic a.	-0.1767
oxoproline	0.1667	Fructose-6-P	-0.1255	serine	0.1969	2-isopropylmalic a.		citulline	0.1578	2-isopropylmalic a.	-0.1640
serine	0.1654	β -sitosterol	-0.0998	phenylalanine	0.1884	pelargonic a.	-0.1683	aspartic a.	0.1534	N-Ac-D-mannosamine	-0.1615
alpha tocopherol	0.1651	Glucose-6-P	-0.0984	ornithine	0.1778	gluconic a.	-0.1634	phytol	0.1469	myo-inositol	-0.1548
citric a.	0.1642	mannitol	-0.0903	threonine	0.1677	phytol	-0.1528	cyclohexylamine	0.1460	leucine	-0.1521
threonine	0.1621	putrescine	-0.0614	citulline	0.1573	lauric a.	-0.1492	PGA	0.1344	N-Ac-D-hexosamine	-0.1507
N-ac-D-hexosamine	0.1587	aspartate	-0.0575	quinic a.	0.1434	PGA	-0.1402	glucose-6-P	0.1269	ribitol	-0.1497
N-ac-D-mannosamine	0.1563	ribonic a.	-0.0432	glucose	0.1308	glycerol	-0.1321	glutamine	0.1210	glutamic a.	-0.1490

Supplementary Table 2: Identified metabolite response ratios of Fe-deficient (-Fe) and Fe-deficient Fe resupplied plants at 6, 12, 18 and 24 hours after Fe resupply vs. Fe-sufficient controls (+Fe) and the correspondent controls at each of the hours after Fe resupply respectively. When the response ratio (level in the -Fe treatment divided by the level in the +Fe treatment) was lower than 1 the inverse was taken and the sign changed. Values in bold indicate significant differences ($p < 0.005$) with the corresponding controls. Different letters indicate significant changes ($p < 0.005$, ANOVA)

Metabolites	-Fe	6 h	12 h	18 h	24 h	KEGG
2-hydroxyglutaric acid	4.6 a	5.9 a	5.6 a	3.7 a	2.3 a	C02630
2-ketoisocaproic acid	-1.4 a	-1.3 a	1.1 a	-1.0 a	1.1 a	C00233
alanine	-2.3 a	-2.2 a	-2.3 a	-1.7 a	-1.6 a	C00041
adipic acid	1.1 a	-3.2 a	-1.0 a	5.1 a	2.3 a	C06104
azelaic acid	-1.5 a	-1.4 a	-1.4 a	4.0 a	2.2 a	C08261
asparagine	2.5 a	3.0 a	1.2 a	3.1 a	1.9 a	C00152
aspartic acid	1.7 b	5.9 a	1.7 b	-1.2 b	1.1 b	C00049
beta alanine	1.5 b	1.8 ab	2.3 a	1.4 b	1.3 b	C00099
glutamic acid	-1.2 b	3.5 a	1.6 b	1.5 b	1.3 b	C00025
glutamine	-1.4 b	-1.2 b	-1.6 b	2.1 a	1.5 ab	C00064
glycine	-3.8 c	-2.7 bc	-2.1 bc	-2.0 ab	-1.5 a	C00037
hydroxylamine	-1.1 a	-1.6 a	-1.9 a	-1.1 a	-1.2 a	C00192
isoleucine	-3.2 b	-4.5 b	-1.4 ab	1.2 a	1.2 a	C00407
leucine	-3.9 b	-5.5 b	-1.2 ab	1.1 ab	1.5 a	C00123
lysine	-5.1 b	-4.9 b	-2.0 b	1.4 a	1.2 a	C00047
maleic acid	4.0 b	19.2 a	3.9 b	2.4 b	2.1 b	C01384
methionine	-3.1 a	-2.2 a	-1.4 a	-1.3 a	-1.3 a	C00073
ornithine	-1.8 b	1.7 a	-1.1 ab	1.4 a	1.1 ab	C00077
quinic acid	-4.2 c	-1.7 ab	-2.7 bc	-1.1 a	-1.4 a	C00296
phenylalanine	-2.8 b	-2.2 b	-1.4 ab	-1.1 ab	1.2 a	C00079
putrescine	-11.8 b	-5.2 b	-3.3 b	-2.1 ab	-1.3 a	C00134
shikimic acid	-4.3 c	-2.2 bc	-2.6 c	-1.3 a	-1.5 ab	C00493
serine	-2.0 b	1.1 a	-1.6 ab	-2.4 b	-1.2 ab	C00065
spermidine	-6.7 c	-2.0 ab	-3.0 bc	-2.0 ab	-1.6 a	C00315
threonine	-3.6 b	-3.8 b	-2.3 ab	-1.1 a	-1.1 a	C00188
tryptophan	6.4 b	5.1 b	2.7 b	14.1 a	3.4 b	C00078
tyramine	-1.5 b	-1.3 b	-4.6 b	5.2 a	1.7 b	C00483
tyrosine	-3.1 b	-4.6 b	1.0 ab	1.5 ab	2.4 a	C00082
urea	-2.9 a	-3.2 a	-1.3 a	-1.2 a	1.4 a	C00086
uric acid	-5.1 a	-1.3 a	-1.2 a	-1.5 a	1.6 a	C00366
valine	-3.0 b	-5.1 b	-1.4 ab	1.1 a	1.4 a	C00183
arabinose	-7.5 c	-5.3 bc	-5.1 bc	-3.4 ab	-2.5 a	C00216
fructose	-5.2 b	-5.2 b	-6.9 b	-1.9 a	-3.0 ab	C00095
galactinol major	-4.7 b	-1.5 ab	-1.9 ab	-1.1 a	-1.0 a	C01235
galacturonic acid	-4.1 c	-2.4 bc	-2.5 bc	-1.5 a	-1.6 ab	C00333
glucuronic acid	-4.2 b	-2.6 b	-2.5 b	-1.6 b	1.8 a	C00191
inulobiose	-5.2 c	-3.7 bc	-3.5 bc	-2.1 a	-2.7 ab	C01711
N-acetyl-D-hexosamine	1.9 a	-1.5 c	-1.3 bc	1.8 ab	1.7 bc	C03136
N-acetyl-D-mannosamine	-2.6 c	1.0 a	-1.4 b	-2.1 bc	-1.5 b	C00645
saccharic acid	-7.1 c	-1.4 a	-2.7 bc	-2.0 ab	-1.6 ab	C00818
suberyl glycine	7.1 a	1.4 b	2.1 b	2.4 b	1.2 b	n/a
sucrose	-2.7 c	1.0 ab	-1.2 b	1.4 a	-1.2 b	C00089
xylose	-3.8 c	-1.5 ab	-1.9 bc	1.0 a	-1.5 ab	C00181
glucose-6-phosphate	-2.3 a	-1.2 a	-1.6 a	-1.1 a	-1.3 a	C00092

glucose	-5.2	b	-6.0	b	-6.0	b	-1.5	a	-2.8	b	C00031
lactic acid	-1.2	a	-2.2	a	1.3	a	-1.2	a	-1.2	a	C00186
1-hexadecanol	-1.2	a	1.4	a	-1.2	a	-1.3	a	-1.1	a	C00823
arachidic acid	1.2	a	-1.8	a	1.2	a	1.3	a	-1.0	a	C06425
behenic acid	-1.2	a	-1.0	a	1.1	a	1.2	a	-1.0	a	C08281
butyl stearate	-4.2	a	-1.5	a	-1.2	a	-1.1	a	1.8	a	n/a
capric acid	-1.2	bc	-1.8	c	1.4	a	1.2	ab	-1.3	bc	C01571
glycerol-alpha-phosphate	-1.9	a	-1.5	a	-1.3	a	1.1	a	-1.1	a	C03189
heptadecanoic acid	-1.2	a	-1.5	a	1.3	a	-1.0	a	1.2	a	n/a
lauric acid	1.3	ab	-1.2	b	1.6	a	-1.4	b	-1.2	b	C02679
myristic acid	1.2	a	1.0	a	1.6	a	-1.2	a	-1.1	a	C06424
octadecanol	-3.4	a	2.8	a	-3.7	a	-1.6	a	-2.6	a	D01924
oleic acid	-2.2	a	-1.4	a	1.1	a	1.3	a	1.1	a	C01712
palmitic acid	1.0	a	-1.0	a	1.5	a	1.0	a	1.3	a	C00249
pelargonic acid	-1.5	a	-1.2	a	-1.0	a	1.0	a	1.4	a	C01601
pentadecanoic acid	-1.4	a	-1.9	a	-1.0	a	-1.2	a	-1.4	a	C16537
phosphoethanolamine	-1.5	b	1.6	b	1.3	b	2.7	a	-1.2	b	C00346
stearic acid	1.0	a	-1.4	a	1.4	a	1.3	a	1.3	a	C01530
ribose	-4.3	c	-1.8	bc	-2.1	bc	1.4	a	1.1	ab	C00121
lyxitol	-2.3	a	-1.5	a	-1.9	a	1.3	a	2.2	a	C00532
2-hydroxyvaleric acid	-1.1		-1.0		1.5		-1.0		1.0		n/a
GABA	-4.4	c	-2.8	bc	-2.8	bc	-1.8	ab	-1.5	a	C00334
inositol-myo	-2.5	c	-1.1	bc	-1.2	bc	1.5	a	1.2	ab	C00137
aconitic acid	2.8	b	5.3	ab	6.5	a	4.5	ab	3.7	b	C00417
alpha ketoglutaric acid	91	b	123	ab	165	a	15	c	31.3	c	C00026
citric acid	5.7	c	29.4	a	14.4	b	18.4	b	6.7	c	C00158
fumaric acid	1.8	b	7.4	a	3.2	b	2.7	b	1.7	b	C00122
malic acid	6.2	a	11.7	a	6.2	a	6.8	a	4.3	a	C00149
succinic acid	4.7	a	5.7	a	3.6	a	4.5	a	2.2	a	C00042
dihydroabiatic acid	4.2	a	1.2	a	1.7	a	-2.2	a	2.0	a	C17920
phosphoric acid	1.1	b	3.7	a	-1.8	b	-2.2	b	-1.4	b	C00009
ribitol	-4.1	c	-2.2	bc	-2.2	bc	-1.1	ab	1.1	a	C00474
threonic acid	-1.6	b	1.2	ab	1.5	ab	2.1	a	1.9	a	C01620

CONCLUSIONS/CONCLUSIONES

Conclusions

1. Complexes of nicotianamine (NA) with Fe(II) and Fe(III) can be determined using electrospray time-of-flight mass spectrometry (ESI-TOFMS).
2. Changes in pH and the concentrations of citrate and metals can have significant effects in NA speciation in plant fluids.
3. Nicotianamine is a candidate for chelating Fe at the pH usually found in the phloem sap, whereas NA is not likely to be involved in xylem Fe transport, conversely to what occurs with other metals such as Cu and Ni.
4. A tri-Fe(III), tri-citrate complex (Fe_3Cit_3) has been found in the xylem sap of Fe-deficient *Solanum lycopersicum* Mill. plants resupplied with Fe, by using an integrated mass spectrometry approach.
5. High Fe-to-citrate ratios favour the formation of Fe-citrate polymeric forms and low ratios (such as those found in Fe deficiency) favour dimeric or monomeric species.
6. An HPLC-ESI-TOFMS method has been developed to determine organic acids in different plant tissues (xylem sap, leaves and fruit juice) with high selectivity, sensitivity and reproducibility.
7. Major increases in the raffinose family of oligosaccharide (RFOs) are elicited by Fe deficiency and resupply in root tips of *Beta vulgaris* plants.
8. Increases in proteins and metabolites related to carbohydrate, TCA cycle and flavin synthesis have been confirmed to occur in roots of *Beta vulgaris* plants grown under Fe deficiency.
9. The major changes in the metabolite profile of xylem sap from *Solanum lycopersicum* and *Lupinus albus* in response to Fe deficiency are an increase in TCA cycle metabolites and a decrease in aminoacids and carbohydrates.
10. The xylem sap metabolite profile of Fe-deficient *Solanum lycopersicum* plants becomes similar to that of Fe-sufficient controls one day after Fe resupply.
11. The main changes in the metabolite profile of leaves from *Solanum lycopersicum* and *Beta vulgaris* in response to Fe deficiency are increases in TCA cycle metabolites, aminoacids and carbohydrates.
12. High correlations between aminoacids and TCA cycle metabolites levels suggest that some anaplerotic reactions using aminoacids as a C source may occur in *Beta vulgaris* leaves in response to Fe deficiency.

Conclusiones

1. Los complejos de nicotianamina (NA) con Fe(II) y Fe(III) se pueden determinar mediante ionización por electrospray y detección por espectrometría de masas de tiempo de vuelo (ESI-TOFMS).
2. Cambios en el pH y las concentraciones de citrato y metales pueden tener efectos significativos en la especiación de NA en fluidos vegetales.
3. La NA podría quelar Fe al pH característico de la savia del floema, mientras que al pH característico de la savia de xilema quelaría preferentemente otros metales como el Cu y/o el Ni.
4. Un complejo de citrato con Fe formado por tres moléculas de citrato y tres átomos de Fe (Fe_3Cit_3) se ha encontrado en la savia del xilema de plantas de *Solanum lycopersicum* Mill. deficientes en Fe después de haber realizado un reaporte de Fe utilizando espectrometría de masas elemental y molecular.
5. Las relaciones de Fe:citrato altas favorecen la formación de especies poliméricas de citrato de Fe mientras que relaciones bajas (como las que se encuentran en el xilema de plantas deficientes en Fe) favorecen la formación de especies diméricas o monoméricas.
6. Se ha desarrollado un método de HPLC-ESI-TOFMS que permite determinar ácidos orgánicos en diferentes tejidos vegetales (savia del xilema, hojas y jugo de fruta) con alta selectividad, sensibilidad y reproducibilidad.
7. Las concentraciones de oligosacáridos de la familia de la rafinosa (RFO) aumentan en puntas de raíz de plantas de *Beta vulgaris* deficientes en Fe y también en puntas de raíz deficientes sometidas a un aporte posterior de Fe.
8. Proteínas y metabolitos relacionados con los hidratos de carbono, el ciclo de Krebs y la síntesis de flavinas aumentan en puntas de raíz de plantas de *Beta vulgaris* deficientes en Fe.
9. Los metabolitos del ciclo de Krebs aumentan mientras que, en general, aminoácidos y carbohidratos disminuyen en la savia de xilema de plantas de *Solanum lycopersicum* y *Lupinus albus* deficientes en Fe.
10. El perfil metabólico de la savia del xilema plantas de *Solanum lycopersicum* deficientes en Fe revierte a valores de plantas control en tan solo 24h después de un reaporte de Fe.
11. Metabolitos implicados en el ciclo de Krebs, aminoácidos y carbohidratos aumentan en hojas de plantas de *Solanum lycopersicum* y *Beta vulgaris* deficientes en Fe.
12. Correlaciones elevadas entre aminoácidos y ácidos orgánicos del ciclo de Krebs sugieren que en las hojas de plantas de *Beta vulgaris* deficientes en Fe se producen reacciones anapleróticas que utilizan aminoácidos como fuente de C.

ANEX I
OTHER ARTICLES OF THE MASTER'S THESIS

Other articles of the Master's Thesis

- 1. Rellán-Álvarez R**, Ortega-Villasante C, Álvarez-Fernández A, del Campo FF, Hernández LE (2006) Stress responses of *Zea mays* to cadmium and mercury. **Plant and Soil** 279, 41-50.
- 2. Rellán-Álvarez R**, Hernández LE, Abadía J, Álvarez-Fernández A (2006) Direct and simultaneous determination of reduced and oxidized glutathione and homoglutathione by liquid chromatography-electrospray/mass spectrometry in plant tissue extracts. **Analytical Biochemistry** 356, 254-264.



Direct and simultaneous determination of reduced and oxidized glutathione and homogluthathione by liquid chromatography–electrospray/mass spectrometry in plant tissue extracts

Rubén Rellán-Álvarez^{a,b}, Luis E. Hernández^a, Javier Abadía^b, Ana Álvarez-Fernández^{b,*}

^a Plant Physiology Laboratory, Department of Biology, Universidad Autónoma de Madrid, Campus de Cantoblanco, E-28049, Madrid, Spain

^b Plant Nutrition Department, Aula Dei Experimental Station, CSIC, Apdo. 202, E-50080, Zaragoza, Spain

Received 12 April 2006
Available online 12 June 2006

Abstract

A simple, highly selective, sensitive, and reproducible liquid chromatography–electrospray ionization/mass spectrometry (time of flight) method has been developed for the direct and simultaneous determination of glutathione and related compounds such as homogluthathione in different plant tissues. These compounds are low-molecular mass antioxidants involved in cellular redox homeostasis in plants, and efforts are being made to develop methods to determine the concentrations of oxidized and reduced forms of these compounds and their ratio. Many of the methodologies developed so far, however, are time-consuming and complex; therefore, analytes can decompose and their redox status can change during the analysis process. The method we have developed allows the simultaneous determination of reduced forms (glutathione [GSH] and homogluthathione [hGSH]) and oxidized forms (glutathione disulfide [GSSG]) of these compounds and is also suitable for the determination of ascorbic acid (ASA) and *S*-nitrosogluthathione (GSNO). Quantification was done using isotopically labeled GSH and ASA as internal standards. All compounds were base peak resolved in less than 6 min, and limits of detection were 60 pmol for GSH, 30 pmol for hGSH, 20 pmol for GSSG, 100 pmol for ASA, and 30 pmol for GSNO. The intraday repeatability values were approximately 0.4 and 7% for retention time and peak area, respectively, whereas the interday repeatability values were approximately 0.6 and 9% for retention time and peak area, respectively. Analyte recoveries found were between 92 and 105%. The method was used to determine the concentrations of GSH, GSSG, hGSH, and ASA in extracts from several plant tissues.

© 2006 Elsevier Inc. All rights reserved.

Keywords: Ascorbate; Glutathione; Homogluthathione; Liquid chromatography; Mass spectrometry; Oxidized glutathione; *S*-Nitrosogluthathione

Reduced glutathione (GSH,¹ L-γ-glutamyl-L-cysteine-glycine) and ascorbic acid (ASA) play an important role in maintaining the intracellular redox status in plant cells. Both metabolites act in the so-called ascorbate–glutathione cycle, helping to prevent and/or minimize damages caused by reactive oxygen species (ROS) [1,2]. ROS are produced

in cell metabolism under normal conditions, but their production in plants is enhanced when plants are submitted to biotic and abiotic stresses. Both GSH and ASA are key metabolites in the control of the redox-signaling cascades that modulate a variety of metabolic processes [3]. GSH is also implicated in the control of reactive nitrogen species

* Corresponding author. Fax: +34 976716145.

E-mail address: ana.alvarez@eead.csic.es (A. Álvarez-Fernández).

¹ Abbreviations used: GSH, reduced glutathione; ASA, ascorbic acid; ROS, reactive oxygen species; GSNO, *S*-nitrosogluthathione; NO, nitric oxide; GSSG, glutathione disulfide; DHA, dehydroascorbic acid; hGSH, homogluthathione; HPLC, high-performance liquid chromatography; MS, mass spectrometry; HPLC–ESI/MS(TOF), high-performance liquid chromatography–electrospray ionization/mass spectrometry (time of flight); MPA, metaphosphoric acid; GSH*, isotopically labeled GSH; ASA*, isotopically labeled ASA; EDTA, ethylenediaminetetraacetic acid; PVPP, polyvinyl–polypyrrolidone; *m/z*, mass/charge ratio; LOD, limit of detection; S/N ratio; signal/noise ratio; LOQ, limit of quantification; hGSSG, oxidized homogluthathione; RSD, relative standard deviation; FWHM, full width, half mass; FW, fresh weight.

[4], and *S*-nitrosogluthathione (GSNO) seems to be a stable transport form of nitric oxide (NO) [5]. When GSH and ASA act as antioxidants in the ascorbate–glutathione cycle, they are oxidized to glutathione disulfide (GSSG) and dehydroascorbic acid (DHA), respectively. On the other hand, GSH is implicated in the detoxification of xenobiotics in conjunction with glutathione *S*-transferases, which react with GSH via the nucleophilic sulfhydryl group of the cysteine moiety [6]. Also, when plants are exposed to heavy metals, GSH is used to synthesize phytochelatin, that is, cysteine-rich peptides able to form complexes with several metal ions [7]. In addition, GSH is the predominant form of reduced sulfur in plants [8]. Homologues of GSH can be found in different plant species, where some of the constitutive amino acids differ from those found in GSH. For instance, homogluthathione (hGSH, *L*- γ -glutamyl-*L*-cysteine- β -alanine) can be found in several tissues and organs of legumes [9,10], whereas other less studied homologues have been found in a number of plant species [11,12].

From a physiological point of view, the GSH/GSSG ratio often is more relevant than the total concentration of GSH in explaining the effects of different stresses [13,14]. For instance, the GSH/GSSG redox pair ratio could be more influential in the control of gene expression and protein function than is the total concentration of GSH [15]. Under normal conditions, the glutathione pool usually is reduced to a large extent, and the oxidized form (GSSG) often is less than 5% of the total pool. The low concentrations of GSSG make quantifying it accurately very difficult, and consequently highly sensitive methodologies are required.

Methodologies for the determination of both GSH and GSSG have been reviewed recently [16,17]. The selectivity and sensitivity of nonseparative techniques, such as UV–Vis spectroscopy, spectrofluorometry, and amperometry, often are inadequate. Improvements in selectivity and sensitivity were achieved using chromatographic techniques such as thin-layer chromatography and high-performance liquid chromatography (HPLC). Recent methods have used HPLC coupled to a variety of detection techniques, including UV–Vis and diode array detection, fluorometry, electrochemical detection, and mass spectrometry (MS). To further enhance sensitivity, common procedures include derivatization of the free thiol group in the GSH molecule with chromophores, such as the Ellman's reagent, or fluorophores, such as monobromobimane. In general, GSSG is measured by reducing it to GSH with the enzyme glutathione reductase. The difference between the total (after reduction) and initial GSH values is used to estimate the GSSG concentration in the sample. Using this procedure, the GSSG concentration found in a given sample often could be similar to the standard deviation between replicates. An improved approach includes a preliminary step where the thiol group of GSH is blocked with vinylpyridine [18]. Subsequently, the derivatization reaction occurs only with GSH formed during the *in vitro* GSSG reduction step. The use of such complex procedures implies a very long analysis

time, and this may result in both losses in analyte concentration and changes in redox status.

HPLC–MS techniques have been a major step toward the determination of GSH and GSSG during recent years [19–25]. These techniques improve selectivity, avoid the GSSG reduction step, and generally have sufficient sensitivity to measure the low concentrations of these compounds without derivatization. In HPLC–MS methods, the autooxidation of the GSH thiol group has been prevented by blocking it with iodoacetic acid [19], Ellman's reagent [20], or *N*-ethylmaleimide [21,22]. So far, only two studies [23,24] have attempted to simultaneously measure GSH and GSSG by MS without blocking the GSH thiol group. Norris and coworkers [23] carried out the extraction of tissue with a methanolic solution, which might not ensure the absence of autooxidation or enzymatic degradation of the thiol groups if they are not blocked [17]. Tissue extraction with acidic solutions can stop γ -glutamyl transpeptidase enzyme activity and prevent GSH autooxidation [17,26], although it may induce ionization problems in MS techniques [17]. The work of Gucek and coworkers [24] was the first attempt to measure both forms of glutathione by HPLC–MS in plant extracts, although information on limits of detection and other validation parameters for GSSG was not provided. Klejduš and coworkers [25] recently measured GSH in maize kernels by HPLC–MS, but quantification of GSSG was not carried out.

Because of the reasons indicated above, new reliable methods to accurately determine the reduced and oxidized forms of GSH and its homologues in plant tissues should be developed. The aim of the current work was to develop and validate a new high-performance liquid chromatography–electrospray ionization/mass spectrometry (time of flight) (HPLC–ESI/MS(TOF)) method to simultaneously measure the concentrations of reduced and oxidized forms of glutathione and homogluthathione in extracts of different plant tissues. The method also allows the simultaneous determination of ASA and GSNO. An extraction procedure with 5% metaphosphoric acid (MPA) was used, and the analytes were measured in the same chromatographic run and without any derivatization step. Isotopically labeled GSH (GSH*) and ASA (ASA*) were used as internal standards to control factors affecting the process during extraction, separation by HPLC, and ESI–MS.

Materials and methods

Chemicals

All eluents, extraction buffers, and standard solutions were prepared with analytical-grade type I water (Milli-Q Synthesis, Millipore, Bedford, MA, USA). Acetonitrile HPLC–gradient grade was purchased from Panreac Química (Barcelona, Spain); formic acid was purchased from Fluka (Sigma–Aldrich, St. Louis, MO, USA); GSH and GSSG were purchased from Calbiochem (San Diego, CA, USA); hGSH was purchased from Bachem (Bubendorf,

Switzerland); ASA, DHA, and GSNO were purchased from Sigma–Aldrich (St. Louis, MO, USA); and labeled GSH ([glycine 1,2-¹³C,¹⁵N]GSH) and ASA ([1-¹³C]ASA) were purchased from Cambridge Isotope Laboratories (Andover, MA, USA).

Standard solutions

Stock solutions containing 10 mM GSH (M_m 307.3), GSSG (M_m 612.6), hGSH (M_m 321.4), ASA (M_m 176.1), DHA (M_m 174.3), GSNO (M_m 336.3), GSH* (M_m 310.3), and ASA* (M_m 177.1) were prepared in 2.5% (w/v) MPA, 1 mM ethylenediaminetetraacetic acid (EDTA), and 0.1% formic acid. Aliquots of the stock solutions were conserved at -80°C . Aliquots were thawed only once to prepare the standards and then were discarded. ASA solutions were prepared in a cold chamber at 4°C and under a green safe-light to avoid degradation, as described in Ref. [26].

Plant material

Different plant species and tissues were used. Materials were chosen to cover a range of different species and tissues having different analytes and concentrations. Materials used included leaves of *Beta vulgaris*, *Prunus persica*, *Medicago sativa*, *Hordeum vulgare*, *Lycopersicon esculentum*, *Oryza sativa*, and *Trifolium* sp.; roots of *Beta vulgaris*; and nodules of *Medicago truncatula*. *B. vulgaris*, *L. esculentum*, and *M. truncatula* were grown in a growth chamber (16 h light/8 h dark photoperiod, 24°C day/ 20°C night). *O. sativa* and *H. vulgare* were grown in a greenhouse during winter at approximately 18°C day/ 10°C night. *P. persica*, *M. sativa*, and *Trifolium* sp. leaves were collected in the field. All material was collected at approximately 12 h solar time.

Tissue extraction

Tissue extraction was performed as described elsewhere [26–31], with some modifications. Plant tissue (100–500 mg) was frozen in liquid N_2 , stored at -80°C until analysis, and ground with mortar and pestle in liquid N_2 . GSH* and ASA* were added at the moment of sample grinding. The dry powder was homogenized with 200–1000 μl of cold (4°C) extraction solution (5% (w/v) MPA and 1 mM EDTA in 0.1% formic acid), supplemented with 1% (m/v) polyvinyl-polypyrrolidone (PVPP) just before use. Homogenates were centrifuged at 15,000g for 20 min at 4°C . Supernatants were collected, and the pellet was resuspended with 150–300 μl of the same extraction solution and centrifuged again under the same conditions. The second supernatant obtained was combined with the first and taken to a final volume of 2 ml with extraction solution. The supernatants were filtered through 0.22- μm polyvinylidene fluoride filters and immediately analyzed or frozen in liquid N_2 and stored at -80°C until analysis. All steps were done in a cold chamber at 4°C and under a green safe-light to avoid ASA degradation. All instruments (e.g., mortar,

pestle) were also precooled. Three replicates of each extract were done.

Using an extraction solution of very low pH stops enzymatic activities, thereby avoiding the degradation of thiols, and also prevents GSH autooxidation [28,30,32]. Extraction with organic solvents, often preferred to acid extraction when using MS for detection, might not prevent thiol group GSH autooxidation [17]. The possible negative influence of MPA on the ionization of analytes was negligible because the signals obtained with standard solutions prepared with 0.1% formic acid or 5% MPA were similar (not shown). This suggests that the effects of the high-ionic strength acidic extraction solvent on ionization possibly are limited to the first minute of the chromatographic run, when the chromatographic front enters the electrospray chamber.

HPLC–ESI/MS(TOF) analysis

Analyses were carried out with a BioTOF II (Bruker Daltonics, Billerica, MA, USA) coaxial multipass time-of-flight mass spectrometer (MS(TOF)) equipped with an Apollo electrospray ionization source (ESI) and coupled to a Waters Alliance 2795 HPLC system (Waters, Milford, MA, USA).

The BioTOF II was operated with endplate and spray tip potentials of 2.8 and 3.3 kV, respectively, in negative ion mode and of 3.0 and 3.5 kV, respectively, in positive ion mode. Drying gas (N_2) pressure was kept at 30 psi. Nebulizer gas (N_2) pressure was kept at 30 and 60 psi in ESI/MS and LC–ESI/MS experiments, respectively. The mass axis was calibrated using Li-formate adducts in negative ion mode and a mixture of 1 μM leucine–enkephaline and 20 μM methionine in positive ion mode. Spectra were acquired in the mass/charge ratio (m/z) range of 100–700.

To optimize the MS signal, direct injection of 20- μM solutions of all standards prepared in 0.1% (v/v) formic acid were carried out using a syringe pump (Cole–Parmer Instrument, Vernon Hills, IL, USA) operated at 2 $\mu\text{l min}^{-1}$. Optimal parameter values after tuning included orifice voltage values of 90 and 120 V in negative and positive ion modes, respectively, and a drying gas temperature of 200°C in both cases. Orifice voltage values were chosen to maximize the GSSG signal without compromising GSH detection because in plant tissue extracts GSSG always occurs in lower concentrations than does GSH.

HPLC–ESI/MS(TOF) analysis was carried out by injecting 20- μl aliquots of standard solutions and sample extracts in a reverse-phase monolithic column (Chromolith Performance RP-18e, 4.6×100 mm, Merck, Darmstadt, Germany) fitted with a 4×30 -mm precolumn packed with Lichrospher RP C_{18} , end-capped 5- μm spherical particle size (Scharlau, Barcelona, Spain). Autosampler and column temperatures were 6 and 30°C , respectively. Samples were eluted at a flow rate of 1 ml min^{-1} . The exit flow from the column was split with a T-connector (Upchurch Scientific, Oak Harbor, WA, USA) that led 200 $\mu\text{l min}^{-1}$ (20% of the

total efflux) from the HPLC into the ESI interface of the MS(TOF) apparatus. The mobile phase was built using two solvents: A (0.1% formic acid in Milli-Q water) and B (0.1% (v/v) formic acid in acetonitrile). For separation of the analytes, a linear gradient from 0 to 10% B (0–5 min) was used. Then, to wash the column, the concentration of B was increased linearly from 10 to 50% from 5 to 6 min, and this solvent composition was maintained until 9 min. Finally, to regenerate the column, the solvent was changed linearly to 0% B until 11 min and then was maintained at 0% B until 15 min, when a new sample could be injected.

Validation was carried out by obtaining calibration curves corrected with internal standards (100 μM ASA* was used for the quantification of ASA, and 75 μM GSH* was used for the quantification of GSH, hGSH, GSSG, and GSNO), limits of detection (LODs, signal/noise (S/N) ratio of 3), limits of quantification (LOQs, S/N ratio of 10), and intra- and interday repeatability and recovery, using standard techniques (for a complete description, see Results).

The system was controlled with the software packages BioTOF (version 2.2, Bruker Daltonics) and HyStar (version 2.3, Bruker Daltonik, Bremen, Germany). Data were processed with Data Analysis software (version 3.2, Bruker Daltonik).

Results

ESI/MS(TOF) analysis

In the negative ion mode ESI/MS(TOF) spectra, standard analyte solutions (20 μM) showed major $[\text{M}-\text{H}]^{-1}$ ions at m/z values 306.2 for GSH (Fig. 1A), 309.2 for GSH* (Fig. 1B), 320.2 for hGSH (Fig. 1C), and 611.4 for GSSG (Fig. 1D). Minor peaks at m/z values 613.3 (Fig. 1A), 619.4 (Fig. 1B), and 641.4 (Fig. 1C) are due to the corresponding dimer $[\text{2M}-\text{H}]^{-1}$ ions. Neither oxidation of GSH nor reduction of GSSG was observed during the ionization process (Figs. 1A and D). Moreover, neither single-labeled GSSG (GSSG*, formed by one GSH and one GSH* molecule, 614.4 m/z) nor double-labeled GSSG (GSSG**, formed by two GSH* molecules, 617.4 m/z) was found in 200- and 1000- μM GSH*-spiked plant extracts, indicating that no GSH oxidation occurs (data not shown). ASA, ASA*, and GSNO spectra show major $[\text{M}-\text{H}]^{-1}$ ions at m/z values 175.1, 176.1, and 335.2, respectively (Figs. 2A–C). Under the conditions used, optimized for GSSG analysis, the GSNO spectrum shows peaks at m/z values 304.2 and 671.4, corresponding to the $[\text{M}-\text{NO}-2\text{H}]^{-1}$ and $[\text{2M}-\text{H}]^{-1}$ ions.

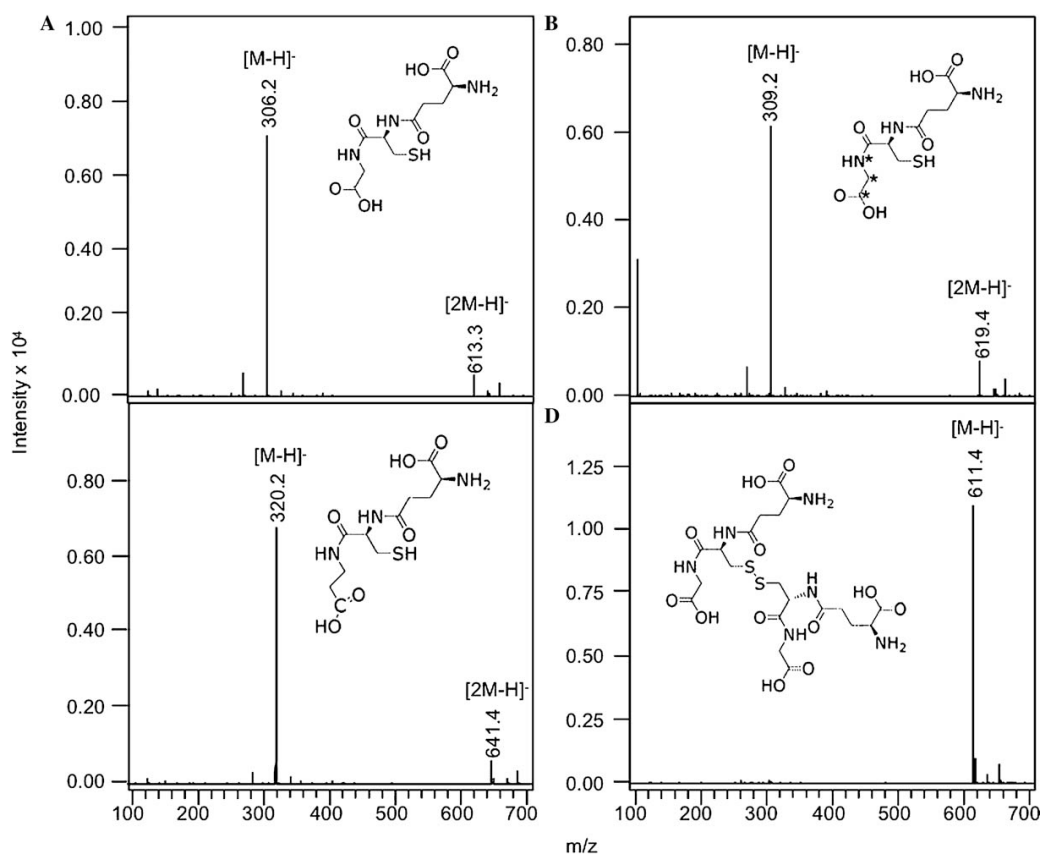


Fig. 1. ESI/TOF mass spectra of GSH (A), GSH* (B), hGSH (C), and GSSG (D) standards in negative ion mode. Data were acquired by injecting 20- μM solutions of each analyte in 0.1% (v/v) formic acid and 50% isopropanol. Labeled atoms are indicated with an asterisk.

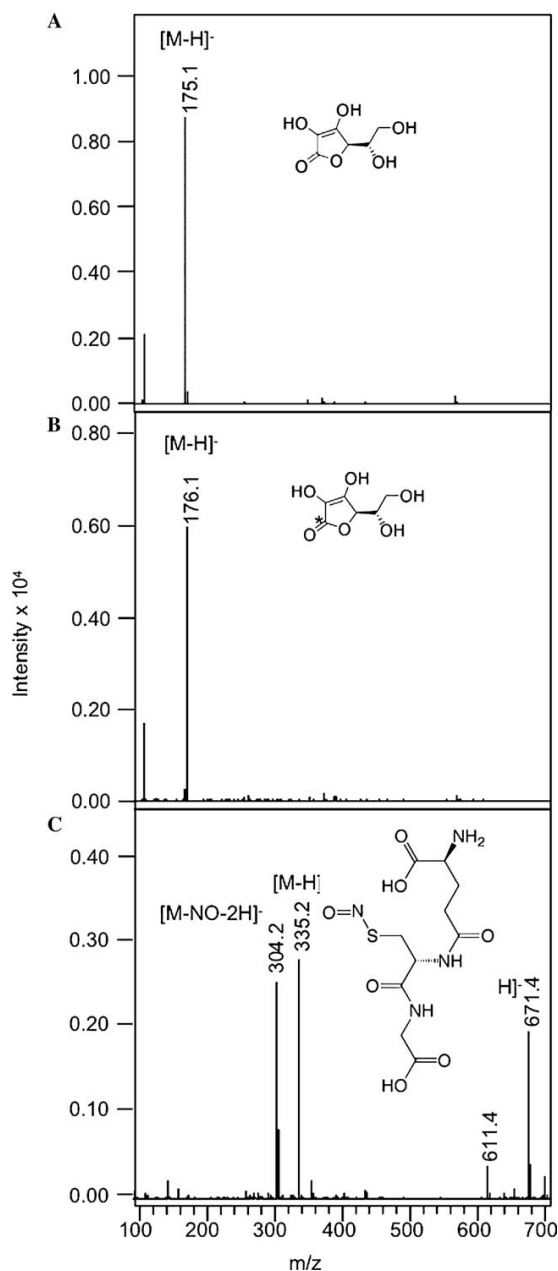


Fig. 2. ESI/TOF mass spectra of ASA (A), ASA* (B), and GSNO (C) standards in negative ion mode. Data were acquired by injecting 20- μ M solutions of each analyte in 0.1% (v/v) formic acid and 50% isopropanol. Labeled atoms are indicated with an asterisk.

The signal obtained under the same conditions for the $[M-H]^{-1}$ ion of DHA was too low to permit analysis (see below). In the positive ion mode, major ions found in the MS spectra were at m/z values 308.2, 322.2, and 613.4 for GSH, hGSH, and GSSG, respectively, and signals obtained were slightly less intense (with a lower S/N ratio) than those obtained in the negative ion mode (data not shown). In the

positive ion mode, signals for the ASA and DHA $[M+H]^{+1}$ ions were too low to permit analysis. Therefore, the negative ion mode was chosen for further experiments.

HPLC-ESI/MS(TOF) analysis

Analytes were separated with a linear solvent gradient in a monolithic C_{18} column, and mass spectra were acquired by ESI/MS(TOF) in the m/z range of 100–700 during the whole chromatographic run, to obtain three-dimensional (time, m/z , and intensity) chromatograms. Ion chromatograms were extracted for the exact m/z values corresponding to the $[M-H]^{-1}$ species of each analyte indicated above. Results show that the HPLC-ESI/MS(TOF) method developed is capable of adequately resolving ASA, GSH, hGSH, GSSG, and GSNO present in a mixed standard solution in a single chromatogram, with retention times of 2.6, 3.2, 4.1, 4.4, and 4.9 min, respectively (Fig. 3). ASA* coeluted with ASA, whereas GSH* eluted at 3.0 min, a slightly shorter retention time than that of GSH (Fig. 3). Although a commercial standard of oxidized homogluthathione (hGSSGh) is not available, legume leaf extract chromatograms show at 5.4 min a peak with m/z 639.2, attributable to the $[M-H]^{-1}$ ion of hGSSGh (Fig. 4). Analysis time for all compounds analyzed was approximately 6 min, with column washing and regeneration time accounting for an additional 9 min, leading to a total analysis time of 15 min per sample.

Validation of the HPLC-ESI/MS(TOF) method

The HPLC-ESI/MS(TOF) method was validated preparing solutions of available standards in extraction solu-

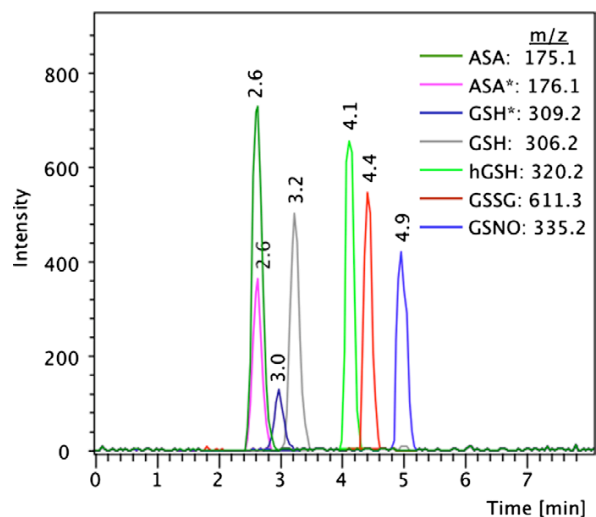


Fig. 3. Chromatogram of a mixture of standards. ASA, ASA*, GSH*, GSH, hGSH, GSSG, and GSNO were at concentrations of 200, 100, 25, 75, 75, 25, and 75 μ M, respectively, in 2.5% (w/v) MPA, 1 mM EDTA, and 0.1% (v/v) formic acid.

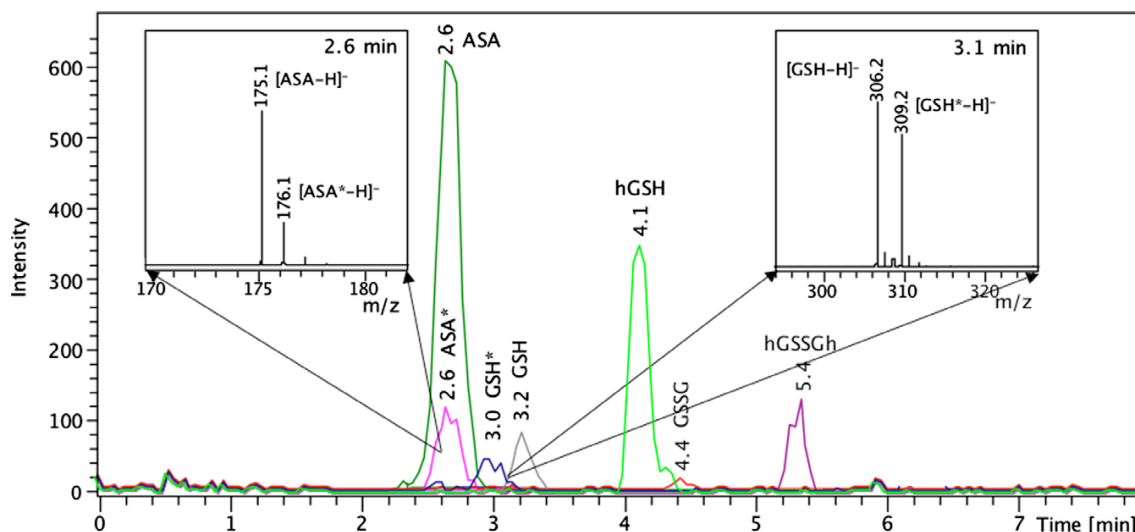


Fig. 4. Chromatogram of a leaf extract from *M. sativa* showing peaks corresponding to ASA (175.1 m/z), GSH (306.2 m/z), hGSH (320.2 m/z), a putative hGSSGh peak (639.2 m/z), and peaks corresponding to ASA* (176.1 m/z) and GSH* (309.2 m/z) used as internal standards. Insets show zooms of the mass spectra at retention times of 2.6 and 3.1 min.

tion (5% (w/v) MPA, 1 mM EDTA, and 0.1% (v/v) formic acid). Calibration curves corrected with internal standardization, LODs, and intra- and interday repeatability and recovery were measured. Real plant extract samples were also analyzed with the method developed.

Calibration curves corrected by internal standardization were obtained by analyzing solutions of standards in the ranges of 5–250 μM (GSH and hGSH), 1–15 μM (GSSG), 25–750 μM (ASA), and 5 to 150 μM (GSNO). Internal standards used were GSH* for GSH, hGSH, GSSG, and GSNO

and ASA* for ASA. In all cases, a linear regression was obtained (r^2 of 0.991–0.998) (Fig. 5).

LODs, defined as the analyte amounts giving an S/N ratio of 3, were 100, 60, 30, 20, and 30 pmol for ASA, GSH, hGSH, GSSG, and GSNO, respectively. Using a 20- μl injection volume, these values are equivalent to analyte concentrations in the injected sample solution of 5.0, 3.0, 1.5, 1.0, and 1.5 μM for ASA, GSH, hGSH, GSSG, and GSNO, respectively. LOQs, defined as the amounts giving an S/N ratio of 10, were 300, 120, 80, 50, and 80 pmol for

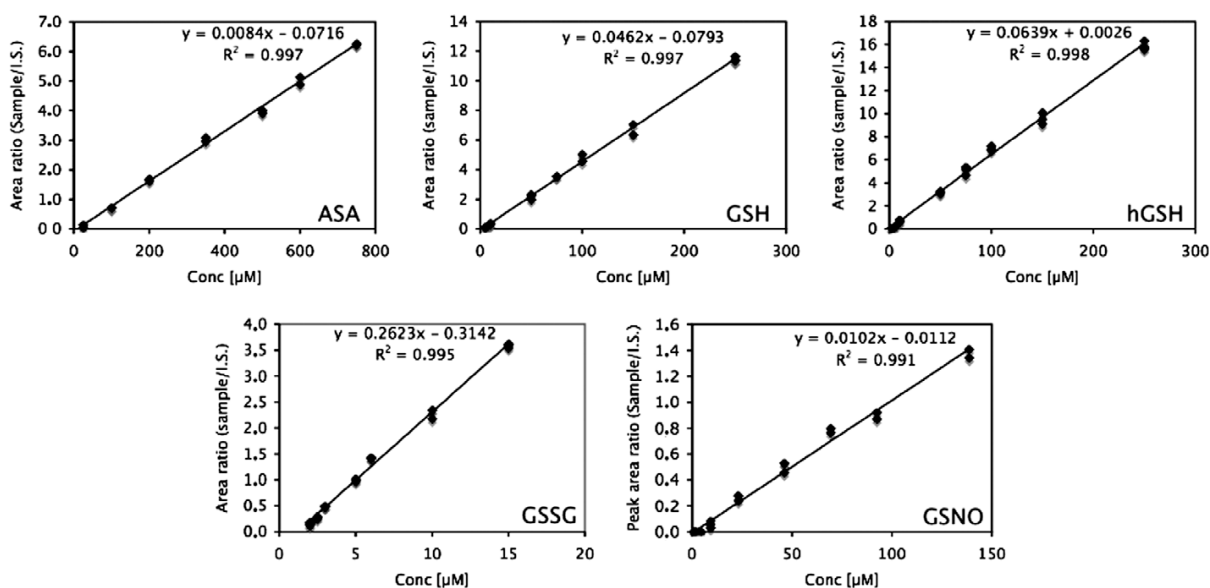


Fig. 5. Calibration curves of ASA, GSH, hGSH, GSSG, and GSNO obtained by analyzing a mixture of standards and internal standards by the ESI/MS(TOF) method. I.S., internal standard.

ASA, GSH, hGSH, GSSG, and GSNO, respectively. For DHA, and possibly due to strong analyte fragmentation, the LOD was higher than 500 μM , a value much larger than the concentrations expected in plant tissue extracts.

The intraday repeatability of the HPLC–ESI/MS(TOF) method was assessed from 10 consecutive chromatographic runs using a standard solution with 75 μM GSH, hGSH, and GSNO; 25 μM GSSG and GSH*; 200 μM ASA; and 100 μM ASA* in 2.5% (w/v) MPA, 1 mM EDTA, and 0.1% (v/v) formic acid. The variation in retention time and peak area was tested for each analyte (Table 1). The interday repeatability of the method was assessed by analyzing the same standard solution for 5 consecutive days (Table 1). The relative standard deviation (RSD) for peak retention time always was lower than 0.41% in the intraday test and 0.95% in the interday test. The RSD for peak area was in the range of 4.4–7.0% in the intraday test and 7.4–13.1% in the case of the interday test.

Recovery assays were carried out for GSH, GSSG, hGSH, ASA, and GSNO by spiking *B. vulgaris* leaf extracts with known amounts of both analyte standards and labeled analytes (GSH* and ASA*). Recovery was calculated by dividing the amount of analyte found in the spiked sample by the sum of the amount found in the sample plus the amount added. Analyte recoveries found were between 92 and 105% (Table 2).

Analysis of plant tissue extracts

A chromatogram example of *M. sativa* leaf extracts is shown in Fig. 4. Five peaks, corresponding to ASA, GSH, hGSH, GSSG, and hGSSG, were detected at retention times of 2.6, 3.2, 4.1, 4.4, and 5.4 min, respectively, as shown in Fig. 4 (in this figure, the internal standards ASA* and GSH* show peaks at 2.6 and 3.0 min, respectively). No trace of double-labeled (617.4 m/z) or single-labeled (614.4 m/z) GSSG was found.

The resolution of the MS(TOF) detector used is higher than 10,000 FWHM (full width, half mass). Therefore, MS(TOF) spectra provide information on the elemental isotopic distribution of any compound detected in the chro-

Table 2
Recoveries obtained for GSH, hGSH, GSSG, ASA, and GSNO using *Beta vulgaris* leaf extracts

	Amount added (pmol)	Amount found (pmol)	Recovery (%)
GSH	0	2328 \pm 64	
	1704 \pm 56	3692 \pm 178	91.5 \pm 3.7
hGSH	0	0	
	1722 \pm 78	1724 \pm 114	100.1 \pm 4.5
GSSG	0	20 \pm 2	
	60 \pm 4	78 \pm 4	94.4 \pm 7.5
ASA	0	3264 \pm 90	
	9514 \pm 210	12,412 \pm 288	98.9 \pm 4.4
GSNO	0	0	
	1888 \pm 214	1872 \pm 52	104.9 \pm 10.6

Note. Results are means \pm SE ($n = 5$).

matographic run. An example can be seen in the insets of Fig. 4, which show the MS resolution of the major ions of ASA and ASA*, coeluting at a retention time of 2.6 min, as well as that of GSH and GSH*, which have slightly different retention times of 3.0 and 3.2 min, respectively, and coelute at an intermediate retention time of 3.1 min.

Analyte concentrations found in these and other plant tissues are shown in Table 3. Concentration ranges found were 43–707 nmol g^{-1} FW (GSH), 47–2300 nmol g^{-1} FW (hGSH), 6–47 nmol g^{-1} FW (GSSG), and 1470–8700 nmol g^{-1} FW (ASA), where FW is fresh weight. These values are within the values reported in the literature for plant tissues (Table 4).

Discussion

The relevance of the GSH/GSSG redox pair in different plant metabolic processes makes necessary having reliable methods to analyze these compounds with high sensitivity while minimizing analyte decomposition and changes in redox status from that originally occurring in the plant. In this work, we have developed and validated an HPLC–ESI/MS(TOF) method capable of measuring GSH, GSSG, hGSH, ASA, and GSNO in plant tissue extracts. The method is based in a separation with reverse-phase HPLC, ionization by electrospray, and highly selective detection of the analytes, using exact mass measurements with a TOF

Table 1
Intraday ($n = 10$) and interday ($n = 5$) repeatability of the LC–ESI/MS(TOF) method

	ASA		GSH		hGSH		GSSG		GSNO	
	RT	A_s/A_{IS}	RT	A_s/A_{IS}	RT	A_s/A_{IS}	RT	A_s/A_{IS}	RT	A_s/A_{IS}
Intraday										
Mean	2.57	2.10	3.17	4.66	4.08	4.99	4.39	3.02	4.93	3.56
SD	0.01	0.09	0.01	0.22	0.01	0.24	0.02	0.21	0.01	0.40
RSD (%)	0.41	4.35	0.33	4.67	0.28	4.91	0.37	6.99	0.29	11.20
Interday										
Mean	2.57	2.13	3.17	4.60	4.08	5.63	4.39	4.03	4.93	3.99
SD	0.01	0.16	0.01	0.42	0.01	0.66	0.02	0.61	0.01	0.45
RSD (%)	0.61	7.36	0.81	9.10	0.62	11.66	0.95	13.11	0.47	11.35

Note. Retention times (RTs) and peak area ratios (sample area/area of internal standard [A_s/A_{IS}]) were obtained using 200 μM ASA, 75 μM GSH, 75 μM hGSH, 25 μM GSSG, 75 μM GSNO (using 100 μM ASA*, and 25 μM GSH* as internal standards) in 2.5% (w/v) MPA, 1 mM EDTA, and 0.1% (v/v) formic acid.

Table 3
Contents of GSH, hGSH, GSSG, and ASA found in plant tissues using the LC–ESI/MS(TOF) method

Plant tissue	GSH (nmol g ⁻¹ FW)	hGSH (nmol g ⁻¹ FW)	GSSG (nmol g ⁻¹ FW)	ASA (nmol g ⁻¹ FW)
<i>Beta vulgaris</i> (leaf)	152.2 ± 8.8	ND	23.7 ± 0.2	2240 ± 78
<i>Prunus persica</i> (leaf)	155.4 ± 9.5	ND	5.8 ± 0.1	8730 ± 225
<i>Medicago truncatula</i> (nodule)	202.8 ± 21.7	47.4 ± 14.7	7.0 ± 1.7	1471 ± 54
<i>Medicago sativa</i> (leaf)	ND	1333.3 ± 152.8	ND	3523 ± 68
<i>Hordeum vulgare</i> (leaf)	187.5 ± 25.1	ND	22.9 ± 0.9	2344 ± 51
<i>Lycopersicon esculentum</i> (leaf)	707.3 ± 54.4	ND	47.3 ± 5.5	4370 ± 306
<i>Beta vulgaris</i> (root)	92.1 ± 14.8	ND	46.1 ± 10.1	ND
<i>Trifolium</i> sp. (leaf)	42.6 ± 24.8	2332.2 ± 7.6	ND	7620 ± 106
<i>Oryza sativa</i> (leaf)	252.1 ± 11.2	ND	12.9 ± 0.4	7928 ± 1288

Note. Values are means ± SE ($n = 3$). ND, not detected (below LOD). FW, fresh weight.

Table 4
Plant tissue contents of GSH, GSSG, and hGSH found in the literature and the analytical techniques used for their determination

Tissue	Analytical technique	Content	Ref.
Sugar beet roots	GR–DTNB	30 and 10 nmol g ⁻¹ FW for GSH and GSSG	[33]
<i>Vigna radiata</i> leaves	GR–DTNB	2000 and 200 nmol g ⁻¹ FW for GSH and GSSG	[34]
Tomato, potato, and broccoli leaves	Amperometric inhibitor biosensor	20–321 µg GSH g ⁻¹ FW	[35]
Sunflower leaves	GR–DTNB	700 nmol GSH g ⁻¹ FW	[36]
<i>Arabidopsis thaliana</i> (protoplasts)	mCB/mBB–CLSM/ TPLSC	8–9 nmol GSH g ⁻¹ FW; 3–4 mM in cells; 3 mM in cytoplasm	[37]
<i>Arabidopsis thaliana</i> trichome cells	mCB/mBB–CLSM	0.24 mM GSH in trichome cytoplasm; 0.08 mM GSH in base cell cytoplasm; 0.14 mM in GSH epidermic cell cytoplasm.	[38]
<i>Arabidopsis thaliana</i> root epidermic cells	mCB–CLSM/TPLSM	2.7 mM GSH in cytoplasmic trichoblasts; 5.5 mM GSH in cytoplasmic atrichoblasts	[39]
<i>Arabidopsis thaliana</i> root epidermic cells	mCB–CLSM	6 mM GSH in external cell cytoplasm; 2–3 mM GSH in other cells	[40]
<i>Populus tremula</i> × <i>Populus alba</i> leaf epidermis	mCB–CLSM and mCB/ mBB–HPLC	0.2–0.3 mM GSH in cytoplasm	[41]
<i>Arabidopsis thaliana</i> root apex	mCB–CLSM	2–4 mM GSH in cytoplasm	[42]
<i>Arabidopsis thaliana</i> leaves	HPLC–DTNB	200–800 nmol GSH g ⁻¹ FW	[43]
Tomato and azuki bean cells	HPLC–DTNB	500–12,500 nmol GSH g ⁻¹ cells	[44]
Nodules, roots, and leaves from different legumes	mBB–HPLC	150–820, 1–147, and 1–445 nmol GSH g ⁻¹ FW in nodules, roots, and leaves, respectively; 0–427, 0–235, and 0–887 nmol hGSH g ⁻¹ FW in nodules, roots, and leaves, respectively	[10]
Poplar leaves	GR–DTNB mBB–HPLC OPA–HPLC	699–1239 nmol GSH g ⁻¹ FW; 640–1169 nmol GSH g ⁻¹ FW; 668–1109 nmol GSH g ⁻¹ FW	[45]

Note. GR, glutathione reductase; DTNB, 5,5'-dithiobis(2-nitrobenzoic acid); mCB, monochlorobimane; mBB, monobromobimane; CLSM, confocal laser scanning microscopy; TPLSC, two-photon laser scanning microscopy; OPA, *o*-phthalaldehyde.

mass spectrometer. This method permits the direct and simultaneous determination of all analytes in a very short time, approximately 6 min, with high sensitivity.

This is the first time, to our knowledge, that GSH, GSSG, ASA, hGSH, and GSNO are determined simultaneously and directly. The method represents significant advantages over traditional methods for the determination of GSH and GSSG. First, the identification of analytes is unequivocal based on both its retention time and its exact m/z ratio. Also, all compounds are measured directly because no reduction step is needed to measure GSSG (thereby reducing by half the number of analyses) and no derivatization step is used. All of these features, along with the short analysis time required for each sample and the fact that the extraction process is carried out under safe conditions (i.e., sample extracted with liquid nitrogen, dim green light, acidic pH), allow a more precise and reliable analysis of the GSH/GSSH redox status in plant tissues.

The method has been validated with respect to LODs, LOQs, calibration curves, reproducibility and analyte recoveries, always using isotopically labeled standards. Sensitivity was good, with LODs for analyte concentrations between 1 and 5 µM. The LOD for GSSG, 1 µM, is similar to the best values obtained in plant analysis using capillary zone electrophoresis (1 µM [30]) but not as good as those found using electrochemical detection (0.02 µM [46]). The LOD found for GSH, 3 µM, compares well with the LODs of other methods based on MS [19–22] and other techniques [17], which are in the ranges of 10 nM to 0.82 µM and 5 nM to 10 µM, respectively. LODs are in any case adequate, considering that the content ranges for the analytes in plant tissues are 6–47 nmol g⁻¹ FW for GSSG, 43–707 nmol g⁻¹ FW for GSH, and 1470–8730 nmol g⁻¹ FW for ASA (Table 3). These contents would result in analyte concentrations in the extracts in the range of 1.5 µM to 2.3 mM, with the lower values being for GSSG. The method

run-to-run interday reproducibility for chromatographic time, with RSD values of 0.8–1.0% for GSH and GSSG, respectively, is better than the reproducibility levels reported previously for other HPLC–MS methods that are in the range of 1.7–6.0% [16–19]. RSD values for peak area, 9 and 13% for GSH and GSSG, respectively, are within the range of values found with other HPLC–MS methods that are between 0.06 and 28.3% [19–23]. If needed in specific tissues, improvements in peak area reproducibility, as well as in LODs, could also be achieved using narrower columns, where lower fluxes are used and no flow split is needed. The recovery for analytes spiked in plant tissue extracts is between 92 and 105%, compared with recoveries found with other methods that are in the range of 70–120% [17].

The method has wide possibilities of application. So far, it has been tested with different plant tissues (leaves, roots, and nodules) from different plant species (*B. vulgaris*, *P. persica*, *Z. mays*, *M. sativa*, *M. truncatula*, *H. vulgare*, *L. esculentum*, *Trifolium* sp., and *O. sativa*), showing its suitability to perform analyses in a variety of studies. In addition to GSH and GSSG, the redox pair hGSH and hGSSG (with the latter putatively assigned to the peak at 5.4 min with a 639.2 *m/z*) could also be analyzed in leaf and nodule legume extracts [10], thereby providing a tool for the study of their redox status [47]. Furthermore, the method also seems to be suitable to analyze other plant thiols such as hydroxymethylglutathione. Unfortunately, with the conditions optimized for GSSG and GSH analysis, it was not possible to determine oxidized ASA, DHA, supporting previous findings that fragmentation occurs with this compound even in mild ionization procedures such as ESI [48].

Recent evidence has shown that micromolar concentrations of GSSG could arise from oxidation of GSH during blood denaturation in acidic conditions [22,49], although it should be kept in mind that these authors did not use low temperature for the extraction procedure. Under the extraction conditions used in this work, which involved the use of liquid nitrogen (–196°C), low safelight, and low pH, no GSH oxidation occurred during the ionization process and no significant oxidation of GSH* spiked to the samples during extraction was found. In fact, no signal at all was found for single- or double-labeled GSSG (*m/z* values 617.4 and 614.4) in the samples spiked with 1 mM GSH* at the time of extraction (data not shown). Because our LOD for GSSG was 1 µM, this would imply that if any oxidation exists, it would account for less than 0.2% of the GSH amount, a value much lower than the 2–3% found in blood by Steghens and coworkers [22]. Therefore, from the GSH and GSSG values found in plant samples (Table 3), one can estimate that less than 0.8–11.6% of the GSSG found may come from GSH oxidation during extraction, depending on the sample considered. This is lower than the interday RSD for GSSG (Table 1). However, the possibility that GSH oxidation may occur should be taken into consideration when analyzing plant materials that cannot be frozen rapidly. For instance, plant fluids such as xylem of phloem

require some time for collection and therefore are prone to GSH oxidation by molecular oxygen and/or oxidizing substances in a similar way to the GSH oxidation mediated by oxyhemoglobin in blood [22]. In this context, it should be investigated whether changing the extraction conditions may affect the GSSG/GSH ratios found in plant fluids.

In summary, the method developed permits the direct and simultaneous analysis of GSH, GSSG and homologues, ASA, and GSNO with extreme selectivity, high sensitivity, and sufficient reproducibility. The rapidity of the analysis allows for a high analysis throughput. Furthermore, the high resolution of the MS(TOF) spectrometer used can give information on isotopic distribution (see insets in Fig. 4), allowing its use as a tool in metabolic studies with stable isotopes. For example, plants can be fed with stable isotopically labeled compounds to follow the analyte metabolic pathways.

Acknowledgments

This work was funded by projects from the Spanish Ministry of Education and Science (MEC) (REN2001-113-C01-02 and REN2002-04229-C02-01 to L. E. Hernández and AGL2004-00194 [cofinanced with FEDER] to J. Abadía). R. Rellán-Álvarez was supported by the Universidad Autónoma de Madrid through a grant of the Ph.D. Student Exchange Program and an FPI fellowship of the Spanish MEC. A. Álvarez-Fernández was supported by a “Ramón y Cajal” research contract from the Spanish MEC. Acquisition of the HPLC/MS(TOF) apparatus was cofinanced with FEDER. The authors acknowledge I. Tacchini and A. Poc for skillful technical assistance and F. Morales for critical reading of the manuscript.

Appendix A. Supplementary data

Supplementary data associated with this article can be found, in the online version, at doi:10.1016/j.ab.2006.05.032.

References

- [1] G. Noctor, C.H. Foyer, Ascorbate and glutathione: keeping active oxygen under control, *Annu. Rev. Plant Physiol. Plant Mol. Biol.* 49 (1998) 249–279.
- [2] M.W. Davey, M. Van Montagu, D. Inzé, M. Sanmartin, A. Kanellis, N. Smirnoff, I.F.F. Benzie, J.J. Strain, J. Fletcher, D. Favell, Plant L-ascorbic acid: chemistry, function, metabolism, bioavailability, and effects of processing, *J. Sci. Food Agric.* 80 (2000) 825–860.
- [3] C.H. Foyer, G. Noctor, Redox homeostasis and antioxidant signaling: a metabolic interface between stress perception and physiological responses, *Plant Cell* 17 (2005) 1866–1875.
- [4] S. Maughan, C.H. Foyer, Engineering and genetic approaches to modulating the glutathione network in plants, *Physiol. Plant.* 126 (2006) 382–397.
- [5] G. Liu, R. Sánchez-Fernández, Z-S. Li, P.A. Rea, Enhanced multi-specificity of *Arabidopsis* vacuolar multidrug resistance-associated protein-type ATP-binding cassette transporter, AtMRP2, *J. Biol. Chem.* 276 (2001) 8648–8656.
- [6] N. Kaplowitz, The physiological significance of glutathione *S*-transferases, *Am. J. Physiol.* 239 (1980) 439–444.

- [7] C. Cobbett, P. Goldsborough, Phytochelatins and metallothioneins: roles in heavy metal detoxification and homeostasis, *Annu. Rev. Plant Biol.* 53 (2002) 159–182.
- [8] C. Herschbach, H. Rennenberg, Influence of glutathione (GSH) on net uptake of sulphate and sulphate transport in tobacco plants, *J. Exp. Bot.* 45 (1994) 1069–1076.
- [9] S. Klapheck, Homogluthathione: isolation, quantification, and occurrence in legumes, *Physiol. Plant.* 74 (1988) 727–732.
- [10] M.A. Matamoros, J.F. Moran, I. Iturbe-Ormaetxe, M.C. Rubio, M. Becana, Glutathione and homogluthathione synthesis in legume root nodules, *Plant Physiol.* 121 (1999) 879–888.
- [11] S. Klapheck, B. Chrost, J. Starke, H. Zimmerman, γ -Glutamylcysteinylserine: a new homologue of glutathione in plants of the family *Poaceae*, *Bot. Acta* 105 (1993) 174–179.
- [12] P. Meuwly, P. Thibault, A.L. Schwan, W.E. Rauser, Three families of thiol peptides are induced by cadmium in maize, *Plant J.* 3 (1995) 391–400.
- [13] C.H. Foyer, N. Souriau, S. Perret, M. Lelandais, K.J. Kunert, C. Pruvost, L. Jouanin, Overexpression of glutathione reductase but not glutathione synthetase leads to increases in antioxidant capacity and resistance to photoinhibition in poplar trees, *Plant Physiol.* 109 (1995) 1047–1057.
- [14] C. Xiang, B.L. Werner, E.M. Christensen, D.J. Oliver, The biological functions of glutathione revisited in *Arabidopsis* transgenic plants with altered glutathione levels, *Plant Physiol.* 126 (1998) 564–574.
- [15] G. Noctor, L. Gomez, H. Vanacker, C.H. Foyer, Interactions between biosynthesis, compartmentation, and transport in the control of glutathione homeostasis and signalling, *J. Exp. Bot.* 53 (2002) 1283–1304.
- [16] J. Lock, J. Davis, The determination of disulphide species within physiological fluids, *Trends Anal. Chem.* 21 (2002) 807–815.
- [17] E. Camera, M. Picardo, Analytical methods to investigate glutathione and related compounds in biological and pathological processes, *J. Chromatogr. B* 781 (2002) 181–206.
- [18] O.W. Griffith, Determination of glutathione and glutathione disulfide using glutathione reductase and 2-vinylpyridine, *Anal. Biochem.* 106 (1980) 207–212.
- [19] A.F. Loughin, G.L. Skyles, D.W. Alberts, W.H. Schaefer, An ion exchange liquid chromatography/mass spectrometry method for the determination of reduced and oxidized glutathione conjugates in hepatocytes, *J. Pharm. Biomed. Anal.* 26 (2001) 131–142.
- [20] X. Guan, B. Hoffman, C. Dwivedi, D.P. Matthees, A simultaneous liquid chromatography/mass spectrometric assay of glutathione, cysteine, homocysteine, and their disulfides in biological samples, *J. Pharm. Biomed. Anal.* 31 (2003) 251–261.
- [21] E. Camera, M. Rinaldi, S. Briganti, M. Picardo, S. Fanali, Simultaneous determination of reduced and oxidized glutathione in peripheral blood mononuclear cells by liquid chromatography–electrospray mass spectrometry, *J. Chromatogr. B* 757 (2001) 69–78.
- [22] J.-P. Steghens, F. Flourié, K. Arab, C. Collombel, Fast liquid chromatography–mass spectrometry glutathione measurement in whole blood: micromolar GSSG is a sample preparation artifact, *J. Chromatogr. B* 798 (2003) 249–343.
- [23] R.L. Norris, G.K. Eaglesham, G.R. Shaw, M.J. Smith, R.K. Chiswell, A.A. Seawright, M.R. Moore, A sensitive and specific assay for glutathione with potential application to glutathione disulphide, using high-performance liquid chromatography–tandem mass spectrometry, *J. Chromatogr. B* 762 (2001) 17–23.
- [24] M. Gucek, S. Makuc, A. Mlakar, J. Bericnik-Vrbovsek, J. Marsel, Determination of glutathione in spruce needles by liquid chromatography/tandem mass spectrometry, *Rapid Commun. Mass Spectrom.* 16 (2002) 1186–1191.
- [25] B. Klejdus, J. Zehnalek, V. Adam, J. Petrek, R. Kizek, J. Vacek, L. Trnkova, R. Rozik, L. Havel, V. Kuban, Sub-picomole high-performance liquid chromatography/mass spectrometric determination of glutathione in the maize (*Zea mays* L.) kernels exposed to cadmium, *Anal. Chim. Acta* 520 (2004) 117–124.
- [26] A. Rizzolo, A. Brambilla, S. Valsecchi, P. Eccher-Zerbini, Evaluation of sampling and extraction procedures for the analysis ascorbic acid from pear fruit tissue, *Food Chem.* 77 (2002) 257–262.
- [27] M.W. Davey, E. Dekempeneer, J. Keulemans, Rocket-powered high-performance liquid chromatographic analysis of plant ascorbate and glutathione, *Anal. Biochem.* 316 (2003) 74–81.
- [28] M.W. Davey, G. Bauw, M.V. Montagu, Simultaneous high-performance capillary electrophoresis analysis of the reduced and oxidized forms of ascorbate and glutathione, *J. Chromatogr. B* 697 (1997) 269–276.
- [29] M. Tausz, I. Kranner, D. Grill, Simultaneous determination of ascorbic acid and dehydroascorbic acid in plant materials by HPLC, *Phytochem. Anal.* 7 (1996) 69–72.
- [30] J.M. Herrero-Martinez, E.F. Simó-Alfonso, G. Ramis-Ramos, V.I. Deltoro, A. Calatayud, E. Barreno, Simultaneous determination of L-ascorbic acid, glutathione, and their oxidized forms in ozone-exposed vascular plants by capillary zone electrophoresis, *Environ. Sci. Technol.* 34 (2000) 1331–1336.
- [31] P.W. Washko, R.W. Welch, K.R. Dhariwal, Y. Wang, M. Levine, Ascorbic acid and dehydroascorbic acid analyses in biological samples, *Anal. Biochem.* 204 (1992) 1–14.
- [32] J. Mendoza, P. Soto, I. Ahumada, T. Garrido, Determination of oxidized and reduced glutathione, by capillary zone electrophoresis, in *Brassica juncea* plants treated with copper and cadmium, *Electrophoresis* 25 (2004) 890–896.
- [33] T.B. Zaharieva, J. Abadía, Iron deficiency enhances the levels of ascorbate, glutathione, and related enzymes in sugar beet roots, *Protoplasma* 221 (2003) 269–275.
- [34] A.K. Shanker, M. Djanaguiraman, R. Sudhagar, C.N. Chandrashekar, G. Pathmanabhan, Differential antioxidative response of ascorbate glutathione pathway enzymes and metabolites to chromium speciation stress in green gram (*Vigna radiata* L.), *Plant Sci.* 166 (2004) 1035–1043.
- [35] M.K. Sezginürk, E. Dinçkaya, An amperometric inhibitor biosensor for the determination of reduced glutathione (GSH) without any derivatization in some plants, *Biosens. Bioelectron.* 19 (2004) 835–841.
- [36] J.M. Ruiz, R.M. Rivero, L. Romero, Preliminary studies on the involvement of biosynthesis of cysteine and glutathione concentration in the resistance to B toxicity in sunflower plants, *Plant Sci.* 165 (2003) 811–817.
- [37] A.J. Meyer, M.J. May, M. Fricker, Quantitative in vivo measurement of glutathione in *Arabidopsis* cells, *Plant J.* 27 (2001) 67–78.
- [38] G. Gutiérrez-Alcalá, C. Gotor, A.J. Meyer, M. Fricker, J.M. Vega, L.C. Romero, Glutathione biosynthesis in *Arabidopsis* trichome cell, *Proc. Natl. Acad. Sci. USA* 26 (2000) 11108–11113.
- [39] A.J. Meyer, M.D. Fricker, Direct measurement of glutathione in epidermal cells off intact *Arabidopsis* roots by two-photon laser scanning microscopy, *J. Microsc.* 198 (2000) 174–181.
- [40] M.D. Fricker, M. May, A.J. Meyer, N. Serrad, N.S. White, Measurement of glutathione levels in intact roots of *Arabidopsis*, *J. Microsc.* 198 (2000) 162–173.
- [41] T.N. Hartmann, M.D. Fricker, H. Rennenberg, A.J. Meyer, Cell-specific measurement of cytosolic glutathione in poplar leaves, *Plant Cell Environ.* 26 (2003) 965–975.
- [42] M.D. Fricker, A.J. Meyer, Confocal imaging of metabolism in vivo: pitfalls and possibilities, *J. Exp. Bot.* 52 (2001) 631–640.
- [43] R. Howden, P.B. Goldsbrough, C.R. Andersen, C.S. Cobbett, Cadmium-sensitive, *cad1* mutants of *Arabidopsis thaliana* are phytochelatin deficient, *Plant Physiol.* 107 (1995) 1059–1066.
- [44] M. Inouhe, R. Ito, S. Ito, N. Sasada, H. Tohoyama, M. Joho, Azuki bean cells are hypersensitive to cadmium and do not synthesize phytochelatin, *Plant Physiol.* 123 (2000) 1029–1036.
- [45] G. Noctor, C.H. Foyer, Simultaneous measurement of foliar glutathione, glutamylcysteine, and amino acids by high-performance liquid chromatography: Comparison with two other assay methods for glutathione, *Anal. Biochem.* 264 (1998) 98–110.
- [46] D. Potesil, J. Petrova, V. Adama, J. Vacek, B. Klejdus, J. Zehnalek, L. Trnkova, L. Havel, R. Kizek, Simultaneous femtomole determination of cysteine, reduced and oxidized glutathione, and phytochelatin in maize (*Zea mays* L.) kernels using high-performance liquid chroma-

- tography with electrochemical detection, *J. Chromatogr. A* 1084 (2005) 134–144.
- [47] M.A. Matamoros, D.A. Dalton, J. Ramos, M.R. Clemente, M.C. Rubio, M. Becana, Biochemistry and molecular biology of antioxidants in the *Rhizobia*-legume symbiosis, *Plant Physiol.* 133 (2003) 499–509.
- [48] N. Cioffi, I. Losito, R. Terzano, C.G. Zambonin, An electrospray ionization ion trap mass spectrometric (ESI-MS-MSⁿ) study of dehydroascorbic acid hydrolysis at neutral pH, *Analyst* 125 (2000) 2244–2248.
- [49] R. Rossi, A. Milzani, I. Dalle-Done, D. Giustarini, L. Lusini, R. Colombo, P. Di Simplicio, Blood glutathione disulfide: in vivo factor or in vitro artifact? *Clin. Chem.* 48 (2002) 742–753.



Stress Responses of *Zea mays* to Cadmium and Mercury

Rubén Rellán-Álvarez^{1,2}, Cristina Ortega-Villasante¹, Ana Álvarez-Fernández²,
Francisca F. del Campo¹ & Luis E. Hernández^{1,3}

¹Laboratory of Plant Physiology, Department of Biology, Universidad Autónoma of Madrid, Campus de Cantoblanco, E-28049, Madrid, Spain. ²Estación Experimental Aula Dei-CSIC Avd. Montañana 1005, 50059, Zaragoza, Spain. ³Corresponding author*

Received 30 November 2004. Accepted in revised form 15 March 2005

Key words: cadmium, heavy metal sensitivity, mercury, oxidative stress, *Zea mays*

Abstract

A hydroponic experiment was carried out to characterize the oxidative stress responses of maize seedlings (*Zea mays* L. cv. Dekalb DK604) to cadmium (Cd) and mercury (Hg). Plants were grown hydroponically for 7 days in a nutrient solution supplemented with several concentrations of Cd and Hg: 0.0 (control), 6 or 30 μM . Growth was inhibited by both metals. The effect was more severe in plants exposed to Hg. Oxidative stress was caused by the exposure to the metals, as quantified by malondialdehyde and carbonyl accumulation, by-products of lipid peroxidation and protein oxidation, respectively. The activity of ascorbate peroxidase (APX) and superoxide dismutase (SOD), enzymes involved in the scavenging of reactive oxygen species, were measured upon metal treatment. We found an activation of a cytosolic APX isoform, as identified by using a specific polyclonal antiserum. However, there were negligible changes in SOD activity. Analysis of thiol-peptides revealed that at 6 μM Cd a remarkable increase in root reduced glutathione (GSH) content occurred, and little effect on the relative content of oxidised glutathione (GSSG) was observed. However, at 30 μM Cd and in plants exposed to 6 and 30 μM of Hg, GSH root content either remained stable or decreased significantly, while the proportion of GSSG increased. Moreover, only Cd was able to induce accumulation of phytochelatin at both assayed concentrations. Apparently, Hg was more toxic than Cd, as inferred from the magnitude of the changes found in the physiological parameters tested.

Introduction

One of the major environmental problems caused by industrialisation is the increment in the concentration of heavy metals in the air, land and water (Nriagu, 1990). In particular, the area around mine facilities in Almadén (Spain) has the largest levels of environmental Hg in the world, due to the extraction and processing of Hg-mineral ore for centuries (Berzas et al., 2003). In

opposition to other metals (i.e. Cu, Zn or Mn), Hg and Cd are not essential nutrients in most higher plants, and the exposure to relative low concentrations results in serious toxicity (Salt et al., 1995). One of the clearest phytotoxic symptoms induced by heavy metals is a diminution in plant growth, which is associated with disturbance of several metabolic processes, alteration of nutrient uptake and degeneration of cell ultrastructure (Hall, 2000). Besides, the appearance of oxidative stress has been well established (Schützendübel and Polle, 2002). It is thought that accumulation of reactive oxygen species (ROS)

* FAX No: + 34 914978344.

E-mail: luise.hernandez@uam.es

increases the cellular damages through oxidation of lipids (Sandalio et al., 2001), proteins (Romero-Puertas et al., 2002) and other macromolecules (Hall, 2000), leading to an oxidative burst. Thus, there is evidence of oxidative stress after exposure of several plants to Cd (Lozano-Rodríguez et al., 1997; Schützendübel et al., 2002) and to Hg (Cho and Park, 2000). Some of these stress responses have been attributed to changes in the activities of ROS scavenging enzymes, such as superoxide dismutase (SOD) and ascorbate peroxidase (APX; for a review see Sanita di Toppi and Gabrielli, 1999). Depending on the organ sampled, the metal concentration and time of exposure, there were increases or losses in the activities of the referred enzymes, as summarized by Schützendübel and Polle (2002).

On the other hand, reduced glutathione (GSH) plays an important role in the defence against oxidative stress in plant cells, being involved in the complex enzymatic machinery that controls the intracellular levels of H_2O_2 (May et al., 1998). Changes in the amount of GSH compared with its oxidised form (GSSG) might be used as stress maker to assess acclimation of plants to their environment (Tausz et al., 2004). There are several reports showing changes in the levels of GSH and GSSG upon exposure of plants to different heavy metals (Schützendübel and Polle, 2002). A common initial response found in Cd-treated plants was a severe depletion of GSH tissue content (Dixit et al., 2001; Xiang and Oliver, 1998), which might recover after prolonged exposure (Schützendübel et al., 2001). This recovery might have been the result of increased GSH synthesis, probably through the over-expression of genes coding for enzymes of the glutathione synthetic pathway (Xiang and Oliver, 1998). Indeed, the importance of GSH to ameliorate Cd and Ni toxicity has been proved using transgenic plants overexpressing serine acetyltransferase (Freeman et al., 2004) or *o*-acetylserine(thiol)lyase (Domínguez-Solis et al., 2001) respectively, that resulted in elevated cellular levels of GSH compared to wild-type plants. Therefore, there is evidence pointing towards the implication, at least partially, of GSH in the tolerance to heavy metals. The depletion of the cellular pool of GSH in the presence of heavy metals, due to accumulation of GSSG and/or its polymerisation during phytochelatins (PCs) syn-

thesis, may result in an increase in oxidative stress symptoms (Rausser, 1991; Xiang and Oliver, 1998).

A characterisation of the oxidative burst induced upon exposure to Hg in higher plants has been described in few reports (Cho and Park, 2000), and very scarce data are available about the content of GSH and GSSG. It is well known the affinity of Hg^{2+} for thiol residues in proteins and peptides (Woolhouse, 1983), which might affect the levels of GSH/GSSG in plant tissues. The aim of the present work was to study physiological responses of maize seedlings to Hg, and compare them with those induced by Cd, a toxic element recurrently described in the literature. In particular, we considered very attractive to examine the relationship between oxidative stress and the depletion of GSH due to its oxidation to GSSG or the synthesis of PCs. According to our preliminary experience, these metals caused distinct phytotoxic effects in maize and pea plants (Lozano-Rodríguez et al., 1997; Hernández et al., 1998). Several oxidative stress indexes and ROS scavenging enzymes were evaluated, as well as changes in GSH, GSSG and other related non-protein thiols.

Materials and methods

Plant material

Maize (*Zea mays* cv. Dekalb DK604) seedlings were cultivated hydroponically as described in detail by Lozano-Rodríguez et al. (1997), using the following nutrient solution adjusted to pH 6.0: 2.0 mM $Ca(NO_3)_2$, 1.5 mM KNO_3 , 1 mM $Mg(NO_3)_2$, 1.0 mM KH_2PO_4 , 0.5 mM $MgSO_4$, 0.1 mM NaCl, 90 μM Fe-EDDHA, 23.5 μM H_3BO_3 , 18 μM $MnSO_4$, 6 μM $CuSO_4$, 3 μM $ZnSO_4$, and 2 μM $(NH_4)_6Mo_7O_{24}$. Seedlings were kept in a long-day photoperiod (200 $\mu mol/m^2s$; 16 h light/8 h darkness) at 25/18 °C, respectively. After 3 days of germination, selected seedlings grew for 5 days in control nutrient solution, and then were transferred to a nutrient solution supplied with Cd and Hg at three concentrations: 0.0 (control), 6 and 30 μM . Hypothetical speciation of both heavy metals in the nutrient solution was carried out by using Visual MINTEQ version 2.30 software with Lindsay's databases

(Gustafsson JP, Dept. of Land and Water Resources Engineering, KTH Stockholm, Sweden). The concentrations calculated for Hg^{2+} were 6 and 30 μM , and for Cd^{2+} were 5.4 and 27.0 μM . Shoots and roots of maize were collected after 7 days treatment, frozen in liquid N_2 and stored at -80°C until analysis.

Analysis of cadmium and mercury

All samples were acid-digested prior to Cd and Hg analysis. Approximately 0.2 g of frozen ground tissue were placed in a boron-silicate chromatographic vial with 4 mL of capacity (capped with Teflon stoppers for digestion), and dried at 60°C for 48 h. After determination of exact dry weight, samples were digested in autoclave (Presoclave-75, Selecta, Spain) for 30 min at 125°C , $24.5 \times 10^4 \text{ N m}^{-2}$, with an acid oxidative mixture $\text{H}_2\text{O}:\text{HNO}_3:\text{H}_2\text{O}_2$ (0.5:0.3:0.2, mL). The volume of the digests was adjusted to 10 mL following filtration. Cd concentration was measured by atomic absorption spectrometry with a hollow cathode Cd lamp using air-acetylene flame ionisation (Perkin Elmer 4000). Hg was also analysed by atomic absorption spectrophotometry using the same spectrophotometer with a hollow cathode Hg lamp, which was equipped with a cold vapour chamber and a NaBH_4 reduction reactor (Perkin Elmer MHS-20).

Lipid peroxidation assay

Lipid peroxidation was quantified as accumulation of the by-product malondialdehyde (MDA), according to Buege and Aust (1978). Prior to analysis, the frozen sample was ground in liquid N_2 . 0.1 g of the powder was then homogenised in 1.0 mL of MDA reagent (15% w/v trichloroacetic acid, 0.37% w/v 2-thiobarbituric acid and 0.25 M HCl), and incubated at 90°C for 30 min. The supernatant was clarified by centrifugation at $12,000 \times g$ for 15 min, the absorbance read at 535 nm, and concentration calculated from the extinction coefficient of $1.56 \times 10^5 \text{ M}^{-1} \text{ cm}^{-1}$.

Protein oxidation

Carbonyl content was measured after protein extraction as described by Romero-Puertas et al.

(2002), with minor modifications. After incubation with 10 mM dinitrophenylhydrazine, proteins were precipitated with 20% TCA, washed with 10% H_2O in ethanol:ethyl acetate (1:1, v/v), and the pellet disrupted. The suspension was clarified by centrifugation at $12,000 \times g$ for 5 min prior to absorbance determination at 370 nm (carbonyl concentration) and at 280 nm (total protein concentration).

APX and SOD activities in non-denaturing gels and Western-blot

After grinding the frozen samples in liquid N_2 , 1 g of the powder was used to prepare an enzymatic extract with 2 mL of extraction buffer (30 mM MOPS, 5 mM Na-EDTA, 10 mM DTT, 10 mM ascorbate, 0.6% (w/v) PVP at pH 7.5), supplemented in fresh with 25 μL 0.1 M PMSF and 50 μL proteinase inhibitor cocktail (SIGMA, USA). To maintain the integrity of APX, special care was taken to add ascorbate in all extraction steps, keeping also all material at 4°C . The homogenate was filtered and centrifuged ($14,000 \times g$ for 15 min at 4°C), and the supernatant was stored at -80°C in several single-use aliquots. Protein concentration of extracts was determined (Protein Assay; BioRad, USA) to load identical amounts of protein in native PAGE (10% and 12% acrylamide for APX and SOD, respectively).

For APX (EC 1.11.1.11) detection, 50 μg protein was separated by electrophoresis following essentially the protocol described by Jiménez et al. (1998). After incubation of gels with 4 mM ascorbate and 2 mM H_2O_2 in 50 mM Na-phosphate buffer at pH 7.0 for 20 min, the presence of APX was detected in the presence of 0.5 mM nitroblue tetrazolium (NBT) and 10 mM TEMED in 50 mM phosphate at pH 7.8. For SOD (EC 1.15.1.1) detection, a similar procedure was followed, although ascorbate was avoided in PAGE-native separation of proteins and subsequent incubations. SOD was detected following the procedure described by Beauchamp and Fridovich (1971), after incubating the gels with 1.25 mM NBT. O_2^- was produced *in situ* by the photooxidation reaction of 50 μM riboflavin in the presence of 55 mM methionine in 50 mM Na-phosphate at pH 7.8.

To identify the bands in the native PAGE observed after *in gel* APX activity, we performed a Western-blot assay using a specific anti-cytosolic APX polyclonal antiserum (Dalton et al., 1996). Following APX staining, gels were incubated for 30 min in semi-dry electroblotting transfer buffer (50 mM Tris-HCl, 40 mM glycine, 1.5 mM SDS, 20% methanol, pH 8.4), and electrotransferred onto a nitrocellulose membrane (Pall, USA) using a Semi-dry Trans Blot SD (Bio Rad, USA), following standard procedures and under the conditions established by the manufacturer. The bonafide of the transfer was analysed by Ponceu's staining (0.2% Ponceau S in 1% acetic acid). The membrane was blocked with 1% BSA in TBS, and incubated overnight with the anti-cytosolic APX antibody (diluted 1/2000). A second incubation was performed with an alkaline phosphatase-conjugated secondary goat anti-rabbit antibody (Sigma, USA; diluted 1/2000), and the immunolabelled protein bands were revealed following standard protocols (Ausubel et al. 1987).

Images obtained were subjected to densitometric semi-quantification to determine changes in band intensity. Scanned images (ScanJet 3300C Hewlett Packard, USA) or pictures taken using a digital camera (Kodak 290, USA) were processed by using the Kodak 1D Image Analysis Software ver. 3.6. Regions of interest (ROIs) were of identical surface and pixel intensity was adjusted to the background. Data are given relative to the intensity of control samples.

Non-protein thiols analysis by HPLC

Prior to extraction of non-protein thiols, the plant tissue was ground in liquid N₂. It is important to avoid prolonged storage of ground frozen samples at -80 °C, since we have observed alterations in the GSH pool by using spikes of thiols added to the samples. 100 mg of the frozen powder was thoroughly mixed with 300 µL of 0.25 N HCl, and a spike of N-acetyl cysteine was added as internal standard (50 µM final concentration). After centrifugation (12,000 × g, 15 min and at 4 °C), the clear extract was injected to a PLRP-S C18 polymer column (250 × 4.6 mm; Polymer Laboratories, U.K.), and eluted according to Meuwly et al. (1995), using the following gradi-

ent program (as for % solvent B): 2 min, 0%; 25 min, 25%; 26 min, 50%; 30 min, 50%; 35 min, 0%; 45 min, 0%; in an Alliance 2695 HPLC system (Waters, USA). Solvent A was 2:98 acetonitrile:H₂O (v/v) plus 0.01% TFA, and solvent B 98:2 acetonitrile:H₂O (v/v) plus 0.01% TFA. Detection was achieved after post-column derivatisation with Ellman's reagent, as described by Rauser (1991), and absorbance was measured at 412 nm. Non-protein thiols were quantified after integration of the peak area against that of the internal standard of N-acetyl cysteine. Identity of cysteine and GSH peaks was achieved by using commercially available standards.

The degree of GSSG was analysed by HPLC coupled to electrospray-mass spectrometry (HPLC-ESI/MS-TOF; Rellán-Álvarez et al., 2005). 100–500 mg of frozen tissue was homogenized in 200–1000 µL of chilled extraction solution (5% meta-phosphoric acid, 1 mM EDTA and 1% polyvinylpyrrolidone in 0.1% formic acid). After centrifugation (15,000 × g, 20 min at 4 °C) the supernatant was filtered through 0.22 µm polyvinylidene fluoride (PVDF) filters, and conserved at -80°C until further analysis. 20 µL of filtered sample were injected onto a Chromolith column (4.6 × 100 mm; Merck, Germany), and eluted (flux of 1 mL/min) with the following linear gradient program (as for % solvent B): 5 min, 10%; 6 min, 50%; 9 min, 50%; 11 min, 0%; 15 min, 0%, in an Alliance 2795 HPLC system (Waters, USA). Solvent A consisted of 0.1% formic acid in Milli-Q water and solvent B of 0.1% formic acid in acetonitrile. After ionisation with an Apollo electrospray ionisation source (ESI), GSH and GSSG ions were detected in a time of flight mass spectrometer (BioTOF II Bruker Daltonics, USA), operated at 2.8 kV of end-plate and at 3.3 kV spray tip potentials in negative ion mode. Identification of peaks corresponding to GSH and GSSG was achieved using commercially available standards. Data of GSSG were calculated as a percentage of total glutathione (GSH + GSSG).

Statistics

One-way analysis of variance was performed using the statistic software SPSS 11.0. Results were expressed as the mean ± S.D. unless noted

otherwise, and the value of $p < 0.05$ was considered significant.

Results and discussion

Growth inhibition, analyses of oxidative stress indexes and heavy metal content

Plants subjected to exposure to Cd and Hg suffered clear symptoms of phytotoxicity, as the fresh weight of shoot and root decreased significantly (Table 1). Similar diminution of organ growth was reported for Cd- (Guo et al., 2004; Sandalio et al., 2001; Schützendübel et al. 2001) and Hg-treated plants (Cho and Park, 2000). In parallel, Cd and Hg accumulated in plant organs at increasing levels concomitantly with the metal concentrations in the nutrient solution (Table 1). Higher proportion of metals was found in roots than in shoots. Thus, in plantlets exposed to metal concentrations of 6 and 30 μM the ratio of metal accumulated in roots to shoots was respectively: for Cd, about 35 and 35, and for Hg, 115 and 300. Therefore, little Cd and even less Hg were transferred to the aerial part of the plants. We also calculated the ratio of the metals that accumulated respectively in shoots and roots (Hg vs. Cd; Table 1). Interestingly, in roots Hg accumulated 2.3 and 3.8 times more than Cd, when supplied respectively at 6 and 30 μM . However, in shoots the ratio was 0.7 at both treatment concentrations. On the other hand, hypothetical speciation of Cd and Hg in the nutrient solution revealed that only Cd^{2+} had a slightly lower concentration than expected: 5.4 μM instead of 6 μM , and 27.0 μM instead of 30 μM . This

meant that the ratio of Hg^{2+} to Cd^{2+} concentration in the nutrient solution was 1.1. Taken together our data, lead to conclude that Hg accumulated in roots at a remarkably higher level than Cd, over the ratio of soluble cations concentration in the nutrient solution.

The inhibition of growth was accompanied by an increase in lipid peroxidation (MDA content) and protein oxidation (carbonyl content) as a result of an oxidative stress (Table 2). Similar responses have been described for MDA in maize (Lozano-Rodríguez et al., 1997), pea (Dixit et al., 2001; Sandalio et al., 2001), poplar (Schützendübel et al., 2002) and barley (Guo et al., 2004) under Cd exposure; and in tomato (Cho and Park, 2000) under Hg treatment. Some differences were observed with respect to the toxic effect caused and tissue susceptibility. In shoots, lipid peroxidation was clearly induced by both metals, but the effect of Cd was more pronounced than that for Hg. In roots, both metals caused a limited, yet significant rise of lipid peroxidation (Table 2). Protein oxidation was also enhanced by both Cd and Hg in roots and shoots. However, the effect of Hg was always larger than that of Cd. In particular, there was a remarkable carbonyl accumulation in plants exposed to 30 μM Hg, indicating an acute stress oxidation. The distinct action of each metal could be due to the different chemical properties and/or to the different rate of accumulation in plant tissues.

Ascorbate peroxidase and superoxide dismutase activities

Several authors have highlighted the activation of ROS scavenging systems to ameliorate the

Table 1. Fresh weight (g/plant) and tissue concentration of heavy metals ($\mu\text{mol/g}$ DW) in shoot and root from maize plants treated with Cd and Hg at the following concentrations (μM): 0.0 (control), 6 and 30 ($n = 5$) \pm SD

Treatment	Fresh weight (g/plant)		Concentration of Cd ($\mu\text{mol/g}$ DW)		Concentration of Hg ($\mu\text{mol/g}$ DW)		Estimated Hg to Cd ratio	
	Shoot	Root	Shoot	Root	Shoot	Root	Shoot	Root
Control	0.83 \pm 0.10 a	0.47 \pm 0.08 a	n.d.*	n.d.	n.d.	n.d.		
6 μM Cd	0.72 \pm 0.08 b	0.45 \pm 0.05 a	0.11 \pm 0.01 a	4.09 \pm 1.20 a				
30 μM Cd	0.47 \pm 0.10 c	0.35 \pm 0.07 b	0.43 \pm 0.14 b	23.45 \pm 2.57 b				
6 μM Hg	0.44 \pm 0.08 c	0.27 \pm 0.04 c			0.08 \pm 0.03 a	9.22 \pm 0.17 a	0.7	2.3
30 μM Hg	0.38 \pm 0.05 c	0.24 \pm 0.05 c			0.29 \pm 0.05 b	89.65 \pm 5.11 b	0.7	3.8

*n.d. Not detected, below limit of sensitivity.

Values carrying different letters were significantly different at $p < 0.05$.

Table 2. Lipid peroxidation (nmol MDA/gFW) and protein oxidation (nmol carbonyl/mg total protein) in maize plants treated with Cd and Hg at the following concentrations (μM): 0.0 (control), 6 and 30 ($n = 3$) \pm SD

	Lipid peroxidation		Protein oxidation	
	Shoot	Root	Shoot	Root
Control	14.66 \pm 1.12 <i>a</i>	6.58 \pm 0.41 <i>a</i>	1.71 \pm 0.54 <i>a</i>	7.14 \pm 0.85 <i>a</i>
6 μM Cd	32.60 \pm 3.34 <i>c</i>	10.98 \pm 1.09 <i>b</i>	3.78 \pm 0.84 <i>b</i>	9.21 \pm 0.90 <i>b</i>
30 μM Cd	45.40 \pm 7.36 <i>c</i>	11.95 \pm 0.61 <i>b</i>	3.23 \pm 0.28 <i>b</i>	13.19 \pm 0.85 <i>c</i>
6 μM Hg	19.26 \pm 2.55 <i>b</i>	9.72 \pm 1.24 <i>b</i>	4.04 \pm 1.05 <i>b</i>	10.58 \pm 2.78 <i>b</i>
30 μM Hg	33.62 \pm 4.94 <i>c</i>	12.30 \pm 0.28 <i>b</i>	7.07 \pm 1.01 <i>c</i>	23.84 \pm 4.85 <i>d</i>

Values carrying different letters were significantly different at $p < 0.05$.

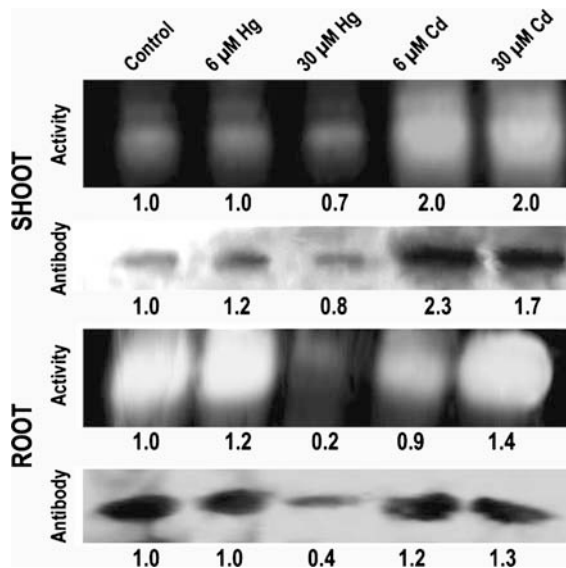


Figure 1. APX activity and Western-blotting of extracts prepared from shoot and root of maize treated with Cd and Hg at the following concentrations: 0 (control), 6 and 30 μM . A representative gel is shown out of least three replicates. Data underneath each band represent pixel intensity relative to control samples.

oxidative burst induced upon exposure of plants to heavy metals. APX, SOD, catalase, and other enzymes had been assessed under various metal concentrations (Schützendübel and Polle, 2002). In maize, by using an *in gel* approach, we analysed APX and SOD activities and found changes in response to increasing concentrations of Cd and Hg (Figures 1 and 2). APX staining resulted in a major colourless band. Western-blot analysis revealed that this major band corresponded to a cytosolic APX isoform, as we used a specific polyclonal antibody (Dalton et al., 1996). When plants were exposed to Cd, shoot APX activity

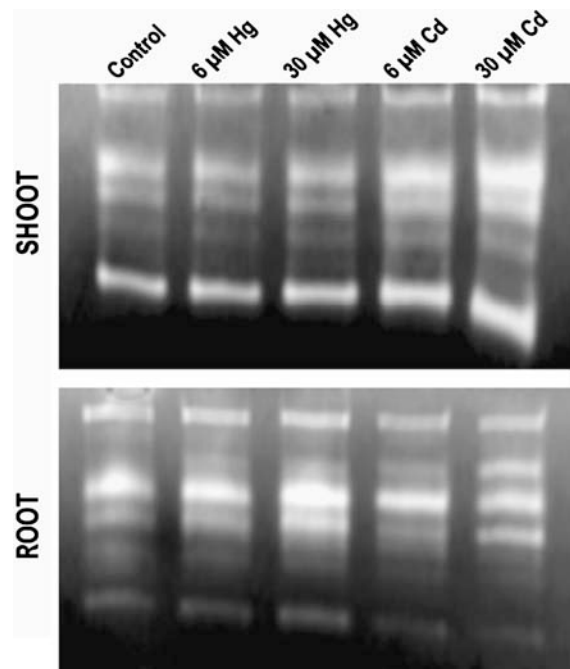


Figure 2. SOD activity of extracts prepared from shoot and root of maize treated with Cd and Hg at the following concentrations: 0 (control), 6 and 30 μM . A representative gel is shown out of least three replicates.

increased, probably due to an increase in cytosolic APX, as visualised by Western-blot. However, APX activity decreased in the presence of 30 μM Hg, the decrease being related to a diminution of cytosolic APX protein (Figure 1). Higher activity was observed in roots than in shoots, but there was a sharp activity loss in the presence of 30 μM Hg. Again, that decrease in activity was concomitant with a diminution of APX cytosolic protein. This decline is in agreement with the high degree of protein oxidation observed in those samples (Table 2), and might

reflect an extreme toxic damage. High concentration of Cd (up to 50 μM) also caused depletion of several enzymes in pea leaf extracts, with a simultaneous increase of protein oxidation (Romero-Puertas et al., 2002). Indeed, a similar pattern in total peroxidase activity has been reported for maize (Lagriffoul et al., 1998), poplar (Schützendübel et al., 2002) and pea (Dixit et al., 2001) under Cd stress. It is conceivable that at mild stress conditions, plants respond by increasing APX activity, but under extreme toxicity a general failure of the metabolism causes its attenuation (Schützendübel et al., 2001, 2002). These effects could be also related to the amount of metals that accumulated differentially in the analysed tissues, at a much higher extent in roots than in shoots (Table 1).

On the other hand, SOD activity was not apparently affected by any of the metals, as no consistent effect related to the treatments with Cd or Hg appeared (Figure 2). The small activity changes were similar for all the enzyme isoforms present in each extract, indicating that those changes were due to protein loading, in spite of having tried to adjust protein concentration by using the Coomassie blue reagent. Several authors observed similar lack of response of SOD in Cd-treated Scots pine seedlings (Schützendübel et al., 2001). Besides, in leaves of pea plants exposed to concentrations of Cd over 40 μM only a diminution in SOD activity was reported, when plants suffered acute damage (Sandalio et al., 2001). In addition, Cho and Park (2000) found that SOD activity increased slightly in tomato seedlings exposed for 10 and 20 days to 10 and 50 μM Hg. Therefore, non-consistent changes in SOD activity might be observed upon exposure to Cd and Hg, as inferred from the data reported in the literature and our own results (Figure 2).

Non-protein thiols concentration

GSH and other non-protein thiols are known to be affected by the presence of several metals (Xiang and Oliver, 1998). Apart from being an essential metabolite in the cellular redox homeostasis (Noctor et al., 2002), GSH is the assembling block of phytochelatins (PCs), a family of cysteine-rich peptides that accumulate under metal exposure (Rauser, 1991). In the presence of

Cd and Hg, the thiol-peptide pattern was altered (Figure 3). New thiol peaks appeared at longer retention time only in Cd-treated maize seedlings (Figure 3B). We have tentatively identified these peaks as corresponding to PCs, according to the retention time of the thiols accumulated upon Cd exposure in maize tissues using a similar chromatographic separation procedure (Meuwly et al., 1995). Moreover, maize plants subjected to prolonged treatment with 30 μM Cd (over 7 days) showed larger peaks of non-protein thiols in root extracts with identical chromatographic properties (data not shown), as it appears to be a typical response to Cd (Rauser, 1991). In

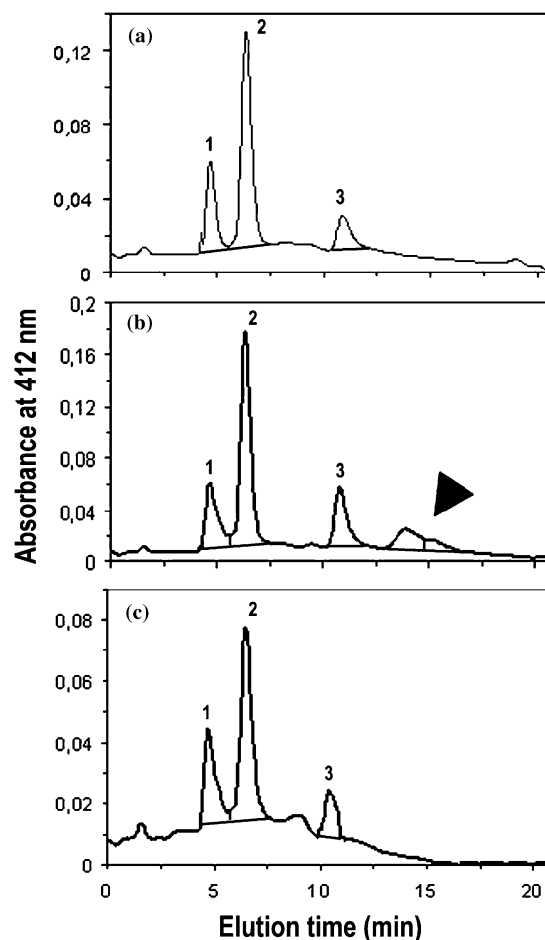


Figure 3. HPLC elution of thiol-peptides extracted from roots of maize treated with control (a), 30 μM Cd (b) and 30 μM Hg (c). 1. Cysteine; 2. GSH and 3. N-acetyl cysteine (internal standard). The solid black arrow indicates the appearance of putative Cd-induced phytochelatins, which were integrated as a unique peak.

Table 3. Thiol-peptide concentration (nmol N-acetyl cysteine/gFW) and percentage of GSSG vs. total content of GSH (%) in maize plants treated with Cd and Hg at the following concentrations (μM): 0.0 (control), 6 and 30 ($n = 3$) \pm SD

	Shoot				Root			
	Cys	GSH	PCs	%GSSG	Cys	GSH	PCs	%GSSG
Control	14.9 \pm 3.9 a	202.3 \pm 27.0 a	n.d.	29.5 \pm 0.1 a	47.3 \pm 21.8 a	206.8 \pm 44.7 a	n.d.	2.3 \pm 0.3 a
6 μM Cd	18.7 \pm 5.7 a	186.1 \pm 44.0 a	n.d.	31.7 \pm 1.5 a	96.0 \pm 39.2 ab	385.2 \pm 53.7 b	12.7 \pm 4.8 a	2.5 \pm 0.4 a
30 μM Cd	36.9 \pm 5.3 b	383.2 \pm 16.6 b	12.2 \pm 0.7 a	28.4 \pm 0.4 a	58.9 \pm 36.0 a	138.8 \pm 48.2 c	37.9 \pm 6.7 b	3.3 \pm 0.7 b
6 μM Hg	14.4 \pm 5.2 a	155.1 \pm 8.8 c	7.6 \pm 4.4 a	27.5 \pm 2.3 a	78.9 \pm 41.2 ab	205.7 \pm 10.0 a	< 2.5	4.9 \pm 0.8 c
30 μM Hg	19.2 \pm 6.8 a	243.3 \pm 46.1 a	< 2.5	24.4 \pm 7.2 a	188.9 \pm 26.6 c	149.5 \pm 25.0 c	n.d.	7.6 \pm 1.4 d

*n.d.: not detected.

Values carrying different letters were significantly different at $p < 0.05$.

addition, lower amount of Cd-induced thiols was observed in shoot extract only at the highest concentration of Cd (Table 3). Under Hg stress, we could not detect peaks corresponding to PCs (Figure 3C). Only in the shoot of plants exposed to 6 μM Hg, we could detect a minor peak at the same elution time as shown for Cd-treated maize (Table 3). Our findings agree with the known poor capability of Hg as a PCs synthesis inductor, as has been observed *in vitro* with recombinant phytochelatin synthase (Ha et al., 1999) or *in vivo* (Maitani et al., 1996). Therefore, it is possible the PCs might play a side role in Hg detoxification in maize seedlings.

On the other hand, GSH concentration varied depending on the metal concentration and the tissue analysed. In the shoot, GSH concentration augmented only at the highest concentration of metal supplied, being Cd a stronger inductor than Hg (Table 3). However, this effect was not accompanied with any significant change in the percentage of GSSG. A similar increment in GSH content was only found in roots of maize treated with 6 μM Cd, while in plants exposed to 6 μM Hg there were no changes. Plants grown in 30 μM of Hg or Cd showed a significant diminution of GSH in roots, which was concomitant with an increase in the percentage of GSSG (Table 3). Apparently, there was a rise under mild toxicity, but it declined when plants suffered acute stress (i.e. in roots of plants given 30 μM). These effects were also accompanied by an increase in the content of cysteine only in the root of plants exposed to 30 μM Hg (Table 3), tissue that showed low concentration of GSH and high GSSG percentage. Our results suggest that GSH might have been accumulated in mild stressed

plants, according to the reported increases to levels above those of controls, which is common in prolonged Cd-exposure (Schützendübel et al., 2001; Vöeli-Lange and Wagner, 1996; Xiang and Oliver, 1998). However, above a certain toxicity threshold the metabolism is unable to attain the putative demand of GSH to keep redox homeostasis under control. In fact, when plants showed higher oxidative stress symptoms in the root upon 30 μM Hg treatment, the proportion of GSSG in root was almost three times that of control plants (Table 3). These results indicate that redox GSH/GSSG homeostasis was only compromised in tissues and organs that were severely affected, in agreement with Xiang and Oliver (1998).

Conclusions

Hg showed a stronger toxic effect than Cd in the root of maize seedlings, as inferred from the found higher proportion of GSSG, enhanced carbonyl content and the negative effects on growth. Similarly, it was also observed that accumulation and activity of the cytosolic APX was severely affected in plants exposed to 30 μM Hg. Under this acute stress conditions, the pool of GSH was reduced, clearly indicating that cellular homeostasis might have been compromised. Only under mild stress, plants could probably acclimate and adjust its metabolism accordingly. It is possible that the higher phytotoxicity caused by Hg might be partially associated to its higher accumulation in the root. In future work, it is important to establish the thresholds of toxicity, either by lowering the metal doses or reducing the exposure

times. Characterisation of the cellular components interacting with the metals might also help to determine different mechanisms underlying metal toxicity and to understand the way plants can cope with those stress conditions.

Acknowledgments

We gratefully appreciate the comments and always helpful discussions of Dr Ramón Carpena-Ruiz (Química Agrícola-UAM, Madrid, Spain). We thank Dr David Dalton (Reed College, Portland, USA) for the donation of the soybean APX cytosolic antibody. We acknowledge funding from the Spanish Ministry of Education and Science (REN2001-113-C01-02 and REN2002-04229-C02-01). R.R.A. recognises the funding from UAM, through a PhD Student Exchange Program grant.

References

- Ausubel F M, Brent R, Kingston R E, Moore D D, Seidman J G, Smith J A and Struhl K 1987 Current Protocols in Molecular Biology. John Wiley and Sons, Inc., USA..
- Beauchamp C O and Fridovich I. 1971 Superoxide dismutase: improved assays and an assay applicable to acrylamide gels. *Anal. Biochem.* 44, 276–287.
- Berzas J L, García L F and Rodríguez R C 2003 Distribution of mercury in the aquatic environment at Almadén, Spain. *Environ. Poll.* 122, 261–271.
- Buege J A and Aust S D 1978 Microsomal lipid peroxidation. *Methods Enzymol.* 52, 302–310.
- Cho U H and Park J O 2000 Mercury-induced oxidative stress in tomato seedlings. *Plant Sci.* 156, 1–9.
- Cobbett C and Goldsbrough P 2002 Phytochelatins and metallothioneins: roles in heavy metal detoxification and homeostasis. *Ann. Rev. Plant Biol.* 53, 159–182.
- Dalton D A, Díaz-Castillo L, Kahn M L, Joyner S L and Chatfield J M 1996 Heterologous expression and characterisation of soybean cytosolic ascorbate peroxidase. *Arch. Biochem. Biophys.* 328, 1–8.
- Domínguez-Solís J R, Gutiérrez-Alcalá G, Vega J M, Romero L C and Gotor C 2001 The cytosolic O-acetylserine(tilo)lyase gene is regulated by heavy metals and can function in cadmium tolerance. *J. Biol. Chem.* 276, 9297–9302.
- Dixit V, Pandey V and Shyam R 2001 Differential antioxidative responses to cadmium in roots and leaves of pea (*Pisum sativum* L. cv. Azad). *J. Exp. Bot.* 52, 1101–1109.
- Freeman J L, Persans M W, Nieman K, Albrecht C, Peer W, Pickering I J and Salt D E 2004 Increased glutathione biosynthesis play a role in nickel tolerance in *Thlaspi* nickel hyperaccumulators. *Plant Cell* 16, 2176–2191.
- Guo T, Zhang G, Zhou M, Wu F and Chen J 2004 Effects of aluminium and cadmium toxicity on growth and antioxidant enzyme activities of two barley genotypes with different Al resistance. *Plant Soil* 258, 241–248.
- Ha S B, Smith A P, Howden R, Dietrich W M, Bugg S, O'Connell M J, Goldsbrough P B and Cobbett C S 1999 Phytochelatins synthase genes from *Arabidopsis* and the yeast *Schizosaccharomyces pombe*. *Plant Cell* 11, 1153–1164.
- Hall J L 2000 Cellular mechanisms for heavy metal detoxification and tolerance. *J. Exp. Bot.* 53, 1–11.
- Hernández L E, Lozano-Rodríguez E, Bonay P and Carpena-Ruiz R O 1998 Fraccionamiento subcelular de Hg en raíz y parte aérea de plantas de maíz y guisante. *In* Nutrición y Producción: VII Simposio Nacional sobre Nutrición Mineral de las Plantas. Ed. Gárate A. pp. 453–458. Madrid.
- Jiménez A, Hernández J A, Ros-Barceló A, Sandalio L M, Río L A del and Sevilla F 1998 Mitochondrial and peroxisomal ascorbate peroxidase of pea leaves. *Physiol. Planta* 104, 687–692.
- Lagriffoul A, Mocquot B, Mench M and Vangronsveld J 1998 Cadmium toxicity effects on growth, mineral and chlorophyll contents, and activities of stress related enzymes in young maize plants (*Zea mays* L.). *Plant Soil* 200, 241–250.
- Lozano-Rodríguez E, Hernández L E, Bonay P and Carpena-Ruiz R O 1997 Distribution of cadmium in shoot and root tissues of maize and pea plants: physiological disturbances. *J. Exp. Bot.* 48, 123–128.
- Maitani T, Kubota H, Sato K and Yamada T 1996 The composition of metals bound to class III metallothionein (phytochelatins and its desglycyl peptide) induced by various metals in root cultures of *Rubia tinctorum*. *Plant Physiol.* 110, 1145–1150.
- May M J, Vernoux T, Leaver C, Montagu M Van and Inzé D 1998 Glutathione homeostasis in plants: implications for environmental sensing and plant development. *J. Exp. Bot.* 49, 649–667.
- Meuwly P, Thibault P, Schwan A L and Rauser W E 1995 Three families of thiol peptides are induced by cadmium in maize. *Plant J.* 7, 391–400.
- Noctor G, Gómez L, Vanacker H and Foyer C H 2002 Interactions between biosynthesis, compartmentation and transport in the control of glutathione homeostasis and signalling. *J. Exp. Bot.* 53, 1283–1304.
- Nriagu J O 1990 Global metal pollution *Environment* 32, 7–33.
- Rauser W E 1991 Cadmium-binding peptides from plants. *Methods Enzymol.* 205, 319–333.
- Rellán-Álvarez R, Hernández L E, Abadía J and Álvarez-Fernández A 2005 Direct and simultaneous determination of reduced and oxidised glutathione by liquid chromatography/electrospray/mass spectrometry in plant tissues. *Anal. Biochem.* (submitted).
- Romero-Puertas M C, Palma J M, Gómez M, Río L A del and Sandalio L M 2002 Cadmium causes the oxidative modification of proteins in pea plants. *Plant Cell Environ.* 25, 677–686.
- Salt D E, Blaylock M, Kumar N P B A, Dushenkov V, Ensley B D, Chet I and Raskin I 1995 Phytoremediation: a novel strategy for the removal of toxic metals from the environment using plants. *Biotechnology* 13, 468–474.
- Sanita di Toppi L and Gabbriellini R 1999 Response to cadmium in higher plants. *Environ. Exp. Bot.* 41, 105–130.
- Sandalio L M, Dalurzo H C, Gomez M, Romero-Puertas M C and Río L A del 2001 Cadmium-induced changes in the

- growth and oxidative metabolism of pea plants. *J. Exp. Bot.* 52, 2115–2126.
- Schützendübel A, Schwanz P, Teichmann T, Gross K, Langenfeld-Heuser R, Godbold D L and Polle A 2001 Cadmium changes in antioxidative systems, hydrogen peroxide content, and differentiation in Scots pine roots. *Plant Physiol.* 127, 887–898.
- Schützendübel A, Nikolova P, Rudolf C and Polle A 2002 Cadmium and H₂O₂-induced oxidative stress in *Populus x canescens* roots. *Plant Physiol. Biochem.* 40, 577–584.
- Schützendübel A and Polle A 2002 Plant responses to abiotic stresses: heavy metal-induced oxidative stress and protection by micorrhization. *J. Exp. Bot.* 53, 1351–1365.
- Tausz M, Sircelj H and Grill D 2004 The glutathione system as a stress marker in plant ecophysiology: is a stress-response concept valid? *J. Exp. Bot.* 55, 1955–1962.
- Vögeli-Lange R and Wagner G W 1996 Relationship between cadmium, glutathione and cadmium-binding peptides (phytochelatins) in leaves of intact tobacco seedlings. *Plant Sci.* 114, 11–18.
- Woolhouse H W 1983 Toxicity and tolerance in the responses of plants to metals. *In* *Physiological Plant Ecology III. Encyclopaedia of Plant Physiology Vol. 12C*. Eds. O L Lange, P S Nobel, C B Osmond and H Ziegler. Springer-Verlag, 246–300.
- Xiang C and Oliver D J 1998 Glutathione metabolic genes coordinately respond to heavy metals and jasmonic acid in *Arabidopsis*. *Plant Cell* 10, 1539–1550.

ANEX II
OTHER COLLABORATION ARTICLES

Other collaboration articles

1- Ortega-Villasante C, **Rellán-Álvarez R**, Del Campo FF, Carpena-Ruiz RO, Hernández LE. (2005) Cellular damage induced by cadmium and mercury in *Medicago sativa*. **Journal of Experimental Botany**. 56 (418): 2239-2251.

Abstract:

Alfalfa (*Medicago sativa*) plantlets were exposed to Cd or Hg to study the kinetics of diverse stress indexes. In the so-called beaker-size hydroponic system, plantlets were grown in 30 IM of Cd or Hg for 7 d. Oxidative stress took place and increased over time, a linear response being observed with Cd but not with Hg. To improve the sensitivity of the stress assays used, a micro-assay system, in which seedlings were exposed for 24 h, was developed. Phytotoxicity of metals, quantified as growth inhibition, was observed well before there was any change in the non-protein thiol tissue concentration. When measured with conventional techniques, oxidative stress indexes did not show significant variation. To trace early and small plant responses to Cd and Hg, a microscopic analysis with novel fluorescent dyes, which had not yet been exploited to any significant extent for use in plants, was conducted. These fluorescent probes, which allowed minute cellular responses to 0, 3, 10, and 30 IM of both metals to be visualized in the roots of the alfalfa seedlings, were: (i) 29,79-dichlorofluorescein diacetate that labels peroxides; (ii) monochlorobimane that stains reduced glutathione/ homogluthathione (GSH/hGSH); and (iii) propidium iodide that marks nuclei of dead cells. Oxidative stress and cell death increased after exposure for 6–24 h to Cd and Hg, but labelling of GSH/hGSH decreased acutely. This diminution might be the result of direct interaction of GSH/hGSH with both Cd and Hg, as inferred from an in vitro conjugation assay. Therefore, both Cd and Hg not only compromised severely the cellular redox homeostasis, but also caused cell necrosis. In plants treated with 1 mM L-buthionine sulphoximine, a potent inhibitor of GSH/hGSH synthesis, only the oxidative stress symptoms appeared, indicating that the depletion of the GSH/ hGSH pool was not sufficient to promote cell death, and that other phytotoxic mechanisms might be involved.

2- Ortega-Villasante C, Hernández LE, **Rellán-Álvarez R**, Del Campo FF, Carpena-Ruiz RO. (2007) Rapid alteration of cellular redox homeostasis upon exposure to cadmium and mercury in alfalfa seedlings. **New Phytologist.**, 176 (1): 96-107.

Abstract:

-Here, the kinetics of oxidative stress responses of alfalfa (*Medicago sativa*) seedlings to cadmium (Cd) and mercury (Hg) (0, 3, 10 and 30 μ M) exposure, expanding from a few minutes to 24 h, were studied. • Intracellular oxidative stress was analysed using 2',7'-dichlorofluorescein diacetate and extracellular hydrogen peroxide (H₂O₂) production was studied with Amplex Red. Growth inhibition, concentrations of ascorbate, glutathione (GSH), homogluthathione (hGSH), Cd and Hg, ascorbate peroxidase (APX) activity, and expression of genes related to GSH metabolism were also determined.

-Both Cd and Hg increased cellular reactive oxygen species (ROS) production and extracellular H₂O₂ formation, but in different ways. The increase was mild and slow with Cd, but more rapid and transient with Hg. Hg treatments also caused a higher cell death rate, significant oxidation of hGSH, as well as increased APX activity and transient overexpression of glutathione reductase 2, glutamylcysteinyl synthetase, and homogluthathione synthetase genes. However, Cd caused minor alterations. Hg accumulation was one order of magnitude higher than Cd accumulation.

-The different kinetics of early physiological responses in vivo to Cd and Hg might be relevant to the characterization of their mechanisms of toxicity. Thus, high accumulation of Hg might explain the metabolism poisoning observed in Hg-treated seedlings.

3- Martí MC, Camejo D, Fernández-García N, **Rellán-Álvarez R**, Marques S, Sevilla F, Jiménez A, Effect of oil refinery sludges on the growth and antioxidant system of alfalfa plants. **Journal of Hazardous Material**, 2009, 171: 879-885.

Abstract:

The refining process in the petrochemical industry generates oil refinery sludges, a potentially contaminating waste product, with a high content of hydrocarbons and heavy metals. Faster degradation of hydrocarbons has been reported in vegetated soils than in non-vegetated soils, but the impact of these contaminants on the plants physiology and on their antioxidant system is not well known. In this study, the effect of the addition of petroleum sludge to soil on the physiological parameters, nutrient contents, and oxidative and antioxidant status in alfalfa was investigated. An inhibition of alfalfa growth and an induction of oxidative stress, as indicated by an increase in protein oxidation, were found. Also, the superoxide dismutase isoenzymes, peroxidase, and those enzymes involved in the ascorbate–glutathione cycle showed significant activity increases, parallel to an enhancement of total homogluthione, allowing plants being tolerant to this situation. This information is necessary to establish successful and sustainable plant-based remediation strategies.

4- Pascual I, Azcona I, Aguirreola J, Morales F, Corpas FJ, Palma JM, **Rellán-Álvarez R**, Sánchez-Díaz M. Growth, yield and fruit quality of pepper plants amended with two sanitized sewage sludges. **Journal of Agricultural and Food Chemistry** 58: 6951-6959.

Abstract:

Organic wastes such as sewage sludge have been successfully used to increase crop productivity of horticultural soils. Nevertheless, considerations of the impact of sludges on vegetable and fruit quality have received little attention. Therefore, the objective of the present work was to investigate the impact of two sanitized sewage sludges, autothermal thermophilic aerobic digestion (ATAD) and compost sludge, on the growth, yield, and fruit quality of pepper plants (*Capsicum annuum* L. cv. Piquillo) grown in the greenhouse. Two doses of ATAD (15 and 30% v/v) and three of composted sludge (15, 30, and 45%) were applied to a peat-based potting mix. Unamended substrate was included as control. ATAD and composted sludge increased leaf, shoot, and root dry matter, as well as fruit yield, mainly due to a higher number of fruits per plant. There was no effect of sludge on fruit size (dry matter per fruit and diameter). The concentrations of Zn and Cu in fruit increased with the addition of sewage sludges. Nevertheless, the levels of these elements remained below toxic thresholds. Pepper fruits from sludge-amended plants maintained low concentrations of capsaicin and dihydrocapsaicin, thus indicating low pungency level, in accordance with the regulations prescribed by the Control Board of “Lodosa Piquillo peppers” Origin Denomination. The application of sludges did not modify the concentration of vitamin C (ASC) in fruit, whereas the highest doses of composted sludge tended to increase the content of reduced (GSH) and oxidized (GSSG) glutathione, without change in the GSH/GSSG ratio. There were no effects of sludge on the transcript levels of enzymes involved in the synthesis of vitamin C, L-galactono-1,4-lactone dehydrogenase (GLDH) or in the ascorbate-glutathione cycle, ascorbate peroxidase (APX), monodehydroascorbate reductase (MDAR), and glutathione reductase (GR). Results suggest that the synthesis and degradation of ASC and GSH were compensated for in most of the treatments assayed. The application of sanitized sludges to pepper plants can improve pepper yield without loss of food nutritional quality, in terms of fruit size and vitamin C, glutathione, and capsaicinoid contents.

5- Rodríguez-Celma J, **Rellán-Álvarez R**, Abadía A, Abadía J, López-Millán A-F. Changes induced by two levels of cadmium toxicity in the 2-DE protein profile of tomato roots. **Journal of Proteomics** 73: 1694-1706

Abstract:

Tomato is an important crop from nutritional and economical points of view, and it is grown in greenhouses, where special substrates and the use of recycled water imply an increased risk of Cd accumulation. We investigated tomato root responses to low (10 μM) and high (100 μM) Cd concentrations at the root proteome level. Root extract proteome maps were obtained by 2-DE, and an average of 121, 145 and 93 spots were detected in the 0, 10 and 100 μM Cd treatments, respectively. The low Cd treatment (10 μM) resulted in significant and higher than 2-fold changes in the relative amounts of 36 polypeptides, with 27 of them identified by mass spectrometry, whereas the 100 μM Cd treatment resulted in changes in the relative amounts of 41 polypeptides, with 33 of them being

identified. The 2-DE based proteomic approach allowed assessing the main metabolic pathways affected by Cd toxicity. Our results suggests that the 10 μM Cd treatment elicits proteomic responses similar to those observed in Fe deficiency, including activation of the glycolytic pathway, TCA cycle and respiration, whereas the 100 μM Cd treatment responses are more likely due to true Cd toxicity, with a general shutdown of carbon metabolism and increases in stress related and detoxification proteins.

6- Jiménez S, Ollat N, Deborde C, Maucourt M, **Rellán-Álvarez R**, Moreno MA, Gogorcena Y. Metabolic response in roots of *Prunus* rootstocks submitted to iron chlorosis. **Journal of Plant Physiology** doi:10.1016/j.jplph.2010.08.010

Abstract:

Iron deficiency induces several responses to iron shortage in plants. Metabolic changes occur to sustain the increased iron uptake capacity of Fe-deficient plants. We evaluated the metabolic changes of three *Prunus* rootstocks submitted to iron chlorosis and their different responses for tolerance using measurements of metabolites and enzymatic activities. The more tolerant rootstocks Adesoto (*Prunus insititia*) and GF 677 (*Prunus amygdalus* \times *Prunus persica*), and the more sensitive Barrier (*P. persica* \times *Prunus davidiana*) were grown hydroponically in iron-sufficient and -deficient conditions over two weeks. Sugar, organic and amino acid concentrations of root tips were determined after two weeks of iron shortage by proton nuclear magnetic resonance spectroscopy of extracts. Complementary analyses of organic acids were performed by liquid chromatography coupled to mass spectrometry. The major soluble sugars found were glucose and sucrose. The major organic acids were malic and citric acids, and the major amino acid was asparagine. Iron deficiency increased root sucrose, total organic and amino acid concentrations and phosphoenolpyruvate carboxylase activity. After two weeks of iron deficiency, the malic, citric and succinic acid concentrations increased in the three rootstocks, although no significant differences were found among genotypes with different tolerance to iron chlorosis. The tolerant rootstock Adesoto showed higher total organic and amino acid concentrations. In contrast, the susceptible rootstock Barrier showed lower total amino acid concentration and phosphoenolpyruvate carboxylase activity values. These results suggest that the induction of this enzyme activity under iron deficiency, as previously shown in herbaceous plants, indicates the tolerance level of rootstocks to iron chlorosis. The analysis of other metabolic parameters, such as organic and amino acid concentrations, provides complementary information for selection of genotypes tolerant to iron chlorosis.

7- Sagardoy R, Morales F, **Rellán-Álvarez R**, Abadía A, Abadía J and López-Millán AF. Carboxylate metabolism in sugar beet plants grown with excess Zn. **Journal of Plant Physiology** *in press*.

Abstract:

The effects of Zn excess on carboxylate metabolism have been investigated in sugar beet (*Beta vulgaris* L.) plants grown hydroponically in a growth chamber. Root extracts of plants grown with 50 or 100 μM Zn in the nutrient solution showed increases in several enzymatic activities related to organic acid metabolism, including citrate synthase and phosphoenolpyruvate carboxylase, when compared to activities in control root extracts. Root citric and malic acid concentrations increased in plants grown with 100 μM Zn but not in plants grown with 50 μM Zn. In the xylem sap, plants grown with 50 and 100 μM Zn showed increases in the concentrations of citrate and malate when compared to the controls. Leaves of plants grown with 50 or 100 μM Zn showed increases in the concentrations of citric and malic acid and in the activities of citrate synthase and fumarase. Leaf isocitrate dehydrogenase increased only in plants grown with 50 μM Zn when compared to the controls. In plants grown with 300 μM Zn the only enzyme showing activity increases in root extracts was citrate synthase, whereas the activities of other enzymes decreased when compared to the controls, and root citrate concentrations increased. In the 300 μM Zn grown plants, the xylem concentrations of citric and malic acids were higher than those of controls, whereas in leaf extracts the activity of fumarase increased markedly and the leaf citric acid concentration was higher than in the controls. Based on our

data, a metabolic model of the carboxylate metabolism in sugar beet plants grown under Zn excess is proposed.

ANEX III
CURRICULUM VITAE

Currículum vitae

Impreso normalizado

Número de hojas que contiene: 10

Nombre: Rubén Rellán Álvarez

Fecha: 31 de Diciembre de 2010

Apellidos: Rellán Álvarez	Nombre: Rubén
Sexo: <i>Hombre</i>	DNI: 71644347Z
Dirección particular: <i>Genova 18-20, Esc 2, 3ºB 50007 Zaragoza</i>	Fecha de nacimiento: <i>08-10-1968</i>

SITUACIÓN PROFESIONAL ACTUAL

Organismo: *Consejo Superior de Investigaciones Científicas (CSIC)*
 Instituto: *Estación Experimental de Aula Dei*
 Dpto.: *Nutrición Vegetal*
 Dirección: *Apartado 202, 50080 Zaragoza*
 Teléfono: *976 716124 y 976 716106* Fax: *976 716145*
 Correo electrónico: rrellan@eead.csic.es
 Página Web: <http://www.stressphysiology.com/>

Especialización (Códigos UNESCO): *Ciencias de La Vida (24), Biología Vegetal (2417), Nutrición Vegetal (241717), Espectroscopia de Masas (2301.10), Metales (2303.18)*

Categoría profesional: *Investigador Contratado* Fecha de inicio: *1 Agosto de 2009*
 Situación administrativa: *Plantilla* Dedicación: *A tiempo completo*

LÍNEAS DE INVESTIGACIÓN

Nutrición vegetal, deficiencia de hierro, metales en plantas, metabólica, cromatografía líquida de alta resolución, espectrometría de masas, complejos metálicos en plantas

FORMACIÓN ACADÉMICA

Titulación Superior	Centro	Fecha
<i>Ciencias Ambientales</i>	<i>Universidad Autónoma de Madrid</i>	<i>2002</i>
Diploma Estudios Avanzados	Centro	Fecha
<i>Biotecnología Vegetal</i>	<i>Universidad Autónoma de Madrid</i>	<i>2005</i>

ACTIVIDADES ANTERIORES DE CARÁCTER CIENTÍFICO O PROFESIONAL

Fechas	Puesto	Institución
<i>Nov 02 – Dic 03</i>	<i>Investigador contratado (no doctor)</i>	<i>Univ. Autónoma de Madrid</i>
<i>Ene 04 – Jul 04</i>	<i>Visiting Scientist Jr.</i>	<i>EEAD-CSIC</i>
<i>Oct 04 – Mar 05</i>	<i>Investigador contratado (no doctor)</i>	<i>EEAD-CSIC</i>
<i>Ago 05 – Jul 09</i>	<i>Doctorando</i>	<i>EEAD-CSIC</i>
<i>Ago 09 – Presente</i>	<i>Investigador contratado (no doctor)</i>	<i>EEAD-CSIC</i>

IDIOMAS DE INTERÉS CIENTÍFICO (R = regular, B = bien, C= correctamente)

Idioma	Habla	Lee	Escribe
Inglés	C	C	C
Frances	B	B	R

PARTICIPACIÓN EN PROYECTOS DE I+D FINANCIADOS EN CONVOCATORIAS PÚBLICAS

ACTIVOS

Título del proyecto:	<i>Homeostasis and Transport of Iron – improving Plant Productivity and Growth (HOT IRON- PLANT PROGROW)</i>
Entidad financiadora:	ERA-NET Plant Genome Research KKBE (PN I+D+I)
Duración desde:	Mar 2009 Hasta: Feb 2012
Investigador principal:	Katrin Philippar (Universidad de Munich, Alemania)
Otros investigadores:	Nico von Wirén (Univ. Hohenheim, Alemania) Jean Francois Briat (INRA-CNRS-SupAgro-Montpellier University) Jose María García-Mina (CIPAV, Timac Agro, España)
Título del proyecto:	<i>Estudios sobre la homeostasis de metales en plantas (AGL2007-61948)</i>
Entidad financiadora:	MEC (Plan Nacional de Investigación)
Duración desde:	Oct 2007 Hasta: Oct 2010
Investigador principal:	Javier Abadía Bayona
Título del proyecto:	<i>Grupo Consolidado DGA (A03)</i>
Entidad financiadora:	Diputación General de Aragón
Duración desde:	2003 Hasta: 2011
Investigador principal:	Javier Abadía Bayona

FINALIZADOS

Título del proyecto:	<i>Adquisición y transporte de metales en plantas (AGL2004-00194)</i>
Entidad financiadora:	CICYT (Plan Nacional de I+D)
Duración desde:	Dic 2004 Hasta: Dic 2007
Investigador principal:	Javier Abadía Bayona
Título del proyecto:	<i>Nutrición de hierro en frutales: estrategias para el control de la clorosis férrica (AGL2003-01999)</i>
Entidad financiadora:	CICYT (Plan Nacional de I+D)
Duración desde:	Dic 2003 Hasta: Dic 2006
Investigador principal:	Anunciación Abadía Bayona
Título del proyecto:	<i>Recuperación de Terrenos Afectados por Mercurio Ambiental (FEDER 2FD97-0314)</i>
Entidad financiadora:	Ministerio de Ciencia y Tecnología
Duración desde:	Ene 2002 Hasta: Dic 2005
Investigador principal:	Rocío Millán

PUBLICACIONES

Artículos en Revistas Internacionales SCI H-Index: 5

- 1** Ortega-Villasante C, **Rellán-Álvarez R**, Del Campo FF, Carpena-Ruiz RO, Hernández LE. (2005) Cellular damage induced by cadmium and mercury in *Medicago sativa*. **Journal of Experimental Botany**. 56 (418): 2239-2251. *Citado 42 veces*.
- 2** **Rellán-Álvarez R**, Ortega-Villasante C, Álvarez-Fernández A, del Campo FF, Hernández LE (2006) Stress responses of *Zea mays* to cadmium and mercury. **Plant and Soil** 279, 41-50. *Citado 22 veces*.
- 3** **Rellán-Álvarez R**, Hernández LE, Abadía J, Álvarez-Fernández A (2006) Direct and simultaneous determination of reduced and oxidized glutathione and homoglutathione by liquid chromatography-electrospray/mass spectrometry in plant tissue extracts. **Analytical Biochemistry** 356, 254-264. *Citado 22 veces*.
- 4** Ortega-Villasante C, Hernández LE, **Rellán-Álvarez R**, Del Campo FF, Carpena-Ruiz RO. (2007) Rapid alteration of cellular redox homeostasis upon exposure to cadmium and mercury in alfalfa seedlings. **New Phytologist.**, 176 (1): 96-107. *Citado 17 veces*.
- 5** **Rellán-Álvarez R**, Abadía J, Álvarez-Fernández A (2008) Formation of metal-nicotianamine complexes as affected by pH, ligand exchange with citrate and metal exchange. A study by electrospray ionization time-of-flight mass spectrometry. **Rapid Communications in Mass Spectrometry** 22, 1553-1562. *Citado 11 veces*.
- 6** Martí MC, Camejo D, Fernández-García N, **Rellán-Álvarez R**, Marques S, Sevilla F, Jiménez A, Effect of oil refinery sludges on the growth and antioxidant system of alfalfa plants. **Journal of Hazardous Material**, 2009, 171: 879-885. *Citado 2 veces*.
- 7** **Rellán-Álvarez R**, Giner-Martínez-Sierra J, Orduna J, Orera I, Rodríguez-Castrillón JA, García-Alonso JI, Abadía J, **Álvarez-Fernández A**. (2010) Identification of a tri-iron(III), tri-citrate complex in the xylem sap of iron-deficient tomato resupplied with iron: new insights into plant iron long-distance transport. **Plant Cell Physiology** 51:91-102. *Citado 4 veces*.
- 8** Pascual I, Azcona I, Aguirreolea J, Morales F, Corpas FJ, Palma JM, **Rellán-Álvarez R**, Sánchez-Díaz M. Growth, yield and fruit quality of pepper plants amended with two sanitized sewage sludges. **Journal of Agricultural and Food Chemistry** 58: 6951-6959.
- 9** Rodríguez-Celma J, **Rellán-Álvarez R**, Abadía A, Abadía J, López-Millán A-F. Changes induced by two levels of cadmium toxicity in the 2-DE protein profile of tomato roots. **Journal of Proteomics** 73: 1694-1706
- 10** **Rellán-Álvarez R**, Andaluz S, Rodríguez-Celma J, Wohlgemuth G, Zocchi G, Álvarez-Fernández A, Fiehn O, López-Millán AF, Abadía J. Changes in the proteomic and metabolic profiles of *Beta vulgaris* root tips in response to iron deficiency and resupply. **BMC Plant Biology**. 10: 120
- 11** Jiménez S, Ollat N, Deborde C, Maucourt M, **Rellán-Álvarez R**, Moreno MA, Gogorcena Y. Metabolic response in roots of *Prunus* rootstocks submitted to iron chlorosis. **Journal of Plant Physiology** doi:10.1016/j.jplph.2010.08.010
- 12** Sagardoy R, Morales F, **Rellán-Álvarez R**, Abadía A, Abadía J and López-Millán AF. Carboxylate metabolism in sugar beet plants grown with excess Zn. **Journal of Plant Physiology** doi:10.1016/j.jplph.2010.10.012

En revisión:

- 13** Abadía J, Vázquez S, **Rellán-Álvarez R**, El Jendoubi H, Abadía A, Álvarez-Fernández A and López-Millán AF. Towards a knowledge-based correction of iron chlorosis. **Plant Physiology and Biochemistry**

- 14** López-Gomollón S*, Rellán-Álvarez R*, Abadía J, Álvarez-Fernández A. Low molecular weight organic acid determination in plant tissue extracts by liquid chromatography–electrospray Time Of Flight mass spectrometry. **Journal of Agriculture and Food Chemistry**
- 15** Rellán-Álvarez R, El Jendoubi H, Wohlgemuth G, Fiehn O, Abadía A, Abadía J and Álvarez Fernández A. Iron deficiency changes induced in metabolite profiles of xylem sap and leaves of different plant species. **Plant Cell and Environment**

Publicaciones en Monografías y Actas de Congresos

- 1** Rellán-Álvarez R, Cristina Ortega-Villasante, Diego F. Rosero, Francisca F. del Campo and Luis E. Hernández. (2004) En *Nutrição Mineral: Causas e consequências da dependencia da fertilização*, MA Martin Loucao and Cristina Cruz (eds). Lisboa, Portugal
- 2** Rellán-Álvarez R, Hernández LE, Abadía J, Álvarez-Fernández A (2006) Direct and simultaneous determination of reduced and oxidized glutathione and homogluthathione by liquid chromatography-electrospray/mass spectrometry in plant tissue extracts. En: *Nutrición Mineral. Aspectos fisiológicos, agronómicos y ambientales* (Lamsfus C, ed.), vol I, pp. 233-240. ISBN 84-9769-165-2.
- 3** Rellán-Álvarez R, Álvarez-Fernández A, Abadía J. Analysis of iron nicotianamine complexes by electrospray-mass spectrometry. **American Journal of Hematology**. 2007, 82 (6): 581-582
- 4** Rellán-Álvarez R, Andaluz S, López-Millán AF, Fiehn O, Álvarez-Fernández A, Abadía J (2009) Changes in the proteomic and metabolomic profiles of beta vulgaris root tips in response to iron deficiency and resupply. En: *The Proceedings of the International Plant Nutrition Colloquium XVI*. UC Davis. Descargar de: <http://www.escholarship.org/uc/item/0jn8d7s6>
-

ESTANCIAS EN CENTROS EXTRANJEROS

CLAVE: D = doctorado, P = postdoctoral, I = invitado, C = contratado, O = otras (especificar).

CENTRO: **University of California, Davis** (Metabolomics Lab, Genome Center)
 LOCALIDAD: Davis PAIS: USA
 AÑO: 2006 DURACION: 2 meses
 TEMA: Metabólica de Plantas. CLAVE: D

CENTRO: **University of California, Davis** (Metabolomics Lab, Genome Center)
 LOCALIDAD: Davis PAIS: USA
 AÑO: 2007 DURACION: 3 meses
 TEMA: Metabólica de Plantas: CLAVE: D
Publicaciones en revistas internacionales n° 8

CENTRO: **University of California, Davis** (Metabolomics Lab, Genome Center)
 LOCALIDAD: Davis PAIS: USA
 AÑO: 2008 DURACION: 2 meses
 TEMA: Metabólica de Plantas: CLAVE: D

ESTANCIAS EN CENTROS NACIONALES

CLAVE: D = doctorado, P = postdoctoral, I = invitado, C = contratado, O = otras (especificar).

CENTRO: **Universidad de Granada** (Dpto Q^aAnalítica)-
 LOCALIDAD: Granada PAIS: España
 AÑO: 2008 DURACION: 1 meses
 TEMA: Determinación complejos metalicos por EC-MS. CLAVE: D

CENTRO: **Universidad de Oviedo** (Dpto Q^aAnalítica)
 LOCALIDAD: Oviedo PAIS: España
 AÑO: 2008-2009 DURACION: 3 semanas
 TEMA: Determinación complejos metalicos por ICP-MS. CLAVE: D

Organización de congresos

XVIII Reunión de la Sociedad Española de Fisiología Vegetal (SEFV). XI Congreso Hispano-Luso de Fisiología Vegetal. Zaragoza, España. Tipo de actividad: Comité Organizador. 8-11 de Sep. 2009.

Conferencias Invitadas de Apertura de Sesión (Keynotes)

I Jornada de Tecnologías para el tratamiento de suelos contaminados/Soil remediation Technologies. Alcalá de Henares, Madrid., *La espectrometría de masas en el estudio de metales pesados en plantas.* 20-21 Nov 2006

VII Jornada de Fisiología Vegetal, Barcelona *Identificación de complejos organometálicos en tejidos vegetales mediante espectrometría de masas.* 6 Nov. 2009.

Comunicaciones orales y paneles

- 2003 *7th International Congress of Plant Molecular Biology Barcelona*
- (1) Cristina Ortega-Villasante, **Rubén Rellán-Álvarez R**, Francisca F. del Campo, Ramón O. Carpena-Ruíz, Luis E. Hernández. Stress responses of *Medicago sativa* seedlings to cadmium and mercury exposure. (*Comunicación, panel*)
- XV Reunión de la Sociedad Española de Fisiología Vegetal y VIII Congreso Hispano-Luso, Palma de Mallorca*
- (2) Luis. E. Hernández, Cristina Villasante-Ortega, **Rubén Rellán-Álvarez R**, Francisca Fdez. del Campo, Ramón O. Carpena-Ruíz. Alteraciones en los niveles de glutatión inducidas por metales pesados en *Medicago* spp.: estrés oxidativo y acumulación de tioles (Comunicación, Panel)
- Achievements and Prospects of Phytoremediation in Europe, Viena, Austria (Asistencia)*
- (3) Luis E. Hernández, Cristina Ortega-Villasante, **Rellán-Álvarez R**, Francisca F. del Campo, Ramón Carpena-Ruiz.Changes in glutathione content induced by heavy metals in *Medicago* spp.: Oxidative stress and phytochelatins. (Comunicación, panel). (Tercer premio al mejor panel)
- 2004 *X Simposio Ibérico de Nutrición Mineral de Plantas. Lisboa. (Asistencia)*
- (4) **Rellán-Álvarez R***, Cristina Villasante-Ortega, Diego F. Rosero, Francisca F. del Campo, Luis E. Hernández. Stress response of *Zea mays* to cadmium and mercury. Oral Presentation. (*Comunicación / oral**)
- 2006 *XIII International Symposium on Iron Nutrition and Interactions in Plants. Montpellier, France. (Asistencia)*
- (5) **Rellán-Álvarez R**, Abadía J, Álvarez-Fernández A. Glutathione and ascorbic levels analysis by HPLC-MS(TOF) in iron deficient plants. (Comunicación / Panel)
- XI Congreso Ibérico sobre Nutrición Mineral de las plantas. Pamplona, España. (Asistencia)*
- (6) **Rellán-Álvarez R**, Hernández LE, Abadía J, Álvarez-Fernández A. Direct and simultaneous determination of reduced and oxidized glutathione and homogluthathione by liquid chromatography-electrospray/mass spectrometry in plant tissue extracts. (Comunicación / Panel)
- 2007 *BioIron meeting. Kyoto, Japan.*

- (7) **Rellán-Álvarez R**, Álvarez-Fernández A, Abadía J. Analysis of nicotianamine metal complexes by electrospray-mass spectrometry (Comunicación / Panel)
- XVII Reunión de la Sociedad Española de Fisiología Vegetal – X Congreso Hispano – Luso de Fisiología Vegetal, Alcalá de Henares, España.*
- (8) Abadía J*, Álvarez-Fernández A, López-Millán AF, Orera I, **Rellán-Álvarez R**, Abadía A. Long-distance metal transport in plants. (Keynote*)
- 2008 *XIV International Symposium on Iron Nutrition and Interactions in Plants. Beijing, China.*
- (8) **Rellán-Álvarez R**, Abadía A, Fiehn O, Abadía J, **Álvarez-Fernández A**. Changes in the xylem sap metabolome of tomato and lupin with Fe deficiency. (Comunicación / Panel)
- (9) **Rellán-Álvarez R**, Andaluz S, López-Millán AF, **Álvarez-Fernández A**, Fiehn O, Abadía J. Proteomic and metabolomic profiles of *Beta vulgaris* root tips: changes induced in response to iron deficiency and resupply. (Comunicación / Panel)
- 2009 *XVI International Plant Nutrition Colloquium. Sacramento, California, USA. (Asistencia)*
- (10) **Rellán-Álvarez R***, Andaluz S, López-Millán AF, Fiehn O, Álvarez-Fernández A, Abadía J. Changes in the proteomic and metabolomic profiles of *Beta vulgaris* root tips in response to iron deficiency and resupply. (Oral*)
- XVIII Reunión de la Sociedad Española de Fisiología Vegetal (SEFV). XI Congreso Hispano-Luso de Fisiología Vegetal. Zaragoza, España. (Asistencia)*
- (11) **Rellán-Álvarez R***, Giner-Martínez-Sierra J, Orduna J, Orera I, Rodríguez-Castrillón JA, García-Alonso JI, Abadía J, Álvarez-Fernández A. Iron is transported as a tri-Fe(III), tri-citrate complex in plant xylem sap. (Comunicación / Oral)
- (12) Rellán-Álvarez R, Rodríguez-Celma J, López-Millán AF, Fiehn O, **Álvarez-Fernández A**, Abadía A, Abadía J. Plant iron deficiency metabolomics. (Comunicación / Panel)
- 2010 *XV International Symposium on Iron Nutrition and Interactions in Plants. Budapest, Hungary. (Asistencia)*
- (13) **Rellán-Álvarez R**, El Jendoubi H, Wohlgemuth G, Abadía A, Fiehn O, Abadía J, Álvarez-Fernández A. Delving into iron deficiency metabolomics (Oral*)
- (14) Abadía J, Álvarez-Fernández A, **Rellán-Álvarez R**, López-Millán AF, Abadía A. Towards a knowledge-based correction of iron chlorosis
- XVII Congress of the Federation of European Societies of Plant Biology. FESPB, Valencia, Spain.*
- (15) **Rellán-Álvarez R**, Abadía J, Álvarez-Fernández, A. Xylem metabolomics and iron deficiency (Poster)
- (16) Azcona I, Pascual I, Aguirreolea J, Morales F, **Rellán-Álvarez R**, Sánchez-Díaz M. Application of sanitized sewage sludges to pepper plants: effects on yield, fruit quality and severity of *Verticillium* wilt. (Poster).
- XIII Simposio Ibérico de Nutrición Mineral de las Plantas, San Sebastián, Spain*
- (17) **Rellán-Álvarez R**, El Jendoubi H, Wohlgemuth G, Abadía A, Fiehn O, Abadía J, Álvarez-Fernández A. Delving into iron deficiency metabolomics (Poster)

6th International Franco-Spanish Workshop on Bio-Inorganic Analytical Chemistry, Pau, France

(18) **Rellán-Álvarez R**, Abadía J, Álvarez-Fernández A. Iron speciation in plant xylem sap using LC-ESI-TOFMS (*Asistencia y Oral*).

GRANDES EQUIPOS QUE UTILIZA O HA UTILIZADO

CLAVE : R= responsable, UA = usuario asiduo, UO = usuario ocasional

<i>EQUIPO</i>	<i>FECHA</i>	<i>CLAVE</i>
Espectrometría de Masas con Plasma de Acoplamiento Inductivo (ICPMS y HPLC-ICPMS)	2009	UO
Espectrometría de masas tándem (HPLC-ESI/MS-MSQ-TOF y Iontrap)	2009	UO
Espectrometría de masas (ESI-MSTOF y HPLC-ESI/MSTOF)	2002-2009	UA
Electroforesis capilar	2007	UO
Espectrometría de masas (GC-MS)	2006-2008	UO
Cromatografía líquida de alta eficacia (HPLC-UV)	2002-2010	UA
Espectrometría de absorción y emisión atómica	1993-2000	UO
Electroforesis capilar	1996-2000	UO

OTROS MÉRITOS O ACLARACIONES QUE SE DESEE HACER CONSTAR

Divulgación Científica

- Semana de la Ciencia de Aragón. Introducción a las labores realizadas de investigación realizadas en la Estación Experimental de Aula Dei a estudiantes de bachillerato como representante del centro de investigación. Dic-2004
- Semana de la Ciencia de Aragón. Introducción a las labores realizadas de investigación realizadas en Aula Dei a estudiantes de Bachillerato Nov-2006.
- Semana de la Ciencia de Aragón. Introducción a las labores realizadas de investigación realizadas en Aula Dei a estudiantes de Bachillerato Oct-2009.
- Pabellón de la Ciencia de Aragón. Introducción a las labores realizadas de investigación realizadas en Aula Dei a todo tipo de público. Oct-2009.
- Semana de la Ciencia de Aragón. Introducción a las labores realizadas de investigación realizadas en Aula Dei a estudiantes de Bachillerato Nov-2010.

Cursos y Seminarios Recibidos

- Curso Práctico de Metodologías de Utilidad Medio Ambiental. 09-Sept-17-Oct 2002 (180 horas) Centro de Biología Molecular Severo Ochoa. CSIC-UAM. Madrid
- XIX Curso de Histoquímica Vegetal. May 2003 (60 horas). Consejo Superior de Investigaciones Científicas. Centro de Ciencias Medio Ambientales. CSIC. Madrid
- Curso de Formación para el Manejo de un ESI-TOF (BioTOF II). Bruker Daltonics. Avanzado. May 2004. (30 h).
- Seminario sobre Detección e identificación de metabolitos y pequeñas moléculas. 28-Nov 2006. Bruker Daltoniks. Barcelona
- Curso de Formación para el Manejo de un ESI-TOF (MicroTOF). Bruker Daltonics. Dic 2008. (aprox. 24 h).
- Seminario de Metabolómica. Agilent Technologies. Mar 2009. (4 h).

